Antonio Luna · Joan C. Vilanova
Pablo R. Ros *Editors*

Learning Abdominal Imaging

LEARNING IMAGING
Ramón Ribes · Antonio Luna · Pablo R. Ros *Series Editors*

Springer

Learning Imaging

Series Editors:

R. Ribes · A. Luna · P.R. Ros

Antonio Luna · Joan C. Vilanova
Pablo R. Ros
(Editors)

Learning Abdominal Imaging

Springer

Antonio Luna
Clinica Las Nieves Sercosa
Carmelo Torres 2
23007 Jaén
Spain

Joan C. Vilanova
Clinica Girona
Dept. Magnetic Resonance
Lorenzana 36
17002 Gerona
Spain

Pablo R. Ros
Case Western Reserve University
Dept. Radiology
Bolwell B124
Euclid Ave. 11100
44106 Cleveland Ohio
USA

ISBN 978-3-540-88002-8 e-ISBN 978-3-540-88003-5

DOI 10.1007/978-3-540-88003-5
Springer Heidelberg Dordrecht London New York

Library of Congress Control Number: 2012931857

Printed on acid-free paper

9 8 7 6 5 4 3 2 1

Springer is part of Springer Science+Business Media (www.springer.com)

Contents

Contributors

Sandra Baleato
Department of Radiology
CHUS Complexo Hospitalario
Universitario de Santiago
Santiago de Compostela
Coruña
Spain

Joaquim Barceló
Department of Radiology
Clínica Girona-Hospital Sta. Caterina
University of Girona
Girona, Spain

Maria Boada
Magnetic Resonance
Clinica Girona
Girona
Spain

Enrique Ramón Botella
Body Section
Radiology Department
Gregorio Marañon Hospital
Madrid
Spain

Gabriel C. Fernández
Department of Radiology
HNSS (Hospital Nuestra
Señora de Sonsoles)
Avila, Spain

Guadalupe Garrido
Radiology Department
Hospital Clínico
Málaga
Spain

Antonio Luna
Health Time Group and
MRI Section
Clinica Las Nieves Sercosa
Jaén
Spain

Luis Luna
Clinica Las Nieves
Sercosa
Jaén
Spain

Carmen Villalba Martín
Department of Radiology
Complexo Hospitalario Universitario de Santiago de Compostela
Santiago de Compostela, Spain

Lidia Alcalá Mata
Clinica Las Nieves Sercosa
Jaen
Spain

Xavier Merino-Casabiel
Unitat RM, Servei Radiologia
Hospital Vall d'Hebrón
Barcelona
Spain

Joaquina Paz López Moras
Centro de Diagnostico "Dr Enrique Rossi"
Buenos Aires
Argentina

Anaberta Bermúdez Naveira
Department of Radiology
Complexo Hospitalario Universitario de Santiago de Compostela
Santiago de Compostela
Spain

Teodoro Martín Noguerol
MRI Section
Clinica Las Nieves Sercosa
Jaén
Spain

María Mercedes Liñares Paz
Department of Radiology
Complexo Hospitalario Universitario de Santiago de Compostela
Santiago de Compostela
Spain

Pablo R. Ros
Department of Radiology
University Hospitals Case Medical Center
Theodore J. Castele University
Case Western Reserve University
Cleveland, OH
USA

Verónica Patricia Rubio
Centro de Diagnostico "Dr Enrique Rossi"
Buenos Aires
Argentina

Mario Santamarina
Hospital Naval Neff
Viña del Mar
Chile

Anna Pérez de Tudela
Department of Radiology
Hospital Sta. Caterina Slat
Girona
Spain

Andrés Enrique Madrid Vallenilla
Radiology Department
Gregorio Marañon Hospital
Madrid
Spain

Joan C. Vilanova
Department of Radiology
Clínica Girona-Hospital Sta. Caterina
University of Girona
Girona
Spain

Mariano Volpacchio
Centro de Diagnostico "Dr Enrique Rossi"
Buenos Aires, Argentina
Hospital de Clínicas "José de San Martín",
Buenos Aires
Argentina

Liver

1

Andrés Enrique Madrid Vallenilla, Enrique Ramón Botella, and Antonio Luna

Contents

A. Luna et al., *Learning Abdominal Imaging*, Learning Imaging,
DOI 10.1007/978-3-540-88003-5_1,

Case 1
Hemangioma

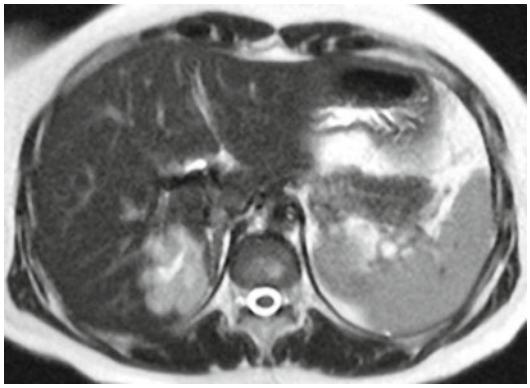

Fig. 1.1.1

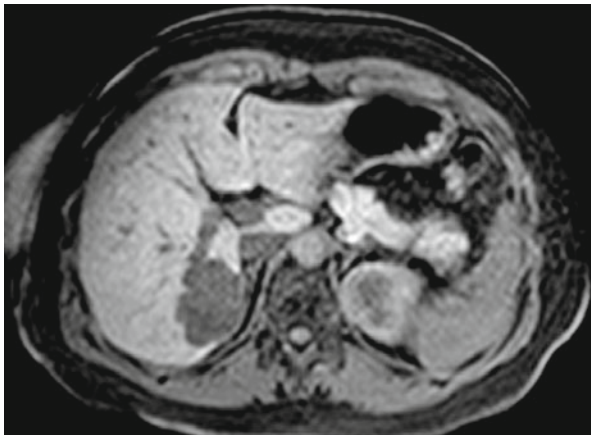

Fig. 1.1.2

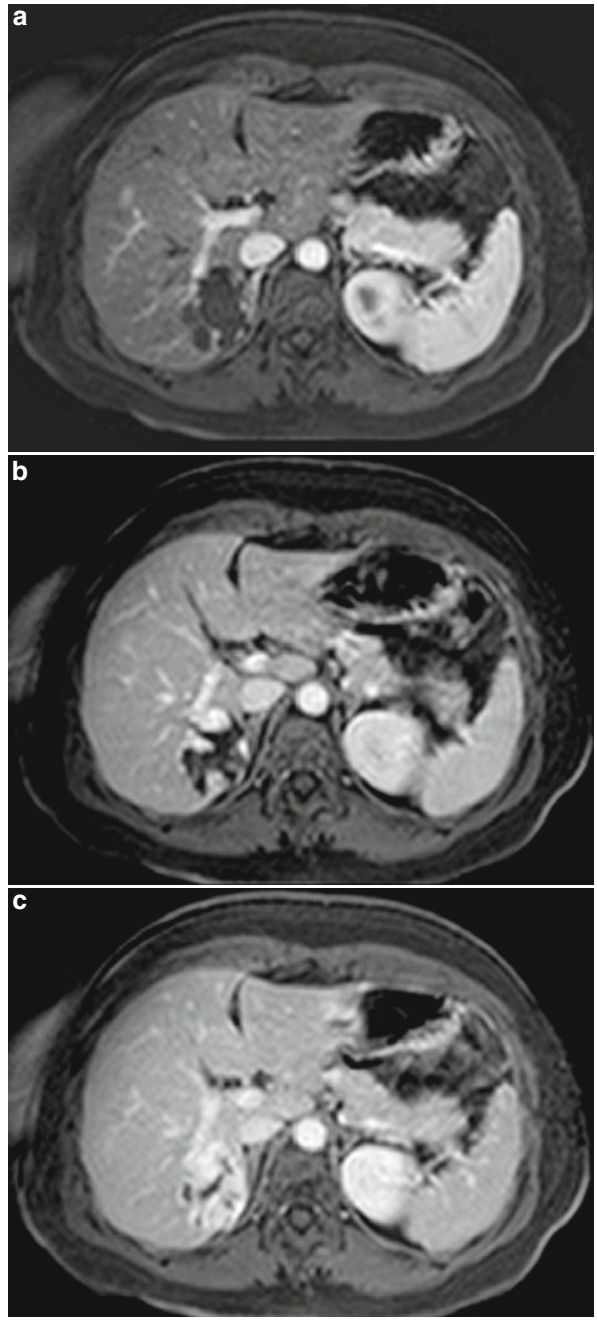

Fig. 1.1.3

A 35-year-old woman that in an abdominal ultrasound is diagnosed with a hyperechoic liver nodule in the posterior segments of the right lobe, was submitted to our MRI unit. An MRI exploration is conducted, with standard sequences, including T1-weighted, T2-weighted, and a dynamic study, after the administration of a gadolinium-based contrast media.

Comments

Hemangiomas are the most common benign tumor of the liver. Histologically they are composed of multiple vascular channels, lined by a single layer of endothelial cells, and supported by a thin fibrous stroma. They are usually detected as an incidental finding in ultrasound scans, being hyperechoic lesions with well-defined margins, which may have a slight posterior acoustic enhancement. However, sometimes, they can show atypical features. In these cases, it is crucial to perform a contrast-enhanced CT or MRI study, where they behave as hypervascular lesions, with three different possible patterns of enhancement:

Type I shows a homogeneous and rapid enhancement and tend to be small lesions.

Type II consists of a peripheral nodular enhancement with homogenous centripetal filling.

Type III is similar to type II, but there is a central scar that is not opacified with contrast; this type of enhancement is characteristic of large hemangiomas.

On T2-weighted sequences, its characteristic feature is a marked hyperintense signal, due to the high content of low-flow vascular channels. These tumors coexist very frequently with other liver lesions, and in oncologic patients with cirrhosis may cause a diagnostic problem; when the doubt exists, the T2-weighted sequence is especially useful, as it allows the radiologist to separating malignant tumor nodules from hemangiomas and cystic lesions, based on T2-relaxation differences, with an excellent diagnostic confidence.

In conclusion, the main clues to diagnose a hemangioma on MRI are the typical pattern of enhancement and its marked hyperintensity on T2.

Imaging Findings

Axial TSE T2-weighted sequence shows a focal liver lesion, measuring 4 cm in the posterior aspect of the right lobe, within the limits between segments 6 and 7 (Fig. 1.1.1). The lesion shows a lobulated shape and is markedly hyperintense, with a small central scar (*arrow*). In precontrast THRIVE (T1-weighted image), the lesion is hypointense (Fig. 1.1.2), and after contrast media injection it undergoes a peripheral nodular enhancement, with progressive centripetal filling (Fig. 1.1.3: dynamic postcontrast THRIVE series on arterial (a), venous (b), and equilibrium phases (c), respectively).

Case 2

Focal Nodular Hyperplasia

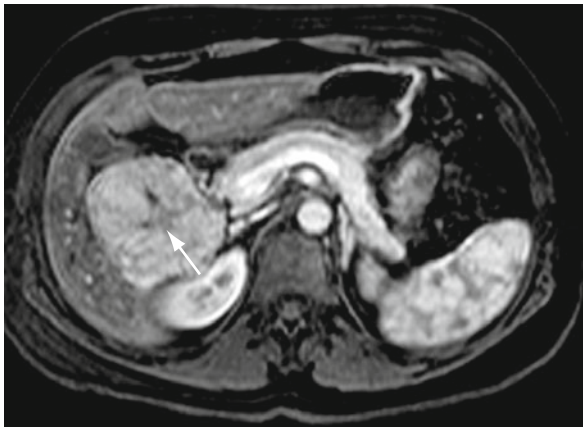

Fig. 1.2.1

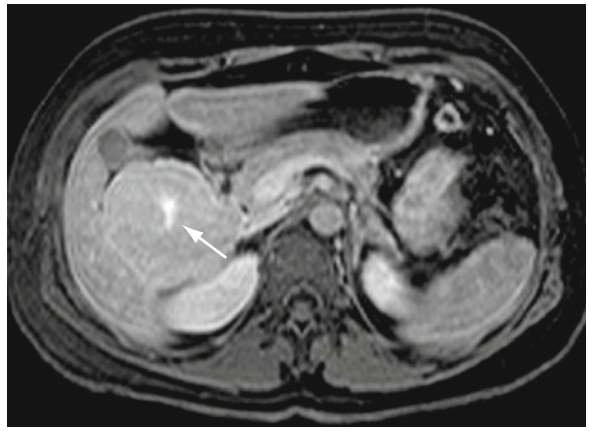

Fig. 1.2.2

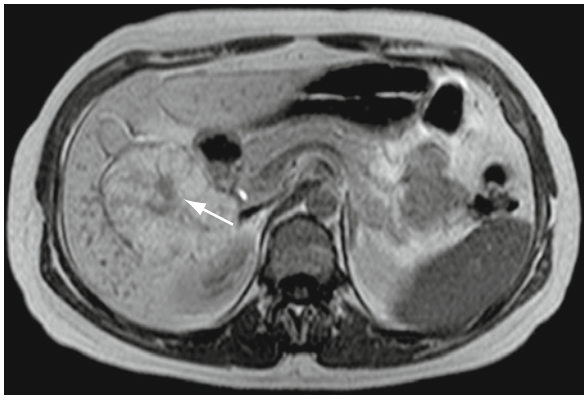

Fig. 1.2.3

A 40-year-old woman with history of epigastric pain, without any other symptom or laboratory abnormality, had an incidental finding on ultrasound of a 5-cm hepatic lesion. The lesion was subcapsular, homogeneous, and slightly hyperechoic in appearance, with a peripheral halo. An MRI was performed for further characterization.

Comments

FNH is the second most common primary solid lesion in the liver after hemangioma. It is characteristic of middle-aged women. It is usually discovered as an incidental finding. FNH is habitually a single lesion, with a homogeneous appearance in a subcapsular location. A central scar is identifiable in up to 70% of the cases, published in different series, but this finding is not pathognomonic.

In ultrasound, FNH is iso- or slightly hyperechoic compared to liver parenchyma. In Doppler or after administration of ultrasound contrast with a vascular distribution (i.e., sulfur hexachloride microbubbles), it demonstrates the characteristic pattern of centrifugal flow pattern ("spoke-wheel sign"). In dynamic CT or MRI scans, FNH shows early enhancement without washout in the equilibrium phase. The use of dual contrast at MRI allows a greater degree of diagnostic confidence. FNH is composed of functioning hepatocytes and characteristically captures the dual contrasts (Gd-BOPTA and Gd-EOB-DTPA) during biliary excretion. The dual contrasts permit to obtain a dynamic T1-weighted study, in the extracellular distribution phase, and after a variable delay between 20 and 60 min, depending on the contrast chelate used, an active intracellular transport allows to exploring the hepatocytes function, by means of their ability to secrete bile. Hepatobiliary contrast agents allow an accurate differentation between FNH and adenoma which is crucial for their management, as adenoma larger of 3 cm should be resected due to the risk of hemorrhage.

FNH as the reticuloendothelial system retains the contrasts media based on microparticles of iron (SPIO or USPIO). When this type of contrasts is used, T2-weighted sequences must be acquired, which improves the visualization of the septa and the central scar.

It has recently been marketed an ultrasound contrast that is captured by the reticuloendothelial system (perfluorobutane bubbles), and therefore it has also applicability to characterize FNH.

Imaging Findings

The lesion was isointense on both T1-weighted and T2-weighted sequences, with a central scar (images not shown). The dynamic study was performed after intravenous administration of Gd-BOPTA (gadobenate dimeglumine). The lesion showed early and intense uptake of contrast on the arterial phase with lack of enhancement of the central scar (*arrow*) (Fig. 1.2.1). During the equilibrium phase, the mass was isointense to liver parenchyma and also retains contrast at the central scar, which appeared hyperintense (*arrow*) (Fig. 1.2.2). Image in the hepatobiliary phase acquired 60 min after contrast injection shows how the mass retains contrast as much as the liver does, with lack of enhancement of the central scar (*arrow*) (Fig. 1.2.3).

Case 3
Adenoma

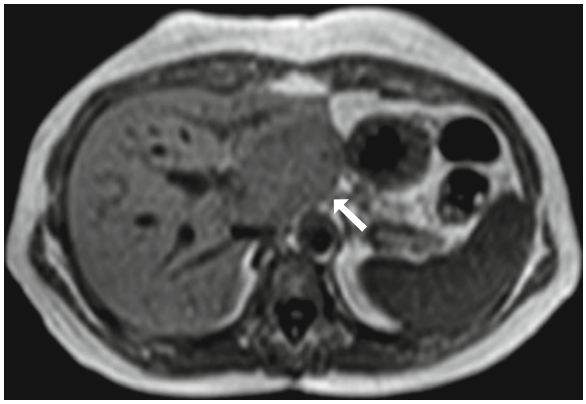

Fig. 1.3.1

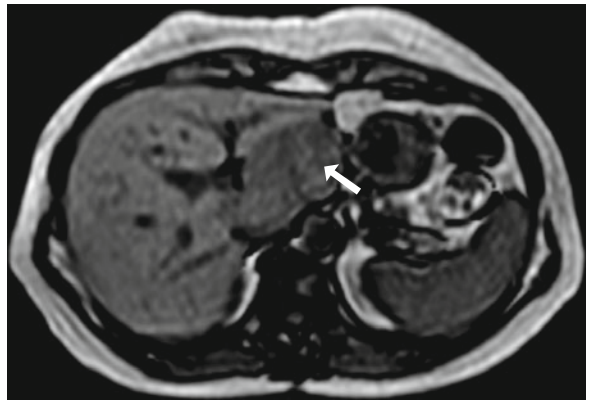

Fig. 1.3.2

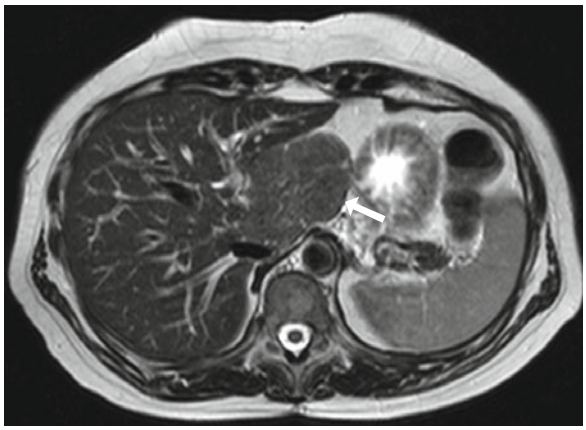

Fig. 1.3.3

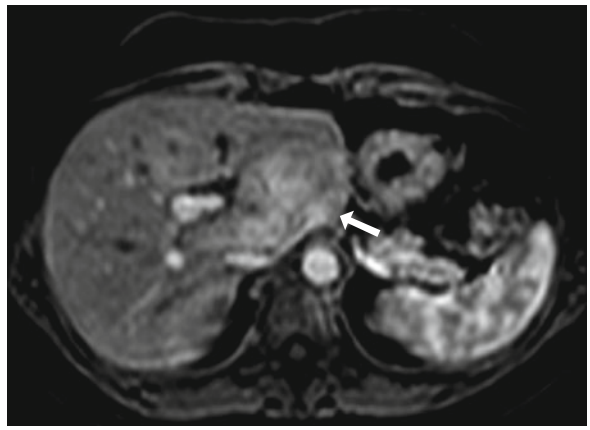

Fig. 1.3.4

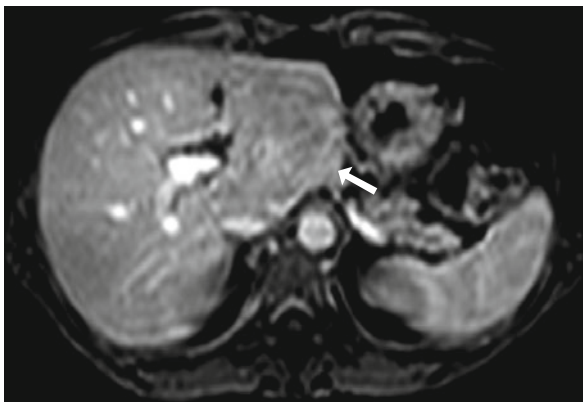

Fig. 1.3.5

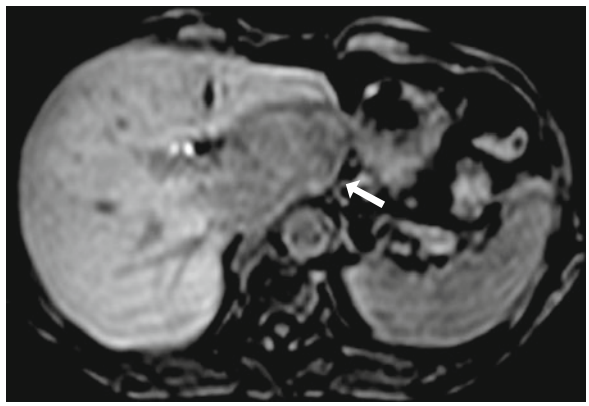

Fig. 1.3.6

A 34-year-old woman, with an incidental focal liver lesion in segment 1 on ultrasound and personal history of use of oral contraceptives, is referred to our department to perform an MRI for further characterization.

Comments

Liver adenoma is a lesion composed of hepatocytes arranged in cords. It usually has intracellular lipids and, histologically, lacks of lobules, centrilobular vein, or portal triad but shows large venous and arterial vessels in a predominant peripheral location. The presence of Kupffer cells is very rare. Large lesions may be more heterogeneous due to different components: fat, different stages of bleeding, and/or necrosis. In a considerable proportion of cases, a fibrous capsule is identifiable. The most important clinical fact is the history of oral contraceptives or anabolic steroids use.

Knowing these histological characteristics, its behavior could be predictable, in each of the imaging techniques. In US it usually correspond to hyperechogenic lesions with sharp borders. The detection of vessels is characteristic with the use of Doppler technique.

MRI is the technique of choice for characterization. The presence of fat is readily detected in GRE T1-weighted in-phase and out-of-phase images sets. The signal drop in out-of-phase with respect to in-phase images allows for the intracellular fat detection. Sometimes, adenoma may show signs of bleeding.

In the dynamic postcontrast sequence, using an extracellular contrast media, adenoma tipically shows an intense enhancement in the arterial phase, without washout in the equilibrium phase. This absence of washout helps in the distinction from hepatocellular carcinoma, which characteristically presents with washout in the equilibrium phase.

Focal nodular hyperplasia (FNH) is the main differential diagnosis of adenoma. If there is no characteristic morphological features, of either FNH, such as a scar, or adenoma, such as the presence of fat or adenoma, the distinction between both types of lesions is very challenging with both CT and MRI. However, the use of MRI dual contrasts with biliary excretion, such as dimeglumine gadobenate and gadoxetic acid, allows this distinction with a sufficient degree of diagnostic confidence. The contrast enhancement during the biliary excretion, at an intensity similar or greater than liver parenchyma, supports the diagnosis of FNH. Adenomas are characteristically hypointense compared to liver parenchyma, during the hepatospecific phase. There are between 10 to 20% of FNH with atypical features, which are classified as nonclassic. These nonclassic FNHs often present a diagnostic challenge at imaging, as they may show features typical of adenomas in different degrees.

Imaging Findings

Figure 1.3.1 In-phase GE T1 sequence confirms the presence of a slightly hypointense mass compared with liver parenchyma (*arrow*). In the out-of-phase sequence, regional signal drop within the mass is identified, revealing fat content (Fig. 1.3.2, *arrow*). In TSE T2 sequence, this lesion is isointense to liver parenchyma (Fig. 1.3.3, *arrow*). After administration of dimeglumine gadobenate, uptake in the arterial phase by the lesion is shown (Fig. 1.3.4, *arrow*). In the portal venous phase, the lesion is isointense to liver (Fig. 1.3.5, *arrow*). During the biliary excretion phase (approximately 60 min after contrast injection), the lesion does not retain the contrast, and it appears hypointense (Fig. 1.3.6, *arrow*). This enhancement pattern is typical for hepatic adenoma.

Case 4
Hepatic Lesion with Cystic Appearance: Liver Abscess

A 31-year-old woman, who came to the ER because of thoracolumbar pain, irradiating to the shoulder, and poor control with analgesics, was referred to perform an abdominal ultrasound to our department. She also refers mild malaise and was afebrile. Laboratory tests showed mild LFTs elevation and hyperbilirubinemia.

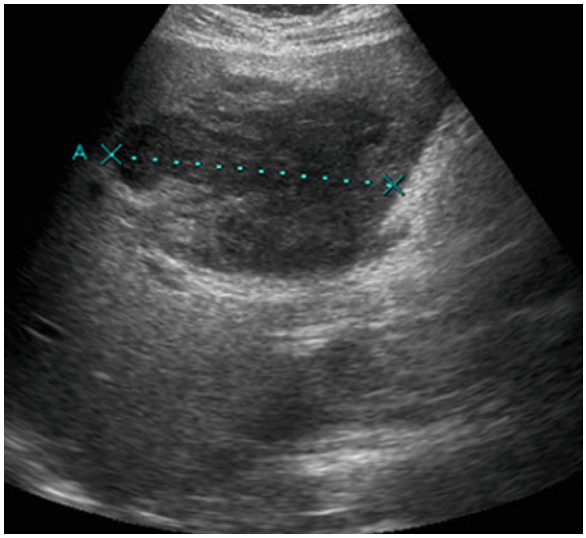

Fig. 1.4.1

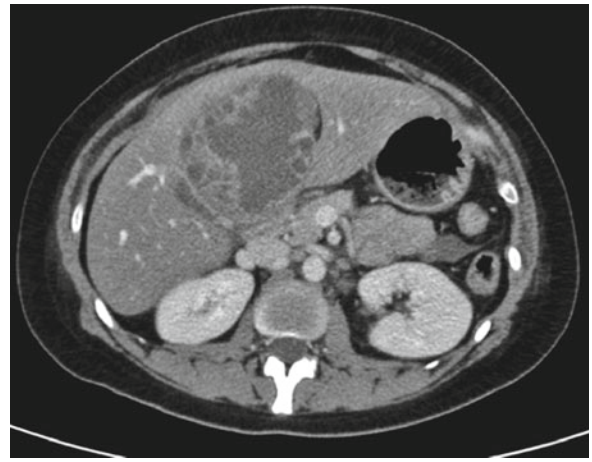

Fig. 1.4.2

Fig. 1.4.3

Comments

Liver abscesses are relatively common lesions in clinical practice and can present with very different morphology and appearance. This diagnosis must be suspected when there is a suggestive clinical scenario and a compatible liver image. They have typically a necrotic central portion with a cystic appearance, which can only be distinguished of a simple cyst because of a thick and enhancing wall. Multifocality suggests a bacterial infection, and the biliary system is the most common origin. Single lesions are more common in parasitic etiologies.

In MRI studies, abscesses may have varying intensities on T1 and T2 sequences; although often similar to a cyst, the only sign that can suggest the diagnosis is the relative restriction on DWI sequences of their content. The behavior in the dynamic study is similar to that described in CT scans.

If the clinical scenario is not supportive, other options in the differential diagnosis of the cystic lesions must be considered. Simple cysts are the most common focal lesion in the liver, usually rounded, multifocal, and lacking of an identifiable wall. The ultrasound may show septa not demonstrable with other techniques, and the typical posterior acoustic reinforcement is present. In CT scans, cysts show attenuation values between −10 and 20 HU. On MRI, cysts are markedly hyperintense on T2-weighted images and hypointense on T1-weighted sequences with lack of enhancement, on diffusion-weighted sequences, they show a similar appearance of that of the gallbladder content and should have high values on ADC maps. Cysts associated to Caroli's disease may have the "central dot" sign that corresponds to the portal triad structures, encompassed by the biliary dilatation. MRCP demonstrates communication with the bile ducts. In hepatic hydatidosis, there is usually a dominant lesion with some peripheral/satellite images. Peripheral calcification may present inside vesicles.

The group of neoplastic lesions with cystic appearance must also be taken into account. In patients above 65 years old, the cystic metastases must be considered within the diagnostic possibilities. Hepatocellular carcinoma may also present with cystic degeneration, but often preserve a solid extrinsic nodule. Biliary cystadenomas and cystadenocarcinomas are also cystic lesions. The presence of mural nodules and calcifications favors the diagnosis of malignancy.

Finally, solid tumoral lesions may undergo cystic changes when treated either by interventional techniques or chemotherapy treatments. In this setting, it can be difficult to assess the presence of tumoral tissue, MRI is particularly useful with the use of DWI and dynamic contrast enhanced sequences that helps in distinguishing necrotic degeneration from viable tumor tissue.

Imaging Findings

A lesion was identified in liver segment 4, which had irregular margins, measuring approximately 8 cm in its long axis, with heterogeneous echogenicity and mild posterior acoustic reinforcement (Fig. 1.4.1, liver ultrasound). The Doppler signal was increased in the periphery, and there was no evidence of vessels inside (not shown). The CT study identified a well-defined lesion, ovoid in shape, presenting two different components within it: a peripheral heterogeneous layer, mildly hyperdense in comparison to the surrounding liver parenchyma, and a central portion, homogeneous and with lower density (Figs. 1.4.2 and 1.4.3, enhanced CT on the portal phase and coronal MPR of enhanced CT on the portal phase). No satellite lesions or bile duct communication were detected.

Case 5

Iron Deposition in the Liver

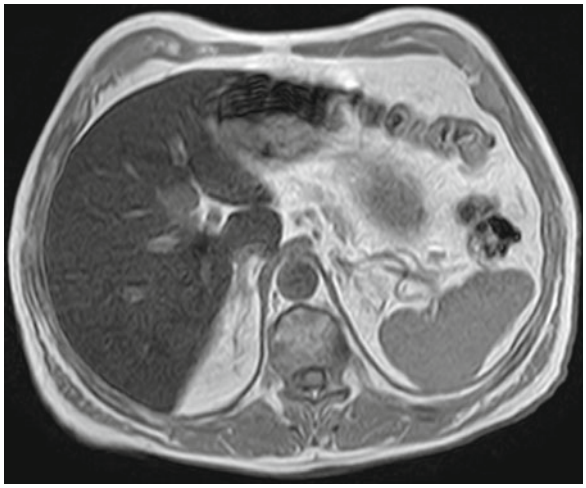

Fig. 1.5.1

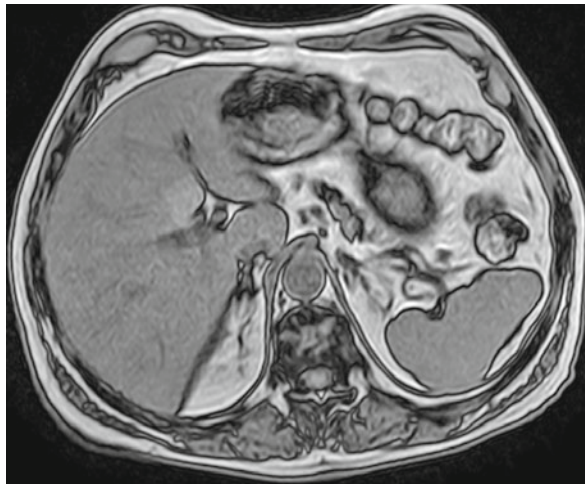

Fig. 1.5.2

Fig. 1.5.3

Clinical Information

A 32-year-old man, who complains of arthralgias, fatigue, and decreased libido, revealed hyperpigmentation of the skin on physical examination. The blood test drawn detected an increased transferrin saturation, high ferritin values, and slight increase in LFTs. With the suspicion of hemochromatosis, an MRI scan was requested. The protocol includes chemical shift and multi-echo T2-weighted images.

Comments

Iron can accumulate in the liver in the clinical setting of either primary or secondary hemochromatosis.

Primary hemochromatosis, idiopathic or genetic, is a common hereditary disorder secondary to a genetic mutation that determines an excessive gastrointestinal iron absorption with a consequent increase in tissue deposits: liver, heart, pancreas, pituitary, joints, and skin, among others. Without treatment, it produces organ damage and, in the liver, develops cirrhosis, and even a hepatocellular carcinoma could appear. Iron and hemosiderin accumulate in hepatocytes and induce cell damage with the development of fibrous septa and a micronodular cirrhosis. There is no significant accumulation of iron in the biliary epithelium or in the reticuloendothelial system. The detection of iron in the pancreatic parenchyma correlates with irreversible changes associated to cirrhosis.

Transfusional iron overload is the most common cause of increased iron storage in the liver and secondary hemochromatosis. Cirrhosis is rare, and iron deposition occurs predominantly in the reticuloendothelial system. The spleen is affected, and the pancreas is spared.

In hemolytic anemia, the findings of primary and secondary hemochromatosis coexist, as there is an increased iron absorption and a history of multiple transfusions. Cirrhosis also causes increased cellular levels of iron in the liver, by a mechanism that is not well understood.

In unenhanced CT scans, liver density is uniformly elevated, between 75 and 135 HU (normal values are below 65 HU).

MRI is probably the noninvasive technique of choice for the determination of hepatic iron. Increased levels of iron in the liver can be detected in MRI based on magnetic susceptibility artifact. The most effective sequences to detect such artifacts are gradient-echo T2-weighted sequences. There is a direct correlation between the liver signal to muscle intensity ratio and the amount of hepatic iron. Multiecho T2 sequences with assessment of liver parenchyma signal decay allow an accurate quantification of iron deposits, and it is a useful tool for posttreatment monitorization.

Chemical-shift imaging is also a standard part of the liver MRI scan protocols. Characteristically, the increase in hepatic iron deposits produces a liver signal drop in GE T1-weighted in-phase sequences with respect to out-of-phase ones. This is explained because the echo time in in-phase is longer than in out-of-phase, and the magnetic susceptibility produced by the iron excess is detected.

Imaging Findings

In-phase GE T1-weighted image (Fig. 1.5.1) shows a marked reduction in liver parenchyma signal, more evident when the in-phase acquisition is compared with the out-of-phase GE T1-weighted image (Fig. 1.5.2). The T2-weighted sequence (Fig. 1.5.3) identifies the liver with a lower intensity than that of the paraspinal muscles. The iron deposit estimation with a gradient-echo T2-weighted sequences with different TE was 200 μmol/g in this case (not shown), which is in the limit between moderate and major overload.

Case 6
Liver Cirrhosis

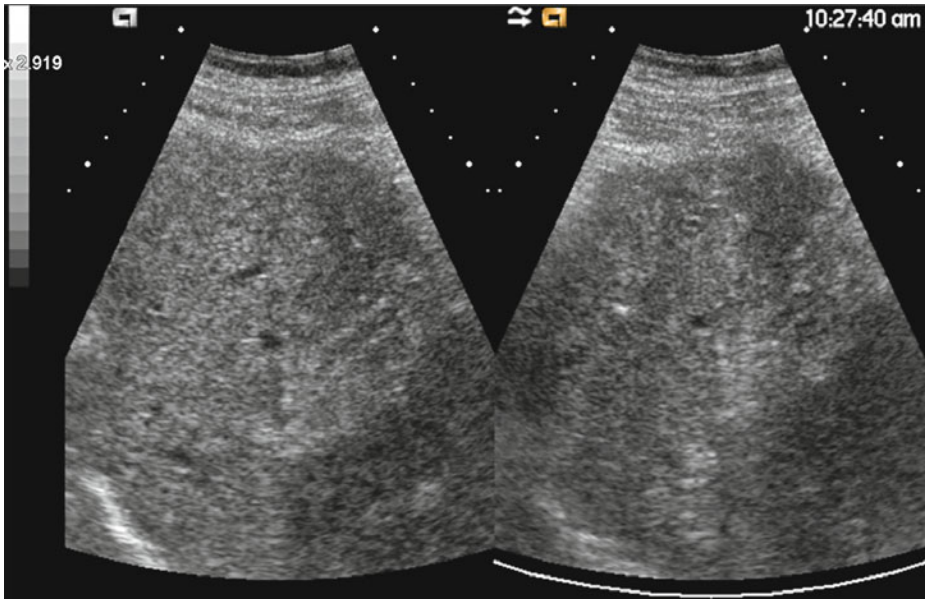

Fig. 1.6.1

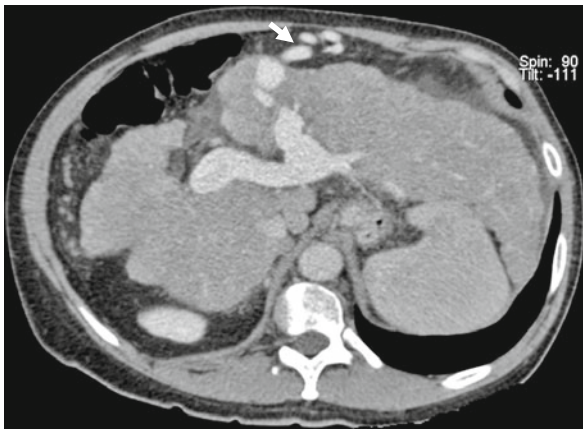

Fig. 1.6.2

Fig. 1.6.3

Clinical Information

A 53-year-old male with personal history of hepatitis C virus infection. He did not receive any specific treatment. Physical examination identified increased abdominal girth, with ascites, periumbilical centrifugal superficial venous circulation, and splenomegaly. Blood test drawn showed altered LFTs, high ammonium, mild hyperbilirubinemia, and hypoalbuminemia. Ultrasound is requested for suspected chronic liver disease, with probable cirrhosis and portal hypertension.

Comments

Liver cirrhosis is a chronic disease characterized by parenchymal extensive fibrosis and architectural distortion by regenerative liver nodules. Cirrhosis prevalence in autopsy series has been estimated between 5% and 10%. The most common causes of cirrhosis include hepatitis C virus (55% of cases), hepatitis B (16%), alcoholism (13%), and other causes, such as nonalcoholic steatohepatitis (NASH) and biliary cirrhosis. Morphologically, cirrhosis can be classified in macronodular (alcoholism), micronodular (hepatitis B), or mixed (bile duct obstruction). The diagnosis of cirrhosis has been traditionally established by liver biopsy but can often be suggested by imaging findings. Portal hypertension is commonly associated to advanced cirrhosis. It is due to increased elevated pressure despite formation of portal collateral vessels.

Generally, the monitorization of patients with cirrhosis is done with ultrasound; CT and MRI studies are performed, when a nodular lesion is detected or when there is an alteration of the hepatic architecture.

The key factors in imaging studies are a nodular contour, widened fissures, enlargement of segment 1 or caudate lobe, ascites, splenomegaly, and portacaval shunts, as signs of portal hypertension. There are other causes of segment 1 hypertrophy, not associated with cirrhosis, as is seen in sclerosing cholangitis and Budd-Chiari disease. The morphological changes in the metastatic liver, which occur in response to chemotherapy, may mimic cirrhosis.

In patients with cirrhosis, a relatively common finding in enhanced CT or MRI studies is the existence of arteriovenous shunts and regional disturbances of hepatic perfusion that sometimes simulate hypervascular nodules. Splenic siderotic nodules can also be detected (Gamna-Gandy bodies) as a sign of portal hypertension. These nodules are seen primarily on MRI scans with GE T2-weighted sequences that show a higher magnetic susceptibility between all the rest of common sequences of a liver MRI protocol.

Cirrhosis is a predisposing factor for portal vein thrombosis and is essential to make the distinction between neoplastic and benign thrombus. Demonstration of vessels within the thrombi or enhancement of the thrombus is a diagnostic sign of malignant thrombosis.

Imaging Findings

Figure 1.6.1 Abdominal ultrasound showed an enlargement of liver segments 2 and 3 and atrophy of segment 4 and right lobe. The liver contour is nodular, and its echotexture is altered. The caliber of the hepatic veins is reduced.

It was decided to perform a CT because the liver echotexture disturbances can hide nodular lesions. We performed a CT protocol that consists of 3 phases: late arterial liver

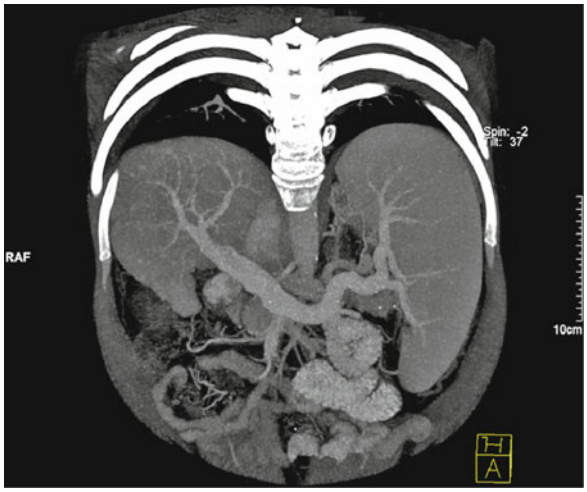

Fig. 1.6.4

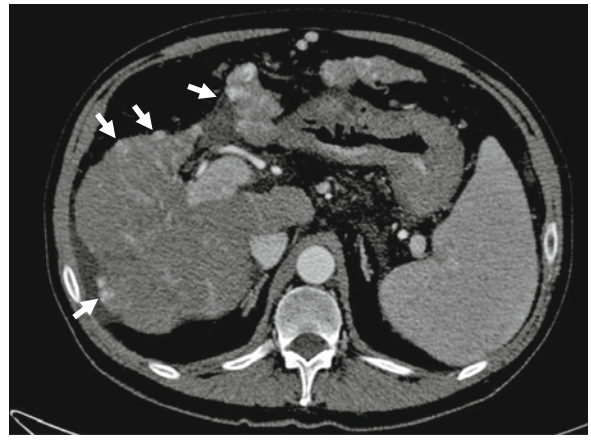

Fig. 1.6.5

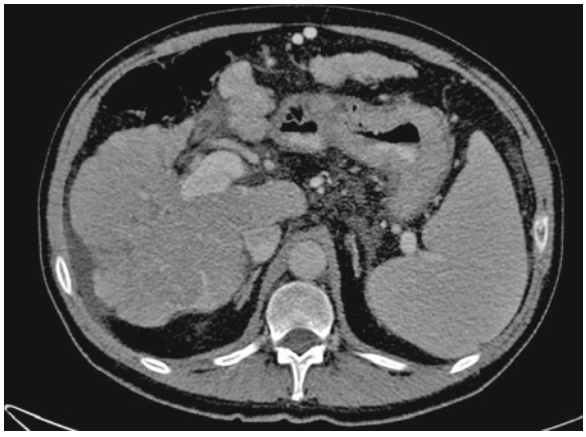

Fig. 1.6.6

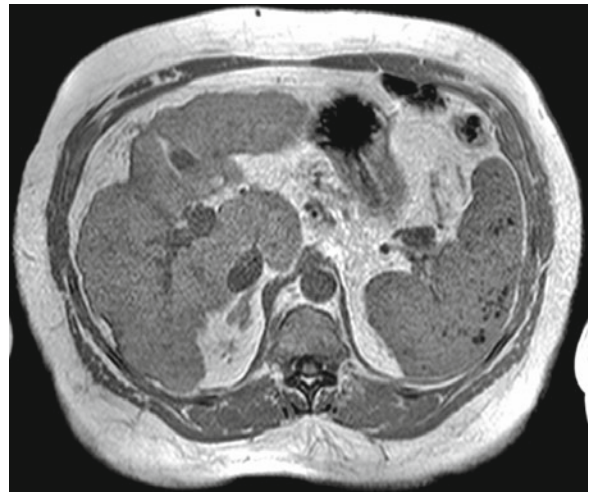

Fig. 1.6.7

(6 s delay after aortic arterial enhancement above 200 HU, using bolus detection technique), portal phase at 70 s, and a late or equilibrium phase (180 s after the start of contrast media injection). The contrast dose is 2 mL/kg of body weight, and a powered injector was used. The CT findings confirmed the altered liver morphology, demonstrating atrophy with capsular retraction of segment 4 (Fig. 1.6.2, enhanced CT on the portal phase). Paraumbilical venous system recanalization was confirmed (*arrows* on Figs. 1.6.2 and 1.6.3) (Fig. 1.6.3, volume rendering of CT on portal phase). There was an important splenomegaly, and the portal vein diameter was increased (Fig. 1.6.4, oblique coronal MPR of enhanced CT on portal venous phase). Multiple arteriovenous anomalous communications (*arrows* on 1.6.5) were demonstrated (Figs. 1.6.5 and 1.6.6, enhanced CT on the arterial and venous phases, respectively). Splenic Gamna-Gandy bodies were also demonstrated in an MRI study (Fig. 1.6.7, in-phase GE T1-weighted sequence).

Case 7

Hepatic Pseudolesion: Focal Fatty Area

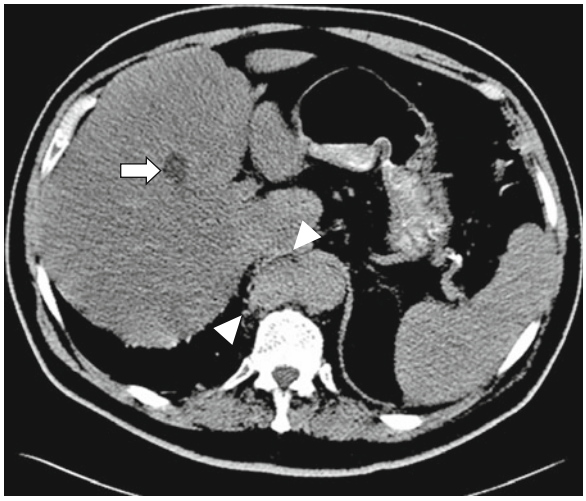

Fig. 1.7.1

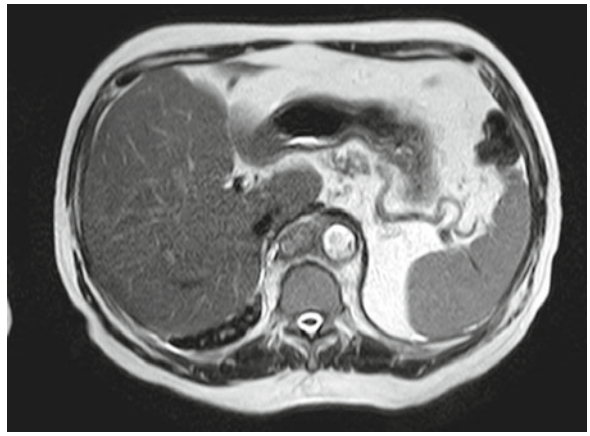

Fig. 1.7.2

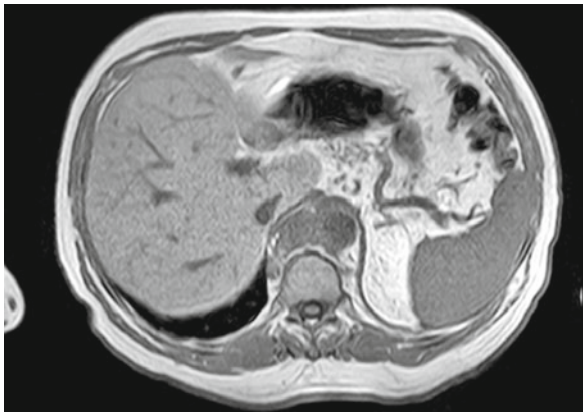

Fig. 1.7.3

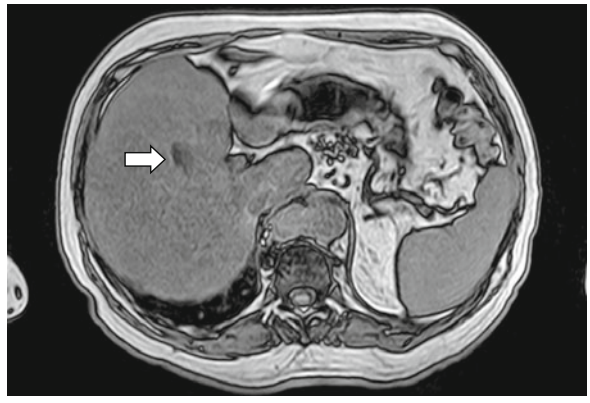

Fig. 1.7.4

A 67-year-old male with personal history of lung and colon carcinomas was treated with surgery and chemotherapy and followed with CT exams during the last years. Last CT showed a focal liver lesion, and an MRI was performed to discard the possibility of metastasis.

Comments

Focal fatty infiltration and sparing of fatty infiltration are frequent findings in imaging tests, and they should be known, because they can mimic inflammatory, vascular, or neoplastic disease, in a considerable proportion of cases.

Both events are more frequent in the segment 4b of Couinaud's classification. This increased regional susceptibility in the metabolism of fat is explained by the existence of systemic venous contributions from phrenic, falciform ligament, remnants of the paraumbilical vein, and parabiliar vascular network. These aberrant veins enter directly into the liver parenchyma, replacing the portal system inflow and explaining the regional absence of fatty infiltration. These areas of focal fatty infiltration appear as hypodense/hypoenhancing regions during the portal phase.

The origin of focal steatosis is intimately related to the development of aberrant pancreaticoduodenal veins, which generates portion of liver with a high concentration of endocrine pancreatic hormones, as is shown in this case. These findings are relatively common in cancer patients undergoing chemotherapy, because cytotoxic agents cause liver damage and increase the cytoplasmic deposits of fat. Similar lesions can be seen, when surgical resections have altered the pancreaticoduodenal vascular territory, and a new collateral flow is developed.

In CT scans, negative attenuation values of fat may mimic focal hypovascular lesions. In cancer patients, it is of particular significance because they can simulate metastases. To further characterize this type of lesions, an MRI scan should be performed. Liver scan protocols should include T1-weighted GE in-phase and out-of-phase to detect intracellular fat. During the in-phase, the sum of the vectors resulting from the populations of the water and fat protons is greater than the reading obtained; during the out-of-phase, and comparing the former with the last images, the presence of intracellular fat results in signal loss.

Hepatic perfusion disorders can also be found, by the existence of arteriovenous fistulae that resemble real nodular lesions in multiphase liver studies. Characteristically, they appear as small, wedge-shaped, hypervascular, polygonal, peripheral, and subcapsular areas that are homogeneous in late phases. These arterioportal communications are common in cirrhosis and may mimic tumors.

Imaging Findings

Abdominal-enhanced CT scan on the portal phase shows a hypodense, focal lesion in the right lobe (Fig. 1.7.1, *arrow*). Retrocrural lymphadenopathies can also be identified (*arrowheads*). The MRI scan of the liver shows a widespread hyperintensity on T2-weighted sequence (Fig. 1.7.2) and on in-phase GE T1-weighted sequence (Fig. 1.7.3). In the out-of-phase GE T1-weighted sequence, a patchy loss of intensity of the liver parenchyma is evident, and there is a marked decline of the signal intensity of the lesion under study (Fig. 1.7.4, *arrow*), representing a focal area of fatty infiltration within a liver with severe and diffuse steatosis.

Case 8
Hepatocellular Carcinoma

A 62-year-old male being followed up because of cirrhosis presented an echogenic nodule in segment 8 in an ultrasound. An MRI scan is performed with the following sequences: T1 GE, in-phase and out-of-phase, TSE T2, DWI, and dynamic study after administration of gadolinium, with acquisitions in the arterial, portal, and equilibrium phases. The used dose of gadolinium is 0.2 mL/kg using a power injector.

Fig. 1.8.1

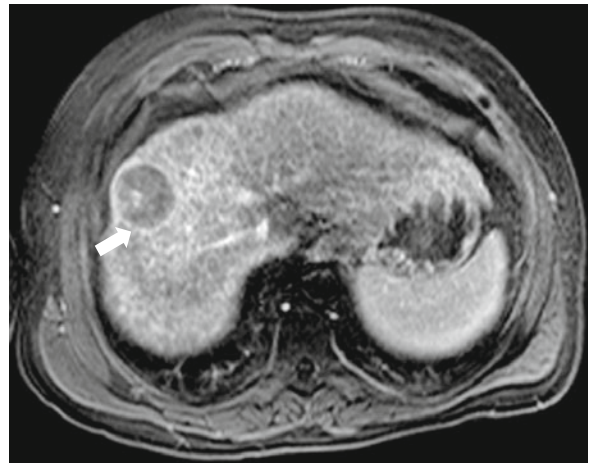

Fig. 1.8.2

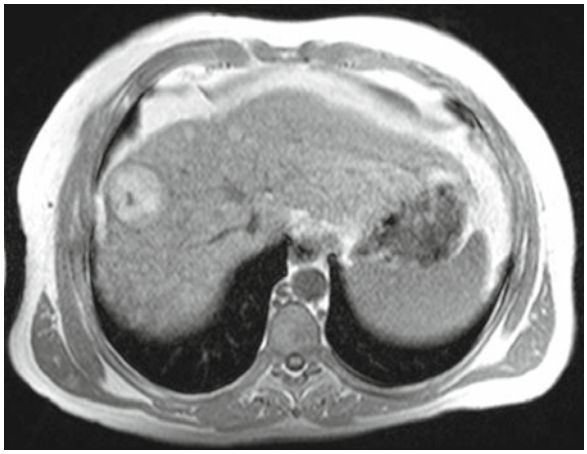

Fig. 1.8.3

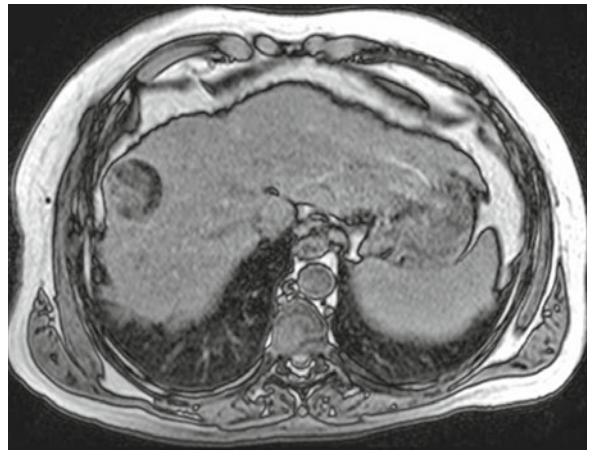

Fig. 1.8.4

Comments

Hepatocellular carcinoma (HCC) is the fifth most common cancer and the third leading cause of cancer-related death, after lung and stomach malignancies. Up to 80% of cases appear on cirrhotic livers. Infection with the hepatitis B and C viruses is the most frequently implicated risk factor in the development of hepatocellular carcinoma; other less common causes of cirrhosis are also implicated in carcinogenesis: alcohol, hemochromatosis, and biliary cirrhosis. An important group of patients infected with hepatitis B virus will develop liver cancer, without cirrhosis.

Hepatocarcinogenesis can be explained, by a "de novo" malignant lesion genesis or by the progression from a regeneration nodule, which evolve to a malignant lesion, passing through low-grade and high-grade dysplastic lesions. The regeneration nodule receives its major blood supply from the venous portal system; this condition makes them indistinguishable from normal liver, in dynamic enhanced CT and MRI studies, when conventional extracellular contrast media are used. In MRI, these nodules may retain iron and show hyperintensity in T1-weighed and T2-weighted sequences. The dysplastic nodules still receive more blood from the portal system than from arterial hepatic system, but sometimes can be detected on portal phases as hypovascular nodules. Some dysplastic nodules, mainly those of high grade, receive predominantly arterial supply and can be detected in this specific study phase.

In this progressive carcinogenesis process, a gradual reduction of the normal portal venous structures and blood supply occurs, finally disappearing and being replaced by the arterial inflow, from neoformed arterial structures (neoangiogenesis). This process of vascular conversion explains the main semiological finding in the imaging of HCC, the arterial phase enhancement, being homogeneous in small lesions and heterogeneous in the large ones. In the portal and equilibrium phases, HCC are detected as hypovascular lesions and could show capsular enhancement. This dynamic behavior practically ensures the diagnosis and thus avoids biopsy.

A further sign of great value in the specificity of the diagnosis of hepatocellular carcinoma, in the context of cirrhosis, is fatty metamorphosis. The existence of intracellular lipids can be detected with chemical-shift sequences, as intratumoral areas with signal drop in out-of-phase acquisitions, when compared to the images acquired in phase. A moderate hyperintensity on T2-weighted images is also a fairly specific finding of HCC.

In conclusion, the specific MRI findings of HCC include: enhancement during the arterial phase, washout and late capsular enhancement, hyperintensity on T2-weighted sequence, and signal drop in chemical-shift sequence (fatty metamorphosis).

Imaging Findings

The nodule located in the periphery of segment 8 is showed in the arterial and equilibrium phases of a postcontrast dynamic MRI study, using a THRIVE sequence (3D GE T1-weighted sequence with selective fat suppression and isotropic voxel). The hypervascularity of the lesion justifies the enhancement during the arterial phase (Fig. 1.8.1). During the equilibrium phase (Fig. 1.8.2), the washout of the lesion is seen. Notice the presence of capsular enhancement (*arrow*). The mass is spontaneously hyperintense in in-phase GE T1-weighted sequence (Fig. 1.8.3), with signal drop in the out-of-phase GE T1-weighted sequence (Fig. 1.8.4), that is proportional to the degree of fatty metamorphosis.

Case 9

Peripheral Cholangiocarcinoma

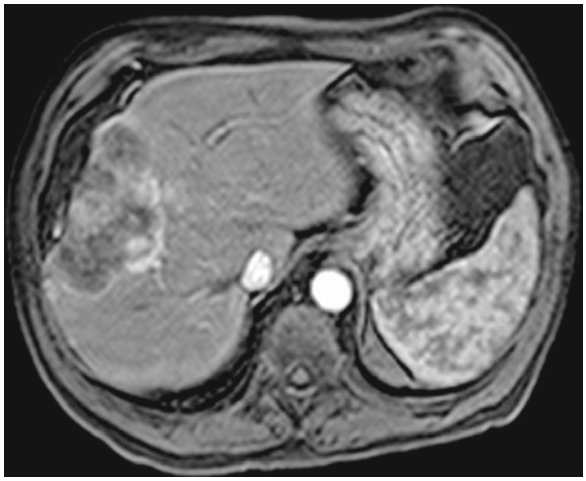

Fig. 1.9.1

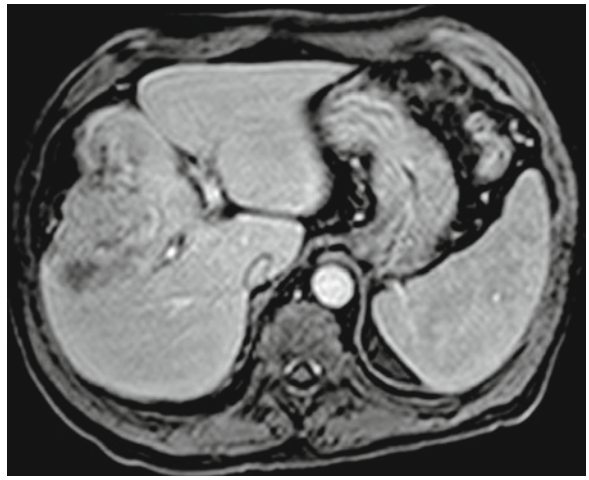

Fig. 1.9.2

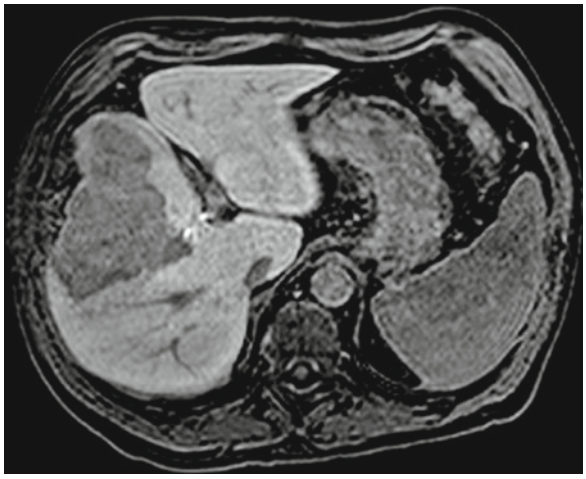

Fig. 1.9.3

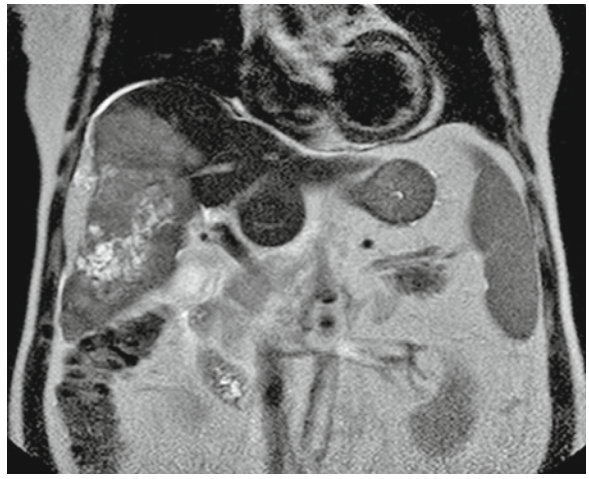

Fig. 1.9.4

A 65-year-old male patient, with malaise, abdominal pain, and weight loss, has a lab test showing mild anemia and an elevated carcinoembryonic antigen. An ultrasound was performed showing a heterogeneous, hyperechoic lesion, located in the liver periphery causing capsular retraction, so it was decided to carry out an MRI for further characterization.

Comments

Cholangiocarcinoma is an adenocarcinoma originated in the bile duct epithelium that arises from intra- and extrahepatic bile ducts. Traditionally, cholangiocarcinoma has been classified according to its anatomical location as intra- and extrahepatic, and intrahepatic cholangiocarcinoma is further classified as either peripheral or hilar (Klatskin's tumor). The peripheral subtype arises distal to the second bifurcation of the left or right hepatic ducts, and the hilar subtype arises directly from one of the hepatic duct or the bifurcation.

Peripheral cholangiocarcinoma is the most common primary malignant tumor after hepatocellular carcinoma, and it represents approximately 10% of liver malignancies.

Peripheral cholangiocarcinoma is usually asymptomatic, until they reach a large size, and its clinical manifestations are often nonspecific, such as weight loss, pain, jaundice, and anemia. Most commonly, it presents as a mass with exophytic growth that does not obstruct the central bile ducts. Macroscopically, it presents as a large, white tumor with dense fibrosis. It is an undifferentiated or poorly differentiated ductal adenocarcinoma with expansive growth beyond the bile duct margins and oftenly containing mucin or showing variable areas of necrosis.

On MR, it usually presents as a well-defined heterogeneous mass hypointense on T1-weighed image and mildly to moderately hyperintense on T2-weighted images. Enhancement is heterogeneous and predominantly peripheral during the immediate postcontrast phase, showing a more prominent enhancement during the portal and delayed phases, with a characteristic centripetal pattern. Its MR appearance correlates well with its histological composition. Tumors with more prominent areas of fibrosis are iso- or slightly hyperintense compated to liver on T2-weighted images and show centripetal enhancement, with delayed enhancement of the fibrotic areas. On the other hand, tumors with extensive necrosis or mucin content demonstrate higher signal intensity on T2-weighted images, and progressive centripetal enhancement is less common. Secondary findings associated to peripheral cholangiocarcinoma are: peripheral bile duct dilatation, multifocal presentation, lobar atrophy, or hilar lymphadenopathies. Vascular invasion is an unusual finding.

It is histologically composed of abundant fibrous and myxomatous stroma, which explains the delayed contrast retention in the extracellular space (intercellular interstitium).

An important characteristic, but not specific finding, is the liver capsule retraction.

In the healthy parenchyma distal to the tumor, dilated bile ducts can be seen; this is due to the intracanalicular growth of this kind of tumor. This sign is also characteristic of peripheral cholangiocarcinoma, but it has been described secondary to metastases and hepatocellular carcinoma.

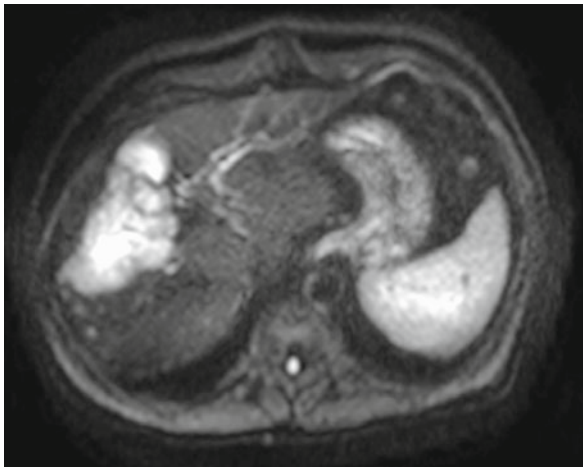

Fig. 1.9.5

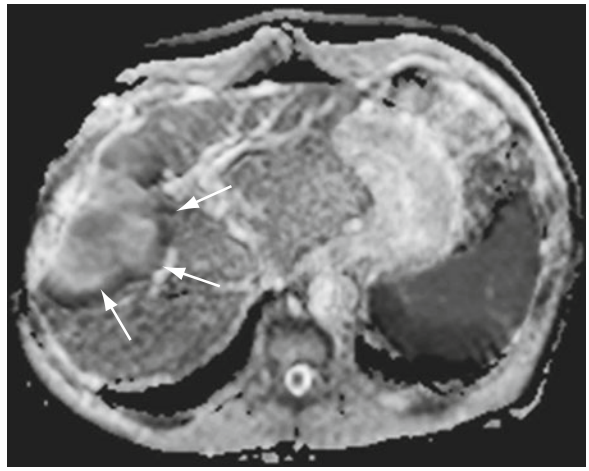

Fig. 1.9.6

After the administration of contrast, it usually enhances peripherally, and the surrounding healthy parenchyma may also experience premature enhancement, because of early invasion of portal structures and a predominant arterial supply. As previously said, the extensive fibrous stroma justifies the enhancement during the late phases of dynamic studies. This delayed enhancement should not be interpreted as cellular uptake, when using dual excretion contrast media (gadobenate dimeglumine and gadoxetic acid).

Imaging Findings

A liver lesion was confirmed with an heterogeneous appearance, lobulated margins and associated shrinkage of the adjacent hepatic capsule. A dynamic study was performed after the administration of gadoxetic acid (Gd-EOB-DTPA) showing early peripheral enhancement (Fig. 1.9.1) and late progressive filling (Fig. 1.9.2). During the biliary excretion phase, it is markedly hypointense compared with liver parenchyma (Fig. 1.9.3). Coronal HASTE image (Fig. 1.9.4) shows the craniocaudal extent of the lesion, occupying almost the entire right lobe. The diffusion-weighted sequence with high b value and corresponding ADC map shows a marked restriction in a ringlike area in the outer portion of the tumor (*arrows* on Fig. 1.9.6), where the major cellular component is located (Figs. 1.9.5 and 1.9.6).

Case 10
Liver Metastases

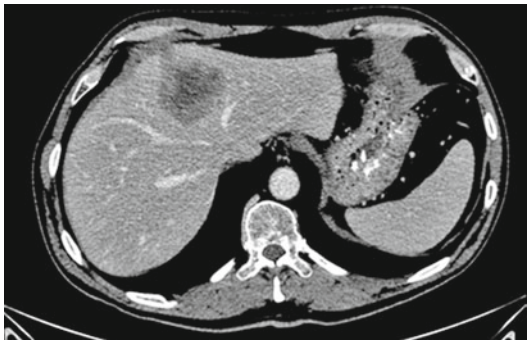

Fig. 1.10.1

Fig. 1.10.2

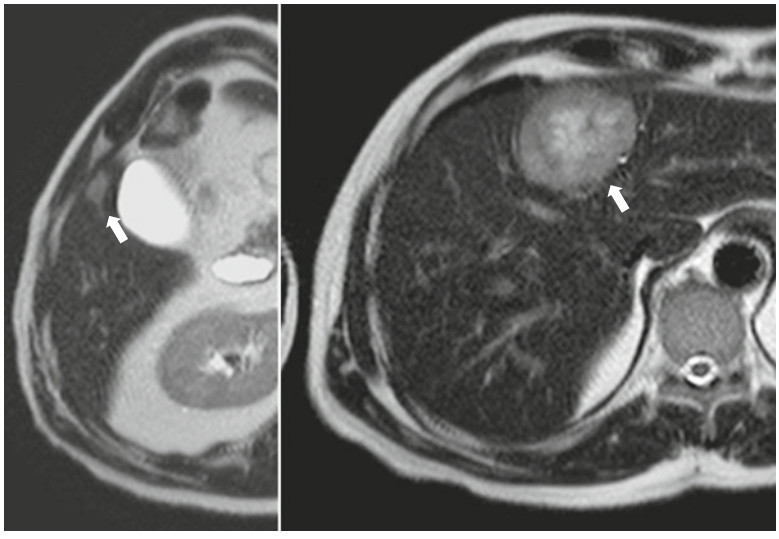

Fig. 1.10.3

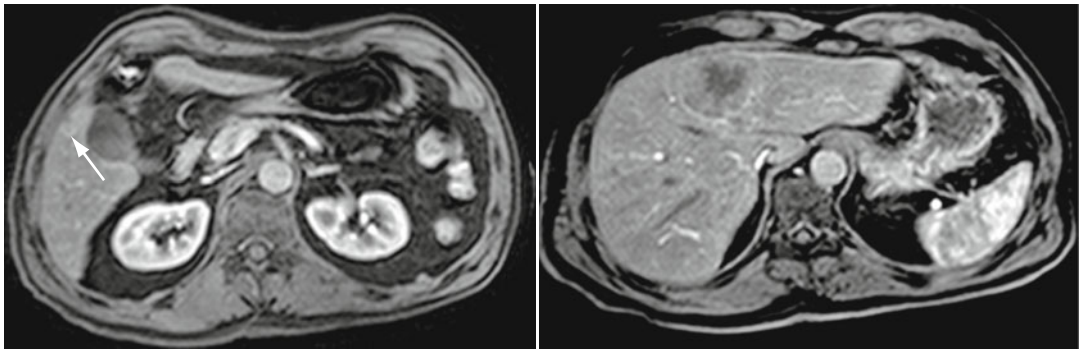

Fig. 1.10.4

A 52-year-old male with malaise and weight loss is found with hepatomegaly on physical examination. On blood tests, there is high LFTs and hypochromic-microcytic anemia. A CT scan is requested for diagnosis, with the suspected diagnosis of a GI origin metastatic neoplasia.

Abdominal CT is performed with a protocol of suspected oncological pathology. In our center, it consists in a first phase which includes a study of the upper abdomen and chest with a delay of 35 s and a second scan with a delay of 70 s of the abdomen and pelvis after administration of intravenous iodinated contrast media at a concentration of 350 mg/mL, with a dose 2 mL/kg and infusion rate of 4–5 mL/seg.

An MRI is also performed, using the following protocol: chemical-shift GE T1-weighted sequence; axial TSE T2-weighted sequence; dynamic THRIVE study; after administration of a liver specific (dual phase) contrast media (Gadoxetic acid/Gd-EOB-DTPA/Primovist) in arterial, venous, equilibrium, and biliary excretion phases; and finally DWI sequences with 5 *b* factors: 0, 50, 150, 500, and 800 mm^2/s).

Comments

Liver metastases have a predominantly arterial vascularization, and the peripheral and linear enhancement pattern ("ring sign") is caused by a thin margin of growing vascularized tumoral tissue. However, most of the metastases, and preferably those of gastrointestinal origin, have less vascular structures than normal tissue Therefore, dynamic studies with extracellular contrast demonstrate them as hypovascular lesions, which are detected with more easily during the portal phase.

CT is usually the first test for the diagnostic approach to patients with cancer, due to its high spatial and temporal resolution, and provides a good diagnostic accuracy for lesions greater than 1 cm. However, the contrast resolution is lower than MRI, being this one the preferred technique, when surgical treatment is going to be performed. MRI provides higher resolution and superior contrast for the detection of small metastases. Organ-specific contrasts, either those with biliary excretion or contrast media based on the iron particles and diffusion-weighted sequences with low b factors, are excellent tools for lesion detection and provide a maximum sensitivity in this task.

In addition, MRI is superior to CT in the characterization of small lesions. Cysts and hemangiomas are very common findings, and it is difficult to diagnose them based only on CT features when they are small. The images obtained in TSE T2-weighted sequences show this kind of benign lesions very hyperintense, being the small metastases generally not noticeable on these sequences. Detection and characterization of the greatest number of secondary lesions as possible, by these techniques, is of great importance, due to the development of the surgical resection techniques and other interventional techniques, such as radiofrequency, microwave thermoablation, and transarterial chemoembolization that allow curative treatment strategies, even in patients with multiple bilobar lesions.

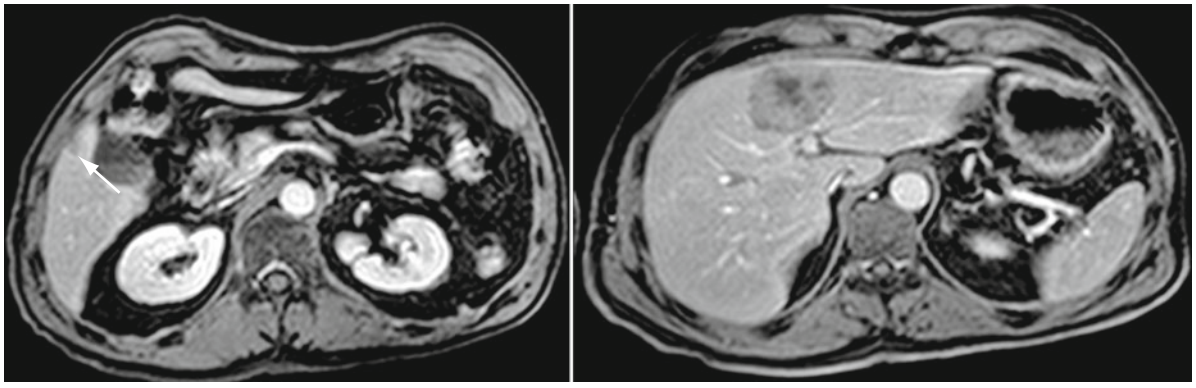

Fig. 1.10.5

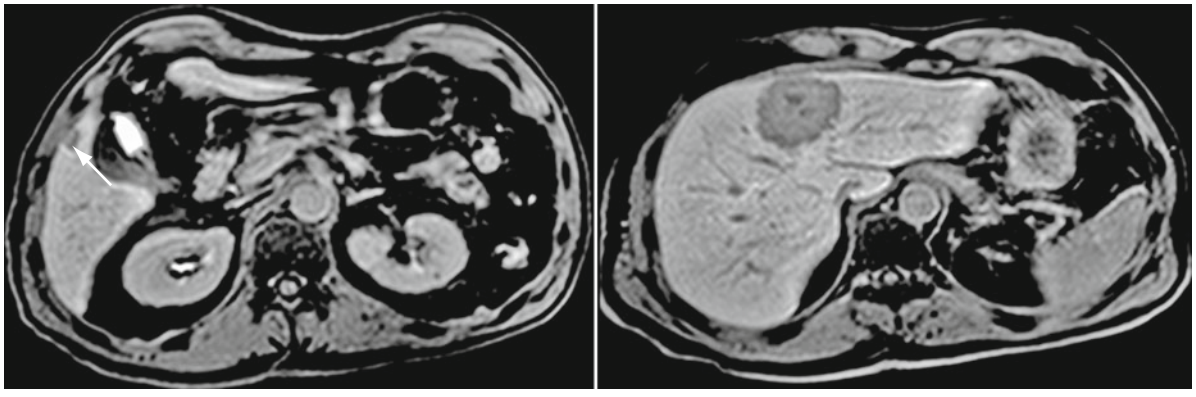

Fig. 1.10.6

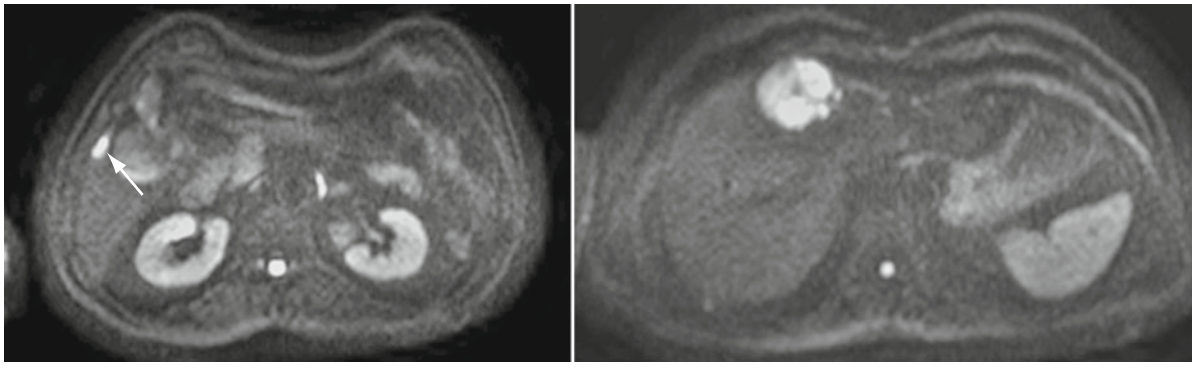

Fig. 1.10.7

Imaging Findings

CT show two hypovascular lesions in the portal venous phase (Figs. 1.10.1 and 1.10.2, *arrow* in 1.10.2).

MRI shows moderate hyperintensity of both lesions in T2-weighted sequence (Fig. 1.10.3, *arrows*), a characteristic enhancing ring in the arterial phase (Fig. 1.10.4, *arrow*), and a hypovascular appearance in the portal images (Fig. 1.10.5, *arrow*). During the biliary excretion of the dual contrast media, both lesions appear hypointense in a liver parenchyma that is diffusely hyperintense (Fig. 1.10.6, *arrow*). The lesions show a high signal on DWI sequence with a *b* value of 800 mm^2/s, consistent with a hypercellular nature (Fig. 1.10.7, *arrow*).

Further Reading

Books

Del Cura JL, Pedraza S, Gayete A (eds) (2009) Radiología Esencial, 1st edn. Madrid, Panamericana

Federle M, Brooke jeffrey R, Woodward PJ, Borhani B (eds) (2009) Diagnostic imaging abdomen, 2nd edn. Amirsys Publishing Inc, Salt Lake City

Hussain S (2007) Liver MRI: correlation with other imaging modalities and histopathology, 1st edn. Springer, Shrewsbury, Springer-Verlag, Berlin-Heidelberg

Lee JKT, Sagel SS, Stanley RJ, Heiken JP (eds) (2005) Computed body tomography with MRI correlation, 4th edn. Lippincott Williams & Wilkins, Philadelphia

Semelka R (2010) Abdominal-pelvic MRI, 3rd edn. Wiley-Blackwell, Chichester/Hoboken

Websites

Casey B (2011) AuntMinnie [Internet] [San Franscisco, CA] [cited July 2011]. Available from: http://www.auntminniecme.com/index.aspx?sec=def

Fishman E. CTisus [Internet] Available from: http://www.ctisus.com/teachingfiles/liver

Lin E (2011) Medscape. WebMD [Internet] [New York (USA)] [cited March 2011]. Available from: http://emedicine.medscape.com/radiology

Smithius R, Van Delden O (2011) The radiology assistant [Internet] [Leiderdop (The Netherlands)]. Radiological Society of The Neteherlands. [cited March 2011]. Available from: http://www.radiologyassistant.nl/en/

University of Rennes 1. [Internet] [Rennes (France)] [cited Feb 2011]. Available from: http://www.radio.univ-rennes1.fr/Sources/EN/HemoAutres.html

Articles

Anderson SW, Kruskal JB, Kane RA (2009) Benign hepatic tumors and iatrogenic pseudotumors. Radiographics 29(1):211–229

Basaran C, Karcaaltincaba M, Akata D, Karabulut N, Akinci D, Ozmen M, Akhan O (2005) Fat-containing lesions of the liver: cross-sectional imaging findings with emphasis on MRI. Am J Roentgenol 184(4):1103–1110

Blachar A, Federle MP, Ferris JV, Lacomis JM, Waltz JS, Armfield DR et al (2002) Radiologists' performance in the diagnosis of liver tumors with central scars by using specific CT criteria. Radiology 223(2):532–539

Boll DT, Merkle EM (2009) Diffuse liver disease: strategies for hepatic CT and MR imaging. Radiographics 29(6):1591–1614

Burns PN, Wilson SR (2007) Focal liver masses: enhancement patterns on contrast-enhanced images—concordance of US scans with CT scans and MR images. Radiology 242(1):162–174

Choi BI (2010) Advances of imaging for hepatocellular carcinoma. Oncology 78(Suppl 1):46–52

Faingold R, Albuquerque PA, Carpineta L (2011) Hepatobiliary tumors. Radiol Clin North Am 49(4):679–687

Fowler KJ, Brown JJ, Narra VR (2011) Magnetic resonance imaging of focal liver lesions: approach to imaging diagnosis. Hepatology. doi:10.1002/hep.24679

Gandhi SN, Brown MA, Wong JG, Aguirre DA, Sirlin CB (2006) MR contrast agents for liver imaging: what, when, how. Radiographics 26(6):1621–1636

Garra BS (2011) Elastography: current status, future prospects, and making it work for you. Ultrasound Q 27(3):177–186

Heiken JP (2007) Distinguishing benign from malignant liver tumours. Cancer Imaging 1(7 Spec No A):S1–S14

Hussain SM, Reinhold C, Mitchell DG (2009) Cirrhosis and lesion characterization at MR imaging. Radiographics 29(6):1637–1652

Jeong YY, Yim NY, Kang HK (2005) Hepatocellular carcinoma in the cirrhotic liver with helical CT and MRI: imaging spectrum and pitfalls of cirrhosis-related nodules. Am J Roentgenol 185(4):1024–1032

Lee JM, Choi BI (2011) Hepatocellular nodules in liver cirrhosis: MR evaluation. Abdom Imaging 36(3):282

Lee JW, Kim S, Kwack SW, Kim CW, Moon TY, Lee SH et al (2008) Hepatic capsular and subcapsular pathologic conditions: demonstration with CT and MR imaging. Radiographics 28(5):1307–1323

Lencioni R, Della Pina C, Crocetti L, Bozzi E, Cioni D (2007) Clinical management of focal liver lesions: the key role of real-time contrast-enhanced US. Eur Radiol 17 Suppl 6:F73–F79

Mortelé KJ, Ros PR (2001) Cystic focal liver lesions in the adult: differential CT and MR imaging features. Radiographics 21(4):895–910

Reeder SB, Cruite I, Hamilton G, Sirlin CB (2011) Quantitative assessment of liver fat with magnetic resonance imaging and spectroscopy. J Magn Reson Imaging 34(4):729–749

Sacks A, Peller PJ, Surasi DS, Chatburn L, Mercier G, Subramaniam RM (2011) Value of PET/CT in the management of primary hepatobiliary tumors, part 2. Am J Roentgenol 197(2):W260–W265

Seale MK, Catalano OA, Saini S, Hahn PF, Sahani DV (2009) Hepatobiliary-specific MR contrast agents: role in imaging the liver and biliary tree. Radiographics 29(6):1725–1748

Silva AC, Evans JM, McCullough AE, Jatoi MA, Vargas HE, Hara AK (2009) MR imaging of hypervascular liver masses: a review of current techniques. Radiographics 29(2):385–402

Sirlin CB, Reeder SB (2010) Magnetic resonance imaging quantification of liver iron. Magn Reson Imaging Clin N Am 18(3):359–381

Vilgrain V, Boulos L, Vullierme M, Denys A, Terris B, Menu Y (2000) Imaging of atypical hemangiomas of the liver with pathologic correlation. Radiographics 20(2):379–397

Willatt JM, Hussain HK, Adusumilli S, Marrero JA (2008) MR imaging of hepatocellular carcinoma in the cirrhotic liver: challenges and controversies. Radiology 247(2):311–330

Yoshimitsu K, Honda H, Kuroiwa T, Irie H, Aibe H, Shinozaki K et al (2001) Unusual hemodynamics and pseudolesions of the noncirrhotic liver at CT. Radiographics 21(Suppl 1): S81–S96

Gallbladder and Biliary System 2

Mariano Volpacchio, Joaquina Paz López Moras,
Verónica Patricia Rubio, and Mario Santamarina

Contents

A. Luna et al., *Learning Abdominal Imaging*, Learning Imaging,
DOI 10.1007/978-3-540-88003-5_2, © Springer-Verlag Berlin Heidelberg 2012

Case 1
Cholangiocarcinoma

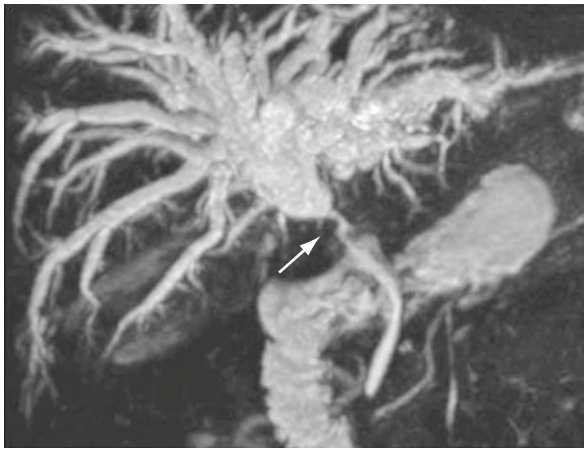

Fig. 2.1.1

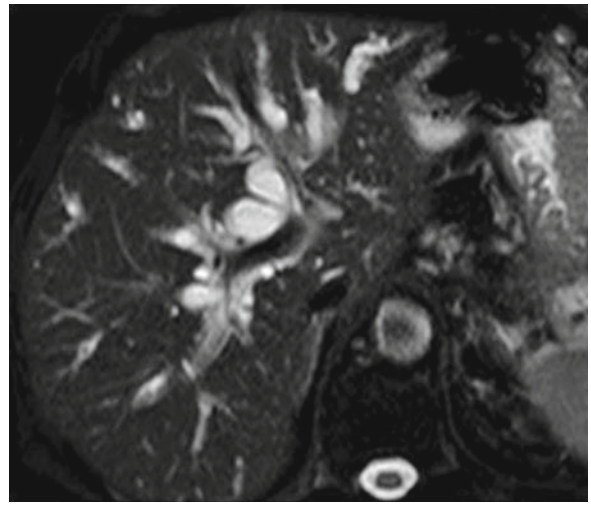

Fig. 2.1.2

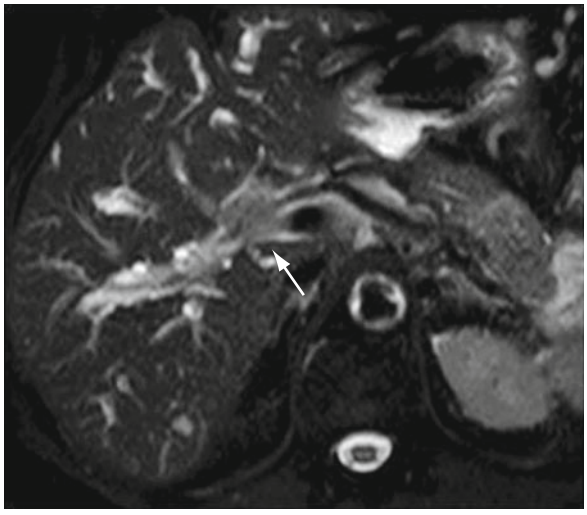

Fig. 2.1.3

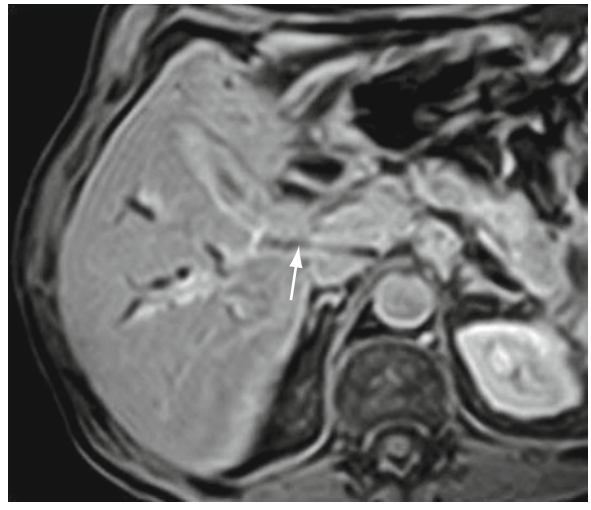

Fig. 2.1.4

A 62-year-old man presents with jaundice, choluria, clear stools, and weight loss.

Comments

Bile duct carcinomas are overwhelmingly adenocarcinomas of ductal origin although other histologic variants also exist. Cholangiocarcinoma (CGC) is the second most common hepatic malignancy after hepatocellular carcinoma. Its incidence varies geographically being more prevalent in Southeast Asia. There are various predisposing conditions including chronic parasitic infestation with *Clonorchis sinensis*, intrahepatic stone disease, congenital choledochal cysts, Caroli disease, sclerosing cholangitis, inflammatory bowel disease, particularly ulcerative colitis, and previous thorotrast exposure among others.

Clinical presentation is variable but typically consists of obstructive jaundice, right upper quadrant dull pain, and weight loss.

According to the site of origin, CGC is classified as peripheral intrahepatic, arising from small intrahepatic ducts including tumors with origin distal to the secondary bifurcation of the right or left hepatic ducts (20–25%), perihilar tumor (50–60%), and distal ductal (20–25%). Classically, peripheral and perihilar types are grouped together as intrahepatic CGC and distal as extrahepatic one.

When a perihilar tumor involves the bifurcation of right and left hepatic ducts, is known as Klatskin tumor. CGC may also be classified, from a morphological standpoint, as exhophytic or mass-forming, periductal-infiltrating, and polypoid types, including the papillary variant in the last group. Although peripheral tumors tend to be of the mass-forming type, hilar CGC of the infiltrating type, and distal lesions of the polypoid type, considerable overlapping exists with regard to morphological type and site. It is generally believed that these different forms of CGC share actually similar biological features, and variations emerge as a consequence of localization, resulting, in different clinical radiological and therapeutic implications. Different morphologic types may coexist in the same patient. Imaging evaluation objectives not only demand to propose a CGC as the cause responsible of obstruction, but also accurate delineation of the extent of disease with special interest in determining feasibility of resection such as proximal extension, liver parenchyma invasion, the presence of vascular compromise, lymphadenopathies, and peritoneal seeding.

Imaging Techniques

Ultrasound (US) is the front-line imaging modality to evaluate a patient with jaundice. US allows for detection of bile duct dilatation, but its ability to detect the cause of obstruction decreases as it approaches the ampulla. It is thus, no surprising, that many CGC, particularly those extrahepatic, are difficult to identify. Historically, opacification of the biliary tract via a percutaneous approach (transhepatic percutaneous cholangiography) or more recently through an endoscopic approach (endoscopic retrograde cholangiopancreatography) was the most accurate way to diagnose the site and cause of obstruction besides allowing to perform therapeutic maneuvers. More recently, computed tomography, particularly multidetector technology, and especially magnetic resonance cholangiopancreatography (MRCP) have allowed for a precise evaluation of the cause of obstruction as well as to stage various pathologic processes in a noninvasive fashion.

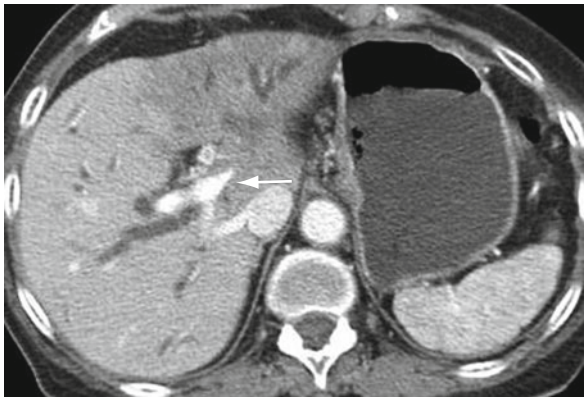

Fig. 2.1.5

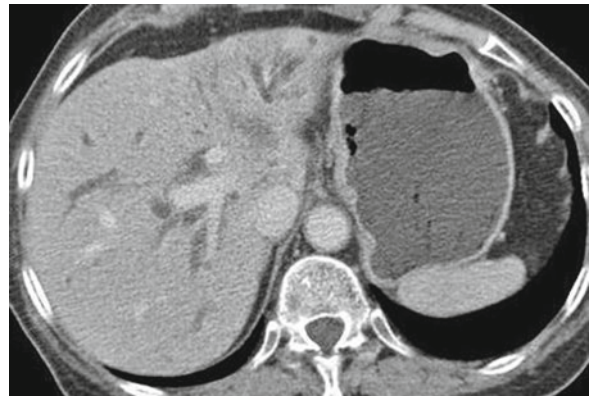

Fig. 2.1.6

The complementary addition of T1 -weighted, T2 -weighted, and diffusion-weighted images to MRCP protocols is crucial in assisting to that purpose when using MRI. Imaging appearance varies according to the subtype of CGC. CT shows a hypoattenuating lesion with rim enhancement and proximal obstruction. Delayed imaging may show contrast material retention due to the fibrous component of these tumors. MRCP usually reveals an abrupt stricture with shouldered margins. T1-weighted images show a low-signal lesion and delayed enhancement similar to CT during the acquisition of contrast-enhanced dynamic series. T2-weighted images demonstrate a high-signal lesion. Small tumors often prove difficult to be detected on cross-sectional images. Both, enhanced CT and MRI may show periductal infiltration and are used to obtain information about local extent and feasibility of resection.

Imaging Findings

Contrast-enhanced MRCP (Fig. 2.1.1) shows a severe biliary duct stricture with abrupt margins (*arrow*) producing a severe proximal dilatation. Sequential axial T2-weighted images (Figs. 2.1.2 and 2.1.3) show a mildly hyperintense lesion located at the hilum (*arrow* on 2.1.3) and bilateral proximal duct dilatation. Contrast-enhanced T1-weighted image (Fig. 2.1.4) demonstrates delayed enhancement of the hilar lesion (*arrow*). Contrast-enhanced MDCT on the aterial phase (Fig. 2.1.5), showing a hypodense infiltrating lesion radiating from the hilar region to invade both left and caudate lobes with obliteration of periportal fat and tapering of portal vein (*arrow*) consistent with vascular compromise. Delayed image (Fig. 2.1.6) demonstrates typical contrast retention within the extracellular space of the lesion.

Case 2
Acute Cholecystitis

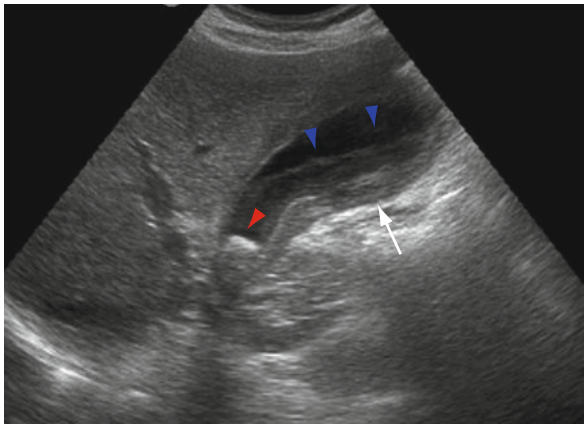

Fig. 2.2.1

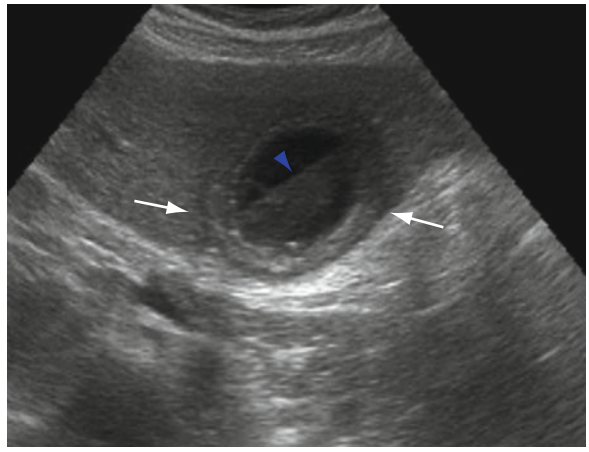

Fig. 2.2.2

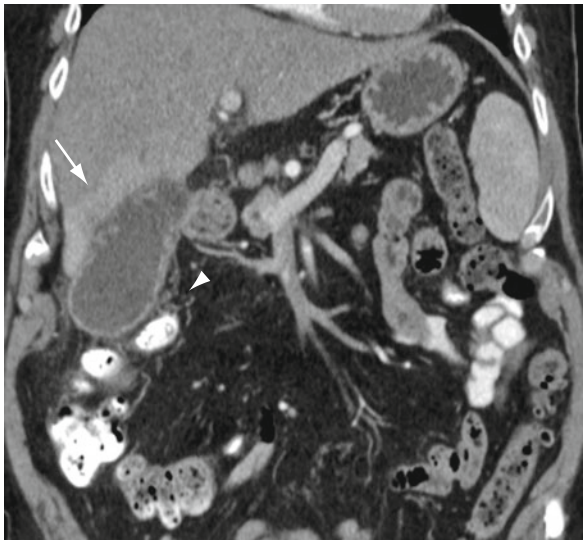

Fig. 2.2.3

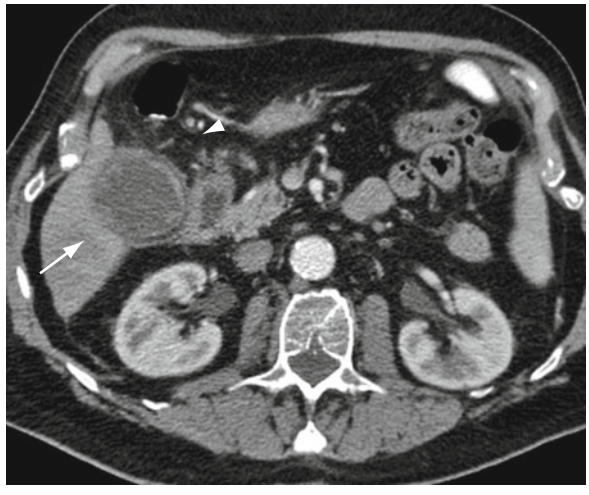

Fig. 2.2.4

A 52-year-old female patient presents with right upper quadrant pain, fever, and leukocytosis.

Comments

Acute cholecystitis (AC) is a very common cause of acute abdominal pain. Most AC (95%) are secondary to cholelithiasis, and an impacted stone leads to obstruction, lumen distention, and ischemia of the wall with subsequent bacterial proliferation. A spectrum of pathologic findings may ensue including hemorrhage, gangrenous changes, and perforation. Not all patients present with typical clinical and laboratory findings, and the elderly and patients very ill such as those in the ICU are a typical example of that group. Consequently, diagnosis may be delayed, and the condition may be misinterpreted as other entities such as pancreatitis, perforated ulcer, or hepatic abscess. Because of this, patients may be initially evaluated with CT. Diabetic patients are prone to develop emphysematous cholecystitis which is generally, a serious condition.

Imaging Techniques

US is the imaging modality of choice for the diagnosis of suspected cholecystitis. US finding supporting a diagnosis of AC includes gallbladder distention (greater than 4 cm), wall thickening (greater than 3 mm), gallstones or sludge, especially demonstration of a nonmobile stone impacted in the gallbladder neck, hyperechogenicity of pericholecystic fat, and hyperemia of the wall as shown by color Doppler. Other US finding is a positive Murphy sign, which consists of pain elicited by the transducer pressure on the patient's hypochondrium during exploration. Patients may be initially evaluated by CT. Furthermore, CT may be choses as the first diagnostic test in obese patients, as it may be difficult the evaluation by US. CT diagnosis of AC is based on similar findings, i.e., GB distension of a lumen which may show increased bile attenuation or stones, mural thickening, increased wall enhancement and a pericholecystic fat stranding. Adjacent liver parenchyma may exhibit transient hyperattenuation on early phase contrast-enhanced CT. CT evaluation also plays a role in the evaluation of complications such as perforation and hepatic abscess.

MRI shows similar imaging findings as CT and is not generally indicated as a primary modality with the exception of certain settings such as pregnant patients. It is noteworthy to emphasize that other causes of GB wall thickening due to submucosal edema are a common finding and include: heart failure, hypoalbuminemia, ascites, and nephrotic syndrome, but they do not produce hyperemia and particularly fat stranding. All modalities may suggest wall necrosis as part of gangrenous evolution as the presence of membranes and discontinuity of the wall as well as diminished enhancement. If patients with AC are not operated on, chronic cholecystitis generally ensues, and the most striking finding is marked wall enhancement which may be heterogenous and irregular, making differential diagnosis with gallbladder carcinoma sometimes extremely difficult. In the chronic phase, imaging markers of acuity (e.g., hyperemia, pericholecystic fat changes) are generally absent.

Imaging Findings

Longitudinal and transverse US images (Figs. 2.2.1 and 2.2.2) show marked GB wall thickening (*arrows*) and an impacted stone in the neck (*red arrowhead*). Notice also layering echogenic bile (*blue arrowheads*). Coronal MPR and axial MDCT on the arterial phase (Figs. 2.2.3 and 2.2.4) reveals GB wall thickening with submucosal edema, pericholecystic fat stranding (*arrowheads*), and hyperemia of adjacent liver parenchyma (*arrows*).

Case 3
Mirizzi Syndrome

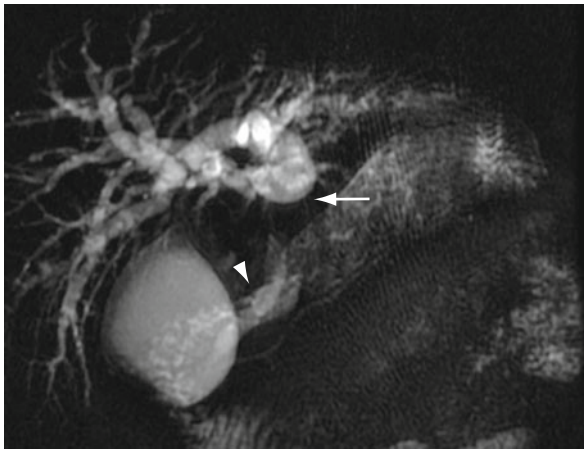

Fig. 2.3.1

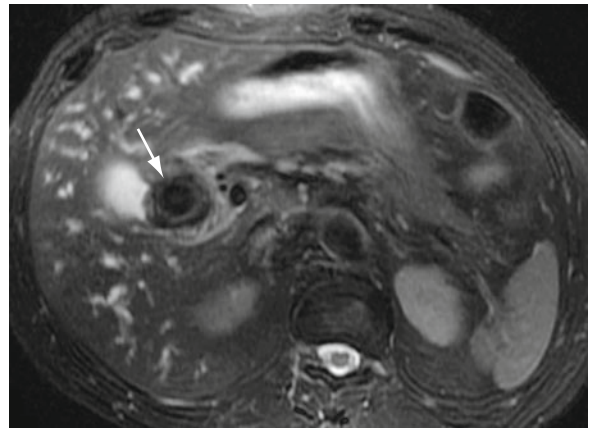

Fig. 2.3.2

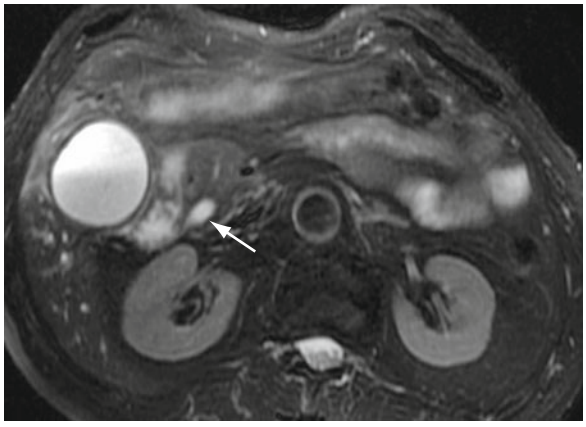

Fig. 2.3.3

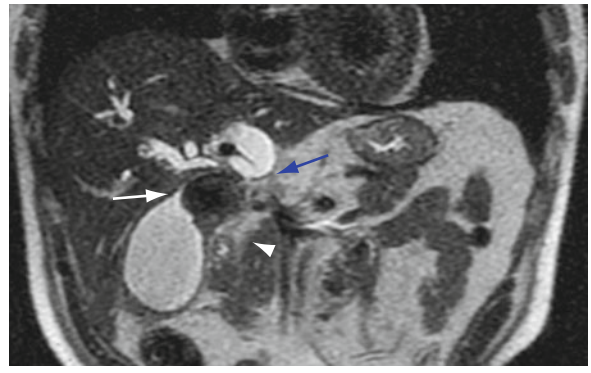

Fig. 2.3.4

A 69-year-old woman complaining of right upper quadrant abdominal pain, fever, leukocytosis, and hyperbilirubinemia.

Comments

Mirizzi syndrome (MS) is an uncommon complication of gallstones which consists of impaction of a stone in the GB neck or cystic duct with subsequent compression and eventually erosion over the common hepatic duct causing upstream biliary dilatation. A long parallel course of the cystic duct is a predisposing factor, and this condition is usually associated with GB dilatation and inflammation. There are two types of MS: type 1 is obstruction by extrinsic compression, and type 2 is characterized by erosion on the common hepatic duct wall. This entity is usually accompanied by marked wall inflammation with imaging findings that may resemble GB carcinoma. Preoperative diagnosis is crucial because MS poses an increased risk of bile duct injury during surgery.

Imaging Techniques

US shows the impacted stone and dilatation of both the GB lumen and proximal biliary ducts. CT scan demonstrates similar finding and shows a normal-caliber common bile duct. MDCT with acquisition of volumetric datasets allows for multiplanar reconstructions that are crucial to delineate the biliary anatomy which often proves complex on axial images.

Imaging Findings

Thick-slab MRCP (Fig. 2.3.1) shows intrahepatic biliary duct dilatation secondary to obstruction at the common hepatic duct with normal-caliber common bile duct (*arrowhead*). There is distension of the GB. Axial sequential FSE T2-weighted images (Figs. 2.3.2 and 2.3.3) reveal an ovoid calculus (*arrow*) and dilatation of the GB with layering of its luminal contents as well as inflammation of pericholecystic fat. Coronal T2-weighted image (Fig. 2.3.4 clearly depicts the impacted stone at the GB neck (*arrow*) with proximal dilatation of biliary ducts (*blue arrow*) and a normal common nile duct (*arrowhead*).

Case 4
Gallbladder Carcinoma

A 72-year-old woman presents with weight loss, malaise, jaundice, and a dull right upper quadrant pain.

Comments

Gallbladder carcinoma (GBC) is the most common primary biliary malignancy and represents the fifth most frequent gastrointestinal cancer. Women are more frequently involved (female to male ratio 3-4:1). GBC occurs most commonly in the elderly. GBC has a variable and nonspecific clinical presentation. Because of this, diagnosis is made, unfortunately, often on an advanced state. GBC may be an unsuspected finding during a laparoscopic procedure or pathologic analysis of a resected GB specimen. Chronic inflammation

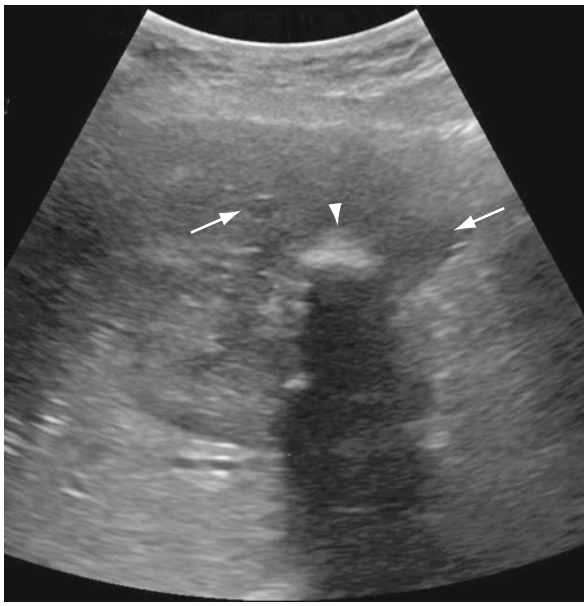

Fig. 2.4.1

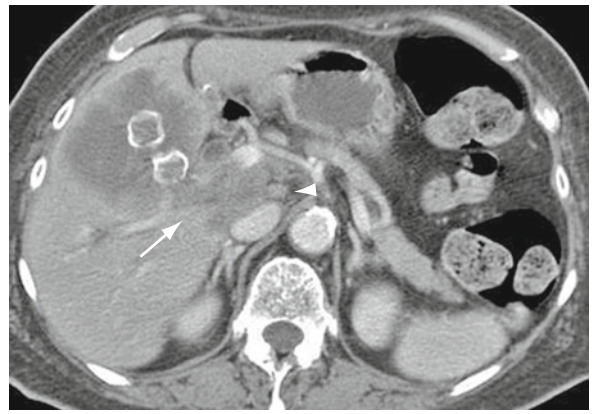

Fig. 2.4.2

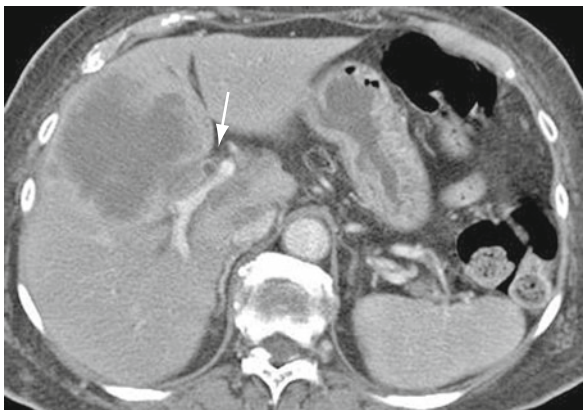

Fig. 2.4.3

associated with the presence of stones is the main risk factor for development of GBC. It is estimated that less than 1% of patients with cholelithiasis develop GBC, but more than 90% of patients with this malignancy have stones. Long-standing inflammation may lead to dysplasia and, eventually, to development of cancer. Other associated predisposing factors include presence of GB polyps, porcelain GB, and anomalous pancreatobiliary duct junction. Ninety percent are carcinomas, and 98% are adenocarcinoma. Other less common tumors are sarcoma, lymphoma, carcinoid, and metastases.

Morphologically, three patterns with corresponding imaging correlates are described: mass-filling tumor, focal or diffuse wall thickening, and polypoid type.

GBC patterns of dissemination include invasion of adjacent liver parenchyma, peritoneal spread, colonic, duodenal, and, less frequently, pancreatic invasion. Lymphatic dissemination is typical to hilar and portocaval nodes although in more advanced disease retroperitoneal lymphadenopathies are not uncommon. Finally, hematogenous dissemination to distant organs is also found. GBC implants may be detected in trocar sites of previous laparoscopic surgery. GBC has a tendency to invade the hepatic hilum and biliary tract and as result may present with obstructive jaundice.

Differential diagnosis must be made with other conditions that result in GB wall thickening and luminal masses such as chronic cholecystitis especially xantogranulomatous cholecystitis, adenomyomatosis, benign polyps (generally adenomas), tumefactive sludge, and other causes of GB wall thickening.

Imaging Techniques

US is the initial imaging modality to approach GB evaluation and shows typical findings corresponding to the patterns previously cited. In the mass type, an echogenic tumor is seen replacing part or the whole of the GB lumen. In advanced cases, a heterogeneous process is seen in the liver with its epicenter in the GB fossa, but the latter may not be recognized. In these instances, CT plays a crucial role because it demonstrates the mass in the expected location of the GB with stones within it. CT also allows for an optimal delineation of the extent of the tumor as well as the demonstration of liver metastases, peritoneal implants, and lymphadenopathies. MRI reveals similar findings as CT but, because of its superior contrast resolution, may demonstrate more heterogeneity as a result of necrosis and areas of hypervascularity and also may better show compromise on the biliary tract. In GBC producing wall thickening, all modalities demonstrate an irregular and asymmetric mural thickening which is generally heterogeneous, and mural stratification is not appreciated. Finally, the polypoid type presents a nonmobile nodule attached to the wall. As polyps in the GB are not an unusual finding, special attention is given to those greater than 10 mm and to sessile polyps (independent of size). Other factors such as the age of the patient and coexistence of stones are considered as risk factors for this type of tumor.

Imaging Findings

Transverse US (Fig. 2.4.1) shows a mass expanding the GB (*arrows*) with echogenic foci that produce acoustic shadow representing a lithiasis (*arrowhead*). Axial contrast-enhanced MDCT during the portal phase at two different levels (Figs. 2.4.2 and 2.4.3) images depict a low attenuation mass, which shows stones within it, with flagrant invasion of segments IV and V and infiltration of the hilum (*arrows*) with resulting biliary obstruction. Notice perihepatic fat compromise as well as portocaval space lymphadenopathies (*arrowhead*).

Case 5
Adenomyomatosis

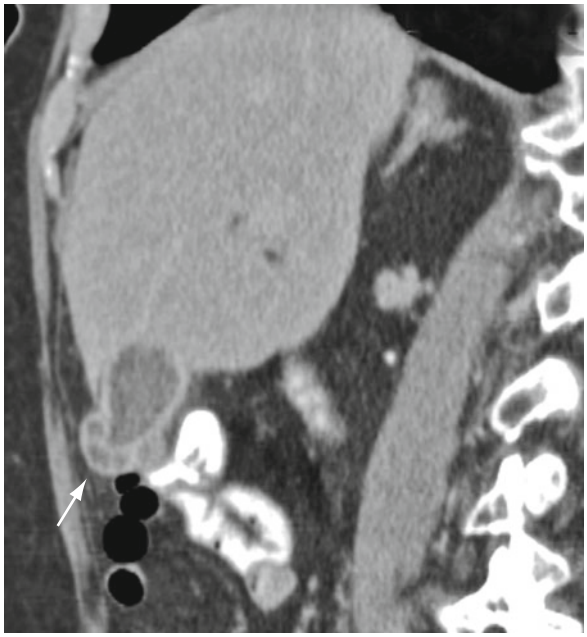

Fig. 2.5.1

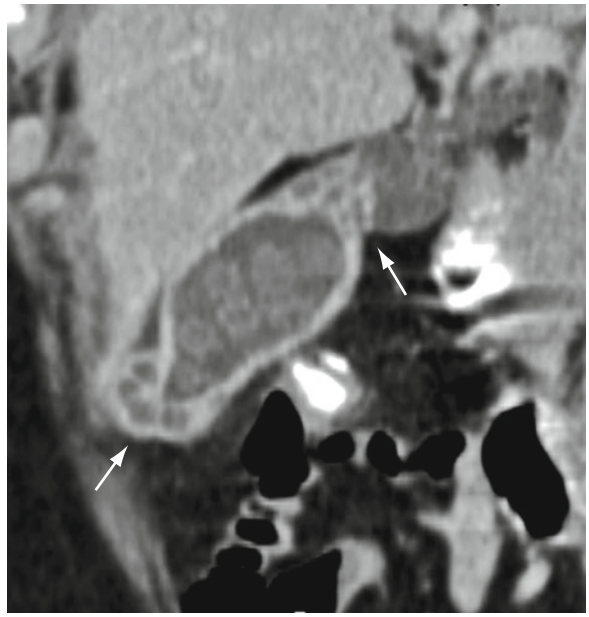

Fig. 2.5.2

A 58-year-old woman with chronic mild right upper quadrant abdominal pain.

Comments

Adenomyomatosis is a hyperplastic benign condition found in 2–5% of GB specimens. It is characterized by epithelial proliferation and invagination into the thickened muscularis tunica of the GB wall. This invaginations produce outpouchings in the wall known as Aschoff-Rockitansky sinuses. It is usually associated with stones. It may be focal, typically occurring in the fundus, segmental, or diffuse. It is important to recognize adenomyomatosis as the cause of wall thickening because it may mimic a gallbladder carcinoma. A relation between adenomyomatosis and gallbladder carcinoma has been suggested though development of dysplastic changes, but probably this is related to the presence of gallstones and chronic inflammation.

Imaging Techniques

Ultrasound shows echogenic foci with "dirty" shadowing due to reverberation producing the so-called "comet-tail" sign. Cystic areas with stones within are also characteristic. Widespread use of CT nowadays reveals very often the presence of adenomyomatosis as an unexpected finding, and it may simulate other causes of wall thickening, particularly the localized form, which may resemble GB carcinoma. The diffuse form may be similar to other causes of GB wall thickening, and the segmental form produces a characteristic narrowing (waist) resulting in an "hourglass" configuration of the GB. Demonstration of cystic spaces within the thickened wall is helpful to establish the diagnosis of adenomyomatosis.

MRI and MRCP are probably the best modalities to confirm the diagnosis, as they reveal the typical cystic cavities surrounding the GB wall, and in the case of the diffuse type, it resembles the classic "pearl necklace" pattern analogous to the classic pattern shown by oral cholecystography.

Imaging Findings

Sagittal and coronal MPR contrast-enhanced MDCT images (Figs. 2.5.1 and 2.5.2) show GB wall thickening with the presence of intramural cystic spaces (*arrows*).

Case 6
Choledocholithiasis

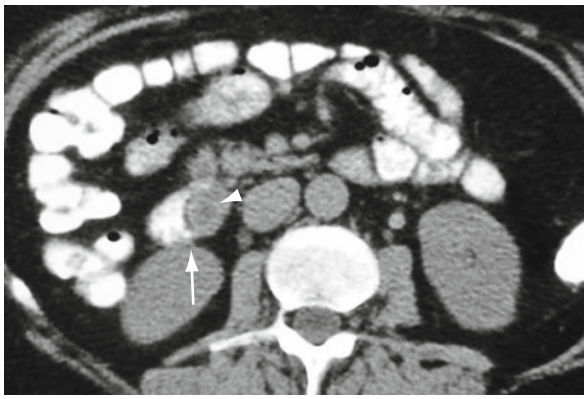

Fig. 2.6.1

Fig. 2.6.2

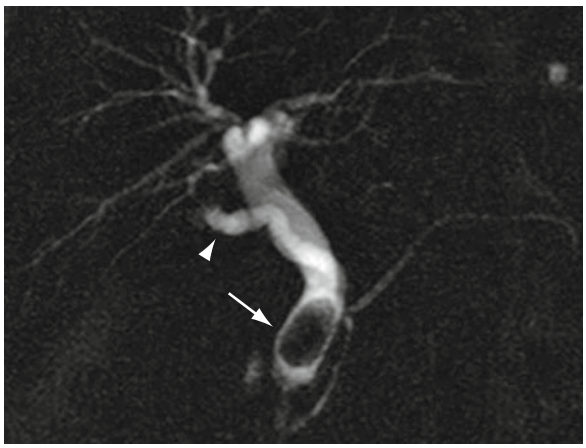

Fig. 2.6.3

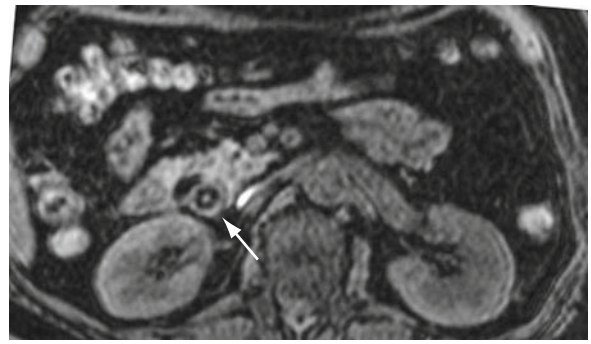

Fig. 2.6.4

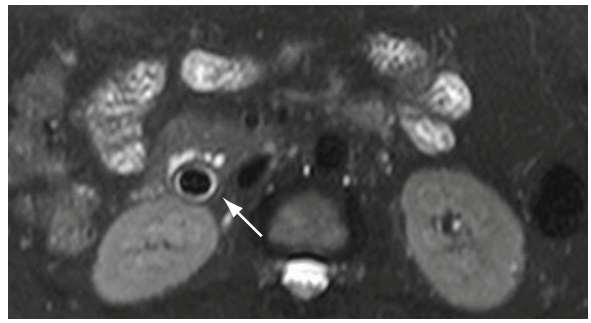

Fig. 2.6.5

A 55-year-old woman with a history of cholecystectomy presents with right upper quadrant pain, yellow-colored skin and sclerae, and laboratory findings of cholestasis.

Comments

Most stones present in the extrahepatic bile ducts migrated from the GB, and a minority form "de novo" in the ducts. Patients present classically with colicky right upper quadrant pain, nausea, vomiting, and laboratory findings of cholestasis. Surprisingly, biliary dilatation is not always present. After an acute obstruction of the biliary ducts, dilatation may take some days to develop, and many times is intermittent with the possibility that a patient being evaluated during a period of no dilatation. This explains why one may find stones in the common bile duct as an incidental finding in patients that may have experienced a biliary colic in the past whose diagnosis was missed.

Imaging Techniques

Although US has the greatest sensitivity and specificity for the diagnosis of gallstones, that is not the case for detecting choledochal stones. This is in part due to the inadequate acoustic window and complex anatomy and is also limited by body habitus. Furthermore, US may even show no abnormality but gallstones and probably, but not necessarily, biliary duct dilatation. On US, stones are seen as echogenic foci with acoustic shadowing. Although CT is not the primary modality to diagnose biliary tract stones, universal CT evaluation in the emergency setting and particularly its use in patients with jaundice and other symptoms related to the biliary tract often show biliary duct stones whether they are suspected or not. MDCT has a mean sensitivity of 80%. Stones are usually seen in a dependent location or filling the whole duct lumen. Its appearance is variable reflecting its varied composition, some are low density (especially those rich in cholesterol), others are isodense, whereas many show soft tissue density. Some stones are calcified, most partially and peripherally, and few densely calcified. An impacted lithiasis in the common bile duct frequently leads to a protrusion of the papilla and rarely may produce pancreatic duct dilatation. Often, biliary stones are more conspicuous on unenhanced images than on those obtained after contrast material administration. MRCP is the noninvasive imaging modality of choice to diagnose biliary duct stones. This is due to many reasons including: noninvasiveness, high sensitivity and specificity, and a large field of view potentially providing information about other entities such as extrinsic biliary tract compression. MRCP is more subject to artifacts that may result in pseudostrictures or false intraductal filling defects. Stones smaller than 3 mm may escape detection by MRCP.

Imaging Findings

Unenhanced (Fig. 2.6.1) and contrast-enhanced (Fig. 2.6.2) CT images at the same level show a marked dilatation of the common bile duct with luminal mixed density material. Notice the ringlike calcification better seen on unenhanced image (*arrowhead*). There is associated papillary protrusion (*arrows*). Single-shot MRCP (Fig. 2.6.3) reveals an oblong filling defect in the dilated CBD (*arrow*) consistent with a calculus. The cystic remnant is also dilated (*arrowhead*). Unenhanced axial fat-suppressed GE T1-weighted volumetric image (Fig. 2.6.4) and axial fat-suppressed TSE T2-weighted image (Fig. 2.6.5) at the same level demonstrate a rounded calculus filling the whole CBD lumen with a very low-signal intensity (*arrows*). There is a central high-signal spot on T1-weighted image reflecting the heterogeneous composition of the calculus.

Case 7
Choledochal Cyst

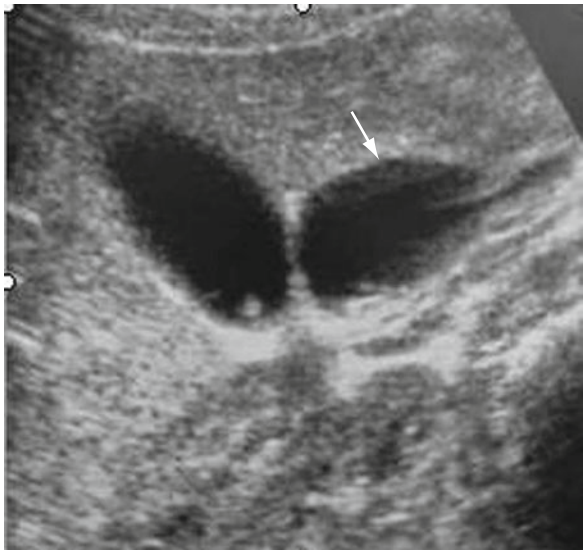

Fig. 2.7.1

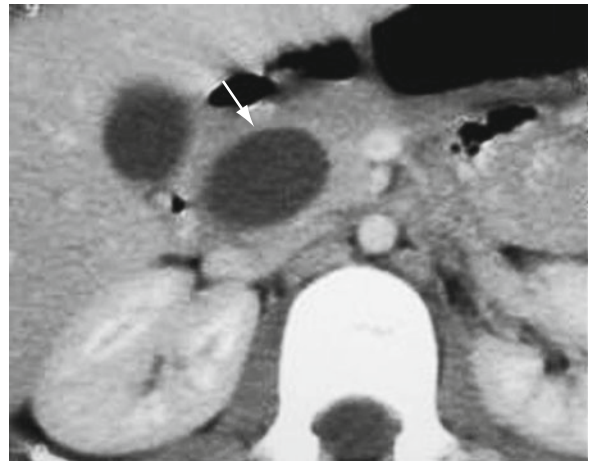

Fig. 2.7.2

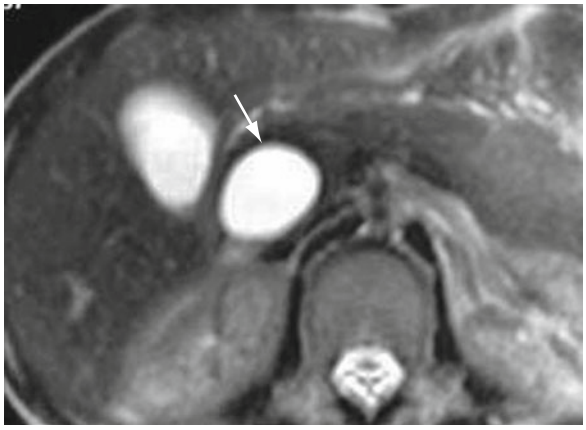

Fig. 2.7.3

Fig. 2.7.4

A 3-year-old boy with jaundice.

Comments

Choledochal cysts are congenital or possibly acquired abnormal dilatations of the biliary tree. It is postulated that it may be the result of reflux of pancreatic secretions due to abnormal pancreatobiliary ductal junction. Choledochal cyst predisposes to ascending cholangitis and cystolithiasis and poses a risk of malignant transformation. Because of that surgical resection is indicated. The classic triad of jaundice, pain, and abdominal mass is not always present, especially in the adult patient. Todani classification includes five types of choledochal cyst. Type 1 consists of fusiform or cystic dilatation of the extrahepatic bile duct as in the case illustrated and represents 80–90%. Type 2 is a diverticulum. Type 3 is a protrusion of the CBD into the duodenal wall known as choledochocele. Type 4 is divided into two classes: 4A fusiform dilatation of extrahepatic ducts, and 4B is rare and consists of multiple dilatation of extrahepatic duct. Type 5 is characterized by multiple cystic dilatation of intrahepatic ducts and is known as Caroli disease.

Imaging Techniques

US evaluation is the initial imaging technique to investigate the biliary tract and is especially suited to study pediatric patients. Although CT may provide important information, its role is supplanted by MRI and particularly MRCP. These modalities afford exquisite contrast resolution, multiplanar capabilities, and the anatomic information necessary to diagnose cystic biliary malformations as well as a road map for surgery in a noninvasive fashion. MRI also permits detection of complications such as lithiasis, cholangitis, or malignant transformation.

Imaging Findings

Transverse US image (Fig. 2.7.1) shows an ovoid cystic thin-walled structure adjacent to the gallbladder (*arrow*). Contrast-enhanced CT scan and axial fat-suppressed TSE T2-weighted image (Figs. 2.7.2 and 2.7.3) depict the same structure in the expected location of the intrapancreatic common bile duct (*arrows*). MRCP (Fig. 2.7.4) shows a cystic fusiform structure in the common bile duct course, typical finding of choledochal cyst (*arrows*).

Case 8

Acute Bacterial Cholangitis

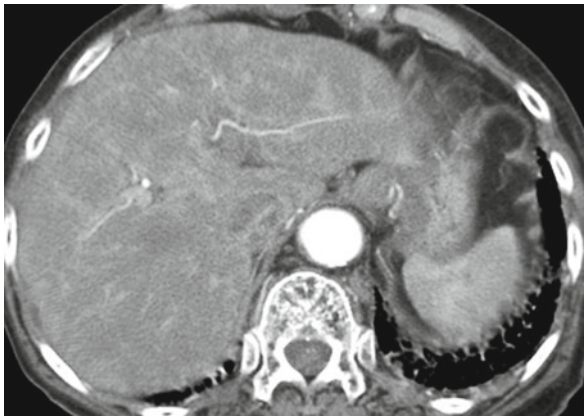

Fig. 2.8.1

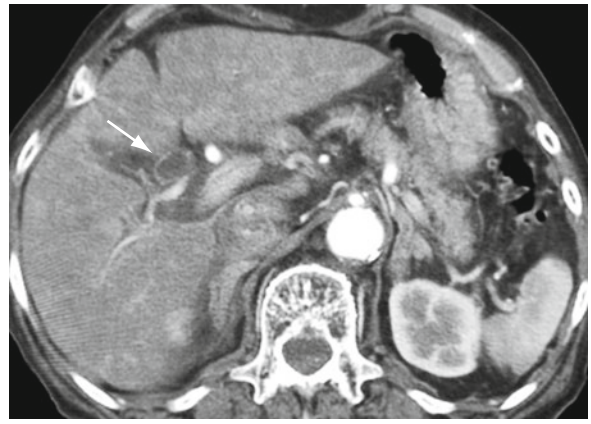

Fig. 2.8.2

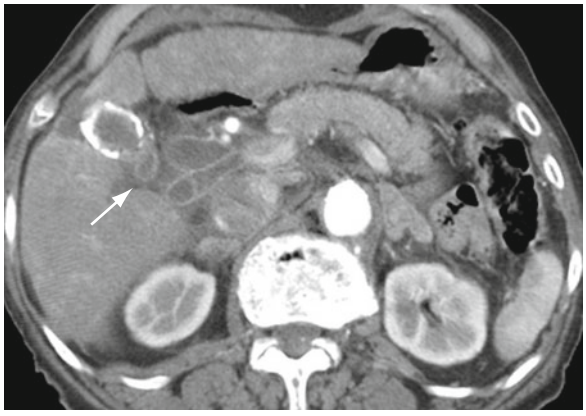

Fig. 2.8.3

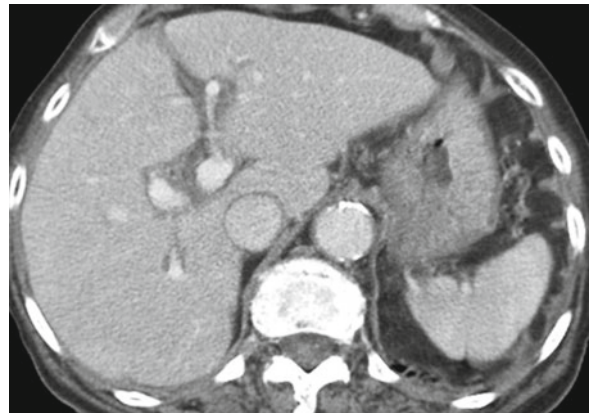

Fig. 2.8.4

A 68-year-old woman complaining of fever, sepsis, and jaundice.

Comments

Acute bacterial cholangitis is a serious condition usually occurring in the setting of biliary obstruction. It is more frequently associated with choledocholithiasis, and other causes include: stenosis associated with surgical injury, papillary stenosis, biliary instrumentation, and obstruction secondary to malignancies such as pancreatic carcinoma and cholangiocarcinoma. Predisposing factors are age (elderly patients), previous biliary surgery (biliodigestive anastomosis), and periampullary diverticula. Patients present typically with jaundice, fever, and abdominal pain (Charcot triad), and more severe evolution is accompanied by mental confusion and shock (Reynolds pentad). Infection of the biliary tract is more commonly secondary to gram-negative bacteria and cultures. Infection of the biliary ducts may derive in pericholangitic pyogenic abscesses, portal vein thrombosis, and rarely biliary peritonitis. Typical clinical presentation often suggests the diagnosis of acute bacterial cholangitis, particularly in those with predisposing factors. Imaging is reserved to aid in the diagnosis, especially in cases with vague clinical manifestations. On the other hand, imaging evaluation is crucial to detect complications such as abscess formation.

Imaging Techniques

Imaging affords several pieces of information regarding acute bacterial cholangitis, namely, biliary dilatation and its cause, as well as specific findings concerning cholangitis itself. These findings include duct wall thickening with increased enhancement and parenchymal changes such as heterogeneous enhancement, particularly transient areas of hyperattenuation on arterial phase that have a predilection for periductal zones. More importantly, cross-sectional imaging allows for the detection of abscess and portal vein branches thrombosis. CT and MRI are both effective modalities for that purpose, and both techniques are probably equally effective toward that goal.

Imaging Findings

Axial arterial phase CT mages at three consecutive levels (Figs. 2.8.1, 2.8.2, and 2.8.3) show a transient heterogeneous enhancement of the liver, with a patchy-appearing density. Biliary duct dilatation, wall thickening, and increased wall enhancement of the biliary system, typical of cholangitis, is evident (*arrows*). Portal venous phase CT at the same level than 2.8.1 (Fig. 2.8.4) demonstrates a homogeneous isoattenuating parenchyma.

Case 9
Caroli Disease

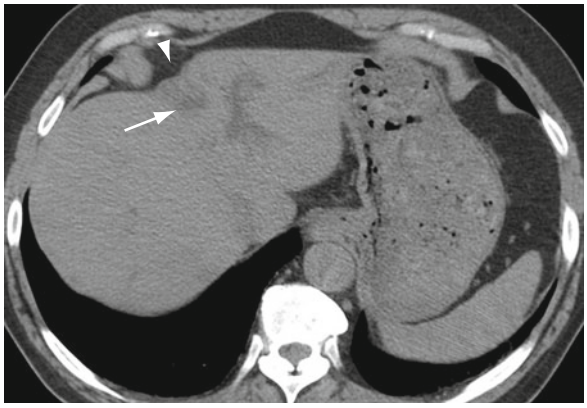

Fig. 2.9.1

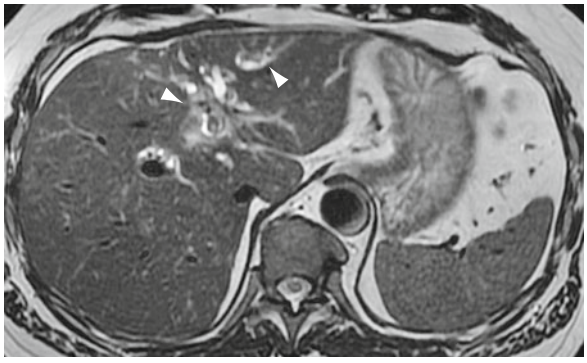

Fig. 2.9.3

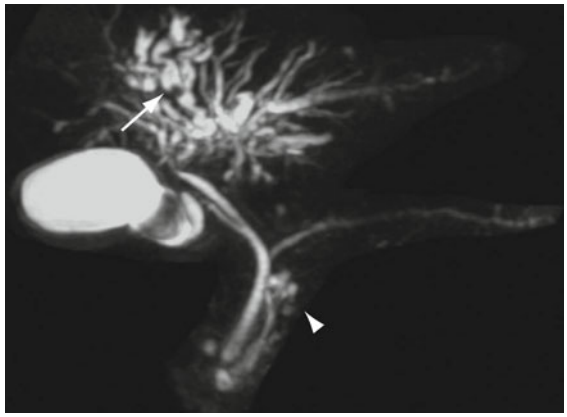

Fig. 2.9.5

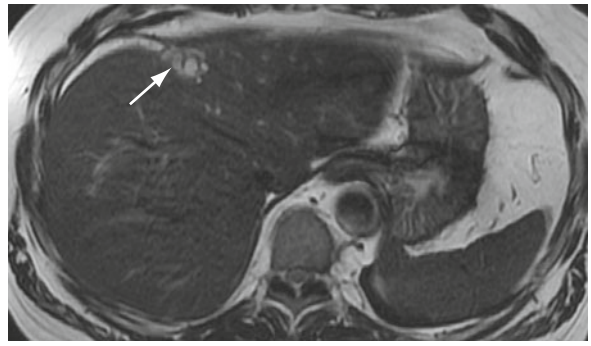

Fig. 2.9.2

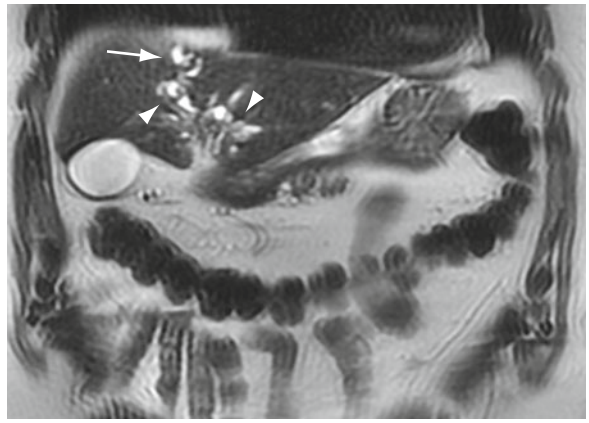

Fig. 2.9.4

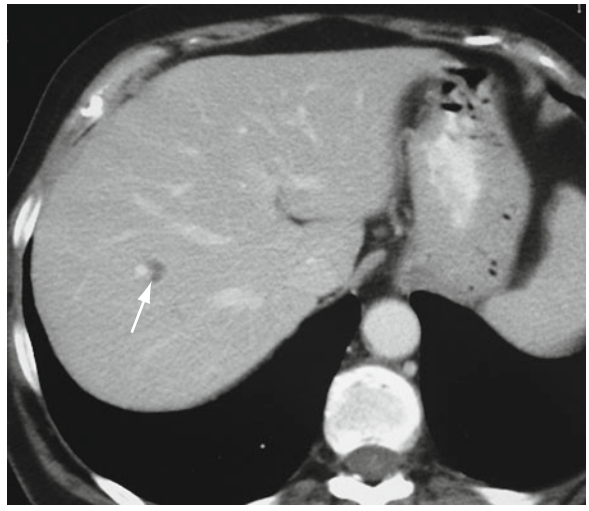

Fig. 2.9.6

A 59-year-old female patient with recurrent episodes of right upper quadrant pain, fever, and jaundice.

Comments

Caroli disease is part of the spectrum of ductal plate malformation that takes place during embryogenesis and may result in abnormal nonobstructive biliary dilatation (communicating cavernous ectasia) and hepatic fibrosis (abnormal development at the level of interlobular ductules). Coexistence of both abnormalities is known as Caroli syndrome. Patients may have associated renal abnormalities.

Clinical presentation usually consists of pain, obstructive jaundice, and cholangitis. Less frequently, patients may be asymptomatic. Age of presentation is variable, and the condition may be recognized in infancy or childhood or in adult patients, and there is a moderate female preponderance. Patients with Caroli disease are prone to intrahepatic lithiasis, recurrent cholangitis, and eventually biliary malignancy.

Imaging Techniques

US is an excellent modality to show biliary dilatation and stones but has a limited field of view. CT scan is effective in both demonstration of biliary dilatation and exclusion of obstruction. It also allows evaluating for complications such as stone formation, cholangitis, and pyogenic abscesses and the exclusion of a cholangiocarcinoma. In Caroli disease, CT shows dilated cystic-appearing biliary structures often encircling an enhancing fibrovascular structure, the so-called "central dot" sign which may be also located at the edge of the cystic space (Fig. 2.9.6). Biliary dilatation may be segmental or diffuse and, from a morphological viewpoint, may be saccular or, less commonly, fusiform. Luminal higher attenuation material may be seen secondary to sludge, stones, debris, or malignant tissue. Signs of cholangitis may be present as well as abscesses. MRI and MRCP are excellent modalities to show the spectrum of imaging findings that characterizes Caroli disease, and particularly MRCP is ideally suited to investigate in a comprehensive and noninvasive fashion the biliary tract. Similarly to CT, MRI may show luminal material as filling defects. Chronic biliary stasis and recurrent episodes of inflammation may result in lobar or segmental atrophy that can be better appreciated on cross-sectional imaging Liver fibrosis or cirrhosis may also occur in the lattest stage of the disease.

Imaging Findings

Unenhanced CT image (Fig. 2.9.1) shows dilated biliary ducts in segment IV (*arrow*) with capsular retraction. (*arrowhead*). Axial and coronal TSE T2-weighted MRI images (Figs. 2.9.2, 2.9.3, and 2.9.4, respectively) demonstrate cystic biliary dilatation in segment IV (*arrows*), as well as, dilated ducts in segments II and III (*arrowheads*). Decreased signal intensity within ducts is due to lithiasis and sludge. Three-dimensional MRCP (Fig. 2.9.5) confirms typical imaging appearance of Caroli disease and stone in segment IV duct (*arrow*). Incidentally, a cystic lesion compatible with an intraductal papillary mucinous neoplasm in pancreatic head is seen (*arrowhead*). Contrast-enhanced CT (Fig. 2.9.6) demonstrates a dilatation of a peripheral branch of the biliary system encircling peripherally an enhancing vessel (*arrow*).

Case 10
Porcelain Gallbladder

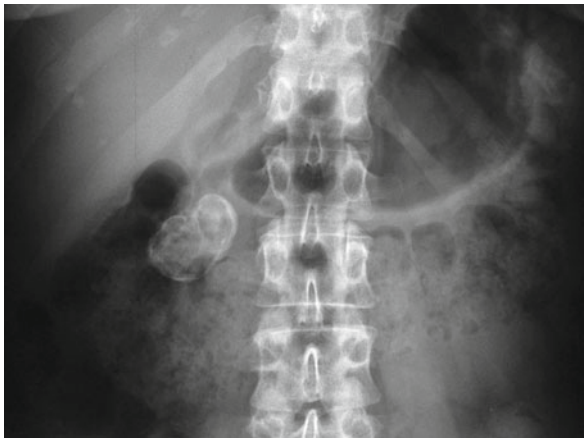

Fig. 2.10.1

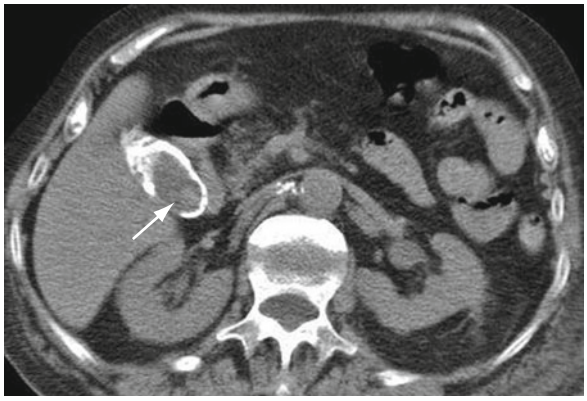

Fig. 2.10.3

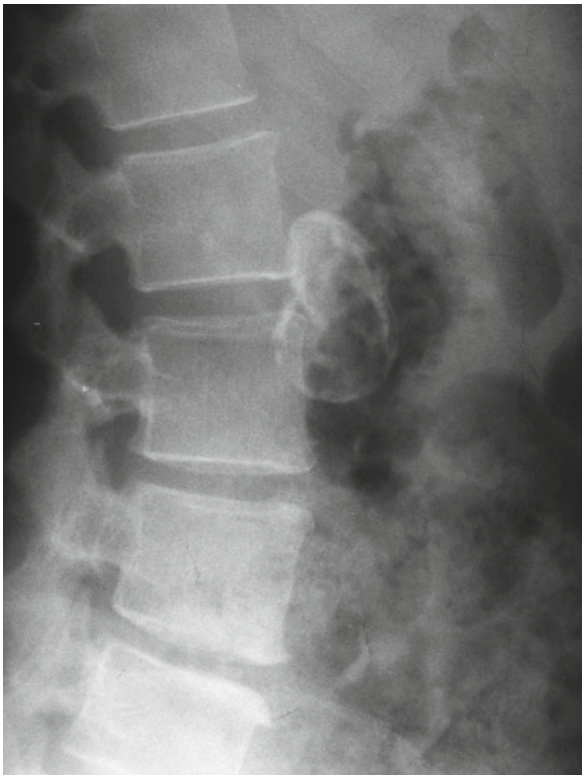

Fig. 2.10.2

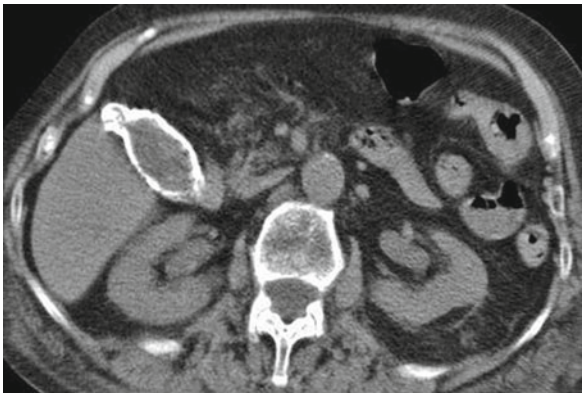

Fig. 2.10.4

A 75-year-old woman with dull chronic right upper quadrant abdominal pain.

Comments

Porcelain gallbladder is a term that denotes a gallbladder with a diffusely calcified wall and is thought to represent an uncommon form of chronic cholecystitis. The term derives from its bluish color and brittle consistency at surgery. Porcelain gallbladder incidence is calculated to range between 0.06% and 0.08% and is far more common in female (ratio male to female 1:5) and elderly patients. It is associated with gallstones in more than 95% of patients. Historically, an association between porcelain gallbladder and gallbladder carcinoma has been recognized although probably with a minor rate than previously thought.

Imaging Techniques

Plain abdominal radiographs show a typical calcified pear-shaped structure projected over the right upper quadrant. Main differential diagnosis includes a large gallstone, hydatid cyst, and old hematoma. Addition of a lateral projection assists in tridimensional localization of a calcified structure. US may demonstrate a hyperechoic semilunar structure with posterior acoustic shadowing that mimics a large stone filling the gallbladder lumen or an irregular clump of echoes with acoustic shadow.

CT is the most accurate imaging modality to depict a porcelain gallbladder as the cause of a calcified mass over the right upper quadrant. It also permits to evaluate any associated mass. MRI is limited to evaluate calcified lesions but may be useful to detect any soft tissue mass associated.

Imaging Findings

Coned-down view of AP and lateral radigraphs of the abdomen (Figs. 2.10.1 and 2.10.2) show a grossly and heterogeneously calcified structure. Uenhanced CT images at two consecutive levels (Figs. 2.10.3 and 2.10.4) show a gallbladder with densely calcified wall. Notice also the presence of a gallstone (*arrow*).

Further Reading

Books

Bennett GL (2008) Cholelithiasis, cholecystitis, choledocholithiasis, and hyperplastic cholecystoses. In: Gore RM, Levine MS (eds) Textbook of gastrointestinal radiology, 3rd edn. Elsevier, Philadelphia

Dooley JS, Lok A, Burroughs A et al (2011) Sherlock's Diseases of the Liver and Biliary System. 12th edition. Willey-Blackwell, Chichester, West Sussex

Lin JH, Kim KW, Choi D (2008) The gallbladder and biliary tract. In: Haaga JR, Gilkeson RC Dogra VS, Forsting M, Ha HK (eds) CT and MR imaging of the whole body, 5th edn. Mosby, St. Louis

Roberts EA, Portmann BC (2007) Developmental abnormalities and liver disease in childhood. In: Burt AD, Portmann BC, Ferrel LD (eds) Pathology of the liver, 5th edn. Churchill Livingstone, Edinburgh

Spicák J, Boyer JL, Gilat T et al (1999) Diseases of the Liver and the Bile Ducts. Springer-Verlag, Berlin-Heidelberg

Web Pages

http://www.ceessentials.net/article41.html
http://www.szote.u-szeged.hu/radio/a7.htm
http://chorus.rad.mcw.edu/index/46.html
http://emedicine.medscape.com/radiology#gastrointestinal
http://www.eurorad.org/

Articles

Adusumilli S, Siegelman ES (2002) MR imaging of the gallbladder. Magn Reson Imaging Clin N Am 10:165–184

Anderson SW, Lucey BC, Varghese JC et al (2006) Accuracy of MDCT in the diagnosis of choledocholithiasis. AJR Am J Roentgenol 187:174–180

Catalano OA, Singh AH et al (2008) Vascular and biliary variants in the liver: implications for liver surgery. Radiographics 28(2):359–378

Fayad LM, Kamel IR, Mitchell DG et al (2005) Functional MR cholangiography: diagnosis of functional abnormalities of the gallbladder and biliary tree. AJR Am J Roentgenol 184:1563–1571

Gore RM, Yaghmai V, Newmark GM et al (2002) Imaging benign and malignant disease of the gallbladder. Radiol Clin North Am 40:1307–1323

Hanbidge AE, Buckler PM et al (2004) Imaging evaluation for acute pain in the right upper quadrant. Radiographics 24: 1117–1135

Hashimoto M, Itoh K, Takeda et al (2008) Evaluation of biliary abnormalities with 64-channel multidetector CT. Radiographics 28(1):119–134

Irie H, Honda H, Kuroiwa T et al (2001) Pitfalls in MR cholangiopancreatographic interpretation. Radiographics 21:23–37

Kim PN, Outwater EK, Mitchell DG (1999) Mirizzi syndrome: evaluation by MR imaging. Am J Gastroenterol 94: 2546–2550

Lee NK, Kim S, Lee JW et al (2009) Biliary MR imaging with Gd-EOB-DTPA and its clinical applications. Radiographics 29(6):1707–1724

Levy AD, Rohrmann CA Jr, Murakata LA et al (2002) Caroli's disease: radiologic spectrum with pathologic correlation. AJR Am J Roentgenol 179:1053–1057

Matos C (2007) MR cholangiography: what's new? JBR-BTR 90(6):503–506

Morimoto K, Shiomi M, Shirakawa T et al (1992) Biliary obstruction: evaluation with three-dimensional MR cholangiography. Radiology 183:578–580

Park MS, Yu JS, Kim YH et al (1998) Acute cholecystitis: comparison of MR cholangiography and US. Radiology 209:781–785

Park MS, Kim TK, Kim KW et al (2004) Differentiation of extrahepatic bile duct cholangiocarcinoma from benign stricture: findings at MRCP versus ERCP. Radiology 233:234–240

Park MS, Yu JS, Lee JH et al (2007) Value of manganese-enhanced T1- and T2-weighted MR cholangiography for differentiating cystic parenchymal lesions from cystic abnormalities which communicate with bile ducts. Yonsei Med J 48:1072–1074

Reinhold C, Bret PM, Guibaud L et al (1996) MR cholangiopancreatography: potential clinical applications. Radiographics 16:309–320

Romagnuolo J, Bardou M, Rahme E et al (2003) Magnetic resonance cholangiopancreatography: a meta-analysis of test performance in suspected biliary disease. Ann Intern Med 139:547–557

Smith EA, Dillman JR, Elsayes KM et al (2009) Cross-sectional imaging of acute and chronic gallbladder inflammatory disease. AJR Am J Roentgenol 192:188–196

Thurley PD, Dhingsa R (2008) Laparoscopic cholecystectomy: postoperative imaging. AJR Am J Roentgenol 191:794–801

Tsai HM, Lin XZ, Chen CY et al (2004) MRI of gallstones with different compositions. AJR Am J Roentgenol 182:1513–1519

van Breda Vriesman AC, Engelbrecht et al (2007) Diffuse gallbladder wall thickening: differential diagnosis. AJR Am J Roentgenol 188:495–501

Vilgrain V (2008) Staging cholangiocarcinoma by imaging studies. HPB (Oxford) 10(2):106–109

Vitellas KM, Keogan MT, Spritzer CE et al (2000) MR cholangiopancreatography of bile and pancreatic duct abnormalities with emphasis on the single-shot fast spin-echo technique. Radiographics 20:939–957

Pancreas 3

Luis Luna and Antonio Luna

Contents

A. Luna et al., *Learning Abdominal Imaging*, Learning Imaging,
DOI 10.1007/978-3-540-88003-5_3,

Case 1
Acute Pancreatitis

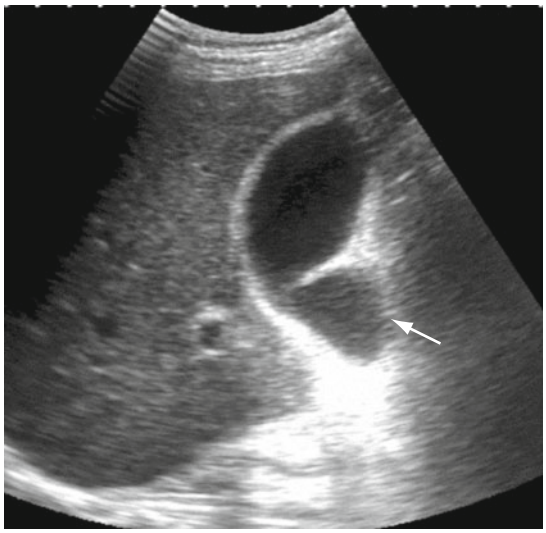

Fig. 3.1.1

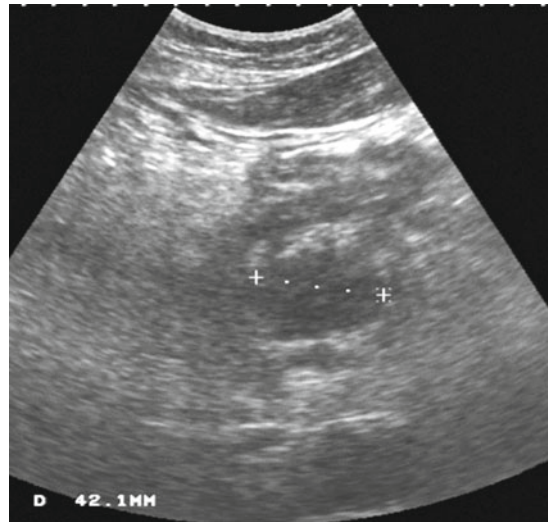

Fig. 3.1.2

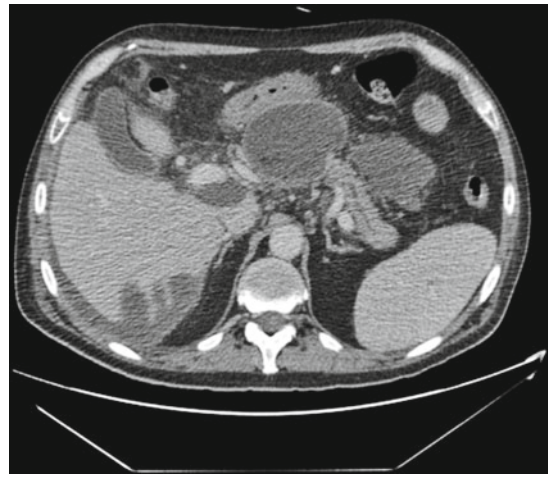

Fig. 3.1.4

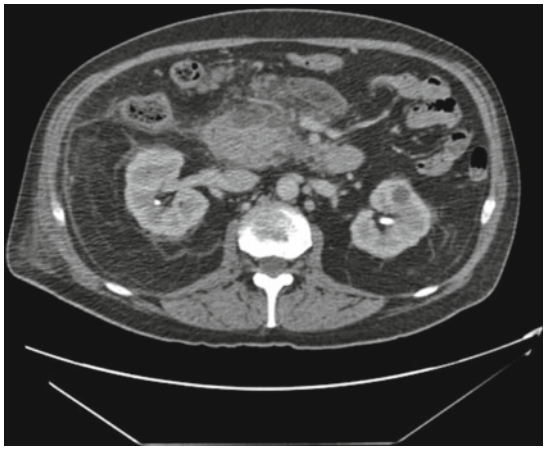

Fig. 3.1.3

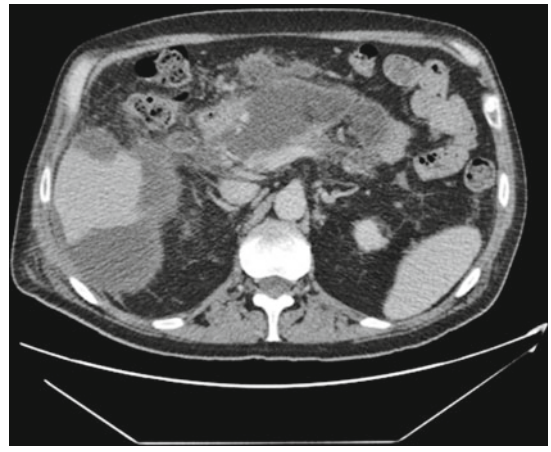

Fig. 3.1.5

A 66-year-old male with abdominal pain presents to the emergency department (ER). Laboratory tests confirm elevation of amylase. Ultrasonography and CT examinations are requested to rule out acute pancreatitis.

Comments

Acute pancreatitis is defined as an acute inflammatory condition of the pancreas with variable involvement of other regional tissues or remote organ systems. Patients typically present with abdominal pain and elevations of pancreatic enzymes (amylase and lipase). It may occur secondary to chronic alcoholism, gallstones, hypercalcemia, hyperlipoproteinemia, blunt abdominal trauma, penetrating peptic ulcer disease, viral infection, and drugs.

Imaging is essential to confirm the diagnosis and to provide an accurate staging, which will have direct implications in treatment and prognosis. Findings in X-ray of the abdomen are nonspecific, although secondary signs such us a sentinel loop may be found. The main role of ultrasonography is to rule out gallstones as etiology of acute pancreatitis. Pancreas may appear enlarged and hypoechoic. It is also possible to detect peripancreatic fluid collections.

Conversely, CT is probably the best imaging method for global assessment of acute pancreatitis. CT is able to distinguish the different types of acute pancreatitis. On one hand, mild acute pancreatitis, also known as edematous or interstitial pancreatitis, is characterized by swelling of the affected portions or the entire gland, appearing slightly enlarged, with decreased attenuation, blurred margins, and thickening of Gerota's fascia. On the other hand, in serous exudative pancreatitis, hypoattenuated, nonenhancing acute fluid collections, that lack of a defined wall, are usually found. Fat necrosis may be difficult to differentiate from these exudates, but it is worse defined with a higher attenuation than fluid. Finally, in severe acute pancreatitis, also known as extensive exudative or hemorrhagic necrotizing pancreatitis, the gland is markedly enlarged, inhomogeneous, and poorly demarcated from surrounding tissues. Necrotic areas appear hypoattenuated, parenchymal sequesters are isoattenuated, and hemorrhagic areas are hyperattenuated compared to pancreatic parenchyma. The use of intravenous contrast is necessary to determinate the extent of pancreatic necrosis, appearing as areas of lack of enhancement. Balthazar and colleagues established a CT severity index to assess the prognosis of acute pancreatitis, based on the evaluation of the existence of fluid collections and the presence of parenchymal gland necrosis and their extension.

MRI may have the same capabilities than CT to evaluate acute pancreatitis, with a greater sensitivity to detect mild areas of inflammation in early acute pancreatitis. The main advantage of MRI is the ability for a better depiction of hemorrhagic areas in severe acute pancreatitis, appearing as areas of high signal intensity on T1-weighted images.

Imaging Findings

On US, the presence of sludge inside the gallbladder is detected (Fig. 3.1.1, *arrow*). An increase in size of the head of the pancreas, which appears hypoechogenic, is also identified (Fig. 3.1.2, area between markers). Postcontrast CT on a delayed phase at three different levels (Figs. 3.1.3, 3.1.4, and 3.1.5) confirmed the diagnosis of complicated acute pancreatitis. The size of the head of the pancreas is increased, with blurred margins and infiltration of the peripancreatic fat, although it shows homogeneous enhancement, demonstrating lack of necrosis (Fig. 3.1.3). Several peripancreatic fluid collections with extension to the right anterior pararenal and subhepatic spaces are also detected (Figs. 3.1.4 and 3.1.5).

Case 2
Pancreatic Pseudocyst

Fig. 3.2.1

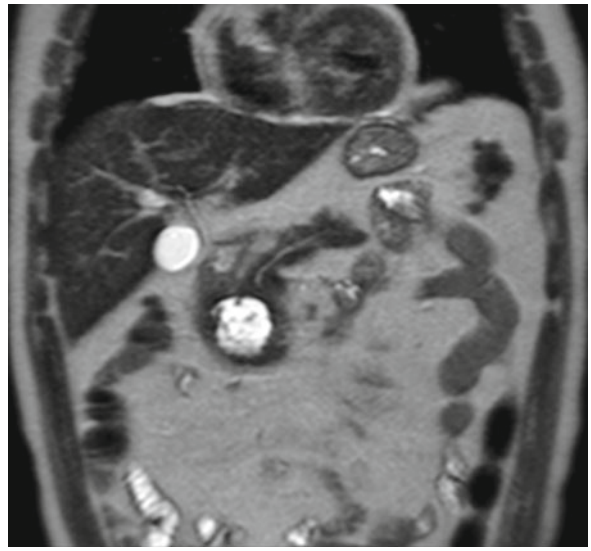

Fig. 3.2.2

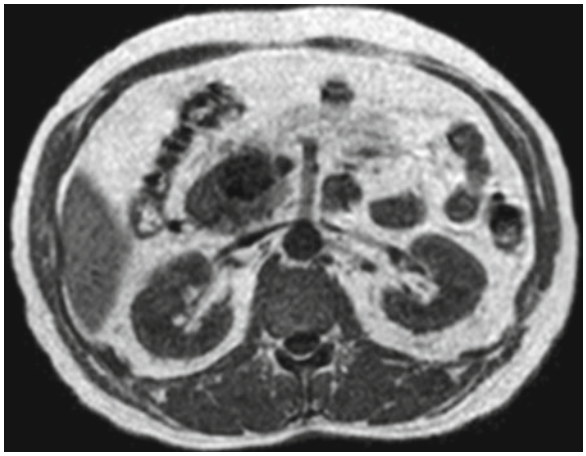

Fig. 3.2.3

Fig. 3.2.4

A 65-year-old male, with history of prior acute pancreatitis, presents persistent abdominal pain. CT and MRI examinations are requested to evaluate possible complications of pancreatitis.

Comments

Pseudocysts are present in approximately 15% of patients with acute pancreatitis. Pseudocysts consist in a collection of pancreatic fluid and inflammatory exudates encapsulated by fibrous tissue. Pseudocysts are delayed complications of acute pancreatitis which are not developed until 4–6 weeks after the onset of the pancreatitis. They are mainly related to fluid collections with origin in exudative acute pancreatitis. In about 50% of the cases, these collections resolve, and in the remainder, pseudocyst formation occurs. They are most frequently located close to the pancreas, but they may be also found in the liver, spleen, or mediastinum.

On ultrasound, pseudocysts appear as hypoechogenic/anechoic fluid collections with through-transmission. On CT, pseudocysts present as rounded, well-encapsulated fluid collections of varying attenuation (0–25 UH). There is contrast enhancement of the cystic walls, with lack of enhancement of their content. Septations are uncommon. Presence of gas bubbles is suggestive of superimposed infection. On MRI, uncomplicated pseudocysts are low in signal intensity on T1-weighted images and homogeneous with high signal intensity on T2-weighted images. Pseudocysts complicated by necrotic debris, hemorrhage, or infection are heterogeneous in signal intensity on T2-weighted images. Pseudocyst walls enhance minimally on early postgadolinium images and show a progressively increase in enhancement on delayed postcontrast images. Pseudocysts may be identified on MR cholangiography (MRCP) as hyperintense cystic lesions contiguous with a dilated pancreatic duct. Absence of areas of restriction on diffusion-weighted images (DWI) helps to rule out solid areas and to distinguish them from malignant cystic tumors.

Imaging Findings

Figure 3.2.1: Postcontrast CT on the venous phase shows an encapsulated cystic lesion (*arrow*) with a density of 15 HU, adjacent to the pancreatic head, demonstrating wall enhancement. Figure 3.2.2: Coronal HASTE demonstrates a cystic lesion close to the head of pancreas, which is hyperintense and slightly heterogeneous. Figure 3.2.3: Axial in-phase GE T1-weighted sequence demonstrates the hypointensity of the lesion, which does not show restriction of free water movement on the diffusion-weighted image acquired with a *b* value of 800 s/mm^2 (Fig. 3.2.4, *arrow*).

Case 3
Focal Chronic Pancreatitis

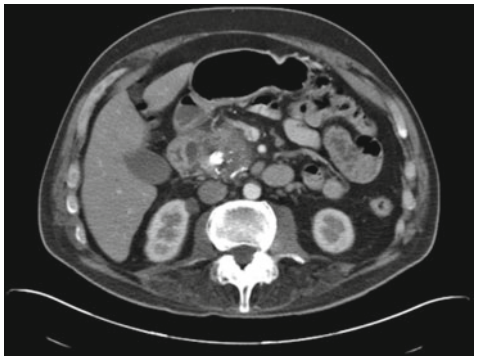

Fig. 3.3.1

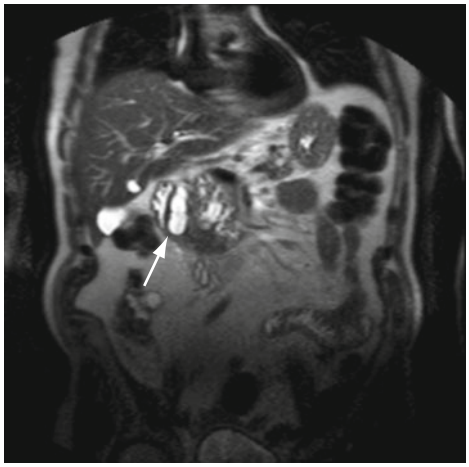

Fig. 3.3.3

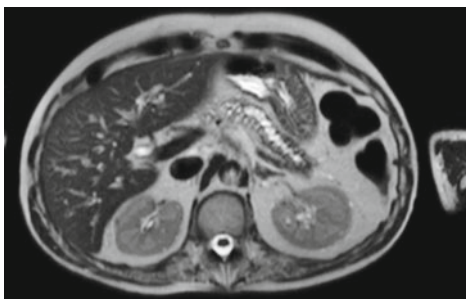

Fig. 3.3.5

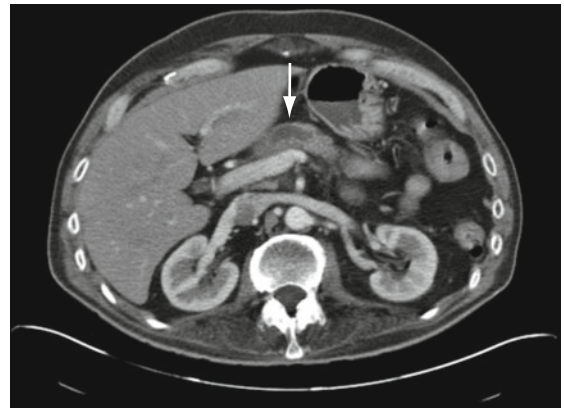

Fig. 3.3.2

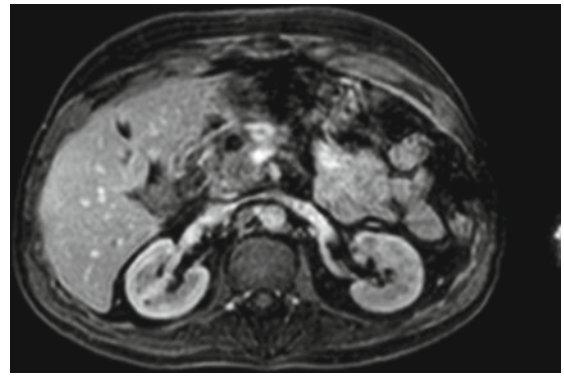

Fig. 3.3.4

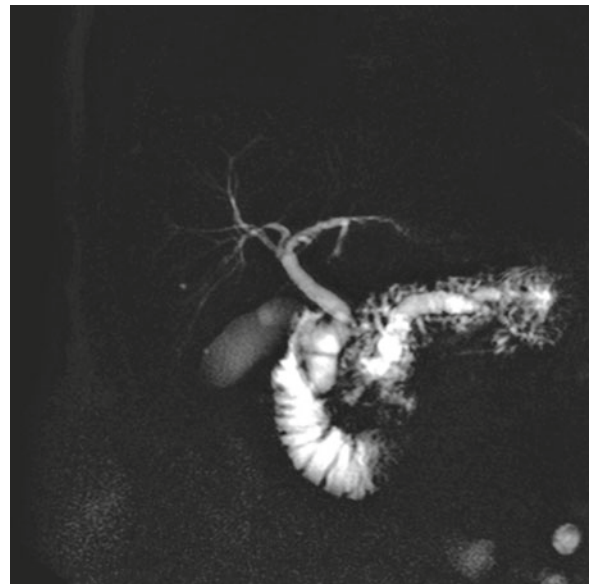

Fig. 3.3.6

A 58-year-old male with nonspecific digestive symptomatology during 2 years is submitted to an ultrasound where a nodular mass in pancreatic head is identified.

Comments

Chronic pancreatitis is defined pathologically by continuous or relapsing inflammation of the pancreas, leading to irreversible morphologic injury and typically leading to impairment of function. It is acquired either as a process distinct from acute pancreatitis or as a complication of repeated attacks of acute pancreatitis. There is a strong association between alcoholism and development of chronic pancreatitis and an increased risk of developing pancreatic cancer.

On ultrasound, the typical sonographic hallmarks are pancreatic calcifications that appear as multifocal punctuate hyperechoic foci with or without shadowing. Calcification is a late occurrence, following developing of fibrosis, and appears only in 50%. Dilatation and tortuosity of pancreatic duct is also frequently seen on ultrasound. On CT, the main features are dilatation of the main pancreatic duct, parenchymal atrophy, calcifications, pseudocysts, and focal pancreatic enlargement. CT is not sensitive at detecting the early changes of fibrosis. However, MRI is more sensitive than CT. MRI detects not only typical morphological findings but also the presence of fibrosis that is shown as areas of diminished signal intensity on fat-suppressed T1-weighted images and diminished heterogeneous enhancement on immediate postgadolinium acquisitions. Most of the cases of chronic pancreatitis show progressive parenchymal enhancement on 5 min postcontrast images, reflecting the same enhancement pattern than fibrous tissue.

MRCP with secretin injection is of value to assess and classify chronic pancreatitis. Secretin induces pancreatic duct secretion, improving the visualization of pancreatic ductal system. In chronic pancreatitis, secretin-MRCP may show early ductal changes, such as areas of dilatation and strictures. This test may also evaluate and grade pancreatic exocrine function.

Mass-forming focal pancreatitis is defined as a focal inflammatory process in the pancreas that may mimic pancreatic cancer. Focal chronic pancreatitis presents as a focal enlargement of the head of the pancreas, which is difficult to distinguish from cancer. Standard cross-sectional imaging techniques including CT, MRI, and even histopathologic analysis of the biopsy material may be inconclusive to distinguish neoplasm from mass-forming focal pancreatitis. Best results in their distinction with imaging have been obtained with functional MRI techniques as dynamic-contrast enhanced and DWI series. Apparent diffusion coefficient values (ADC) of focal chronic pancreatitis is similar to those of normal pancreas. Conversely, pancreatic cancer usually shows lower ADC values than normal pancreas.

Imaging Findings

On postcontrast CT on arterial phase at two different levels, a hypodense pseudonodular mass with calcifications in the pancreatic head is detected (Fig. 3.3.1), associating dilatation of the main pancreatic duct (Fig. 3.3.2, *arrow*).

Coronal HASTE demonstrates a heterogeneous focal enlargement of the head of the pancreas, presenting a pseudocyst (*arrow*) between the head of pancreas and the duodenum (Fig. 3.3.3). This nodule-like enlargement of pancreatic head shows progressive enhancement on the dynamic series, being heterogeneously hypovascular on delayed postcontrast THRIVE (Fig. 3.3.4). Atrophy of body and tail of pancreas and marked dilatation of pancreatic main duct are also visualized on axial HASTE and coronal thick-slice 2D MRCP (Figs. 3.3.5 and 3.3.6).

Case 4
Serous Cystoadenoma

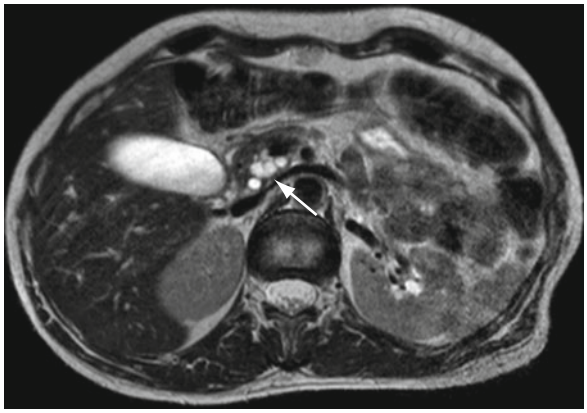

Fig. 3.4.1

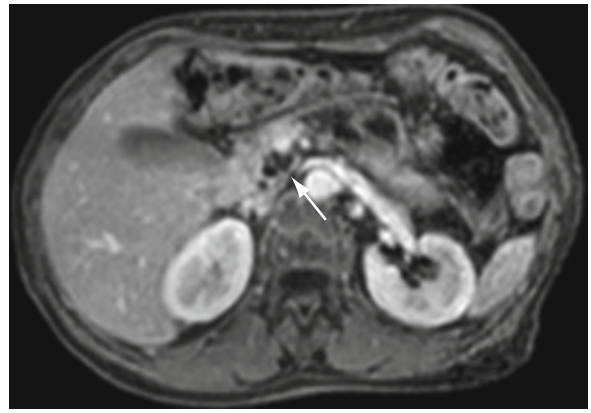

Fig. 3.4.2

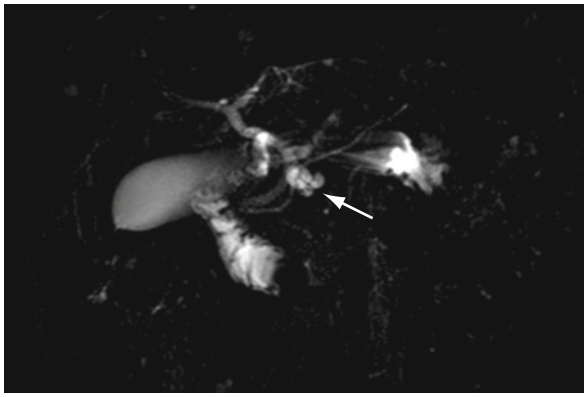

Fig. 3.4.3

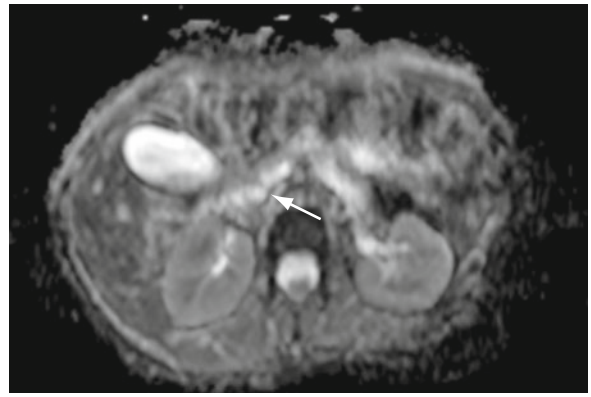

Fig. 3.4.4

A 52-year-old female was sent to our institution for better characterization of a cystic mass located in pancreatic head, seen on a prior US examination.

Comments

Serous cystoadenoma of the pancreas is a benign neoplasm characterized by numerous tiny serous fluid-filled cysts, which are usually microcystic and multilocular, with a size inferior to 1 cm. This neoplasm uncommonly may show macrocystic areas. It is more frequently located in the head of pancreas but may be located in any part of the pancreas. It may occasionally contain a central fibrotic scar with calcification.

On ultrasound, serous cystoadenoma of the pancreas may appear as a hyperechoic solid mass due to the interfaces produced between the numerous cysts. On CT, its appearance is that of multiple cysts with enhancing septa, presenting a multilobulated contour and a honeycomb configuration. It may resemble a solid lesion in noncontrast images, but after contrast administration, enhancing septations become visible, delineating the cystic spaces. A central fibrotic scar is typically seen with stellate or sunburst calcifications in 15–40% of the cases. This scar shows prolonged enhancement on delayed images.

On MRI, serous cystoadenoma of the pancreas appears as a well-defined mass, which does not demonstrate invasion of fat or adjacent organs. On T2-weighted images, this tumor shows a cluster of small grape-like high-signal-intensity cysts. Thin uniform septations and absence of locally aggressive features help to distinguish serous cystoadenoma from serous cystoadenocarcinoma. Tumor septations enhance minimally with gadolinium on early and late postcontrast images. Delayed enhancement of the central scar when present, is another typical finding. Serous cystoadenoma is not communicated with the pancreatic duct.

Imaging Findings

Figure 3.4.1: On axial TSE T2-weighted image, a multiseptated cystic mass, formed by multiple tiny cysts, adopting a honeycomb configuration is seen at the uncinate process of the pancreas (*arrow*). Figure 3.4.2: Postcontrast THRIVE on the portal phase demonstrates septal enhancement within the lesion (*arrow*). This lesion has no communication with the main pancreatic duct (*arrow*), as demonstrated on coronal thick-slice 2D MR cholangiography (Fig. 3.4.3). The mass does not demonstrate restriction of diffusion, appearing hyperintense on the ADC map (Fig. 3.4.4), excluding areas of hypercellularity.

Case 5

Mucinous Cystic Pancreatic Tumor

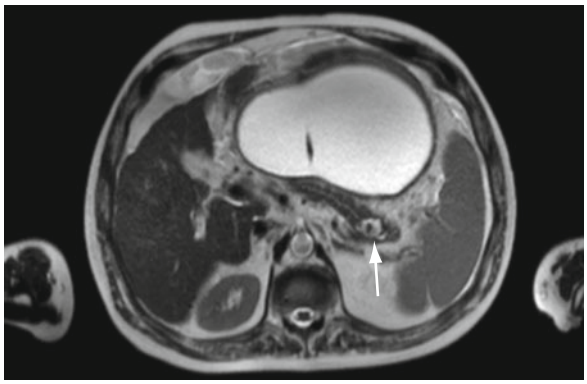

Fig. 3.5.1

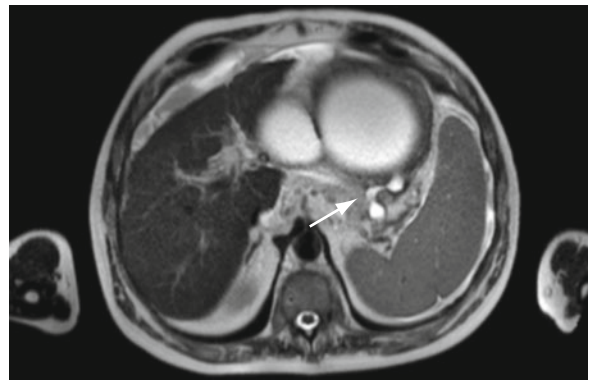

Fig. 3.5.2

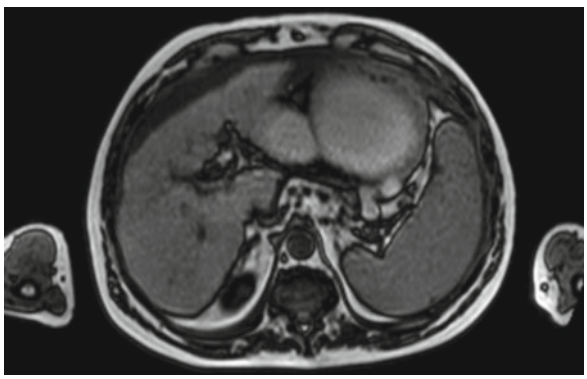

Fig. 3.5.3

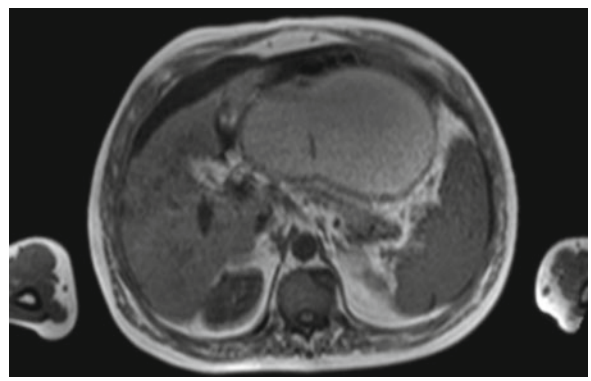

Fig. 3.5.4

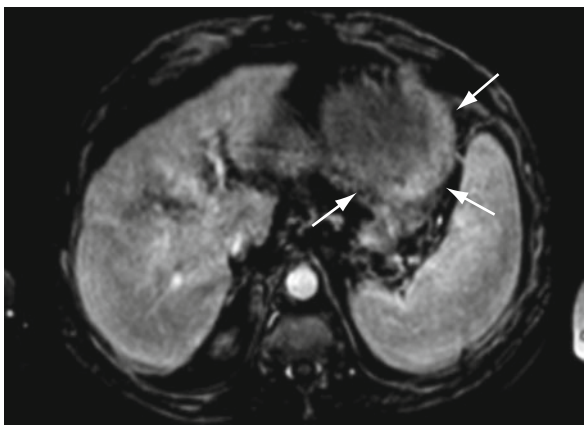

Fig. 3.5.5

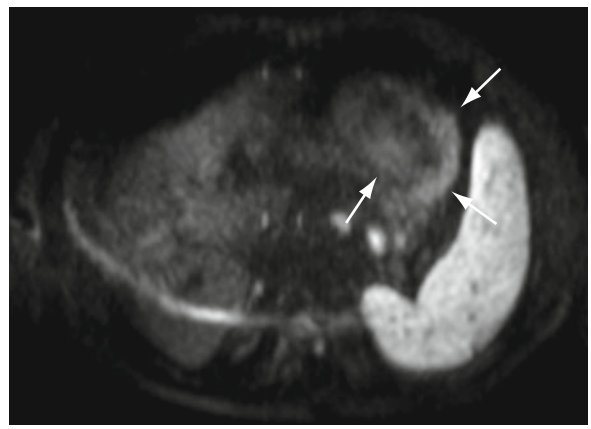

Fig. 3.5.6

A 53-year-old alcoholic male, with a huge incidental abdominal mass detected on CT, is sent to our imaging department to perform a pancreatic MRI for further characterization of the mass.

Comments

Mucinous cystic neoplasms of the pancreas are characterized by the formation of large unilocular or multilocular cysts filled with abundant, thick gelatinous mucin. Histopathologically, these tumors are divided into benign (mucinous cystoadenoma), borderline, and malignant (mucinous cystoadenocarcinoma) variants. They are usually located in the body and tail of the pancreas. Mucinous cystic neoplasms may be large (mean diameter of 10 cm), often multiloculated and encapsulated, although with great propensity for invasion of local organs and tissues. They are not connected to the main pancreatic duct. Up to 10% of them have scattered peripheral calcifications.

On ultrasound, mucinous cystic neoplasms of the pancreas appear as a hypoechoic cystic mass that may be unilocular and simulate a pseudocyst. Presence of internal debris is common. On CT, they appear as a uni- or multilocular cystic mass that may show water or soft tissue density. Small daughter cysts may be found on the inner surface of a larger cyst. Septa are hyperattenuated on postcontrast images and are generally thicker and more irregular than in microcystic serous cystoadenoma. Peripheral calcifications are quite specific of this neoplasm. Malignant transformation may occur, and the presence of solid papillary excrescences and thick septations which show enhancement after contrast administration helps to distinguish malignant variants from benign type of mucinous cystoadenoma, although CT does not allow a confident differentiation between both entities. MRI performs better in this regard, as gadolinium-enhanced fat-suppressed T1-weighted images demonstrate large, irregular cystic spaces separated by septa. Cyst walls and septations are usually thicker in mucinous cystoadenocarcinoma than those of mucinous cystoadenomas. The presence of solid component is suggestive of malignancy. Mucin produced by these tumors results in high signal intensity on T1-weighted and T2-weighted images of both the primary tumor and liver metastasis, which are generally hypervascular in nature.

Imaging Findings

Figure 3.5.1: Axial HASTE demonstrates a large cystic mass located in the lesser sac. Notice the presence of another cystic mass in the pancreatic tail (*arrow*). These lesions show very high signal intensity on T2-weighted images. Figure 3.5.2: Axial HASTE at a different level demonstrates that both lesions are connected by a narrow cystic-like structure (*arrow*). Figures 3.5.3 and 3.5.4: Axial out-of-phase and in-phase GE T1-weighted images at two different levels demonstrate hyperintensity of the lesion, consistent with mucinous content. Figure 3.5.5: Postcontrast THRIVE at portal phase demonstrates marked parietal enhancement of the inferior and lateral aspects of the lesion (*arrows*), which also show restriction on DWI with high *b* value (Fig. 3.5.6, *arrows*), being suspicious for solid areas and malignancy of the lesion (*arrows*), as posteriorly confirmed on histological analysis.

Case 6

Islet Cell Tumors: Malignant Insulinoma

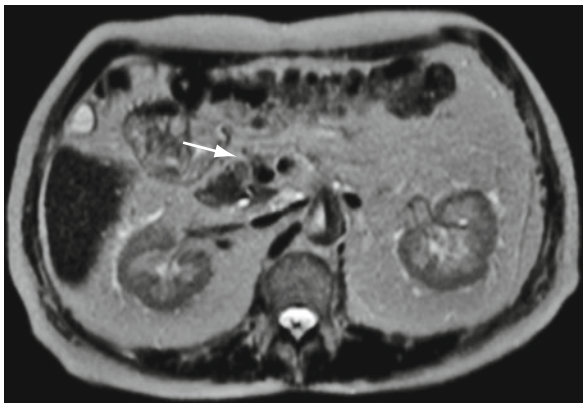

Fig. 3.6.1

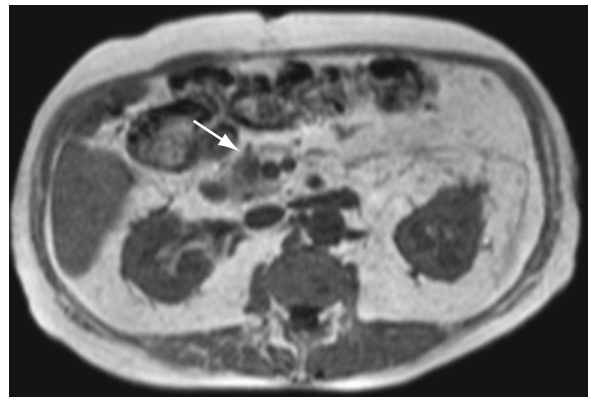

Fig. 3.6.2

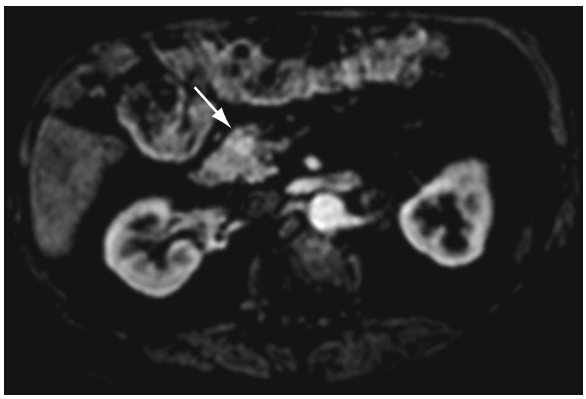

Fig. 3.6.3

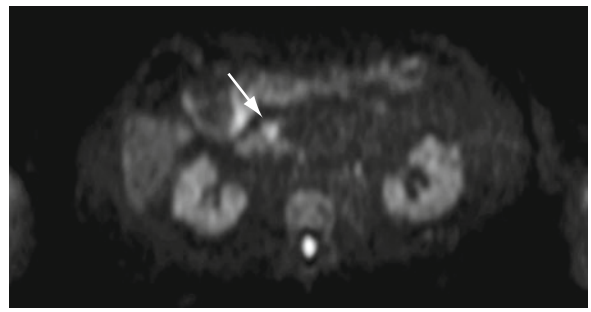

Fig. 3.6.4

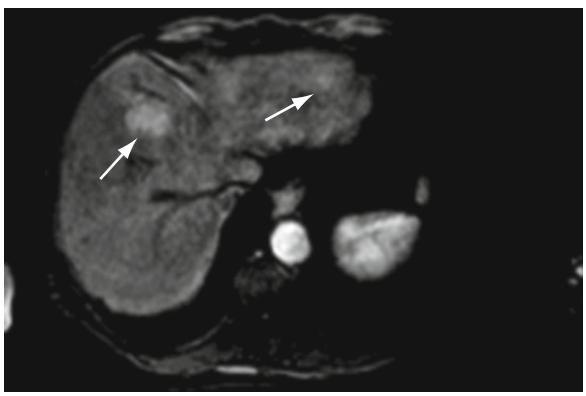

Fig. 3.6.5

A 75-year-old male, with repetitive episodes of hypoglucemia and with clinical and analytical suspicion of insulinoma. A prior CT scan failed to locate the tumor, but a hypervascular focal liver lesion was detected. MRI is performed for further assessment.

Comments

Islet cell tumor is a collective term applied to tumors arising from endocrine cells of the islet cell apparatus of the pancreas. Up to 90% of these tumors are benign, and 75% are functional (hormonally active). Insulinomas are one of the most common islet cell tumors, and they are frequently functionally active. Insulinomas are usually benign lesions but may be malignant in 5–10% of the occasions. They can appear on any location of the entire pancreas, as a richly vascular lesion. They typically present with signs and symptoms of hypoglucemia, and they are early diagnosed with a small size (<2 cm).

The diagnosis is based on hormonal determination in an appropriate clinical setting. Imaging is requested to locate them and to exclude multiplicity. On US, detection of islet cell tumors is generally difficult due to small tumor size. When located, they appear like a small solid hypoechoic mass, with lack of calcification or necrosis. Internal color Doppler signal is a common feature.

Functional islet cell tumors are usually isoattenuated and rarely hypoattenuated compared to the surrounding pancreas on unenhanced CT. Most of insulinomas are hypervascular lesions on arterial phase. Some tumors remain visible in the parenchymal or portal venous phase of enhancement, but most of them become isodense to the pancreas and cannot be detected on this phase. Calcifications can appear in up to 25% of cases.

On MRI, insulinomas are low in signal intensity on T1-weighted images and high in signal intensity on T2-weighted images. Small insulinomas typically enhance homogeneously on immediate postgadolinium images. Larger tumors, greater than 2 cm, often show a ring enhancement. Liver metastases typically have peripheral ringlike enhancement, although small metastases tend to enhance homogeneously. Enhancement of small metastases frequently occurs transiently in the capillary phase of enhancement, and they completely fade on images acquired 1 min after injection. Signs of local invasion and the detection of metastases are the only means available for distinguishing malignant from benign variants.

MRI performs superiorly to CT and angiography for their detection, although endoscopic ultrasound and percutaneous transhepatic catheterization of the portal vein and immunoassay for insulin of blood samples taken from the splenic and portal veins for localization of insulinoma usually show better performance than other noninvasive imaging tests. Despite of these imaging methods in preoperative location of insulinomas, they may not replace through and careful palpation of the pancreas at the time of surgery, especially if intraoperative ultrasound is added.

Imaging Findings

Figure 3.6.1: Axial TSE T2-weighted sequence demonstrates a small hyperintense lesion in the pancreatic head of 1.2 cm (*arrow*). This lesion is also hypointense on axial GE T1-weighted sequence (Fig. 3.6.2, *arrow*). Figure 3.6.3: On postcontrast dynamic THRIVE in arterial phase, this nodule presents homogeneous and intense enhancement (*arrow*). This lesion also shows an important restriction on DWI with high *b* value (Fig. 3.6.4, *arrow*). Hypervascular focal liver lesions during arterial phase of postcontrast dynamic series are identified in segments 8 and 2 (Fig. 3.6.5, *arrows*). A malignant insulinoma with hypervascular liver metastases was confirmed posteriorly.

Case 7

Unresectable Pancreatic Carcinoma

Fig. 3.7.1

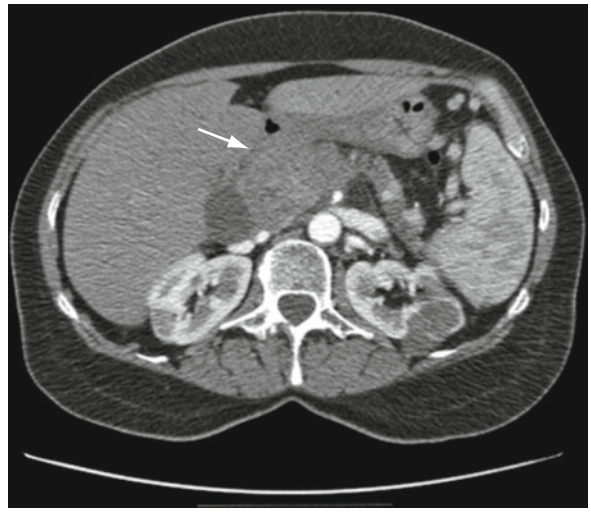

Fig. 3.7.2

Fig. 3.7.3

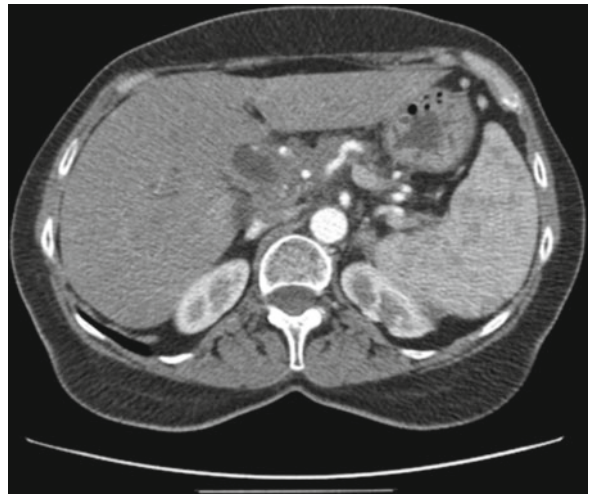

Fig. 3.7.4

A 62-year-old female with painless obstructive jaundice was sent to our imaging department to exclude obstruction of the biliary system.

Comments

Pancreatic adenocarcinoma is a malignancy that arises from ductal epithelium of the exocrine portion of the gland. It accounts for 95% of malignant tumors of the pancreas. Approximately 60–70% of pancreatic adenocarcinomas occur in the head, 15% in the body, 5% in the tail, and 10–20% show a diffuse involvement. Tumors in pancreatic head tend to encroach on the common bile duct, major papilla, and duodenum. At the moment of diagnosis, tumors of the pancreatic head usually are smaller in size than those in the body, because of the development of obstructive painless jaundice. Diagnosis of pancreatic adenocarcinoma is made when the tumors are relatively large (about 5 cm) and have extended beyond the pancreas in up to 85% of cases. Carcinomas involving the body and tail of the pancreas grow insidiously and have often already metastasized widely at the time of diagnosis. The rich lymphatic supply and lack of a capsule of the pancreas account for the early spread of cancer to regional lymph nodes. The only effective treatment is surgical resection. Only a small percentage of pancreatic cancers are resectable at the time of diagnosis, because of early lymphogenous and hematogenous spread and propensity for invasive growth. Imaging is essential to correctly stage pancreatic adenocarcinoma, which will mark both therapeutic management and prognosis.

Imaging criteria of unresectable pancreatic carcinoma

- Vascular invasion is a relative criterion for the lack of resectability, depending on the extent of vascular involvement. A circumferential vessel involvement over 50% makes tumor unresectable. However, in between 25% and 50% of vascular invasion makes its resectability questionable.
- Metastatic spread outside the pancreas makes tumor irresectable.
- Tumor invasion into adjacent organs signifies unresectability.
- Ascites is seen in advanced stages and implies peritoneal carcinomatosis or invasion of the lesser sac. Irregular increase in density of the omental fat is highly suggestive of peritoneal carcinomatosis.

Figure 3.7.1: On US, an enlarged, slightly hypoechoic, pancreatic mass is identified at the head of the pancreas (*arrow*). Fig. 3.7.2: On enhanced CT scan on the arterial phase, a hypodense and hypovascular mass in the head of the pancreas is identified (*arrow* on Fig. 3.7.2) which infiltrates the portal vein, as shown on Fig. 3.7.3, coronal MPR of portal phase postcontrast CT (*arrow*) and the bifurcation of celiac trunk (Fig. 3.7.4, enhanced CT scan on the arterial phase). This lesion produces an obstruction of common bile duct (*arrow* on Fig. 3.7.5, coronal MPR of portal phase postcontrast CT (*arrow*), with secondary dilatation of the proximal biliary system. The mass is in contact with the pylorus (Fig. 3.7.6, enhanced CT scan on the portal phase), indicating infiltration at this level (*arrow*). MRI confirmed the presence of a huge mass in the pancreatic head, appearing hypointense on T1-weighted GE image (Fig. 3.7.7, *arrow*), and demonstrating the hypovascular nature of the lesion (*arrow*), showing less contrast enhancement than the rest of the pancreatic parenchyma (Fig. 3.7.8, axial postcontrast THRIVE at portal phase).

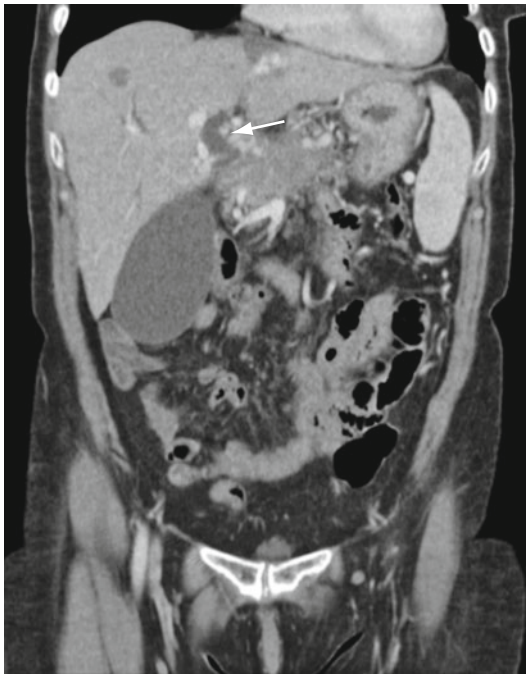

Fig. 3.7.5

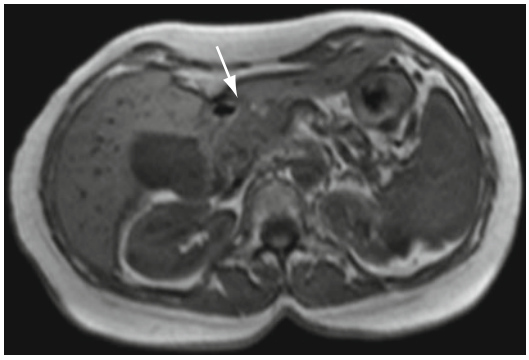

Fig. 3.7.7

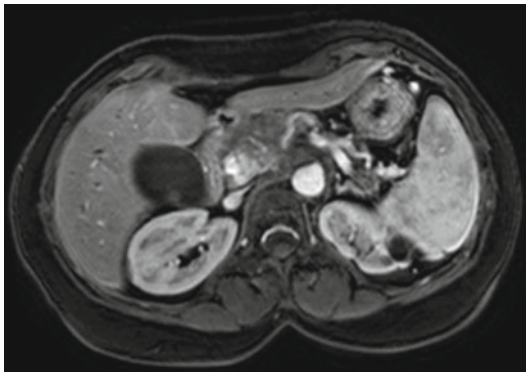

Fig. 3.7.9

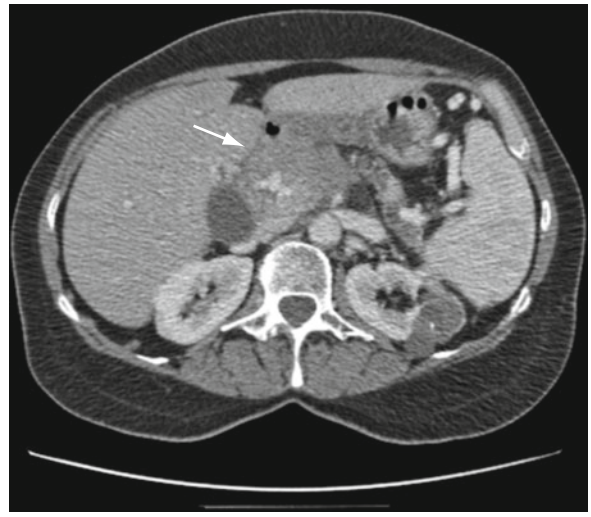

Fig. 3.7.6

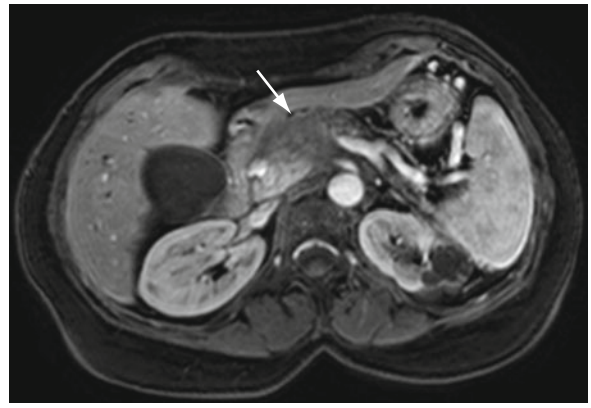

Fig. 3.7.8

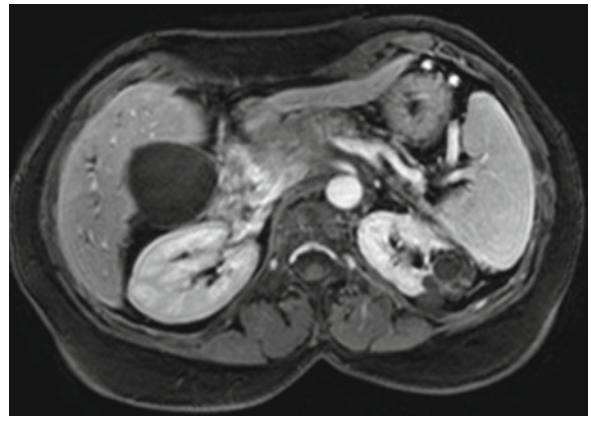

Fig. 3.7.10

The vascular invasion of the celiac trunk at its bifurcation (Fig. 3.7.9, axial postcontrast THRIVE at arterial phase), portal and splenic veins invasion (Fig. 3.7.10, axial postcontrast THRIVE at portal phase), and infiltration of the pylorus (Fig. 3.7.8) as well as the obstruction of common bile duct (Fig. 3.7.11, coronal HASTE, *arrow*) are confirmed with MRI. DWI shows hyperintensity of the mass with high *b* value consistent with biological aggressiveness (Fig. 3.7.12, *arrow*). The invasion of vascular structures and adjacent organs are criteria of unresectability.

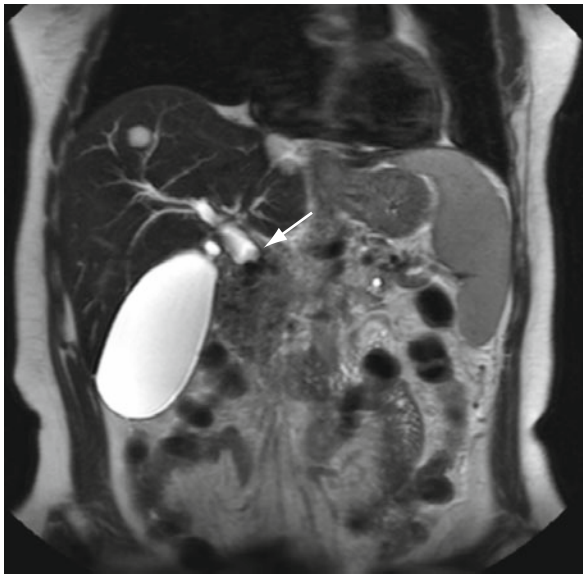

Fig. 3.7.11

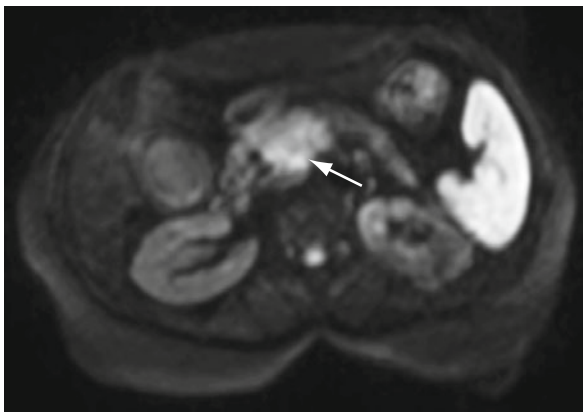

Fig. 3.7.12

Case 8
Resectable Pancreatic Carcinoma

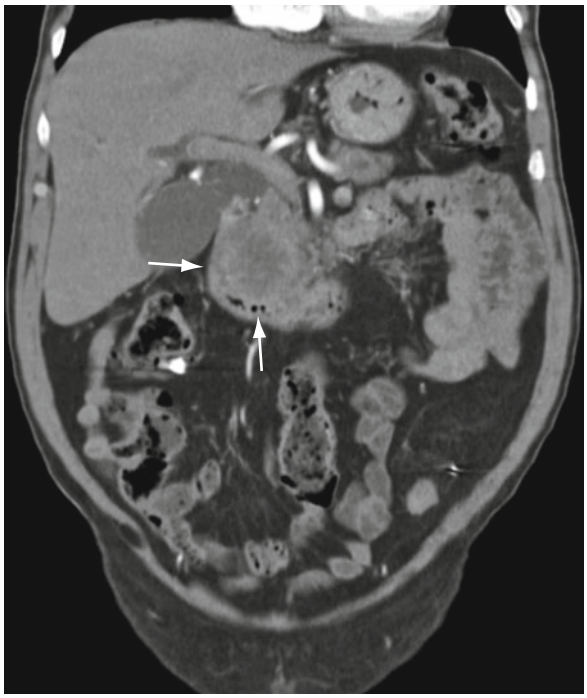

Fig. 3.8.1

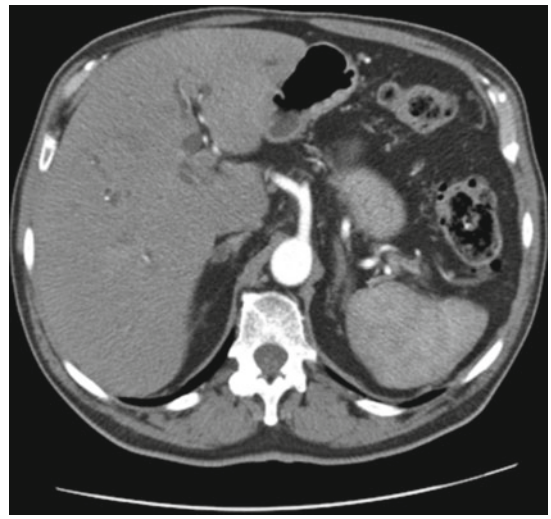

Fig. 3.8.2

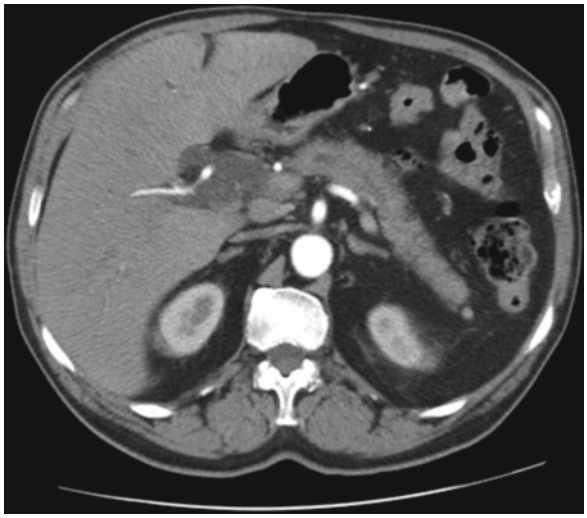

Fig. 3.8.3

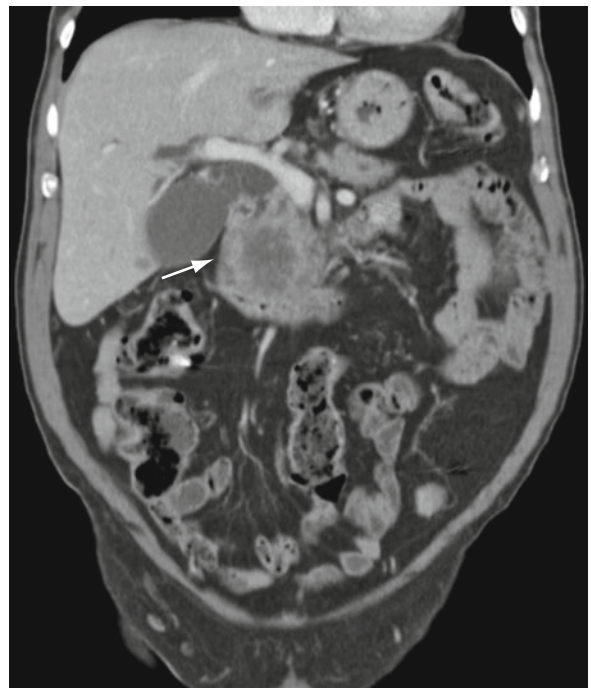

Fig. 3.8.4

A 67-year-old male in study because of great weight loss and painless jaundice was submitted to CT for further assessment.

Imaging criteria of resectable pancreatic carcinoma are:

- When no vascular invasion is seen or the circumferential vessel involvement is 25% or less.
- Lack of distant metastases.
- No invasion of adjacent organs, except duodenum, which is resected anyway.
- Presence of regional lymph node metastases does not necessarily render the tumor unresectable.

Imaging Findings

US is not a very effective tool for diagnosis of pancreatic carcinomas due to the often limitation for an adequate visualization of the pancreas. When a pancreatic carcinoma is detected, it appears as a poorly defined, homo- or heterogeneous hypoechoic mass.

On CT, pancreatic carcinomas are almost always isoattenuated compared to the parenchyma on unenhanced CT. On contrast-enhanced acquisitons, during the parenchymal phase, it appears as a hypoattenuated mass. Foci of intratumoral necrosis can simulate a pseudocyst.

MRI is the most sensitive tool to detect pancreatic carcinomas, which usually appear as low signal intensity masses on unenhanced T1-weighted sequences with fat suppression. Pancreatic tissue distal to pancreatic cancer often shows lower signal intensity than normal pancreatic tissue, secondary to tumor-associated pancreatitis distal to the tumor, because of obstruction of main pancreatic duct. When chronic inflammation occurs, there is progressive fibrosis and glandular atrophy, and the depiction of tumor is poorer. Tumors are usually minimally hypointense relative to pancreas on T2-weighted images and are difficult to visualize. Detection of carcinomas is best performed by immediate postgadolinium GE T1-weighted sequences, appearing as hypovascular lesions that enhance to a lesser extent than surrounding normal pancreatic tissue, because of their abundant fibrous stroma and relative sparse vascularity. DWI can also help in the diagnosis of pancreatic carcinoma, showing high signal intensity with high *b* values and lower ADC values compared to normal pancreas.

On CT, a huge mass located in the pancreatic head is clearly seen (*arrows*), presenting a hypodense central area, related to central necrosis (Fig. 3.8.1, coronal MPR of contrast-enhanced CT on the arterial phase). There is lack of invasion of the main arterial vessels, including the celiac trunk and its branches (Fig. 3.8.2, contrast-enhanced CT on the arterial phase) and superior mesenteric artery (Fig. 3.8.3, contrast-enhanced CT on the arterial phase). The portal vein is also resected (Fig. 3.8.4, Fig. 3.8.1, coronal MPR of contrast-enhanced CT on the portal phase). There is infiltration of the duodenum (Fig. 3.8.4), but this fact is not a contraindication for surgery. On MRI, a large stenosis of the common bile duct caused by the mass of the pancreatic head (*arrow*), as well as dilatation of main

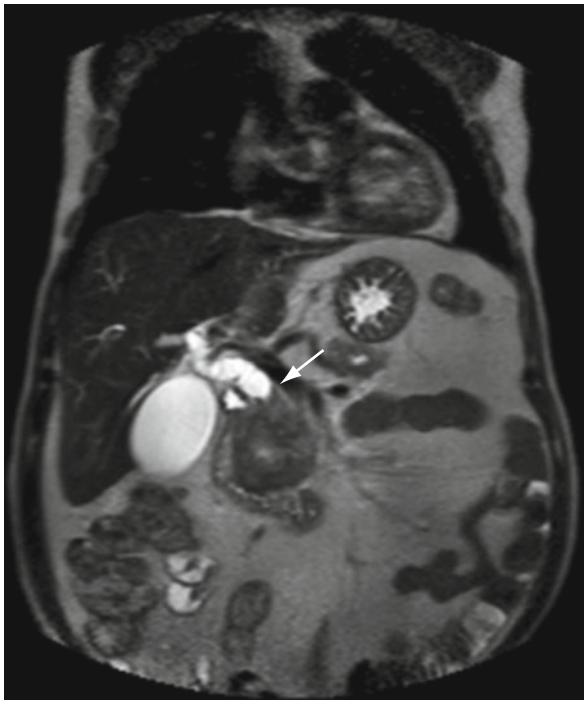

Fig. 3.8.5

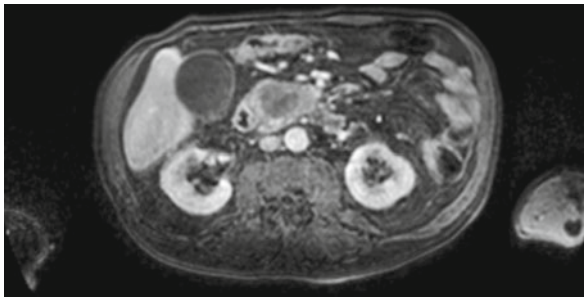

Fig. 3.8.7

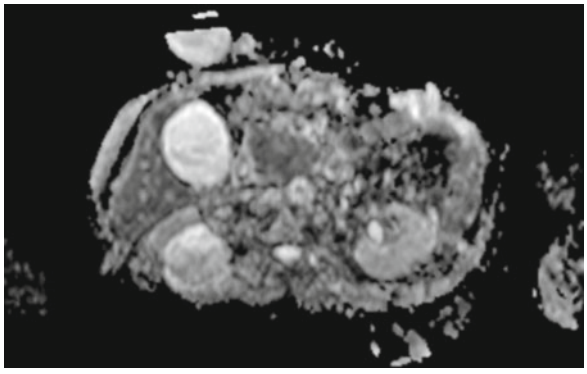

Fig. 3.8.9

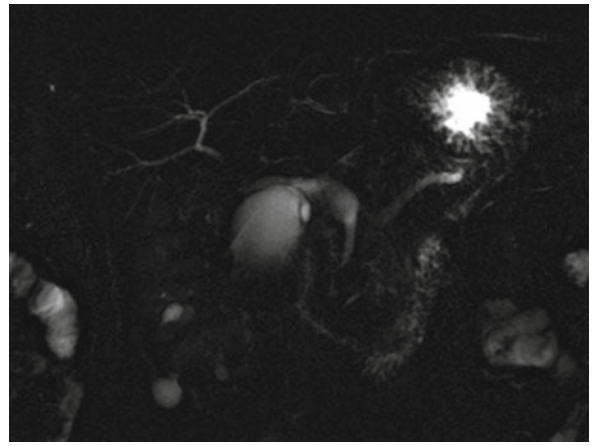

Fig. 3.8.6

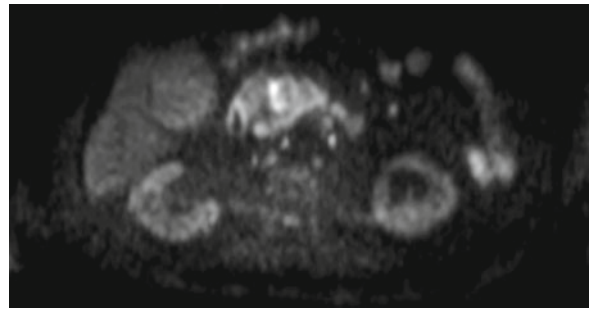

Fig. 3.8.8

pancreatic duct is visible (Figs. 3.8.5, coronal HASTE and 3.8.6, coronal thick-slice 2D MRCP). In postcontrast dynamic series during the portal phase, a hypovascular mass with a large necrotic center is demonstrated (Fig. 3.8.7). This lesion shows marked restriction of diffusion, appearing hyperintense on DWI with high *b* value (Fig. 3.8.8) and very hypointense on the ADC map (Fig. 3.8.9), confirming its hypercellularity.

Case 9

Traumatic Pancreatic Laceration

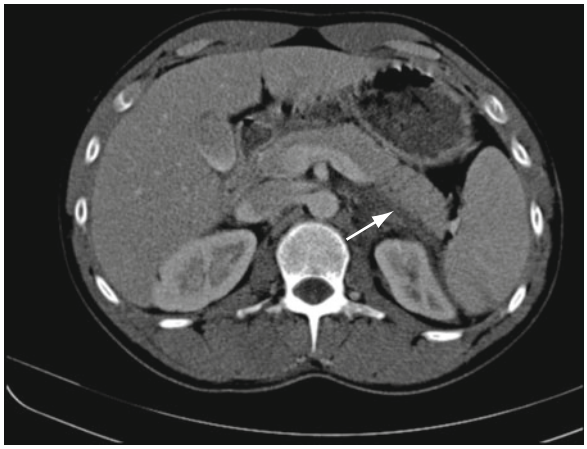

Fig. 3.9.1

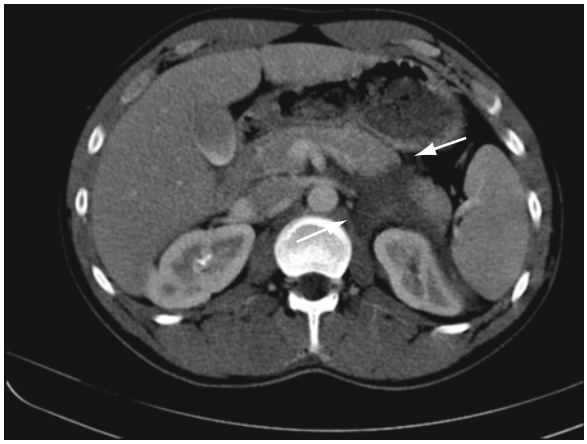

Fig. 3.9.2

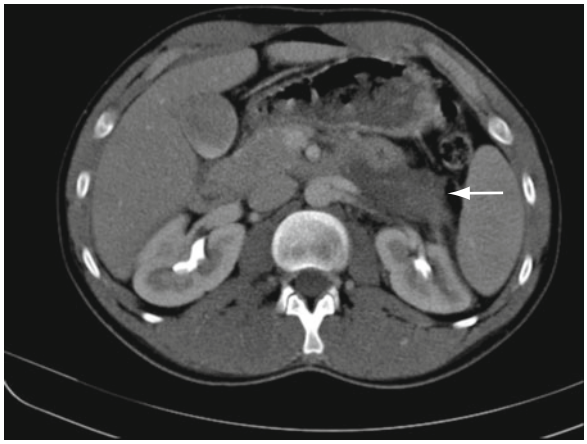

Fig. 3.9.3

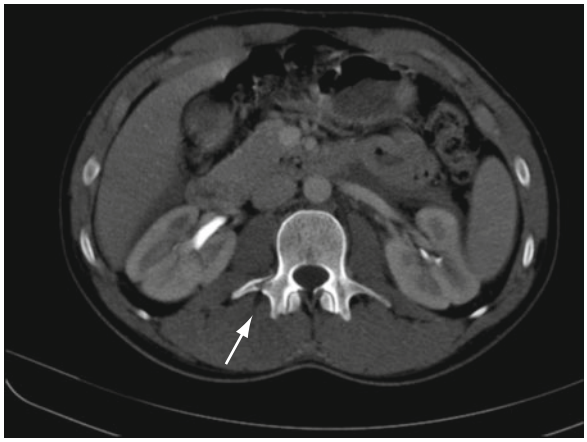

Fig. 3.9.4

An 18-year-old male, with blunt abdominal trauma and diffuse abdominal pain, presented to the ER with a slight decrease of blood pressure. A CT scan is performed.

Comments

Pancreatic injury is infrequent in blunt trauma, and it is usually associated with injuries to other organs such as duodenum and liver. It is seen more frequently in children or young adults. The pancreas is usually compressed against the spinal column, producing either a contusion, hematoma, laceration, or fracture.

Lacerations and fractures that rupture the pancreatic duct require emergency surgery. Stenosis of the pancreatic duct with distal ductal dilatation may be observed as a sequel of trauma.

In pancreatic laceration or fracture, CT shows interruption of the pancreatic body with associated hemorrhage in the anterior pararenal space. Less severe injuries may present as edematous swelling, a focal mass, or contour deformities, which may be associated with peripancreatic fluid collections. Indirect signs to look for are fluid collections around the superior mesenteric artery, transverse mesocolon, lesser sac, and between the pancreas and splenic vein. Evaluation of duct integrity is the terrain of MRCP.

Imaging Findings

On postcontrast CT examination during the portal phase, a subtle decrease of enhancement of the pancreatic tail is noticed (Fig. 3.9.1, *arrow*). In a caudal location of the same scan, a complete discontinuity of the pancreatic body and tail is identified along with a focal fluid collection, related to a complete pancreatic laceration (Fig. 3.9.2, *arrows*). There is also a moderate amount of fluid in the left anterior pararenal space (Fig. 3.9.3, *arrow*). Notice the presence of a fracture of the right transverse vertebral apophyses at this level (Fig. 3.9.4).

Case 10
Pancreatic Lipoma

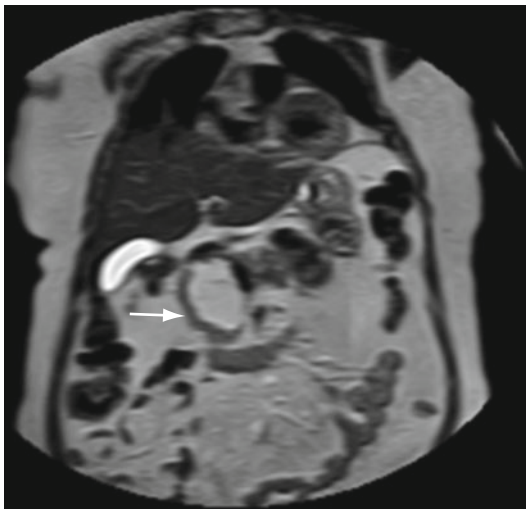

Fig. 3.10.1

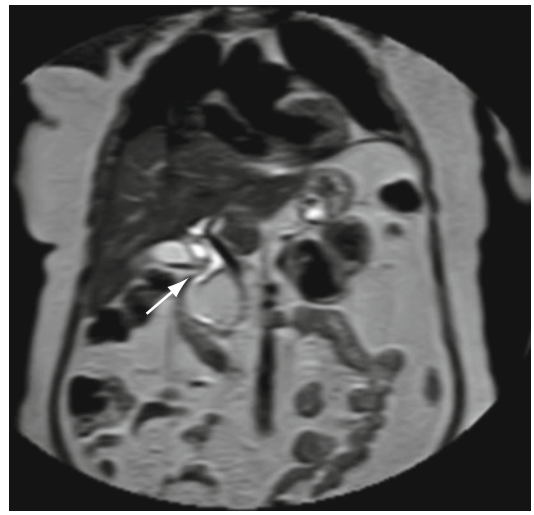

Fig. 3.10.2

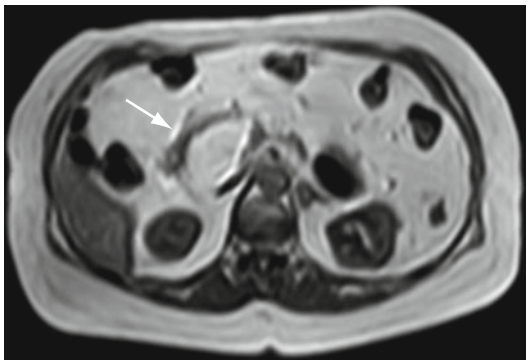

Fig. 3.10.3

Fig. 3.10.4

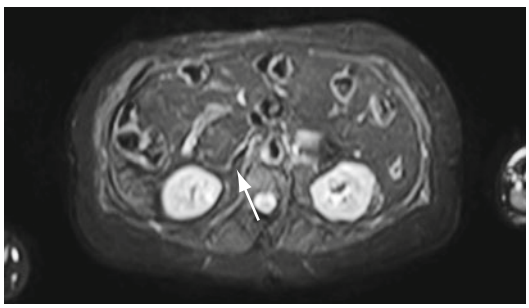

Fig. 3.10.5

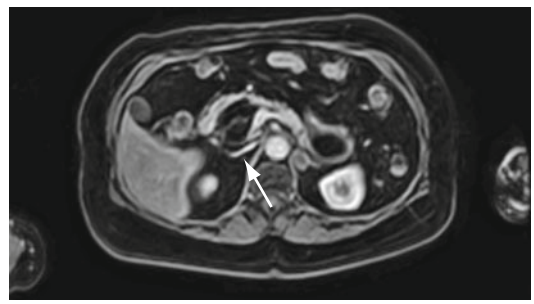

Fig. 3.10.6

A 67-year-old female with symptoms of dyspepsia and a cholestasis pattern in laboratory tests was submitted to the ER to perform a US where a mass in the head of pancreas was identified. MRI was requested for better characterization of this mass.

Comments

Pancreatic mesenchymal tumors are rare, accounting for only 1–2% of all pancreatic tumors, being pancreatic lipoma a very rare variant of them. This is a benign mesenchymal tumor consisting of mature adipose cells and thin collagen capsule.

This lesion appears on US as a well-demarcated, homogeneous, and almost isoechoic mass, compared to normal pancreatic parenchyma. On CT, pancreatic lipoma is seen as a capsulated very hypodense and homogeneous mass, with very low attenuation values in the range of fat. On basal MRI examination, these lesions present the same signal intensity than adjacent fat, appearing markedly hyperintense both on T1-weighted and T2-weighted images, losing signal with fat-suppressed sequences in a similar fashion to mesenteric fat. These features allow an accurate diagnosis of lipoma as in other body regions.

Imaging Findings

Figure 3.10.1: A mass, highly hyperintense on coronal HASTE, located in the pancreatic head, with internal septa is identified (Fig. 3.10.1, *arrow*). This mass produces mass effect over the common bile duct with displacement, extrinsic compression, and subsequent choledochal dilatation (Fig. 3.10.2, coronal HASTE, *arrow*). On axial in-phase GE T1-weighted image, the lesion is also very hyperintense (Fig. 3.10.3, *arrow*), not showing loss of signal in out of phase sequence (Fig. 3.10.4, *arrow*). In fat-suppressed images, the mass appears hypointense, confirming its content in macroscopic fat (Fig. 3.10.5, *arrow*). In dynamic postcontrast series during the portal phase, the lesion shows only delayed septal and capsular enhancement (Fig. 3.10.6, *arrow*). Therefore, the lesion mimics the behavior of the surrounding intra-abdominal fat, confirming the diagnosis of intrapancreatic lipoma.

For Further Reading

Books

Ahuja AT, Griffith JF, Wong KT (2007) Diagnostic imaging: ultrasound. Amirsys, Salt Lake City

Balthazar EJ, Pozzi Muccelli R, Megibow AJ (2009) Imaging of the pancreas: acute and chronic pancreatitis. Springer-Verlag, Berlin-Heidelberg

Federle M (ed) (2009) Diagnostic imaging abdomen, 2nd edn. Amirsys Publishing Inc, Salt Lake City

Heiken J (2009) Pancreatic Cancer (Contemporary Issues in Cancer Imaging). Cambridge University Press, New York

Semelka RC (2010) Abdominal-pelvic MRI, 3rd edn. Wiley/Blackwell, Chichester/Hoboken

Webs

http://www.esgar.org/
http://www.ctisus.com/
http://chorus.rad.mcw.edu/index/48.html
http://emedicine.medscape.com/radiology#gastrointestinal
http://www.eurorad.org/

Articles

Balthazar EJ (2002) Acute pancreatitis: assessment of severity with clinical and CT evaluation. Radiology 223:603–613

Bluemke DA, Cameron JL, Hruban RH, Pitt HA, Siegelman SS, Soyer P, Fishman EK (1995) Potentially resectable pancreatic adenocarcinoma: spiral CT assessment with surgical and pathologic correlation. Radiology 197:381–385

Braganza JM, Lee SH, McCloy RF, McMahon MJ (2011) Chronic pancreatitis. Lancet 377(9772):1184–1197

Brun A, Agarwal N, Pitchumoni CS (2011) Fluid collections in and around the pancreas in acute pancreatitis. J Clin Gastroenterol 45(7):614–625

Buetow PC, Miller DL, Parrino TV, Buck JL (1997) Islet cell tumors of the pancreas: clinical, radiologic, and pathologic correlation in diagnosis and localization. Radiographics 17:453–472

Cohen-Scali F, Vilgrain V, Brancatelli G, Hammel P, Vullierme M-P, Sauvanet A, et al (2003) Discrimination of unilocular macrocystic serous cystadenoma from pancreatic pseudocyst and mucinous cystadenoma with CT: initial observations. Radiology 228:727–733

Di Maggio EM, Solcia M, Dore R, Preda L, La Fianza A, Rodino C, et al (1996) Intrapancreatic lipoma: first case diagnosed with CT. Am J Roentgenol 167:56–57

Fatih Akisik M, Aisen AM, Sandrasegaran K, Gregory Jennings S, Lin C, Sherman S, et al (2009) Assessment of chronic pancreatitis: utility of diffusion-weighted MR imaging with secretin enhancement. Radiology 250:103–109

Gabata T, Matsui O, Kadoya M, Yoshikawa J, Miyayama S, Takashima T, et al (1994) Small pancreatic adenocarcinomas: efficacy of MR imaging with fat suppression and gadolinium enhancement. Radiology 193:683–688

H'ng MW, Kwek JW, Liao KH, Vu CK (2010) Cystic pancreatic lesions: a pictorial review and management approach. Singapore Med J 51(8):668–675

Ichikawa T, Haradome H, Hachiya J, Nitatori T, Ohtomo K, Kinoshita T, Araki T (1997) Pancreatic ductal adenocarcinoma: preoperative assessment with helical CT versus dynamic MR imaging. Radiology 202:655–662

Ichikawa T, Erturk SM, Sou H, Nakajima H, Tsukamoto T, Motosugi U, Araki T (2006) MDCT of pancreatic adenocarcinoma: optimal imaging phases and multiplanar reformatted imaging. Am J Roentgenol 187:1513–1520

Jeffrey RB Jr, Federle MP, Crass RA (1983) Computed tomography of pancreatic trauma. Radiology 147:491–494

Johnson PT, Outwater EK (1999) Pancreatic carcinoma versus chronic pancreatitis: dynamic MR imaging. Radiology 212:213–218

Katz DS, Nardi PM, Hines J, Barckhausen R, Math KR, Fruauff AA, et al (1998) Lipomas of the pancreas. Am J Roentgenol 170:1485–1487

Kim YH, Saini S, Sahani D, Hahn PF, Mueller PR, Auh YH (2005) Imaging diagnosis of cystic pancreatic lesions: pseudocyst versus nonpseudocyst. Radiographics 25:671–685

Kim SY, Lee JM, Kim SH, Shin KS, Kim YJ, An SK, et al (2006) Macrocystic neoplasms of the pancreas: CT differentiation of serous oligocystic adenoma from mucinous cystadenoma and intraductal papillary mucinous tumor. AJR Am J Roentgenol 187(5):1192–1198

Kim SH, Lim JH, Lee WJ, Lim HK (2008) Macrocystic pancreatic lesions: differentiation of benign from premalignant and malignant cysts by CT. Eur J Radiol 71(1):122–128

Macari M, Finn ME, Bennett GL, Cho KC, Newman E, Hajdu CH, et al (2009) Differentiating pancreatic cystic neoplasms from pancreatic pseudocysts at MR imaging: value of perceived internal debris. Radiology 251:77–84

Menassa-Moussa L, Halaby G, Braidy C (2010) Multiple pancreatic insulinomas: multislice CT. Abdom Imaging 35(6):690

Miller FH, Rini NJ, Keppke AL (2006) MRI of adenocarcinoma of the pancreas. Am J Roentgenol 187:W365–W374

Semelka RC, Cumming MJ, Shoenut JP, Magro CM, Yaffe CS, Kroeker MA, et al (1993) Islet cell tumors: comparison of dynamic contrast-enhanced CT and MR imaging with dynamic gadolinium enhancement and fat suppression. Radiology 186:799–802

Spanier BW, Bruno MJ (2011) Use of early CT scanning in patients with acute pancreatitis. Radiology 260(2):606

Wang Y, Miller FH, Chen ZE, Merrick L, Mortele KJ, Hoff FL, Hammond NA, et al (2011) Diffusion-weighted MR imaging of solid and cystic lesions of the pancreas. Radiographics 31(3):E13–E30

Xiao B, Zhang XM (2010) Magnetic resonance imaging for acute pancreatitis. World J Radiol 2(8):298–308

Spleen

4

Teodoro Martín Noguerol, Guadalupe Garrido, and Antonio Luna

Contents

A. Luna et al., *Learning Abdominal Imaging*, Learning Imaging,
DOI 10.1007/978-3-540-88003-5_4,

Case 1
Hemangioma

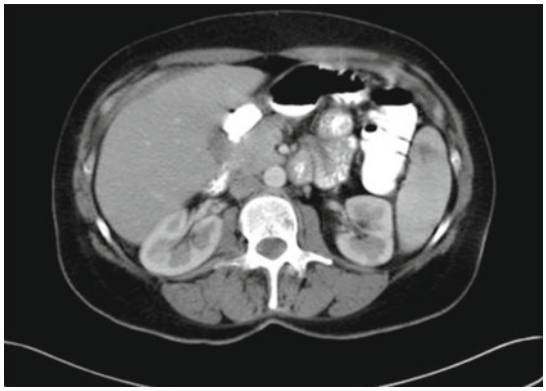

Fig. 4.1.1

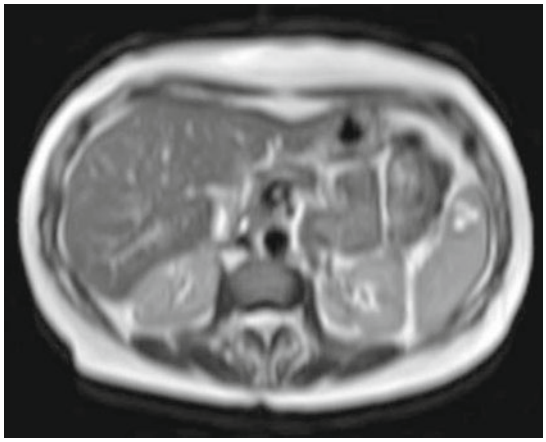

Fig. 4.1.2

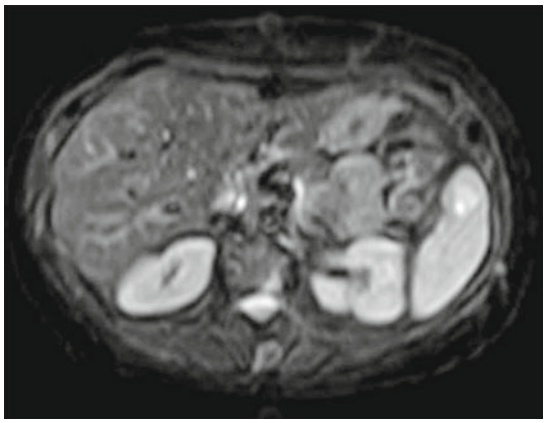

Fig. 4.1.3

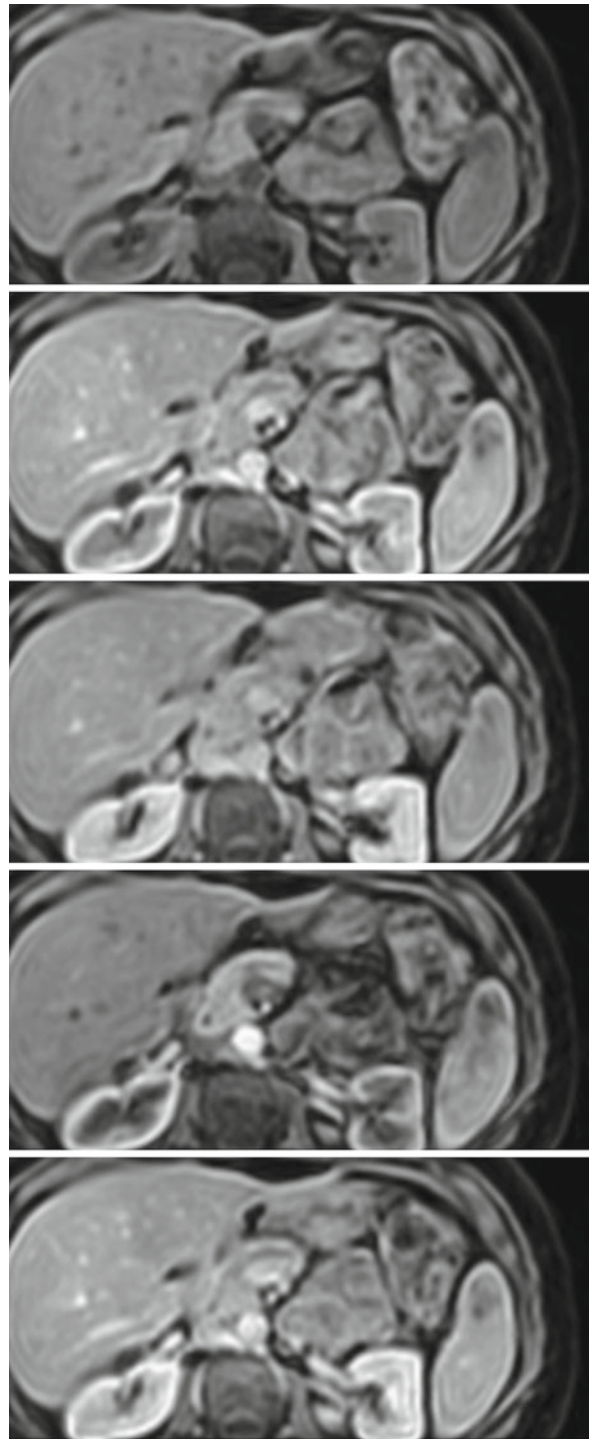

Fig. 4.1.4

A 59-year-old woman, who presents nonspecific abdominal discomfort of long duration, is derived for abdominal CT.

Comments

Hemangiomas are the most common primary neoplasms of the spleen. They are composed by endothelium-lined vascular channels filled with blood. They are usually asymptomatic, although symptoms appear when they reach a large size, either by compression or by bleeding. They can be single or multiple; in that case, they are often associated with angiomas in other locations as in the Klippel-Trenaunay syndrome. The two most common types of splenic hemangiomas are capillary and cavernous types. On ultrasound, hemangiomas behave as hyperechoic solid lesions. Those larger, cavernous hemangiomas may have internal cystic areas. On CT, capillary hemangiomas usually present as hyper- or isodense homogeneous nodules with enhancement on the arterial phase. Cavernous hemangiomas are hypodense in the baseline study with cystic areas of low attenuation, and they show progressive centripetal enhancement after contrast administration. They may show gross calcifications.

On MRI, splenic hemangioma typically appears as iso- or slightly hypointense on T1-weighted sequences and slightly hyperintense on T2-weighted images, as often occurs with hepatic hemangiomas. The dynamic sequence after administration of gadolinium may reveal three different enhancement patterns: immediate homogeneous enhancement that persists over time; peripheral enhancement in both early and late postcontrast phases; and, the most typical, progressive centripetal peripheral enhancement with a central fibrous scar. In contrast with liver hemangiomas, splenic hemangiomas do not have well-defined nodules that coalesce over time. Large hemangiomas can have variable appearance due to the existence of areas of necrosis, intralesional bleeding, or thrombosis.

Imaging Findings

Figure 4.1.1: Postcontrast CT on portal phase. A hypodense lesion with peripheral nodular enhancement margins is seen at anterior pole of spleen.

Figures 4.1.2 and 4.1.3: T2-weighted and STIR images show a hyperintense splenic lesion.

Figure 4.1.4: Dynamic-enhanced THRIVE series. Progressive centripetal peripheral enhancement is seen within the splenic lesion, consistent with hemangioma.

Case 2
Abscess

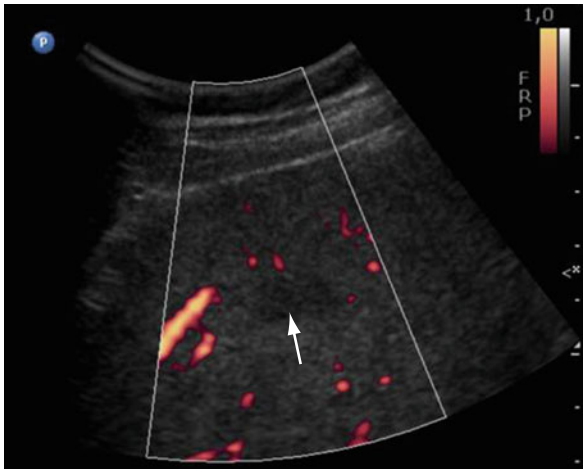

Fig. 4.2.1

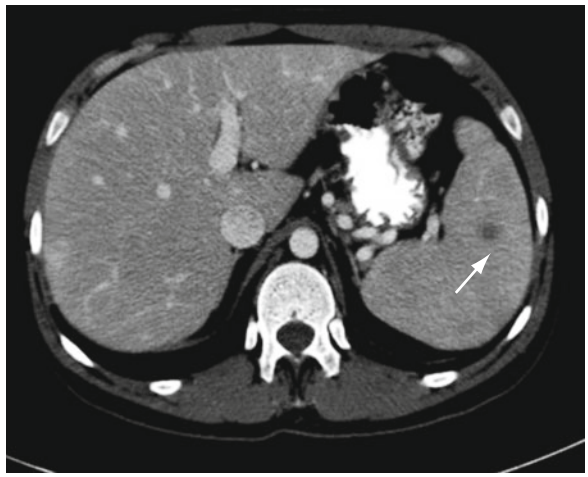

Fig. 4.2.2

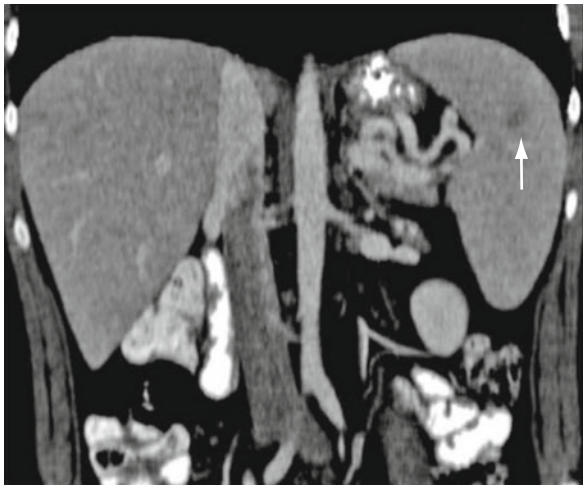

Fig. 4.2.3

Fig. 4.2.4

A 23-year-old man was referred for study of fever of unknown origin with left upper quadrant pain.

Comments

Splenic abscesses, due to inherent immune activity of the spleen are very rare, less than 1% in autopsies. However, there are predisposing factors like pyogenic infections, endocarditis, trauma, splenic infarcts, infections in the vicinity of the spleen, and immunosuppression, where the prevalence rises up to 25%. Bacterial or fungal abscesses are uncommon and frequently secondary to spread of infection, usually associated to endocarditis. Bacterial abscesses are usually larger than fungal ones. The most common infectious agents are *E. coli, Streptococcus, Staphylococcus,* and *Salmonella*. Among the fungi, *Candida* and *Aspergillus* are responsible for the majority of fungal infections in immunocompromised patients. Viral infection may result in splenomegaly but neither abscesses nor focal involvement are common features as in infections of other origins.

Abscesses usually present as fever, malaise, splenomegaly, and pain in the upper left quadrant. The presence of multiple hypodense lesions in the spleen in this clinical setting is very suggestive of abscesses.

On ultrasound, pyogenic abscesses may appear as poorly demarcated lesions, hypoechoic with fine echoes inside. On color Doppler images, typical pyogenic abscess shows no internal flow. Hepatosplenic candidiasis may present with the typical "target pattern", that is, hypoechoic lesion with hyperechoic center.

On unenhanced CT, abscesses appear as ill-defined hypodense lesions, which sometimes can have gas within it. After administration of contrast, they show a wall that enhances persistently with a hypoenhancing core.

MRI can reveal the presence of abscesses and distinguish its evolutionary stage. They are easily distinguished on T2-weighted sequences with fat suppression as hyperintense round foci. All focal infections tend to be hypervascular in their periphery on immediate postcontrast images, showing in delayed acquisitions, alteration of the perilesional perfusion. DWI has become a useful tool to detect and characterize splenic abscesses especially on their early phases.

Multiorganic involvement is the rule in cases of candidiasis, with hepatosplenic and less commonly renal microabscesses. Acute lesions, frequently subcapsular in location, are more evident in the spleen in comparison to those of the liver. They present as very small hyperintense lesions on T2-weighted images. Fat-suppressed SE T2-weighted sequences are useful in order to render these tiny lesions more conspicuous. After the administration of gadolinium, an intense peripheral enhancement is seen in the acute phase which diminishes in older lesions due to a fibrotic reaction. MR surpasses enhanced CT in the evaluation of these lesions.

Imaging Findings

Figure 4.2.1: Abdominal ultrasound. An ill-defined hypoechoic splenic lesion is seen without evidence of Doppler color signal within it (*arrow*).

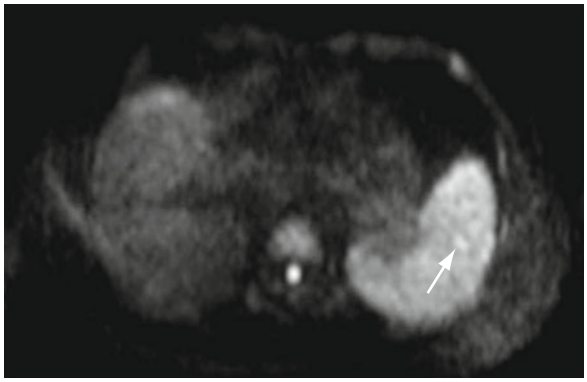

Fig. 4.2.5

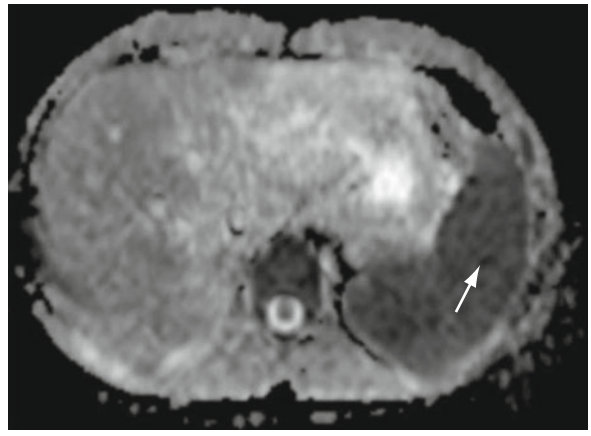

Fig. 4.2.6

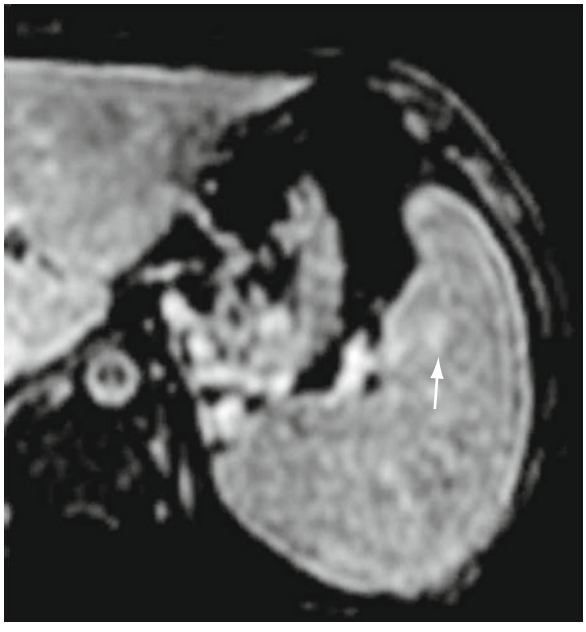

Fig. 4.2.7

Figures 4.2.2 and 4.2.3: Axial and coronal MPR of an enhanced abdominal CT in the portal phase. A hypodense splenic lesion with irregular wedges and slight hypodense peripheral rim is confirmed (*arrows*).

Figures 4.2.4, 4.2.5, and 4.2.6: Coronal HASTE, axial DWI with a *b* value of 1,000 s/mm^2, and corresponding ADC map. A slight isointense lesion with a thin hyperintense ring is seen on T2-weighted sequence at middle third of spleen (*arrow* on 4.2.4), more conspicuous on DWI sequence (*arrow* on 4.2.5), showing mild restriction of free water diffusion, as confirmed in the ADC map (*arrow* on 4.2.6).

Figure 4.2.7: Axial postcontrast THRIVE image in the delayed phase. The splenic lesion shows moderate delayed enhancement (*arrow*).

Case 3:
Metastasis

Fig. 4.3.1

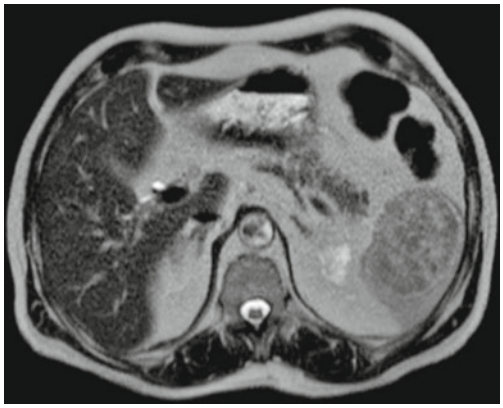

Fig. 4.3.3

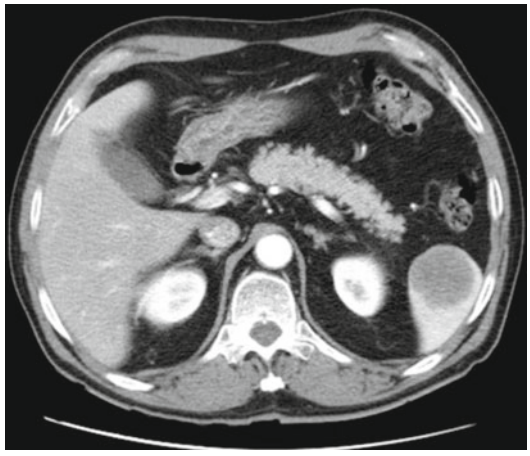

Fig. 4.3.2

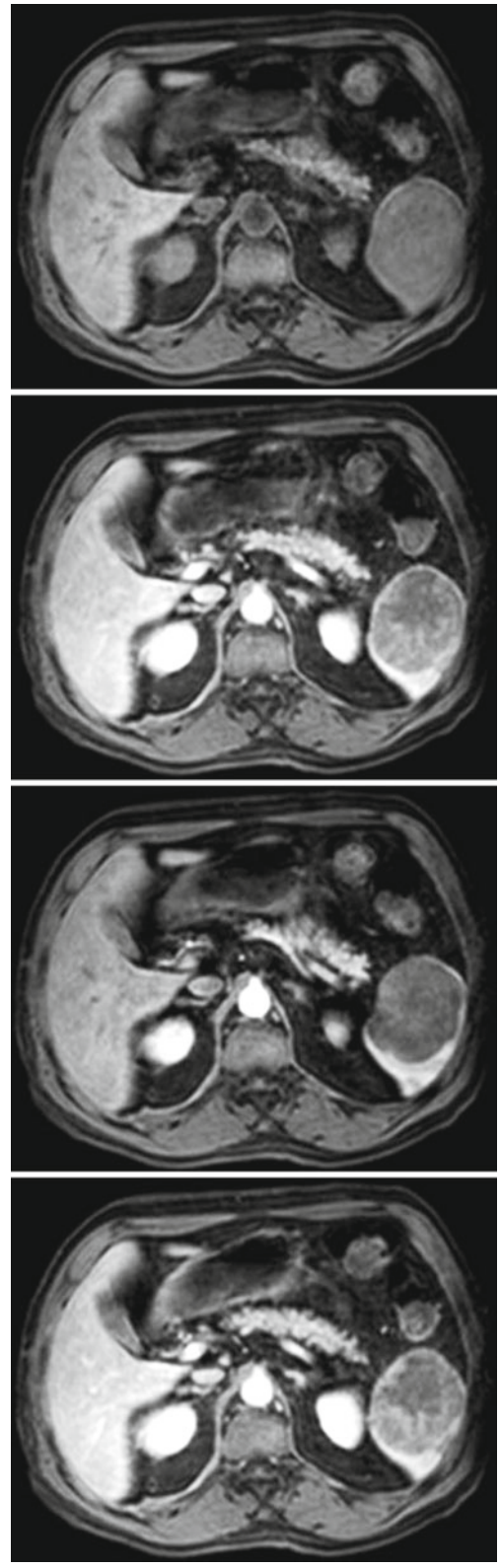

Fig. 4.3.4

A 75-year-old male referred for lung adenocarcinoma staging by CT. A splenic lesion is detected, further evaluated with abdominal MRI.

Comments

Spleen metastasis occurs by hematogenous spread, mainly by an arterial origin and a venous one in cases of portal hypertension. The frequency of splenic involvement by malignant tumors is between 4% and 36%. The tumors that most frequently affect the spleen are melanoma, breast, ovarian, lung, prostate, and gastric malignancies. However, splenic metastases are usually seen in cases of advanced disease, when there is involvement of other organs. Metastases usually appear as solitary or multiple nodules that may alter the splenic contour. They also can show cystic components. By ultrasound, metastases are usually displayed as single or multiple lesions, hypo- or hyperechogenic, with target morphology or infiltrative appearance. On CT, metastases appear as ill-defined nodules of variable size and low attenuation, which may have necrotic areas inside them, especially if they are large. These nodules are best delimited after contrast administration. Cystic metastases may occur in patients with melanoma, breast, ovarian, or endometrial cancer. Calcium-containing metastases are usually secondary to mucinous adenocarcinomas. MRI has proven high effectiveness in the detection and characterization of splenic metastasis. Metastases are more commonly isointense to the spleen on T1- and T2-weighted images, although they can be hyperintense on T2-weighted images mainly when necrosis or cystic components are demonstrated. Sometimes, high signal on T1-weighted images is shown in relation to hemorrhage or melanin within malignant melanoma's metastasis. These last two features can be used to distinguish metastases from lymphoma, as lymphoma rarely shows hemorrhage or necrosis. Metastases appear as hypovascular nodules on immediate postcontrast images, being isointense to spleen after the first postcontrast minute. The use of superparamagnetic iron oxide particles improves their detection.

Imaging Findings

Figure 4.3.1: Thoracic CT scout shows a large pulmonary mass at right superior lobe.

Figure 4.3.2: Enhanced abdominal CT at portal phase. A hypoenhancing lesion is identified at the inferior spleen pole.

Figures 4.3.3: Transverse T2-weighted image shows a heterogeneous lesion within the inferior splenic aspect which shows a thin peripheral hyperintense rim.

Figure 4.3.4: Transverse dynamic-enhanced THRIVE images. Poor and progressive, mainly peripheral, enhancement of the lesion compared with the rest of the splenic parenchyma is demonstrated. A central area of necrosis is also identified.

Case 4
Infarct

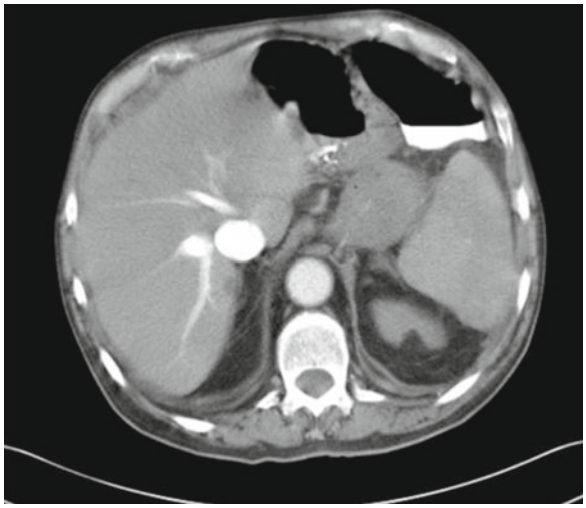

Fig. 4.4.1

Fig. 4.4.4

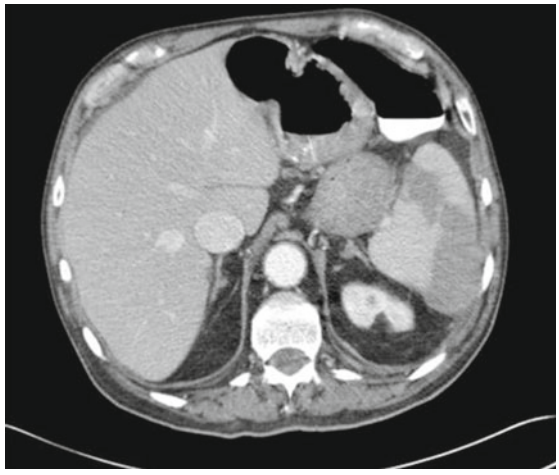

Fig. 4.4.2

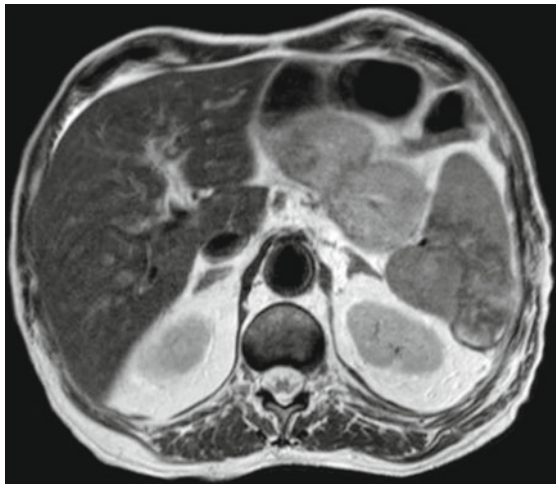

Fig. 4.4.3

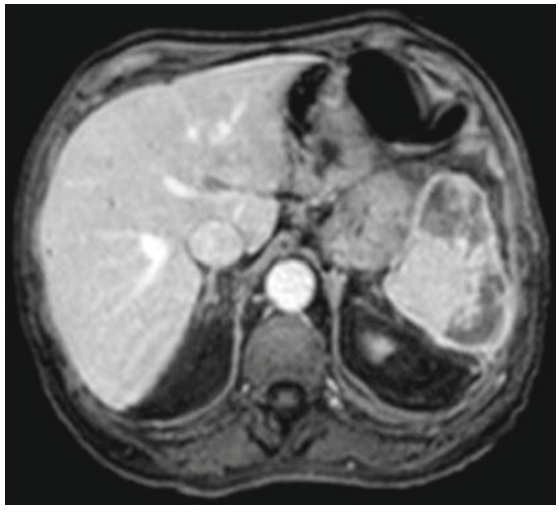

Fig. 4.4.5

A 75-year-old male with sudden abdominal pain is referred for evaluation of cholelithiasis and possible pancreatitis. Both splenic and renal lesions are detected.

Comments

Splenic infarction is due to occlusion of the arterial system of the spleen by local embolism or thrombosis secondary to multiple conditions such as atherosclerosis, stroke, lymphoma, myeloproliferative syndromes, sickle-cell anemia, storage diseases, vasculitis, trauma, and infections/abdominal inflammation such as pancreatitis or due to portal hypertension. Infarcts are usually asymptomatic, although sometimes they can present as sudden pain in left hypochondrium. The sonographic appearance of splenic infarct is a hypoechoic wedge shaped lesion, based to the capsular surface which points towards the hilum. In later stages, due to fibrosis, this area will become slightly hyperechoic. It is very useful for diagnosis of splenic infarction to use Doppler, as it allows us to confirm whether or not blood flow is present and to assess the presence of Doppler signal in the affected parenchymal area.

The semiology of splenic infarction by CT is similar to that described in ultrasound. The lesions have a peripheral, triangular morphology, with low attenuation on both unenhanced acquisitions and postcontrast administration baseline. It is very important to obtain images during the late parenchymal phase (60–70 s after contrast administration) to avoid false positives due to the heterogeneous enhancement experienced by the spleen in the early arterial phase. Using MRI, splenic infarcts appear equally as peripherally located areas of low signal on T1-weighted sequences and hyperintense on T2-weighted images. The absence of enhancement in both early and late phase after gadolinium administration is the key for the differential diagnosis with other entities. The splenic capsule may appear as a thin peripheral linear structure with important enhancement. The infarct may be complicated with infection, leading to abscesses or subcapsular hemorrhage or even splenic rupture as the cause of spontaneous hemoperitoneum.

Imaging Findings

Figures 4.4.1 and 4.4.2: Abdominal CT at arterial and portal phase, respectively. Multiple hypoenhancing splenic peripheral triangular shape areas are seen on portal phase, which are not depicted during the arterial phase.

Figures 4.4.3 and 4.4.4: Transverse and coronal TSE T2-weighted images. Moderate hyperintense areas are seen peripherally located on both upper splenic pole and inferior right renal pole (*arrow*). Note the presence of a slight irregular hypointense rim on the splenic lesion due to chronic microhemorrhage.

Figure 4.4.5: Axial postcontrast THRIVE image during the portal phase. Hypoenhancing areas are identified within splenic parenchyma on peripheral location. The splenic capsule is displayed as a thin hyperenhancing line.

Case 5
Splenic Trauma

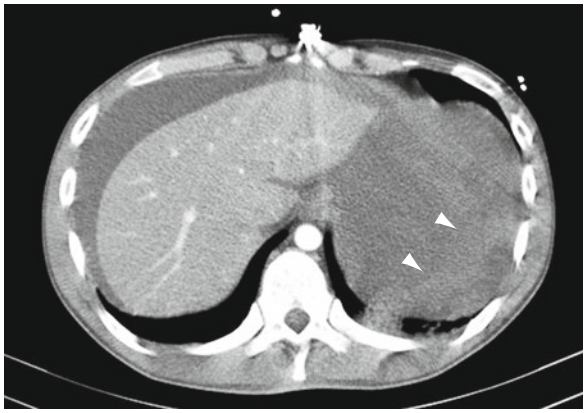

Fig. 4.5.1

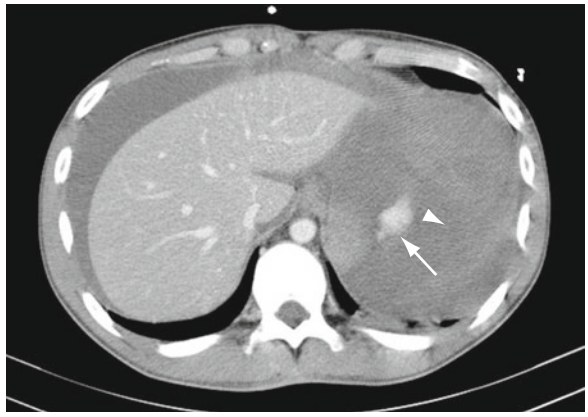

Fig. 4.5.2

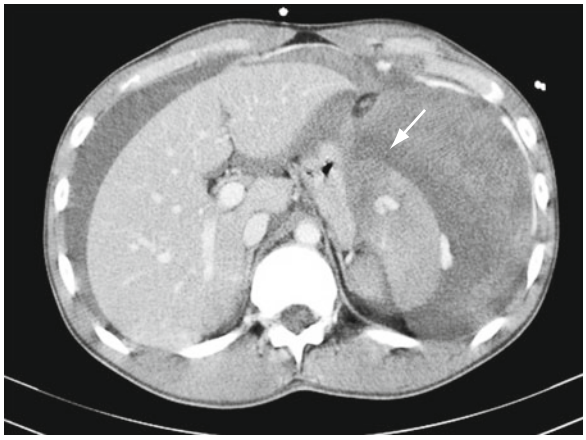

Fig. 4.5.3

Fig. 4.5.4

A 22-year-old boy, who has suffered a motorcycle accident, presents hypotension and abdominal pain. ER requests abdominal CT for evaluation of possible splenic injury.

Comments

Spleen is the abdominal viscera most frequently injured in blunt abdominal trauma and often is accompanied by injuries in other structures. Clinically, it presents with left upper quadrant pain radiating to left shoulder, hypotension, and low hematocrit which may lead to hypovolemic shock. The degree of involvement can vary between subcapsular hematoma to parenchymal laceration or visceral rupture. Ultrasound is a rapid, accessible, and noninvasive technique useful in the diagnosis of abdominal trauma, especially due to its high sensitivity for the detection of free fluid. However, it sometimes can fall short in assessing the parenchymal splenic damage, especially if other injuries are associated, being ultrasound reserved for hemodynamically unstable patients. That is why CT is the study of choice for assessment of splenic trauma in hemodynamically stable patients with a sensitivity above 95% to evaluate the degree of parenchymal involvement, the presence of hemoperitoneum, and to rule out other associated visceral injuries or both thoracic and axial skeleton damages. On CT, a subcapsular hematoma appears as a semilunar collection of low attenuation in the splenic edge. The presence of sentinel clot, a patchy hyperattenuating structure (with a density of about 60 HU) within free fluid in the vicinity of the spleen, increases the suspicion of splenic injury. Tears or lacerations of the spleen appear as dashed line defects of low attenuation, which, if in contact with the surface, are called fractures. Again, caution should be taken with heterogeneous enhancement experienced by the spleen during the early capillary phase. Extravasation of contrast material is a sign of active bleeding that almost always requires immediate surgical treatment. This sign of splenic hemorrhage may be absent in cases of significant hypovolemia. A proper assessment of splenic injury is needed to establish both prognosis and treatment. For this aim, the American Association of the Surgery of Trauma (AAST) developed in 2003 a guide to stage the severity of the injury and to establish which patients would benefit from surgical treatment and which from a conservative one. This classification take into account the integrity of the capsule, the size of the hematoma, the number and length of lacerations, and vascular involvement.

Imaging Findings

Figure 4.5.1: Transverse abdominal CT during the arterial phase. Severe amount of free spontaneous hyperdense (50–60 HU) fluid (*arrowheads*) is seen at both perihepatic and left hypochondrium areas.

Figure 4.5.2: Transverse abdominal CT during the portal phase. At the same level as in Fig. 4.5.1, a hyperdense ill-defined area is displayed due to extravasation of iodine contrast, findings consistent with active bleeding (*arrow*). Note also the increase of attenuation (80 HU) within the free fluid, especially at left hypochondrium (*arrowhead*).

Figures 4.5.3 and 4.5.4: Transverse and coronal MPR images of an abdominal CT during portal phase. A hypoenhanced ill-defined lesion is identified at the superoanterior aspect of the spleen with several hyperdense foci due to active bleeding (*arrows*). Notice the laminar peripheral disposition of the extravasated iodine contrast (*arrowhead*). These findings described are consistent with splenic rupture.

Case 6
Splenic Lymphoma

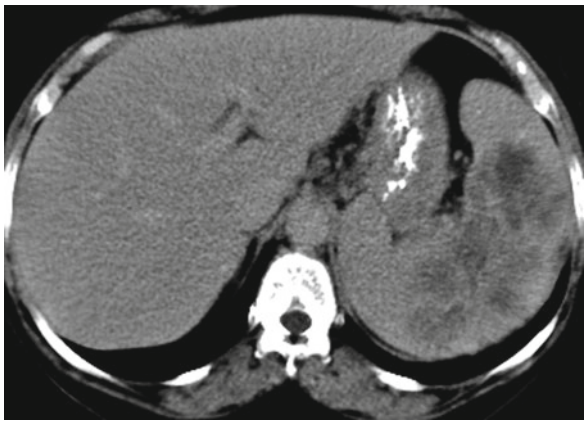

Fig. 4.6.1

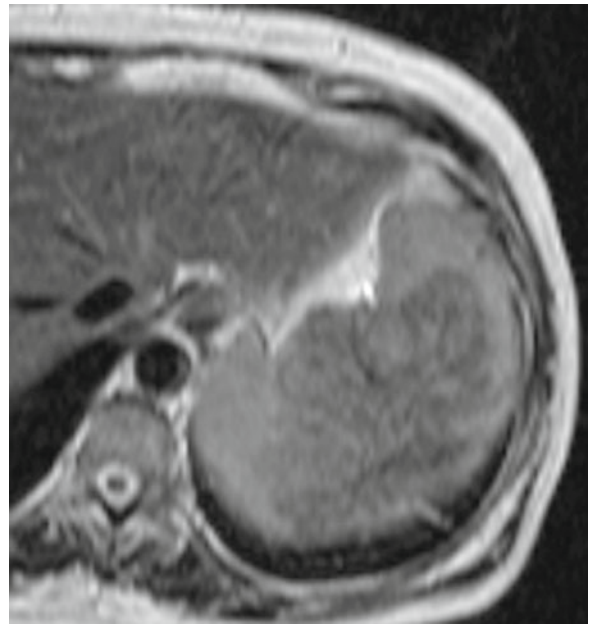

Fig. 4.6.2

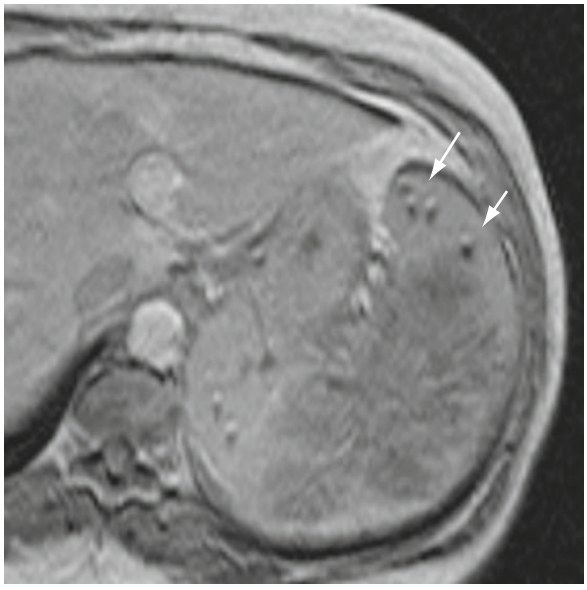

Fig. 4.6.3

Fig. 4.6.4

47-year-old female with left abdominal pain and weight loss during 3 months. A routine ultrasound study demonstrated a splenic mass (not shown). CT and MR were performed for further characterization.

Comments

Lymphoma is the most common malignancy involving the spleen. Both Hodgkin and non-Hodgkin lymphoma may present in the spleen either as the primary site or as a part of systemic involvement. Splenic involvement is present in up to 40% of the patients in both Hodgkin and non-Hodgkin lymphoma at the time of initial diagnosis. Most of the time, patients present with nonspecific clinical symptoms, splenomegaly, and usually with retroperitoneal adenopathy. Pathologically, lesions range from microscopic foci involving the spleen diffusely (infiltrative pattern) to gross lesion varying in size from small miliary nodules to a single or multiple large masses.

Splenic lymphoma is difficult to detect with imaging. Their different presentations make it a challenging diagnosis. In cases of secondary splenic lymphoma, the presence of retroperitoneal adenopathies is almost a constant finding, an associated splenomegaly which should alert the radiologist of the possibility of splenic lymphoma.

Diffuse, infiltrative splenic lymphoma is the most difficult form of presentation to detect by imaging. Focal disease, either solitary or multinodular, is commonly adequately detected by ultrasound, CT, or MR. CT and MR are superior to ultrasound in the detection and characterization of splenic lymphoma. It is very important to perform a dynamic postcontrast series to increase the detection of splenic lymphoma. Acquisition of immediate postcontrast images helps to differentiate normal and abnormal splenic areas. Immediate postcontrast images demonstrate hypovascular nodules which usually become isointense/isodense to the spleen within the first minute after the injection of contrast material, although variable delayed enhancement has also been reported. In a reduced number of cases, lymphoma may present as a solitary mass.

MR is superior to CT in the distinction between splenic lymphoma and metastases, as lymphoma usually is iso- or hypointense, and metastases are more commonly hyperintense on T2-weighted images compared to splenic parenchyma.

Imaging Findings

Figure 4.6.1: Contrast enhanced CT on the equilibrium phase shows a huge hypovascular and heterogeneous mass.

Figures 4.6.2 and 4.6.3: On the MR study, the mass is hypointense on T2 weighted-image (Fig. 4.6.2) and confirms its hypovascular nature on a postcontrast T1-weighted gradient-echo sequence on the portal phase (Fig. 4.6.3). The MR study revealed the spread of the tumor through the splenic capsule and the presence of siderotic nodules in the anterior pole of the spleen (*arrows*).

Figure 4.6.4: Splenectomy specimen reveals the nice correlation between histological and imaging findings. The histological analysis demonstrates a primary non-Hodgkin lymphoma.

Case 7
Gamna-Gandy Bodies in the Spleen

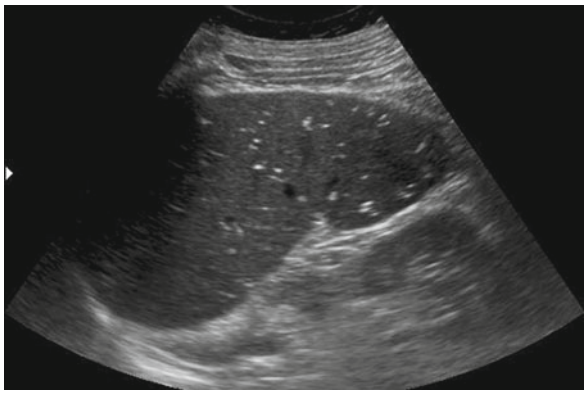

Fig. 4.7.1

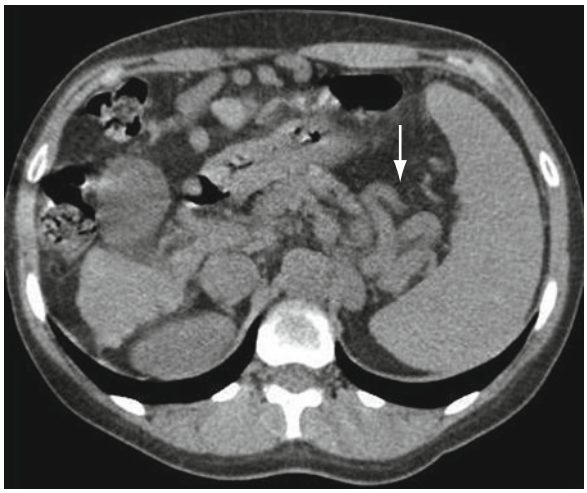

Fig. 4.7.2

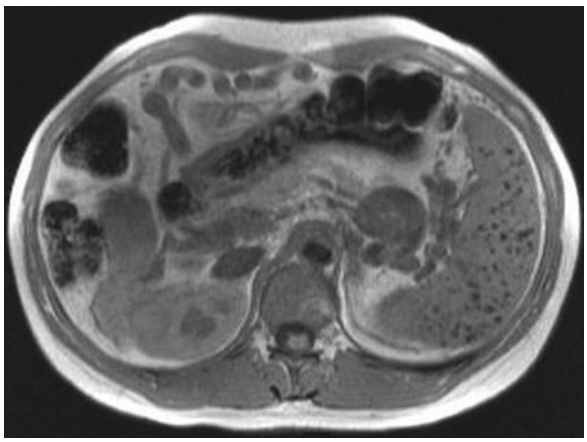

Fig. 4.7.3

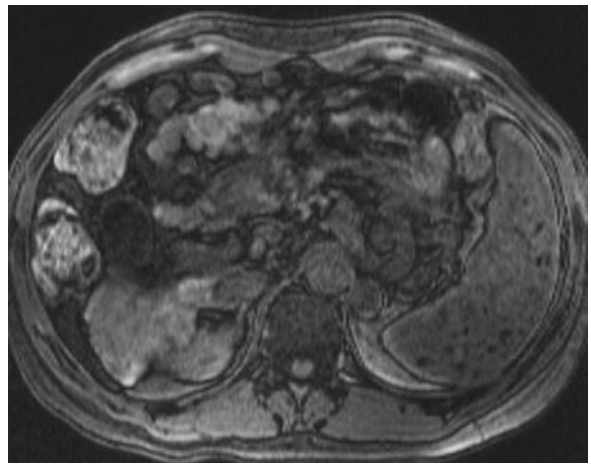

Fig. 4.7.4

Fig. 4.7.5

A 33-year-old woman with liver cirrhosis secondary to autoimmune hepatitis, and portal hypertension, registered on the liver transplant waiting list, underwent an abdominal CT and an MRI to rule out focal lesions in the liver.

Comments

Gamna-Gandy nodules (GGB) or siderotic nodules are small foci of intrasplenic hemorrhage, and they are composed of a combination of fibrous tissue, hemosiderin, and calcium. Their size is variable, being usually subcentimetric. Portal hypertension is the most common cause of Gamna-Gandy bodies development, appearing in about 9–12% of the cases. They can also be seen in other conditions, such as portal or splenic vein thrombosis, hemolytic anemia, leukemia, lymphoma, or paroxysmal nocturnal hemoglobinuria.

On ultrasonography, GGB appear as multiple, punctate, hyperechoic foci without acoustic shadowing scattered throughout the splenic parenchyma.

Nonenhanced CT may occasionally detect GGB, which would present as multiple faint hyperattenuating spots in the spleen, corresponding to calcification in siderotic nodules.

On MRI, Gamna-Gandy bodies appear as multiple small low-signal-intensity nodules on all pulse sequences, especially on T2-weighted SE or T2*-weighted GRE sequences due to "blooming" from susceptibility effects of the intralesional hemosiderin content. Lesion depiction improves on postgadolinium MR images since Gamna-Gandy bodies do not enhance, while normal splenic parenchyma enhances intensely.

In the setting of portal hypertension, splenomegaly, signs of hepatic cirrhosis, dilated collateral veins, or ascites may also be found.

Differential diagnosis should be established with calcified miliary tuberculosis, histoplasmosis, prominent vessels, phleboliths, and microabscesses. Usually, the clinical history and the presence of other extrasplenic findings aid in establishing the diagnosis.

Imaging Findings

Ultrasound image (Fig. 4.7.1) demonstrates mild splenomegaly with multiple hyperechoic spots with no posterior shadowing scattered throughout the parenchyma.

Unenhanced CT scan (Fig. 4.7.2) shows no focal lesion in the splenic parenchyma. Dilated collateral vessels are seen in the splenic hilum (*arrow*) related to portal hypertension.

T1-weighted MR image (Fig. 4.7.3) shows widespread hypointense nodules in an enlarged spleen. On T2*-weighted MR image (Fig. 4.7.4) and postgadolinium contrast MR image (Fig. 4.7.5), these nodules are more apparent. Note the dilated splenoportal collateral vessels (*arrow*).

Case 8

Splenic Invasion by Malignant Pleural Mesothelioma

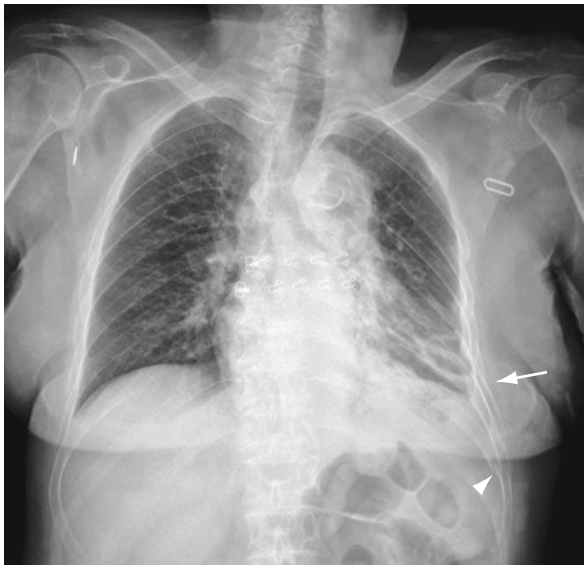

Fig. 4.8.1

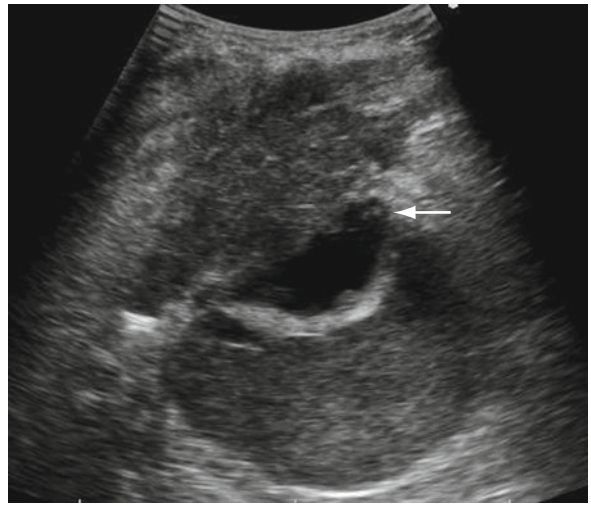

Fig. 4.8.3

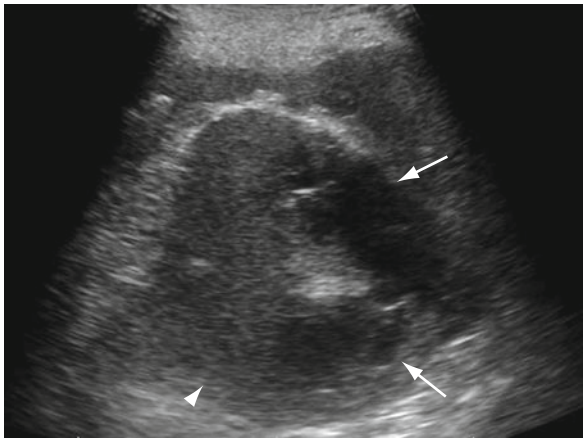

Fig. 4.8.2

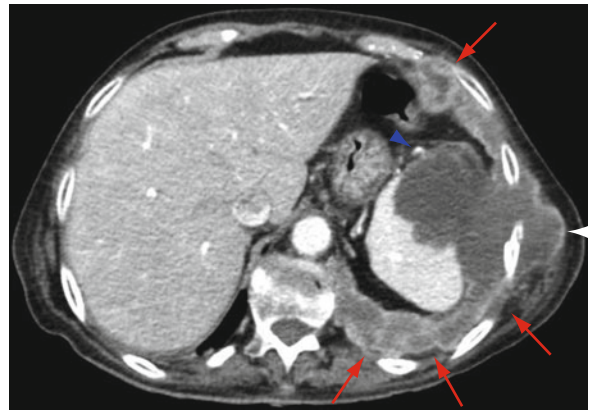

Fig. 4.8.4

A 70-year-old woman with a malignant pleural mesothelioma (MPM) under treatment with chemotherapy came to the ER with severe left upper quadrant pain. During the physical examination, a painful lump was noted in her left abdominal lateral wall, at the level of the eighth and ninth ribs. She underwent a chest and abdominal plain films and an abdominal ultrasound, and afterward, she was admitted in the hospital. An abdominal CT was performed the next day.

Comments

Direct invasion of the spleen by adjacent malignancies is uncommon, but may occur from a variety of neoplasms, most frequently gastric or colonic carcinoma, cancer of the pancreatic tail, renal cell carcinoma, neuroblastoma, or retroperitoneal sarcoma. MPM is a locally aggressive neoplasm, with frequent invasion of the chest wall, mediastinum, and diaphragm, being rare its extrathoracic extension (e.g., direct splenic or hepatic invasion, retroperitoneal spread).

Chest radiograph is not sensitive to demonstrate abdominal extension of MPM.

On ultrasonography, the imaging appearance of splenic invasion by MPM varies depending on the gross morphology ranging from solid to mixed to purely cystic lesion. The lesion can be nearly anechoic if necrosis predominates. In these cases, septations or low-level echoes, due to the presence of internal debris, may be present. Color Doppler ultrasound may show blood flow within the solid portions.

On CT, transdiaphragmatic spread of MPM is suspected when a soft-tissue mass encases the hemidiaphragm. Splenic invasion may be seen as a well-defined mass or as a lesion with lobulated and irregular contours, in contiguity with the adjacent primary MPM. The density of the lesion may be variable, being more hypodense as necrosis progresses.

In contrast to chest radiography and CT, MRI has a superior soft-tissue contrast. It improves the detection of tumor extension offering the possibility to differentiate invasion of the diaphragm from transdiaphragmatic tumor growth. Involvement of the diaphragmatic pleura, infiltration of the diaphragmatic muscle, and invasion of abdominal solid organs can be accurately assessed. Signal intensity of the splenic lesion may be variable, being more hyperintense on T2-weighted images as necrosis or cystic changes increase.

Imaging Findings

Chest film (Fig. 4.8.1) shows left pleural irregular thickening with loss of lung volume and mild pleural effusion. A pathologic fracture of the ninth left rib (*arrowhead*) and the thickening of the chest wall at this level (*arrow*) can be noted.

Ultrasound images (Figs. 4.8.2 and 4.8.3) demonstrate an irregular heterogeneous mass, with areas of high and low echogenicity (*arrowhead* and *arrows* on 4.8.2, respectively) and a cystic area with thickened walls and low-level echoes within it (*arrow* on 4.8.3) occupying the upper part of the spleen. The splenic lesion was in contiguity with the nodular pleural thickening (not shown).

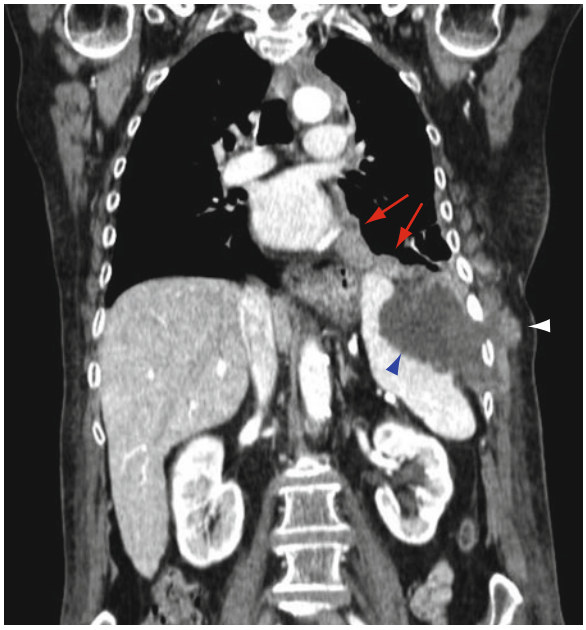

Fig. 4.8.5

Abdominal contrast–enhanced axial and coronal MPR CT images (Figs. 4.8.4 and 4.8.5) show diffuse nodular left pleural thickening with heterogeneous enhancement in relation with the MPM (*red arrows*). It invades ribs, muscles, and the subcutaneous tissue of the chest wall (*arrowheads*) and extends through the diaphragm to the abdominal cavity. The spleen is infiltrated by a well-defined low-attenuated mass with peripheral enhancement (*blue arrowheads*) consistent with extensive central necrosis.

Case 9

Secondary Hemochromatosis to Chronic Transfusion

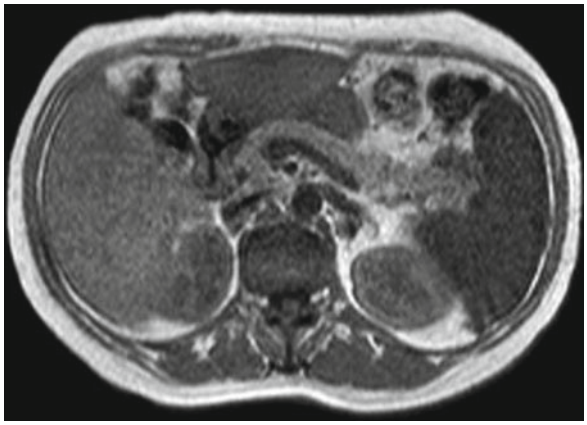

Fig. 4.9.1

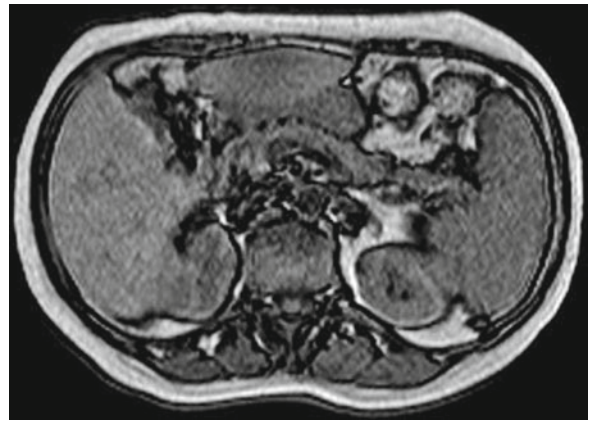

Fig. 4.9.2

Fig. 4.9.3

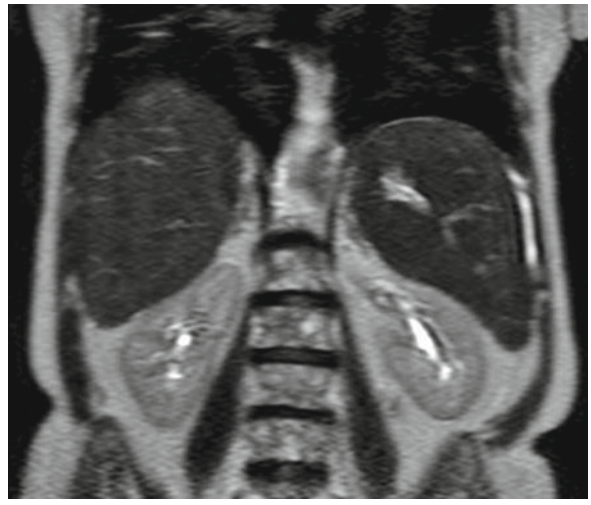

Fig. 4.9.4

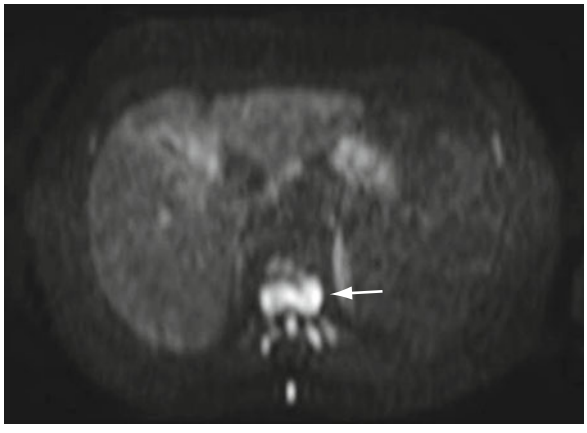

Fig. 4.9.5

A 59-year-old woman with a history of disseminated breast carcinoma, with hepatic and skeletal metastases, was receiving chemotherapy and repeated blood transfusions as part of her treatment. Significant laboratory data included increased levels of serum iron, percent transferrin saturation, and serum ferritin. MR study of the upper abdomen was performed.

Comments

Hemochromatosis is characterized by excess iron accumulation in various parenchymal organs. Hemochromatosis can be primary (genetic hemochromatosis) or secondary. Secondary hemochromatosis most commonly results from chronic blood transfusions. In these cases, excess iron deposits within the reticuloendothelial cells of the liver, spleen, and bone marrow, with sparing of the parenchymal cells. However, later in the disease process, parenchymal cells of other organs may accumulate iron (liver, pancreas, myocardium, and pituitary).

Secondary hemochromatosis due to chronic transfusions may or may not cause splenic enlargement.

Unenhanced CT shows increased attenuation in the spleen from iron deposition in the reticuloendothelial system as well as calcium deposition.

MRI is sensitive to the tissue deposition of iron; the signal intensity correlates with the amount of iron deposited. On T1- and T2-weighted MR images, the spleen shows a diffuse loss of signal intensity relative to the musculature, especially apparent on T2 spin echo (SE) and T2* gradient echo (GRE) sequences, as a result of iron deposition within the reticuloendothelial cells of the spleen. In addition, a decreased signal intensity of the liver may be present secondary to the iron deposition within the Kupffer cells.

On MRI, the signal intensity of the spleen may allow the distinction from primary hemochromatosis, in which the spleen is spared from the iron overload that is often present within the liver and other parenchymal organs.

On unenhanced CT, the differential diagnosis of increased splenic density should include other entities such as Thorotrast exposure or prolonged gold therapy.

Imaging Findings

T1-weighted in-phase (Fig. 4.9.1) and T1-weighted out-of-phase (Fig. 4.9.2) MR images show diffuse low signal intensity in the spleen, more evident on the in-phase acquisition, consistent with iron deposition within its reticuloendothelial cells. The liver and the pancreas are spared.

Axial and coronal T2-weighted MR images (Fig. 4.9.3 and Fig. 4.9.4) show enlargement and low signal intensity of the spleen. Note the hyperintensity in the imaged thoracic vertebra (*arrow*). This vertebra also shows high signal intensity on diffusion-weighted MR image (Fig. 4.9.5), suggestive of metastatic involvement (*arrow*).

Case 10
Gaucher Disease

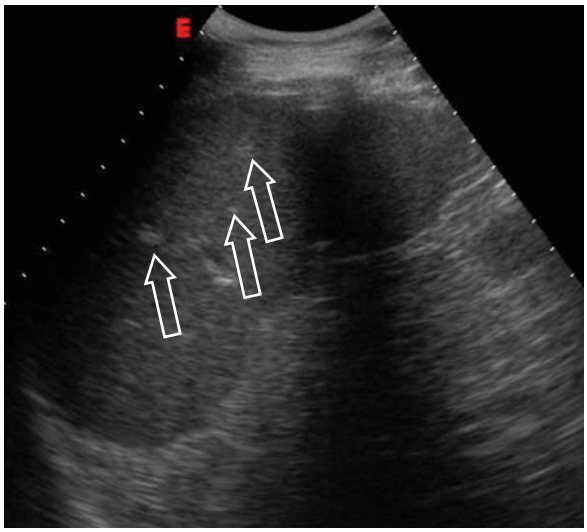

Fig. 4.10.1

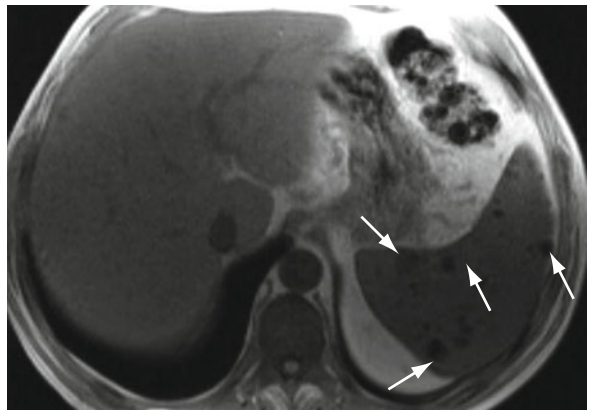

Fig. 4.10.2

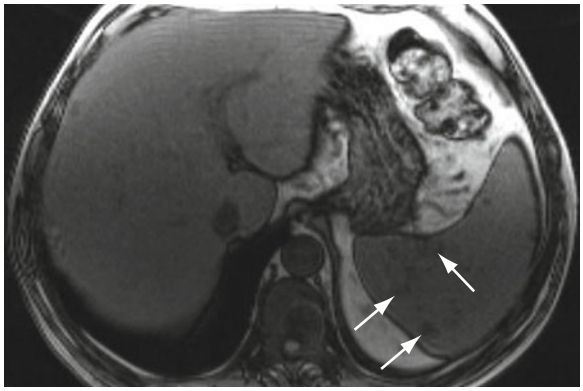

Fig. 4.10.3

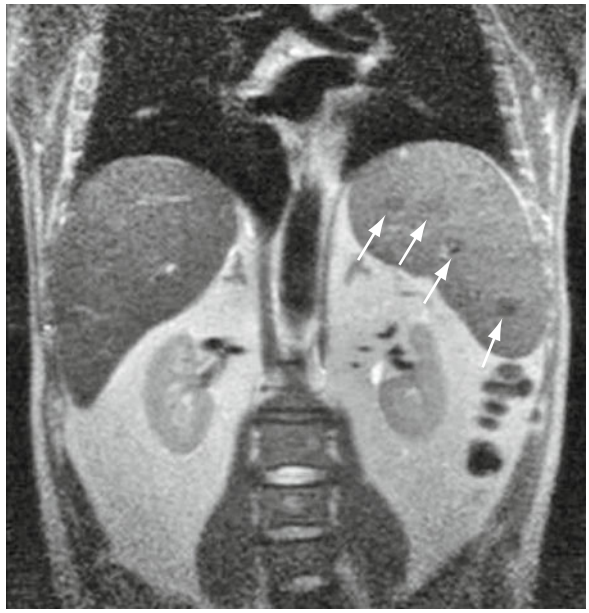

Fig. 4.10.4

A 53-year-old man, previously diagnosed of Gaucher disease with liver and bone marrow infiltration, presented with abdominal pain. Abdominal ultrasound and MRI were performed.

Comments

Gaucher disease is an autosomal recessive lysosomal disorder secondary to glucocerebrosidase deficiency, leading to accumulation of glucocerebrosides in the cells of the reticuloendothelial system and causing hepatosplenomegaly and skeletal disease due to the bone marrow infiltration.

Hepatosplenomegaly is invariably present. In 20–30% of patients, the spleen contains multiple nodules. Splenic nodules are of variable size, ranging from 0.5 to 6 cm in diameter. The nodules are thought to represent reticuloendothelial cells laden with glucocerebroside (the so-called Gaucher cells), fibrosis, or infarction. Splenic infarcts may appear in up to 30% of patients with Gaucher disease.

On ultrasonography, multiple, well-defined discrete hypoechoic or hyperechoic lesions may be found, corresponding to focal clusters of Gaucher cells and to Gaucher cells with fibrosis or infarction, respectively. A geographic pattern of irregular areas of infiltration by Gaucher cells interspersed with normal splenic parenchyma is less common.

On CT, the spleen may demonstrate multiple low-attenuating nodular lesions, without enhancement after intravenous contrast administration.

On MRI, the signal characteristics of the splenic nodules may be variable, with nodules of different signal intensity coexisting in the same spleen. Most of the splenic nodules appear iso- or slightly hypointense on T1-weighted images and hypointense on T2-weighted images without and with fat saturation, indicating nodular Gaucher cell deposits. In some patients, splenic nodules may appear hyperintense on T2-weighted images, finding that is thought to correspond to nodules associated with blood-filled dilated sinusoids.

The differential diagnosis of multiple lesions in an enlarged spleen should include lymphoma, leukemia, metastases, benign tumors, splenic cysts, infarction, and abscesses.

Imaging Findings

Ultrasound image (Fig. 4.10.1) shows an enlarged spleen with some subcentimeter hyperechoic lesions (*open arrows*).

Axial T1-weighted in-phase (Fig. 4.10.2) and opposed-phase (Fig. 4.10.3) and coronal T2-weighted (Fig. 4.10.4) MR images show hepatosplenomegaly and multiple hypointense nodular lesions of variable size in the splenic parenchyma (*arrows*), corresponding to focal clusters of Gaucher cells, fibrosis, or infarction.

Further Reading

Books

Federle M, Brooke Jeffrey R, Woodward PJ, Borhani B (ed) (2009) Diagnostic imaging abdomen, 2nd edn. Amirsys Publishing Inc, Salt Lake City

Lee JKT, Sagel SS, Stanley RJ, Heiken JP (eds) (2005) Computed body tomography with MRI correlation, 4th edn. Lippincott Williams & Wilkins, Philadelphia

Rumack CM, Wilson SR, Charboneau JW, Levine D (2011) Diagnostic ultrasound, 4th edn. Mosby, St. Louis

Semelka R (2010) Abdominal-pelvic MRI, 3rd edn. Wiley-Blackwell, Chichester/Hoboken

Skucas J (2006) Advanced imaging of the abdomen. Springer, Berlin

Web Pages

www.aast.org/
www.esgar.org/
www.sgr.org/
http://www.learningradiology.com/toc/tocorgansystems/tocgi.htm
http://www.eurorad.org/

Articles

Ahmed S, Horton KM, Fishman EK (2011) Splenic incidentalomas. Radiol Clin North Am 49(2):323–347

Benter T, Klühs L, Teichgräber U (2011) Sonography of the spleen. J Ultrasound Med 30(9):1281–1293

Clark R, Hird K, Misur P et al (2011) CT grading scales for splenic injury: why can't we agree? J Med Imaging Radiat Oncol 55(2):163–169

Clark TJ, Cardoza S, Kanth N (2011) Splenic trauma: pictorial review of contrast-enhanced CT findings. Emerg Radiol 18(3):227–234

Comarmond C, Jauréguiberry S, Vaillant JC et al (2010) Giant splenic abscess due to Salmonella enteritidis in a returning traveler. J Travel Med 17(4): 271–273

Dormagen J, Meyerdierks O, Gaarder C et al (2011) Contrast-enhanced ultrasound of the injured spleen after embolization – comparison with computed tomography. Ultraschall Med 32(5):485–491

Elsayes KM, Narra VR, Mukundan G et al (2005) MR imaging of the spleen: spectrum of abnormalities. Radiographics 25(4):967–982

Ertan G, Tekes A, Mitchell S et al (2009) Pediatric littoral cell angioma of the spleen: multimodality imaging including diffusion-weighted imaging. Pediatr Radiol 39(10):1105–1109

Forest F, Duband S, Clemenson A et al (2010) Traumatic subcapsular splenic hematoma revealing littoral cell angioma and Gaucher's disease. Ann Hematol 89(10): 1061–1062

Franco F, Monaco D, Volpi A et al (2011) The role of arterial embolization in blunt splenic injury. Radiol Med 116(3):454–465

Jakhere SG, Chemburkar VC, Yeragi BS et al (2011) Imaging findings of disseminated cysticercosis with unusual involvement of spleen and pancreas. J Glob Infect Dis 3(3):306–308

Jolobe OM (2010) Splenic infarct is a plausible alternative diagnosis in suspected splenic abscess. Eur J Intern Med 21(1):52

Karlo C, Gnannt R, Frauenfelder T et al (2011) Whole-body CT in polytrauma patients: effect of arm positioning on thoracic and abdominal image quality. Emerg Radiol 18(4): 285–293

Kaza RK, Azar S, Al-Hawary MM et al (2010) Primary and secondary neoplasms of the spleen. Cancer Imaging 10: 173–182

Luna A, Ribes R, Caro P et al (2006) MRI of focal splenic lesions without and with dynamic gadolinium enhancement. Am J Roentgenol 186(6):1533–1547

McInnes MD, Kielar AZ, Macdonald DB (2011) Percutaneous image-guided biopsy of the spleen: systematic review and meta-analysis of the complication rate and diagnostic accuracy. Radiology 260(3):699–708

Nagai Y et al (2010) Hepatosplenic alphabeta T cell lymphoma. Int J Clin Oncol 15(2):215–219

Pilz JB, Sperschneider T, Lutz T et al (2011) Littoral cell angioma in main and accessory intrapancreatic spleen presenting as splenic rupture. Am J Surg 201(2):e15–e17

Ray S, Mridha AR, Ahammed M (2011) Diffuse splenic infarction in a case of severe acute pancreatitis. Am J Surg 201(3): e23–e25

Rezai P, Tochetto SM, Galizia MS et al (2011) Splenic volume model constructed from standardized one-dimensional MDCT measurements. AJR Am J Roentgenol 196(2): 367–372

Sankar S, Thanka J, Jagdishchandrabose S et al (2011) Splenic hamartoma: a rare vascular space occupying lesion of the spleen. Indian J Pathol Microbiol 54(1):223–225

Warshauer DM, Hall HL (2006) Solitary splenic lesions. Semin Ultrasound CT MR 27(5):370–388

Wells IT, Venkatanarasimha N, Freeman S (2010) Differentiating a benign splenic lesion from an isolated metastasis with contrast-enhanced sonography. J Ultrasound Med 29(9): 1375–1378

Xu GP, Shen HF, Yang LR et al (2011) Splenic cystic lymphangioma in a young woman: case report and literature review. Acta Gastroenterol Belg 74(2):334–336

Yu RS, Zhang SZ, Hua JM (2004) Imaging findings of splenic hamartoma. World J Gastroenterol 10(17):2613–2615

Peritoneum 5

Teodoro Martín Noguerol and Antonio Luna

Contents

A. Luna et al., *Learning Abdominal Imaging*, Learning Imaging,
DOI 10.1007/978-3-540-88003-5_5, © Springer-Verlag Berlin Heidelberg 2012

Case 1

Malignant Peritoneal Mesothelioma

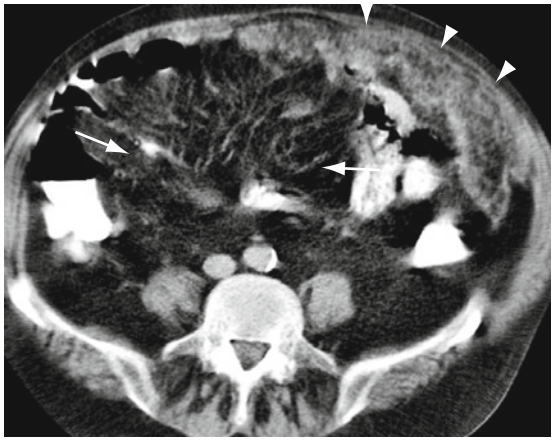

Fig. 5.1.1

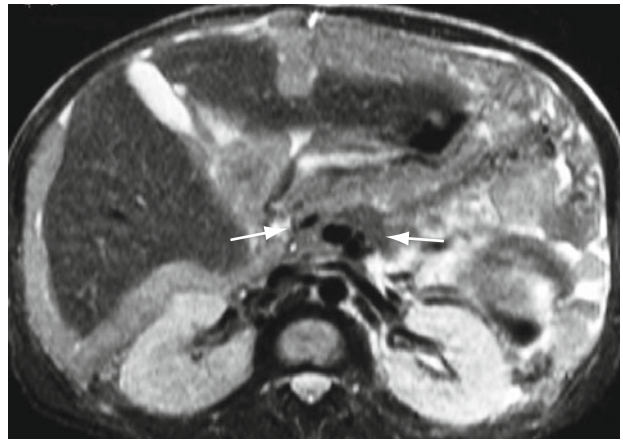

Fig. 5.1.2

A 72-year-old man with abdominal pain and increased abdominal circumference was submitted to our radiology center to perform a CT of abdomen and pelvis.

Comments

Malignant peritoneal mesothelioma is a rare tumor that usually occurs in middle-aged men. A history of previous exposure to asbestos, 20–30 years before the radiological manifestations is common. Clinical manifestations include pain, abdominal distension, anorexia, and weight loss. The abdominal variant of this type of tumor derived from mesothelial cells is much less common than the thoracic one.

The classic imaging findings of malignant peritoneal mesothelioma are the presence of solid masses or peritoneal nodules accompanied by ascites. The infiltration of the omentum is characterized by its thickening and desmoplastic changes within the adjacent mesenteric fat tissue. Large tumoral deposits of peripheral location are seen close to the abdominal wall. Bowel loops acquire a central position with diffuse thickening due to serous infiltration. Ascites, although minimal, is usually present in up to 80% of cases. When infiltration of solid organs occurs, the liver is the most commonly affected. The differential diagnosis of this entity includes peritoneal carcinomatosis secondary to neoplastic processes affecting the stomach, ovary, or colon, which can be challenging, although malignant mesothelioma is often accompanied by thoracic involvement and calcified pleural plaques. Other differential diagnoses include desmoid tumor, carcinoid, lymphoma, and retractile mesenteritis. The most frequent histological pattern of malignant peritoneal involvement is the epithelial or tubulopapillary variant, which may show coarse calcifications.

Imaging Findings

Figure 5.1.1: Abdominal CT with contrast in the venous phase. A stellate pattern within the infiltrated mesenteric fat (*arrows*) and a cake-like appearance of the enhancing omentum (*arrowheads*) are detected.

Figure 5.1.2: Axial fat-suppressed TSE T2-weighted image shows diffuse peritoneal thickening, which causes mass effect over the liver and vascular encasement (*arrows*).

Case 2
Desmoid Tumor

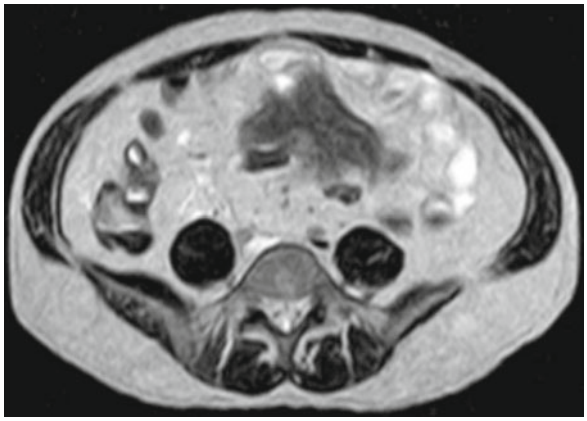

Fig. 5.2.1

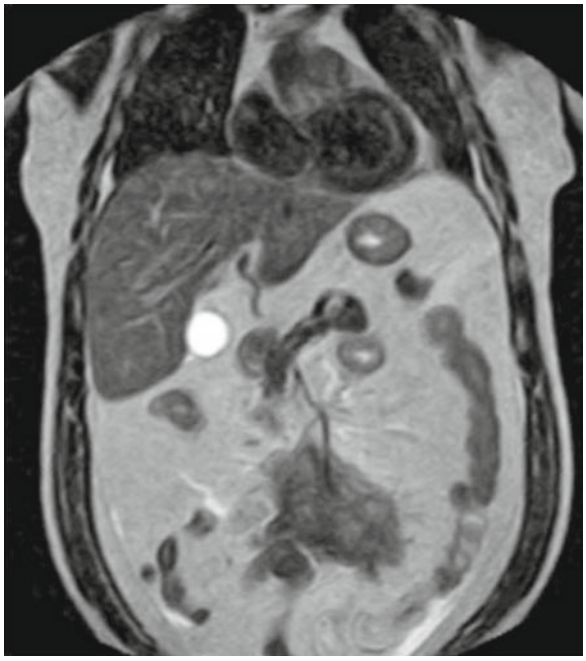

Fig. 5.2.2

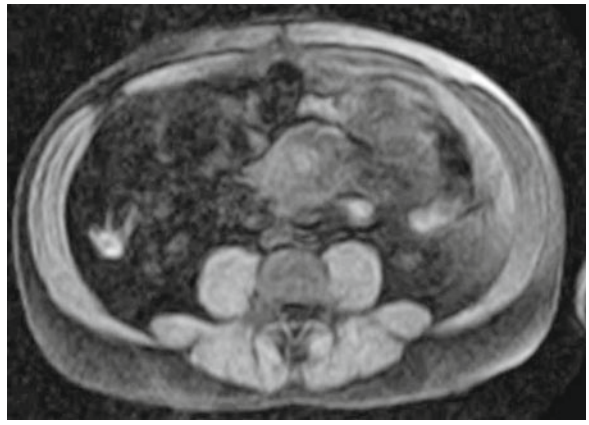

Fig. 5.2.3

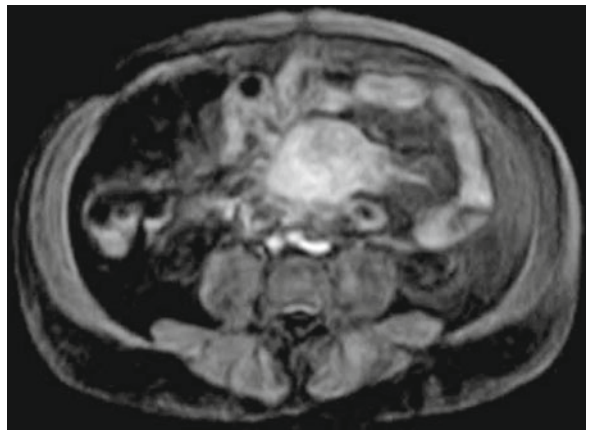

Fig. 5.2.4

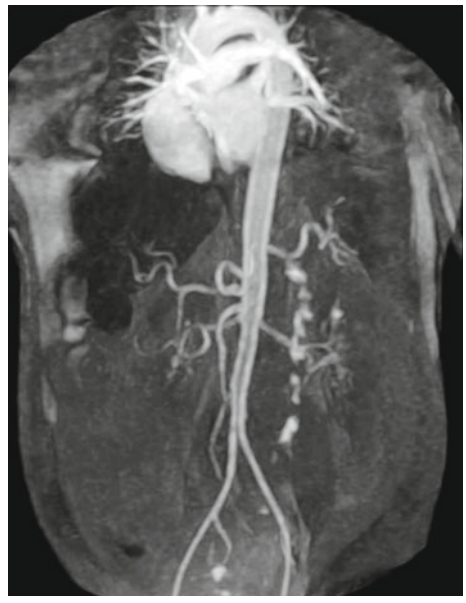

Fig. 5.2.5

A 45-year-old man who presents a mesenteric mass that involves the superior mesenteric artery (SMA) on an ultrasound is referred to our MR unit for further characterization.

Comments

Abdominal desmoid tumor is a pseudotumoral lesion of unknown etiology, including within the group of the fibromatosis. It is a histological benign disease but tends to infiltrate adjacent tissues and structures with a high rate of recurrence after surgical removal. Abdominal desmoid tumor can be located in the abdominal wall, the mesentery, or the retroperitoneum. This type of tumor occurs most often in young women, sometimes related to pregnancy; others can be associated with Gardner syndrome. Desmoid tumor has also been related to previous abdominal surgery, as the tumor is located on the neighborhood of scars. The size of these tumors can vary from a few millimeters up to 15–20 cm.

On abdominal CT scans, desmoid tumor usually presents as a soft tissue mass with well- or ill-defined margins, isodense to muscle, with a great tendency to involve small bowel mesentery. It can show a variable enhancement after contrast administration. On MRI, it appears as hypointense on both T1-weighted and T2-weighted sequences, due to its predominant fibrous composition. Most commonly, desmoid tumor shows restricted diffusion of free water on diffusion-weighted sequences. The main differential diagnosis has to be established with lymphoma, which usually surrounds and involves mesenteric vessels, and with carcinoid tumor, which usually shows a desmoplastic reaction surrounding it.

Imaging Findings

Figures 5.2.1 and 5.2.2: Axial TSE T2-weighted image and coronal HASTE show an ill-defined mass at the inferior aspect of the mesenteric root with low signal intensity, findings consistent with fibrous nature.

Figures 5.2.3 and 5.2.4: Axial THRIVE before and after contrast administration demonstrates a hypointense mass with intense and homogeneous enhancement after gadolinium administration.

Figure 5.2.5: Postcontrast 3D MR angiography is performed to rule out involvement of proximal SMA, which is adequately visualized and patent in its whole extent.

Case 3

Retractile Mesenteritis

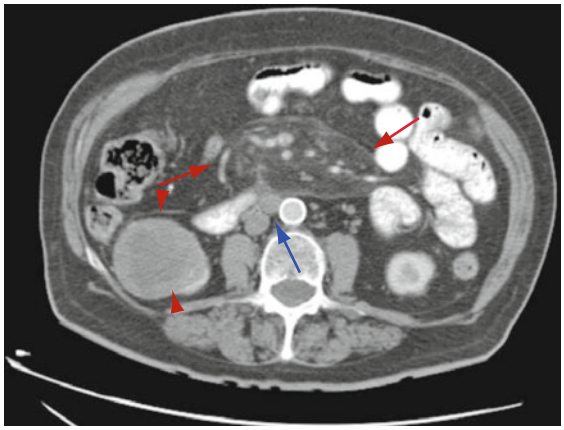

Fig. 5.3.1

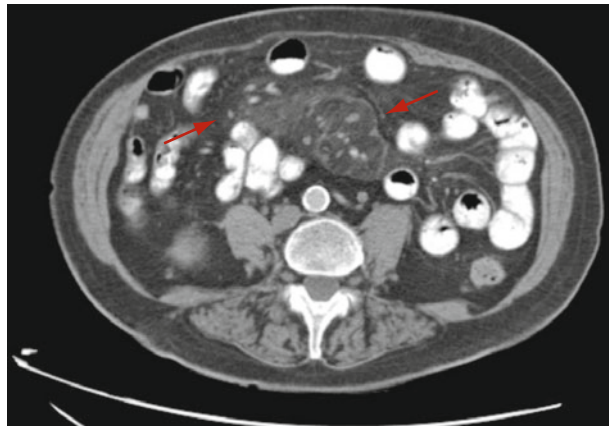

Fig. 5.3.2

A 69-year-old female was referred to our CT unit for study of right renal mass.

Comments

Mesenteric panniculitis and retractile mesenteritis are controversial entities of unknown etiology. History of trauma or previous surgery, ischemia, or autoimmune diseases have been suggested as probable cause. This process is also known as lipodystrophy, mesenteritis, chronic fibrosing, or sclerosing mesenteritis. It is a benign inflammatory process of the mesentery, usually due to focal fat inflammation or fibrosis. This disease is classified depending on the predominant tissue as: mesenteric panniculitis (predominant inflammation and fat necrosis over fibrosis), mesenteric lipodystrophy (when fat necrosis is more evident than inflammation and fibrosis), and retractile mesenteritis (if fibrosis is more evident than fat necrosis).

Many times, this entity shows only imaging manifestations. CT remains as a useful tool for its diagnosis. The classic presentation is that of a well-circumscribed, slightly hyperdense mass. Sometimes, it tends to form a pseudocapsule that enhances after contrast administration surrounded by a hypodense halo of normal fat tissue. Small nodular structures and fiber tracts inside the mass are usually seen. This lesion is usually located around the main mesenteric vascular axis near the root of the mesentery and may have calcifications inside. On MRI, mesenteric panniculitis usually presents with a mixed signal intensity on both T1-weighted and T2-weighted images. Conversely, in cases of retractile mesenteritis, the signal is low in both sequences due to its predominant fibrous content. One fact that helps to its diagnosis is the absence of other inflammatory/infectious intra-abdominal process such as pancreatitis or inflammatory bowel disease. The differential diagnosis of this entity should be established with lymphoma and carcinoid tumors.

Imaging Findings

Figures 5.3.1 and 5.3.2: Axial contrast-enhanced abdominal CT on the arterial phase at two different levels. Ill-circumscribed infiltration of the mesenteric fat with a nodular appearance and surrounded by a pseudocapsule is identified (*red arrows*). Small nodes are visualized within this lesion, which corresponds to incidental mesenteric panniculitis. This appearance has been classically known as "mighty mesentery." A large mass is displayed at right kidney, consistent with renal carcinoma (*arrowheads*). Note the presence of metastatic interaortocaval lymphadenopathy (*blue arrow* on 5.3.1).

Case 4
Epiploic Appendagitis

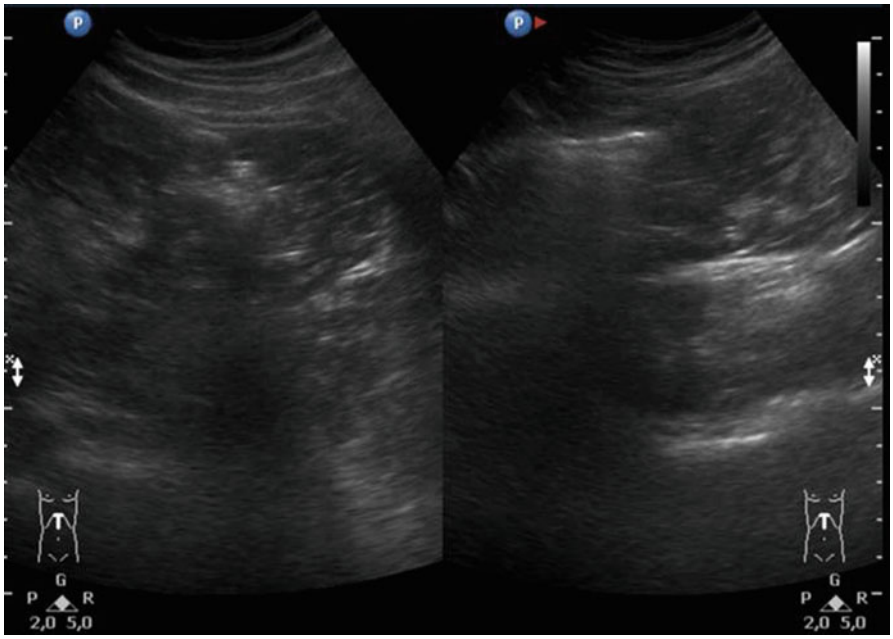

Fig. 5.4.1

Fig. 5.4.2

Fig. 5.4.3

A 70-year-old man that presented left flank pain of acute onset without fever or leukocytosis was referred to our department. Abdominal ultrasound and abdominal CT were performed.

Comments

Epiploic appendagitis is a benign self-limiting process that involves the epiploic appendages of the colon, secondary to vascular pedicle torsion or spontaneous thrombosis of their venous drainage. It appears more frequently in the fourth or fifth decade of life, with a similar incidence between men and women. Less common causes are intestinal obstruction or the introduction of these appendices inside of a femoral, umbilical, or inguinal hernia, with a posterior twisting causing pain. In descending order, epiploic appendagitis may appear adjacent to the sigmoid colon, descending colon, and right colon. The most common clinical manifestation is severe pain in the lower abdomen, especially in the left quadrant that may mimic diverticulitis or acute appendicitis if it occurs on the opposite side. However, it also can occur in any part of the abdomen, depending on the location of the appendix along the colon. Therefore, its clinical symptoms may overlap with those of other diseases such as omental infarction, mesenteric panniculitis, and sclerosing mesenteritis. It is not usually accompanied by changes in bowel habits, fever, or leukocytosis.

Diagnosis is often made through the clinical picture after ruling out other causes of acute abdomen and by imaging, abdominal CT being especially useful. The most common CT feature is a paracolic oval lesion with fat density of less than 5 cm in diameter (2–3 cm) with a central hyperattenuation zone, which corresponds to an epiploic vein thrombus. This lesion is commonly in continuity with the anterior wall of the colon. There is also secondarily increased density of fat around the lesion, revealing adjacent inflammation. Treatment is conservative with oral anti-inflammatory therapy. The clinical symptoms disappear in most cases within 10–14 days, but the radiological changes may take longer to completely come out, up to 6 months.

Imaging Findings

Figure 5.4.1: *Abdominal ultrasound*. An ill-defined pseudomass with mixed echogenicity is identified on the anterior aspect of the left iliac fossa.

Figures 5.4.2 and 5.4.3: Abdominal unenhanced CT at two different levels. Increase of attenuation of peritoneal fat is seen beneath the left rectus muscle, in close vicinity to the antimesenteric aspect of an ileal loop on the left abdominal flank (*arrows*). Minimal amount of free peritoneal fluid is identified within this area.

Case 5
Peritoneal Carcinomatosis

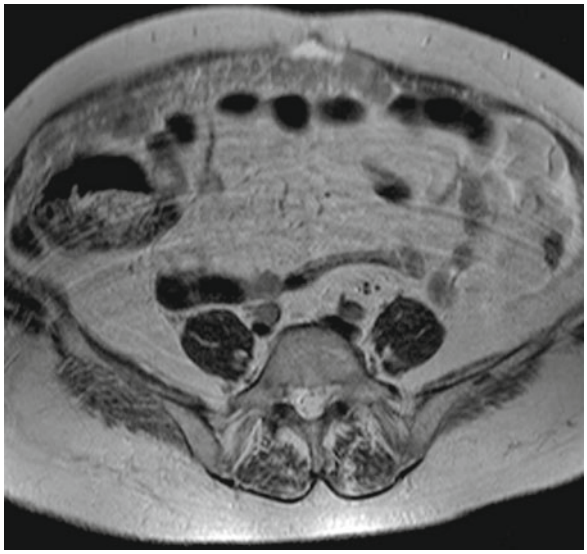

Fig. 5.5.1

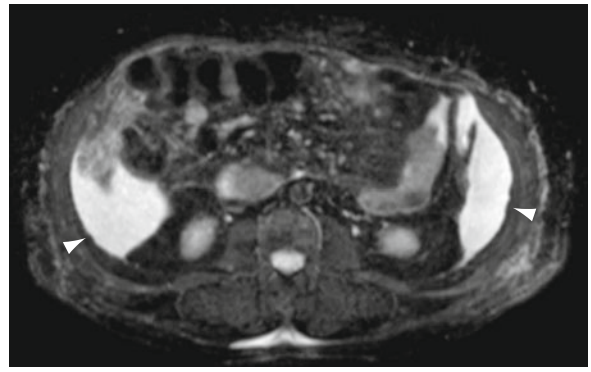

Fig. 5.5.2

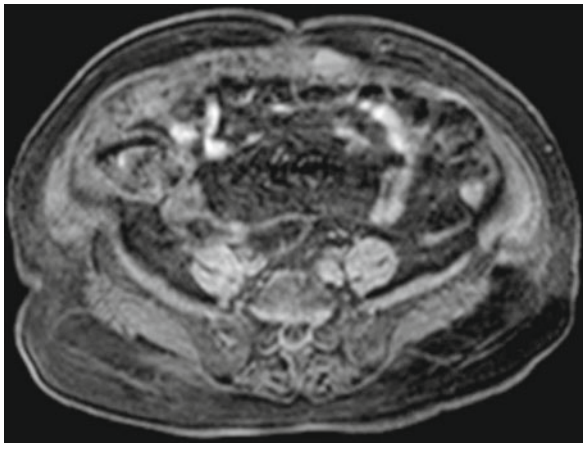

Fig. 5.5.3

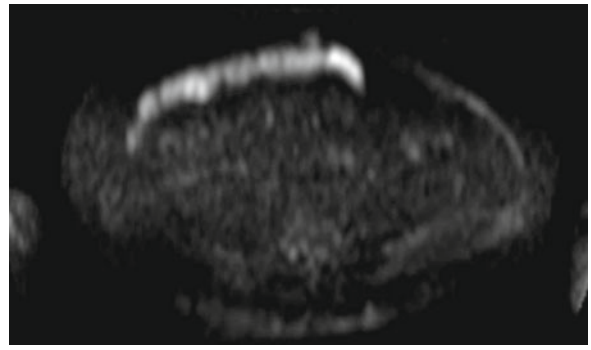

Fig. 5.5.4

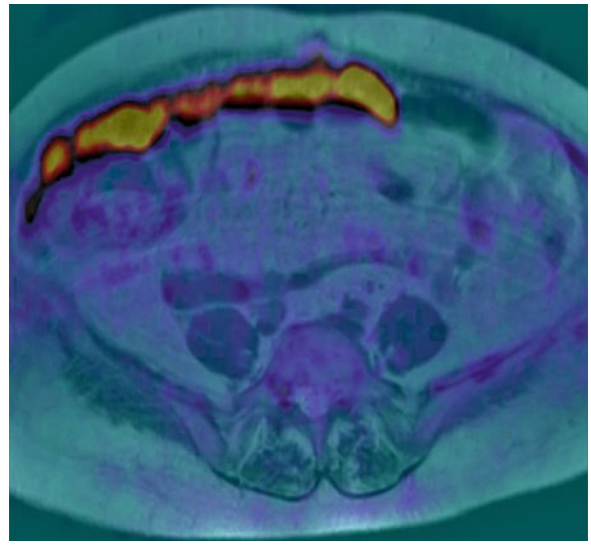

Fig. 5.5.5

A 52-year-old woman presents a paraneoplastic syndrome of probable gynecologic origin.

Comments

The term peritoneal carcinomatosis refers to the spread of a malignant tumor within the peritoneal cavity. Ovarian, colonic, and gastric carcinomas are among the most common tumors that may present with carcinomatosis. This entity can be the first manifestation of a primary tumor. Clinically, it presents with pain, malaise, partial bowel obstruction, or abdominal distension. The classical findings on CT include ascites, up to 80% of cases, and thick nodular enhancing of the peritoneum along with the existence of omental hypovascular masses. Implants are usually located in the pouch of Douglas, right paracolic gutter, and omentum. These masses can merge and give the appearance of an omental cake. The coexistence with metastatic lesions in solid organs, lymph nodes, or bones is not uncommon. The route of spread varies with the type of primary tumor, and it can be made either directly through the mesentery due to peritoneal seeding mediated by ascites or following a lymphatic or hematogenous spread.

MRI can help in the detection of implants; especially fat-suppressed T2-weighted sequences have shown great capability in their depiction, as areas of high signal compared with the low signal of the suppressed peritoneal fat. More recently, diffusion-weighted imaging is able to detect small metastatic deposits of millimeters. However, until now, imaging is not able to adequately detect the early phases of peritoneal carcinomatosis.

The differential diagnosis of this entity has to be established with tuberculous peritonitis, in which there is usually mural thickening of the ileocecal region with splenomegaly and peritoneal calcifications; papillary serous peritoneal carcinoma, rare primary tumor with superimposed findings of peritoneal carcinomatosis, but the absence of a known primary tumor may help in their differential; malignant peritoneal mesothelioma, which usually demonstrates a single mass that infiltrates the mesentery with less ascites than peritoneal carcinomatosis; and pseudomyxoma peritonei, which is characterized by gelatinous masses in the peritoneum, usually in connection with perforation of a mucinous neoplasm of the appendix.

Imaging Findings

Figures 5.5.1 and 5.5.2: Axial TSE T2-weighted and STIR images at two different levels show moderate amount of free peritoneal fluid on both gutters (*arrowheads*) and a diffuse nodular thickening of the omentum.

Figure 5.5.3: Axial postcontrast THRIVE. Nodular and irregular thickening of peritoneum is identified, demonstrating intense enhancement.

Figures 5.5.4 and 5.5.5 EPI DWI with a b-value of 1,000 s/mm^2 and fusion image of DWI and TSE T2-weighted images. Severe restriction of diffusion of the nodular peritoneal thickening, which is better displayed on the fusion image as red areas.

Case 6
Spigelian Hernia

Fig. 5.6.1

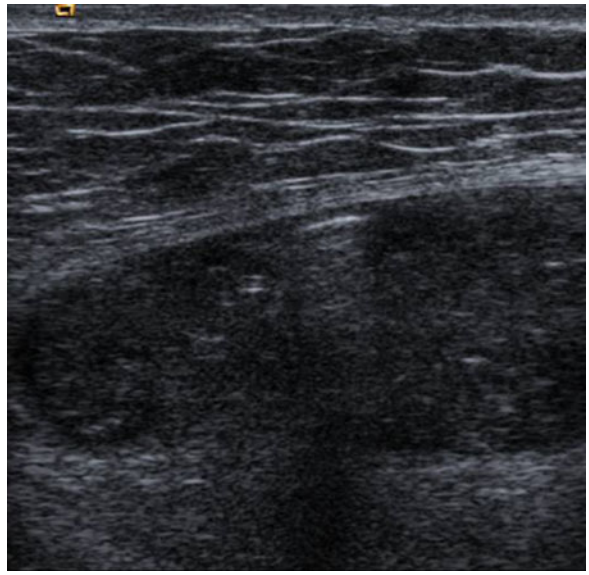

Fig. 5.6.2

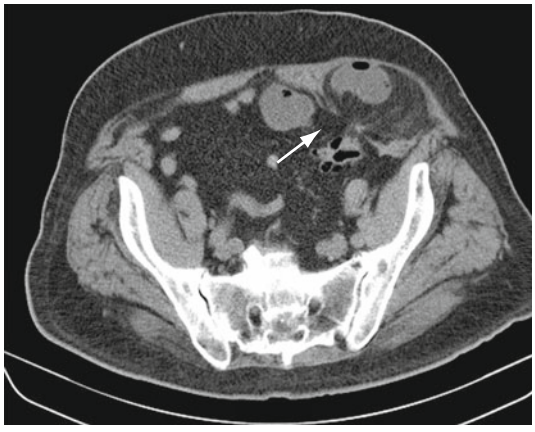

Fig. 5.6.3

Fig. 5.6.4

A 70-year-old man that presented nausea and vomiting with a palpable tender mass in the left lower quadrant was referred to our department for investigation of these findings.

Comments

Hernias through the abdominal wall are the vast majority of external hernias. There are numerous types such as inguinal, femoral, umbilical, incisional, or spigelian hernias, depending on their location or origin. They are caused by the protrusion of a hernial sac through a congenital or acquired defect of the abdominal wall. The sac, covered with peritoneum, may contain inside extraperitoneal fat, omentum, or even bowel loops. The diagnosis is mainly clinical, although in many cases, an imaging study such as ultrasound or CT is needed, especially in cases with suspicion of strangulated hernia or in patients difficult to explore. CT is the modality of choice in case of abdominal wall hernias as it provides precise information about the size, location, content of hernial sac, and secondary complications.

Spigelian hernia occurs due to weakness of the semilunar fascia, between the lateral rectus muscle and the medial margin of the lateral muscles of the abdominal wall, allowing the abdominal content to protrude through the fascia of the transverse and oblique muscles, although it remains covered by the intact external oblique muscle.

Spigelian hernia appears as an anterior peritoneal protrusion located below the umbilicus and lateral to the midline in about 10 cm. Normally, it is located in the left side. The hernial orifice is small and may be difficult to localize. It often contains omental or peritoneal fat or small bowel loops. Typically, the omentum and short segments of bowel protrude through the hernia defect with a high frequency of incarceration. They characteristically cross the complete thickness of the abdominal wall muscles, in contrast to interparietal hernias in which the hernial sac is confined between muscle layers.

It is usually asymptomatic, although it may present with intermittent abdominal pain, as an evanescent anterolateral abdominal mass or as an subocclusive intestinal process. The main complication is intestinal obstruction, more common in irreducible hernias, as a sign of strangulation. In children, although rare, it may be bilateral in up to 15% of cases, and it may be associated with cryptorchidism. Treatment consists of a tension-free repair technique using a prosthetic mesh.

Imaging Findings

Figure 5.6.1: Abdominal plain film. Isolated dilatation of central bowel loops is identified (*arrows*). Notice the presence of severe degenerative changes in the lumbar spine with vacuum disc phenomenon.

Figure 5.6.2: Abdominal ultrasound shows a superficial dilated and fulfilled bowel loop situated within a sac just beneath the aponeurosis of the external oblique muscle.

Figures 5.6.3 and 5.6.4: Abdominal unenhanced CT scan at two different levels. There is a left ventrolateral abdominal wall hernia situated between the lateral edge of rectus abdominis muscle and the medial aspect of transverse muscle (*arrows*). The hernial sac contents are peritoneal fat and a strangulated bowel loop.

Case 7
Pelvic Lipomatosis

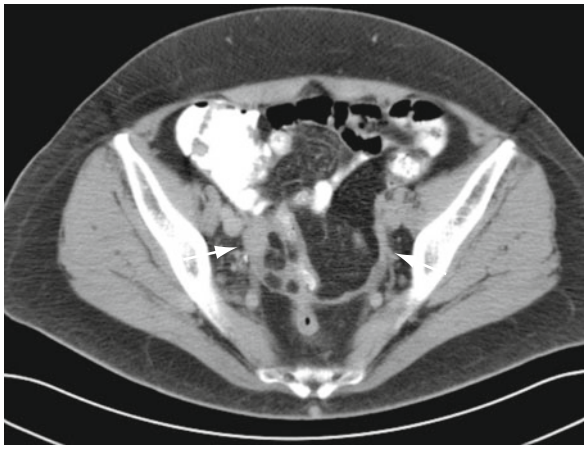

Fig. 5.7.1

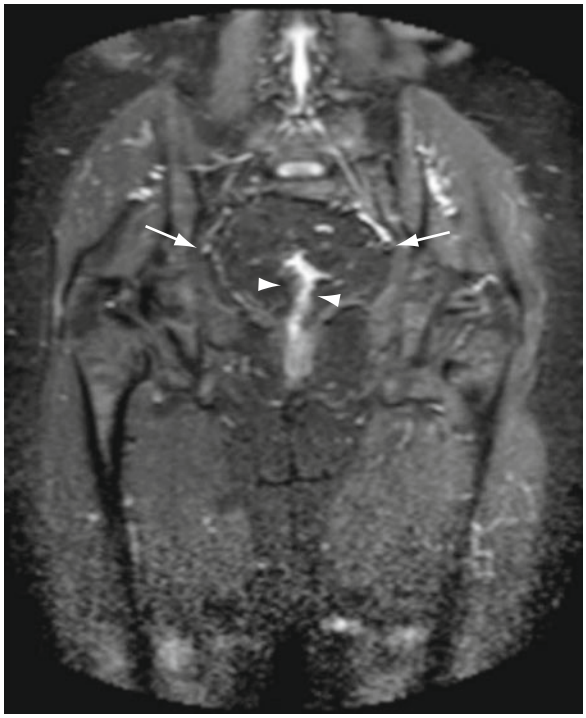

Fig. 5.7.3

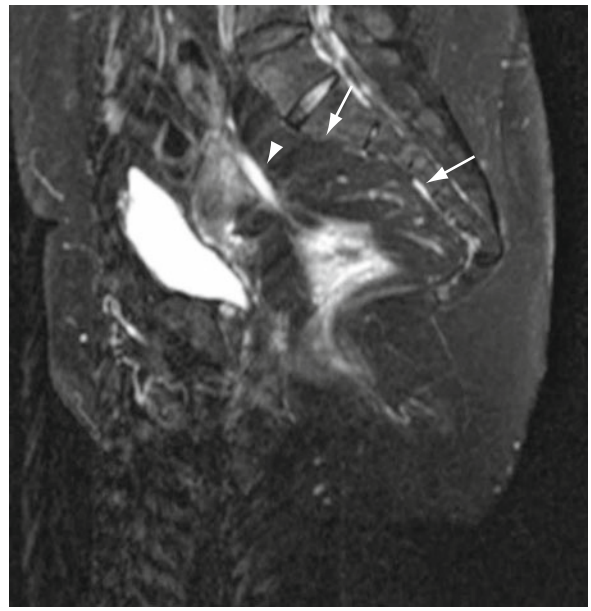

Fig. 5.7.2

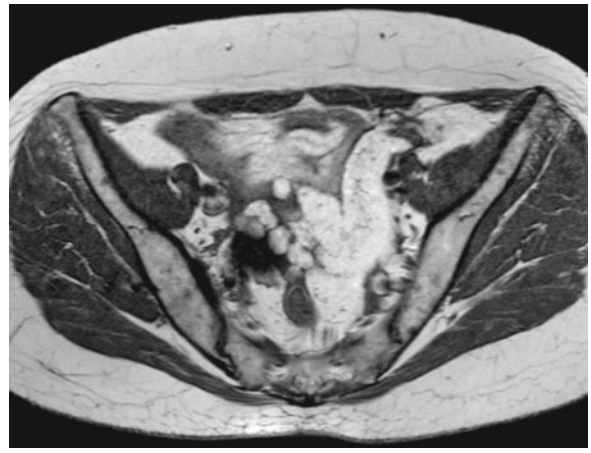

Fig. 5.7.4

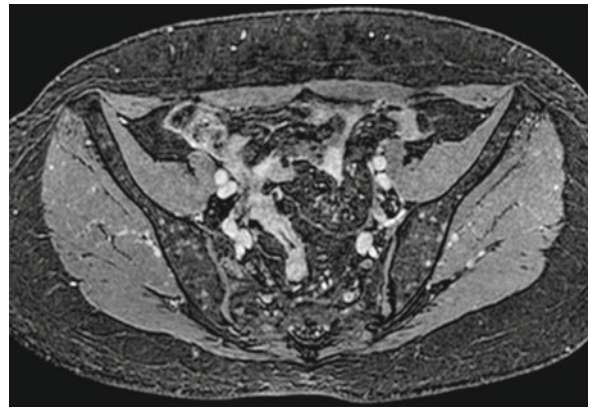

Fig. 5.7.5

A 60-year-old woman with previous history of breast cancer was referred to our department for routinary imaging follow-up.

Comments

Pelvic lipomatosis is a benign overgrowth of adipose tissue with a small amount of inflammatory and fibrotic components. This condition could cause compression of adjacent pelvic structures. The incidence peak of this entity is between 25 and 60 years, with a male predominance of 10:1. Contrary to common belief, obesity is not a factor contributing to this condition.

Pelvic lipomatosis is commonly an incidental finding. Sometimes, symptoms may occur secondary to compression of pelvic structures. Pollakiuria and nocturia are symptoms resulting from bladder compression. Constipation is the most common symptom of intestinal tract compromise. Rarely, there may be manifestations resulting from compression of vascular structures, such as lower extremity swelling. Other symptoms include suprapubic or low back pain.

Plain abdominal X-ray film may show nonspecific diffuse increase of radiolucency at the pelvis. In occasions, patients are referred for constipation screening, and in barium enemas, a symmetric stretching and extrinsic compression upward shift of the sigma may be identified. Cystography can identify a high-positioned bladder acquiring a "pear-shape" morphology. Apart from these indirect imaging signs, a certain diagnosis of this entity can be done both by CT, which is usually sufficient, and MRI. With these techniques, a poorly demarcated and unencapsulated fat mass, which surrounds the pelvic structures, can be identified. Pelvic lipomatosis may show a bilateral urinary tract obstruction with hydronephrosis, as a common complication in up to 40% of the cases.

Imaging Findings

Figure 5.7.1: *Unenhanced* CT shows overgrowth of the pelvic fat that surrounds and compresses ileal bowel loops and causes narrowing of the lumen of the sigmoid colon (*arrows*). Notice the presence of thin linear strips within the pelvic fat.

Figures 5.7.2 and 5.7.3: Sagittal and coronal STIR images show an increase of the amount of the mesorectal and pelvic fat with widening of the presacral space (*arrows*) and narrowing of the lumen of the rectum and sigmoid colon (*arrowheads*).

Figures 5.7.4 and 5.7.5: Axial TSE T1-weighted and postcontrast THRIVE images at the same level confirm an increment of pelvic peritoneal fat that surrounds both adnexa and bowel loops. Notice the presence of multiple hyperenhancing foci within pelvic bones, which are hypointense on T1-weighted sequences, consistent with breast cancer metastasis.

Case 8

Hemoperitoneum Secondary to Rupture of Ovarian Carcinoma

Fig. 5.8.1

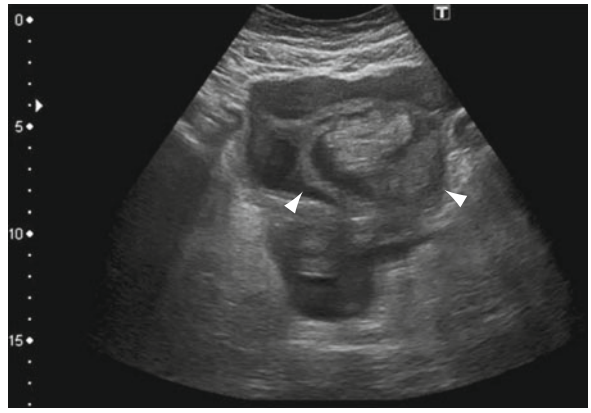

Fig. 5.8.2

Fig. 5.8.3

Fig. 5.8.4

A 44-year-old woman without previous significant clinical history, who presents hypogastric pain of acute onset, came to the ER.

Comments

Spontaneous abdominal hemorrhage is a rare entity. It is defined by the presence of blood in both intraperitoneal and retroperitoneal abdominal spaces. By definition, it is not related to previous trauma. The most common presentation is a sudden abdominal pain with signs of hypovolemic shock.

Leaving aside the causes of traumatic hemoperitoneum, nontraumatic entities that may present with spontaneous hemoperitoneum include:

- Hemorrhage secondary to ruptured intra-abdominal tumors; it is not uncommon that tumoral lesions of solid organs present as spontaneous hemoperitoneum. Hepatocellular carcinoma or hepatic adenomas are tumors which may present as intraperitoneal bleeding, being much more frequent in the case of liver adenoma. Pelvic tumors such as uterine sarcomas or malignant ovarian masses are also included in this group. Portal hypertension or lymphoproliferative disorders with spontaneous splenic hematomas, or more rarely, changes associated with pregnancy and HELLP syndrome may also cause hemoperitoneum.
- In female patients of reproductive age, the most common causes of hemoperitoneum are gynecologic, including ectopic pregnancy and ovarian follicular cyst rupture. The rupture of an ovarian cyst is usually a self-limited process that ceases with conservative therapy. The existence of an adnexal mass with elevated serum beta-HCG and hemoperitoneum raises the suspicion of an ectopic pregnancy.
- The rupture of an aneurysm of the aorta or any other vessel may also present as hemoperitoneum.

Ultrasound and computed tomography are the techniques of choice for the diagnostic approach due to their speed and accessibility. Ultrasound can be used as first diagnostic approach for the assessment of these patients due to its high sensitivity for the detection of intra-abdominal free fluid. Blood, depending on their developmental stage, may present as iso-, hypo-, or hyperechoic. Most often, liquid-liquid levels are displayed with hyperechoic areas inside. However, CT is the modality of choice for the study of spontaneous hemoperitoneum due to their ability not only to detect blood, whose density will also be influenced by the degree of hemodilution and the evolution of bleeding, but also to assess its origin. In general, free blood in the peritoneum has a high density between 30 and 80 HU. Sometimes, a sentinel clot can be identified in the vicinity of the damaged organs that can give us a clue to detect the source of bleeding. It is common to identify liquid-liquid levels due to hematocrit effect. The use of endovenous contrast in CT studies is recommended, as it may demonstrate active bleeding through the existence of contrast extravasation.

Imaging Findings

Figure 5.8.1: Abdominal plain film shows a moderate and ill-defined increase of density on pelvis. Notice the absence of intestinal gas at this level.

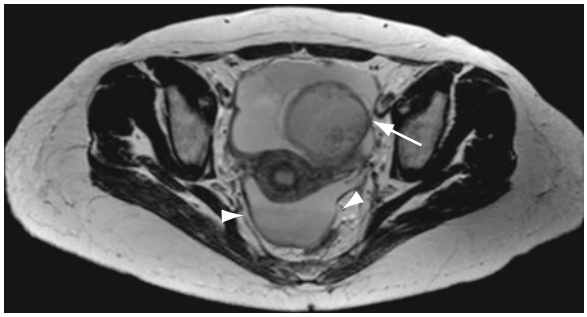

Fig. 5.8.5

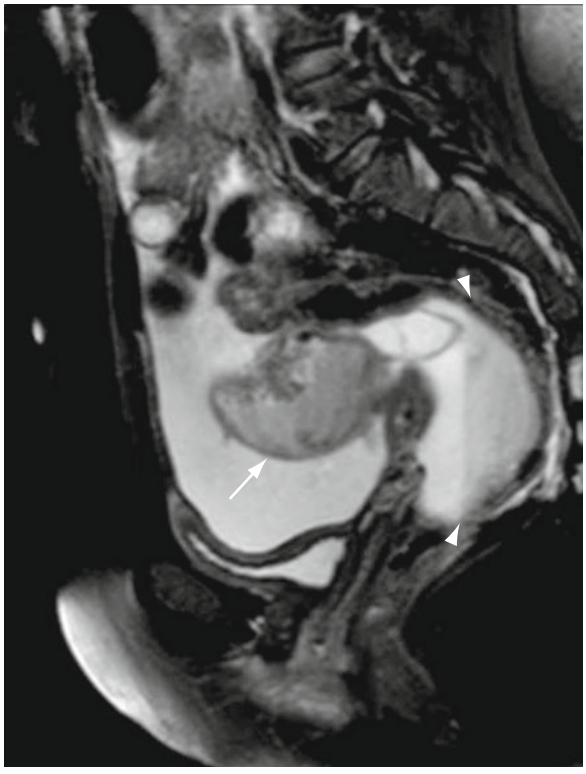

Fig. 5.8.6

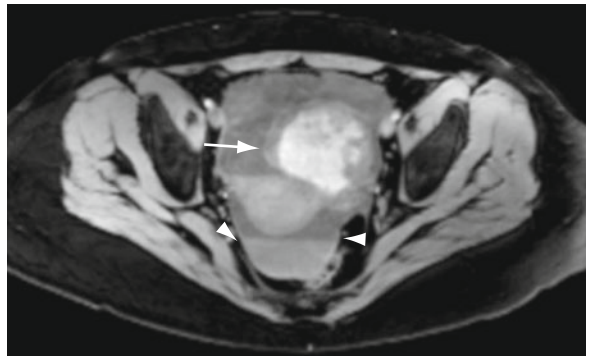

Fig. 5.8.7

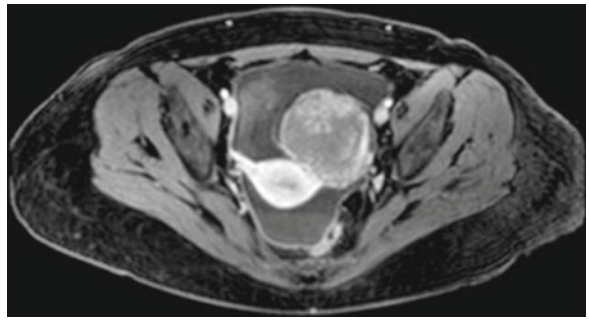

Fig. 5.8.8

Figures 5.8.2 and 5.8.3: Abdominal and pelvic ultrasound shows the presence of an important amount of free fluid with echogenic material inside it (*arrowheads*), identified in right paracolic gutter (Fig. 5.8.3), Morrison's space, and in pelvis surrounding uterus and adnexa (Fig. 5.8.2).

Figure 5.8.4: Coronal MPR of abdominopelvic CT with iodine contrast shows a large left pelvic mass with a heterogeneous appearance, with hyperdense areas within it, corresponding to a left adnexal mass (*arrowheads*). Moderate amount of slight hyperdense free fluid is seen on both abdominal flanks.

Figures 5.8.5 and 5.8.6: Axial TSE T2-weighted and sagittal fat-suppressed TSE T2-weighted images. Severe volume of free fluid that shows a fluid-fluid level is displayed (*arrowheads*). Notice the lower signal intensity of the bottom fluid due to deposit of blood products. The presence of a heterogeneous and hyperintense mass on the left adnexa is confirmed (*arrows*).

Figures 5.8.7 and 5.8.8: Axial THRIVE before and after contrast administration. Precontrast THRIVE shows the blood inside the free fluid as hyperintense (*arrowheads*). The left adnexal mass is also markedly hyperintense due to internal bleeding (*arrow*). This mass shows heterogeneous enhancement, predominantly peripheral. Final diagnosis was that of rupture of bleeding ovarian carcinoma with spontaneous hemoperitoneum.

Case 9
Mesenteric Lymphoma

Fig. 5.9.1

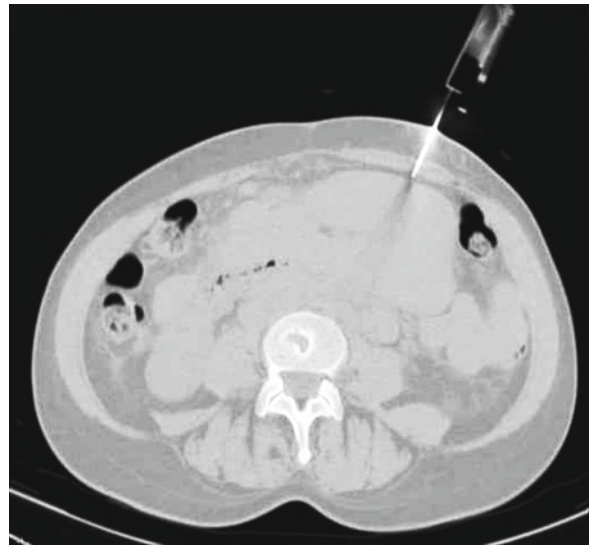

Fig. 5.9.2

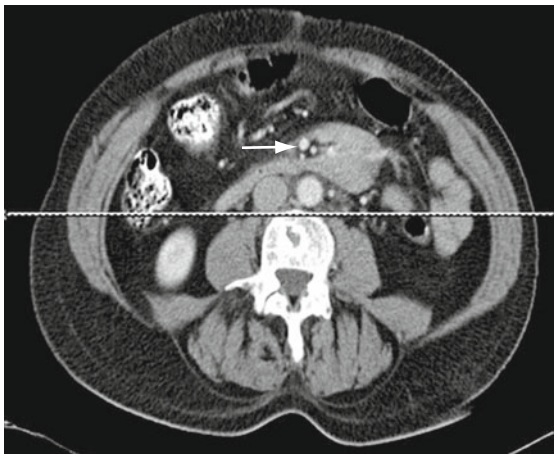

Fig. 5.9.3

A 65-year-old woman came to the emergency room for an abdominal palpable mass. An abdominal CT was performed.

Comments

Independently, if it is a primary gastrointestinal disease or a secondary involvement, intraperitoneal non-Hodgkin lymphomas have a mesenteric compromise in 51% of cases, being the leading cause of neoplastic mesenteric mass. In most patients it corresponds to a diffuse B cell lymphoma, large cell type in adults, or Burkitt type in pediatric patients. The predominant clinical presentation is nonspecific abdominal pain, nausea, vomiting, and weight loss up to one third of cases. There is fever in less than 5%.

Lymph node enlargement is the commonest manifestation of lymphoma on CT. The presence of mesenteric disease is more typical to occur in non-Hodgkin lymphomas. The presence of retroperitoneal lymphadenopathy is a key feature to make the diagnosis. On CT, characteristically multiple rounded homogeneous masses, corresponding to lymphadenopathies, are observed with soft tissue density and fat surrounding mesenteric vessels, which is knwon as "sandwich sign." After intravenous contrast administration, mesenteric vascular structures are enhanced, highlighting the appearance of "sandwich filling." Lymphoma tends to displace small bowel loops and could also present ill-defined mesenteric fat infiltration. MRI can assess the internal composition and biological aggressiveness of lymphoma. Typically, the presence of areas of low signal on T2-weighted sequences with little enhancement after gadolinium administration is in favor of fibrosis rather than active tumor. However, the presence of necrosis will appear as internal areas of high signal intensity. Recently, diffusion-weighted sequences are able to assess the restriction of free water movement, being a biomarker of cellularity, which will increase with higher lymphoproliferative activity. Both CT and MRI have been used for posttreatment monitorization of lymphoma, although 18-FDG PET-CT is currently the best imaging technique in this task.

Imaging Findings

Figure 5.9.1: Unenhanced abdominal CT scan shows a huge homogeneous and well-defined intraperitoneal mass which surrounds the main mesenteric vascular axis. Notice also the presence of retroperitoneal lymphadenopathies.

Figure 5.9.2: A CT-guided core biopsy for histopathological characterization of the mass was performed with result of type B low-grade follicular non-Hodgkin lymphoma.

Figure 5.9.3: Enhanced abdominal CT performed 6 months after treatment shows important reduction of tumoral bulky mass that still surrounds the mesenteric vessels ("sandwich sign") (*arrow*).

Case 10
Gasoma

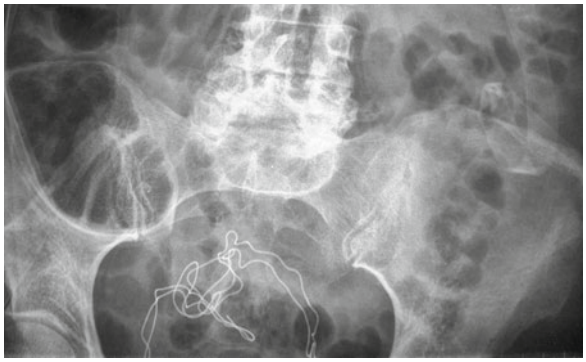

Fig. 5.10.1

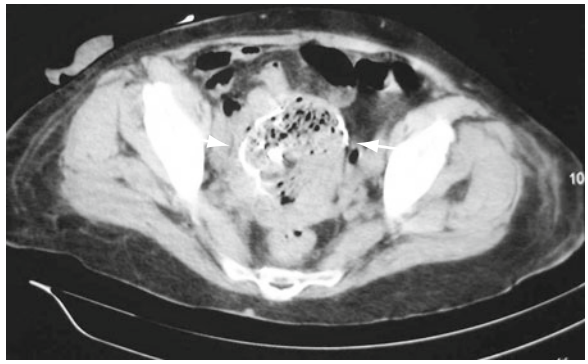

Fig. 5.10.2

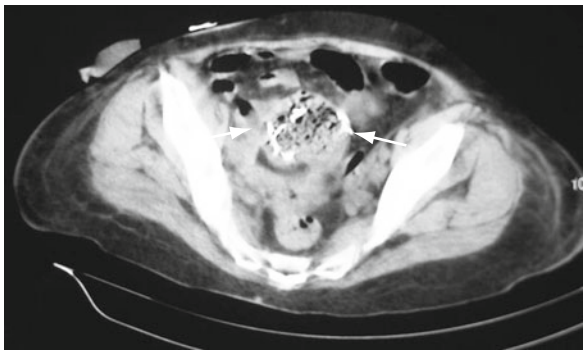

Fig. 5.10.3

A 45-year-old woman with history of recent hysterectomy 2 days ago presented pelvic pain and vomits of acute onset. Plain abdominal X-ray was performed.

Comments

The gasoma (also called gossypiboma or textiloma) is an uncommon complication of surgery. It is the most common type of foreign body forgotten inside a patient. It consists of a mass produced by the retention of surgical gauzes, which generates a reaction body that hosts it. Because the symptoms of gasoma are nonspecific and may appear years after surgery, the initial suspicion usually comes from an imaging study. The low index of suspicion often ends in a misdiagnosis or lack of it, causing delay in treatment with increased morbidity.

Because sponges are inert, they do not suffer any decay or biological reactions. However, it is not uncommon to find either a granuloma, as a consequence of a foreign body response, or an abscess formation. The use of gauze with radiopaque markers has spread universally for the detection of these foreign bodies. In fact, plain film is the test of choice for its detection in the vast majority of cases. In the case of using radiolucent sponge, diagnosis is more challenging, but a spongiform area due to the presence of air bubbles trapped in an unusual extraluminal location can be identified.

Ultrasound also can be useful, detecting hyperechoic structures with strong posterior acoustic shadowing, which are surrounded liquid. CT is the test of choice for the detection of gasomas and associated complications, such as abscesses, fistulas, and obstruction. On CT, gasomas are displayed as well-circumscribed, thick-walled masses, with or without air, calcification, or metal density inside. Contrast enhancement is variable, and it may or may not be present. However, these radiographic and CT findings are nonspecific, and they are not always present. Differential diagnoses of gasoma include fecaloid material, hematoma, abscess, calcified infectious granulomas, and tumors.

Imaging Findings

Figure 5.10.1: Coned view of pelvis plain film shows the existence of radiopaque wire material within the pelvis.

Figure 5.10.2 and 5.10.3: Unenhanced CT at two different levels show an ill-defined mass on pelvis (*arrows*). This mass presents a heterogeneous content with multiple air bubbles trapped inside, and it is surrounded by a metallic density material. These findings are highly suspicious for a forgotten surgical foreign body.

Further Reading

Books

Feberle MP, Jeffrey B, Woodward PJ, Borhani A (2009) Diagnostic imaging abdomen, 2nd edition. Lippincott Williams & Wilkins, Philadelphia

Lee JKT, Sagel SS, Stanley RJ, Heiken JP (2005) Computed body tomography with MRI correlation, 4th edn. Lippincott Williams & Wilkins, Philadelphia

Rossi A, Rossi S, Cardinale AE, Baert AL (2001) CT of the peritoneum. Springer-Verlag, Berlin, Heidelberg

Rumack CM, Wilson SR, Charboneau JW, Levine D (2011) Diagnostic ultrasound, 4th edn. Mosby, St. Louis

Semelka R (2010) Abdominal-pelvic MRI, 3rd edn. Wiley-Blackwell, Chichester/Hoboken

Web Pages

http://www.esgar.org/
http://www.radcentral.com/
http://www.ctisus.com/
http://www.emedicine.com/radio/gastrointestinal.htm
http://www.aast.org/

Articles

Berri RN, Baumann DP, Madewell JE et al (2011) Desmoid tumor: current multidisciplinary approaches. Ann Plast Surg 67(5):551–564

Camera L, Calabrese M, Sarnelli G et al (2011) Pseudopneumoperitoneum in chronic intestinal pseudo-obstruction: a case report. World J Gastroenterol 17(24):2972–2975

Casal Rodriguez AX, Sanchez Trigo S, Ferreira Gonzalez L et al (2011) Hemoperitoneum due to spontaneous rupture of ovarian adenocarcinoma. Emerg Radiol 18(3):267–269

Chen CB, Chiou YY, Chen CH et al (2010) Sonographic and computed tomography findings of intra-abdominal desmoid tumor. J Chin Med Assoc 73(7):393

Clark TJ, Cardoza S, Kanth N (2011) Splenic trauma: pictorial review of contrast-enhanced CT findings. Emerg Radiol 18(3):227–234

Davies RH, Rees BI (2011) Abdominal trauma. BMJ 342:d882. doi:10.1136/bmj.d882

Dormagen J, Meyerdierks O, Gaarder C et al (2011) Contrast-enhanced ultrasound of the injured spleen after embolization – comparison with computed tomography. Ultraschall Med 32(5):485–491

Karaosmanoglu D, Boge M, Akpinar E et al (2010) An unusual cause of pelvic hemorrhage: multidetector CT diagnosis of inferior mesenteric vein injury. JBR-BTR 93(4):186–188

Karcaaltincaba M, Eldem G, Ozdeniz I et al (2012) Omental vascular pedicle sign: multidetector CT finding useful for diagnosis of an omental mass. Eur J Radiol 81(2): e166–e169

Karlo C, Gnannt R, Frauenfelder T et al (2011) Whole-body CT in polytrauma patients: effect of arm positioning on thoracic and abdominal image quality. Emerg Radiol 18(4):285–293

Kim HC, Yang DM, Jin W et al (2011) Infarction of lesser omental fat mimicking an exophytic pancreatic tumor by sonography. J Clin Ultrasound. doi:10.1002/jcu.20806

Kim JW, Chae EJ, Park YS et al (2011) Radiological and clinical features of subcutaneous panniculitis-like T-cell lymphoma. J Comput Assist Tomogr 35(3):394–401

Korley FK, Pham JC, Kirsch TD (2010) Use of advanced radiology during visits to US emergency departments for injury-related conditions, 1998–2007. JAMA 304(13):1465–1471, Erratum in: JAMA. 2010;304(17):1901

Krause J, Bergman A, Graf W et al (2011) Ultrasonography findings and tumour quantification in patients with pseudomyxoma peritonei. Eur J Radiol Feb 22. [Epub ahead of print]

Liao CM, Chang WC, Ko KH et al (2010) Desmoid tumor arising in the site of previous surgery in the left lower quadrant of the abdomen. South Med J 103(2):162–164

Malhotra AK, Carter RF, Lebman DA et al (2010) Preservation of splenic immunocompetence after splenic artery angioembolization for blunt splenic injury. J Trauma 69(5): 1126–1130

Marrannes J, Delvaux S, Verheezen J (2009) Malignant peritoneal mesothelioma: contribution and limitation of imaging for its diagnosis. JBR-BTR 92(5):248–250

Myers JR, Fernando C (2011) Radiology of vernix caseosa peritonitis: case report and discussion. J Med Imaging Radiat Oncol 55(3):301–303. doi:10.1111/j.1754-9485.2011.02271.x

Noguchi T, Kawamura M, Kawamura T et al (2010) A case of diffuse peritoneal malignant mesothelioma – intraabdominal administration of cisplatin is useful for diminishing ascites. Gan To Kagaku Ryoho 37(10):1975–1978

Oei TN, Jagannathan JP, Ramaiya N et al (2010) Peritoneal sarcomatosis versus peritoneal carcinomatosis: imaging findings at MDCT. AJR Am J Roentgenol 195(3): W229–W235

Oh JY, Cho JH, Kang MJ et al (2011) Omental infarction caused by laparoscopy-assisted gastrectomy for gastric cancer: CT findings. Clin Radiol 66(10):966–973

Otani T, Ishimura K, Wakabayashi H (2011) Massive mucinous ascites. Gastroenterology 140(5):e11–e12

Shin SM, Park SM, Hwang BS et al (2010) A case of peritoneal mesothelioma with direct invasion to gastric mucosa. Korean J Gastroenterol 56(6):377–381

Stuart S (2011) Can detection of changes in the motion of abdominal contents using "cine" MRI help in the management of encapsulating peritoneal sclerosis? Perit Dial Int 31(3):267–268

Tandon AA, Lim KS (2010) Torsion of the greater omentum: a rare preoperative diagnosis. Indian J Radiol Imaging 20(4):294–296

Esophagus 6

Anna Pérez de Tudela, Joan C. Vilanova, Lidia Alcalá Mata, and Antonio Luna

Contents

A. Luna et al., *Learning Abdominal Imaging*, Learning Imaging,
DOI 10.1007/978-3-540-88003-5_6,

Case 1
Achalasia

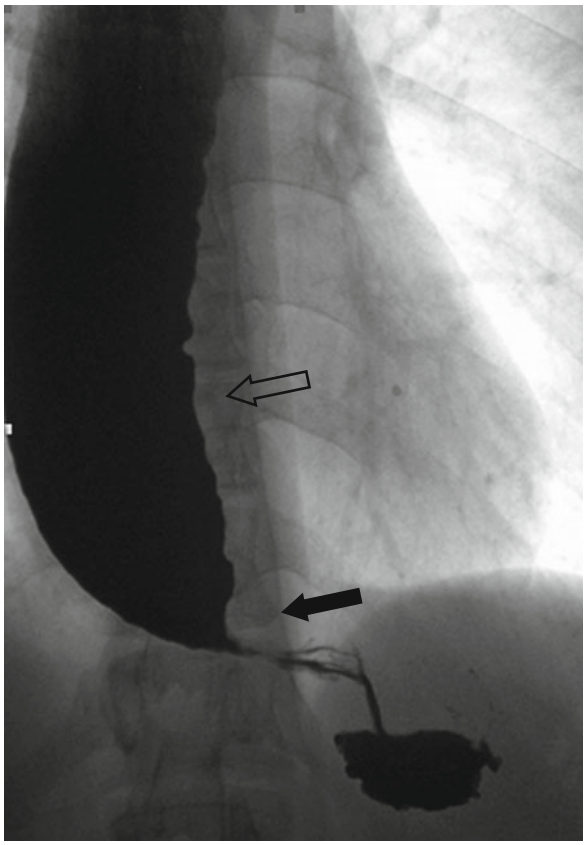

Fig. 6.1.1

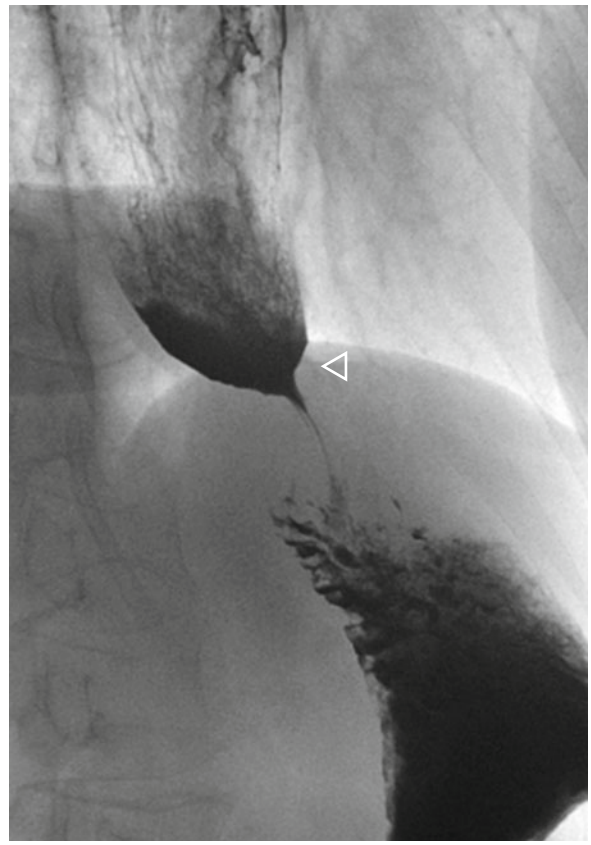

Fig. 6.1.2

A 59-year-old man presented with dysphagia and food regurgitation at night.

Comments

Achalasia is an esophageal motility disorder involving the smooth muscle layer of the esophagus and the lower esophageal sphincter (LES). Its cause is unknown, but the most accepted explanation is a defect in the cholinergic innervation of the esophagus related to a paucity or absence of ganglion cells in the myenteric plexus of the distal esophagus wall.

Achalasia is characterized by incomplete relaxation and increased LES tone, combined with failure of normal peristalsis in the smooth muscle portion of the esophagus, in the absence of other possible causes such as cancer or fibrosis.

The most common symptoms are dysphagia and regurgitation. Other manifestations are chest pain, weight loss, and pneumonia (secondary to regurgitation).

The diagnosis is reached with esophageal manometry and barium swallow radiographic studies.

Several disease processes can mimic achalasia on chest radiographs or barium swallow studies (pseudoachalasia). These include: colon adenocarcinoma, esophageal carcinoma, gastric carcinoma, non-small cell lung cancer, thoracic scleroderma, amyloidosis, Chagas disease, collagen vascular disease, and lymphoma.

Plain chest film findings have low sensitivity and specificity for the diagnosis of achalasia but occasionally offer clues: a double mediastinal stripe, a retrocardiac air-fluid level, and small or absent gastric air bubble because of the paucity of air progressing through the hypertensive LES should raise suspicion of achalasia.

Suspected achalasia should be confirmed with barium swallow study under fluoroscopy. CT may be indicated in the workup of patients with suspected pseudoachalasia.

Imaging Findings

Fluoroscopic imaging shows an abnormal peristaltic movement with the patient in the recumbent position (Fig. 6.1.1, *open arrow*), acute tapering at the lower esophageal sphincter, and narrowing at the gastroesophageal junction producing a "bird's beak" or "rat's tail" appearance (Fig. 6.1.1, *arrow* and Fig. 6.1.2, *open arrowhead*) and dilatation of the esophagus above.

Case 2

Esophageal Carcinoma

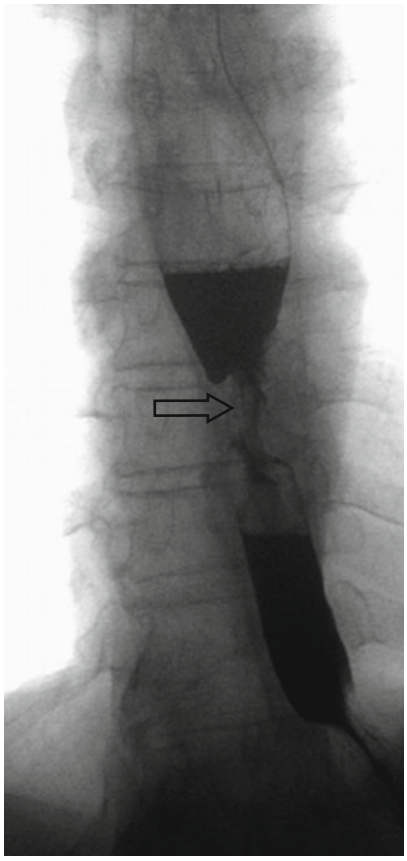

Fig. 6.2.1

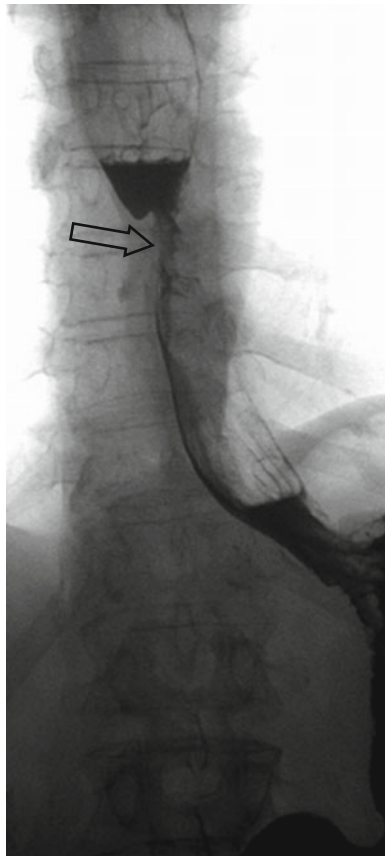

Fig. 6.2.2

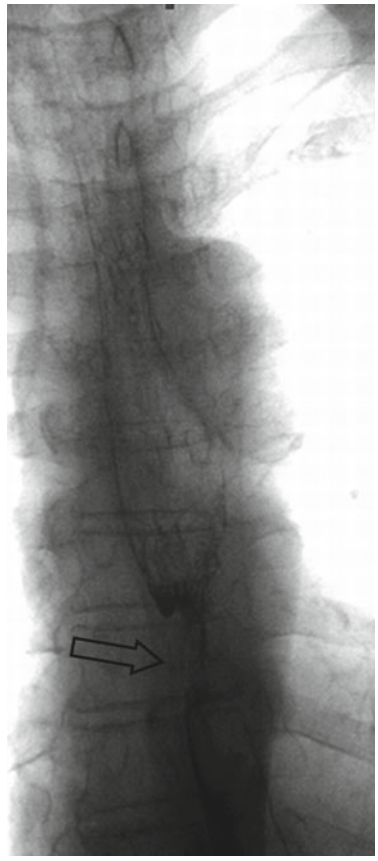

Fig. 6.2.3

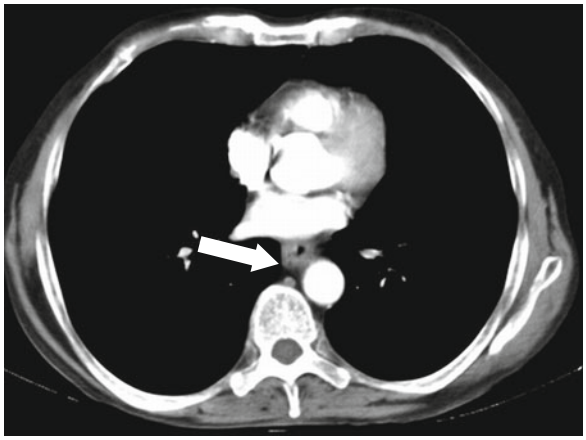

Fig. 6.2.4

A 74-year-old man with progressive dysphagia, odynophagia, and weight loss underwent barium esophagography and CT.

Comments

The most common types of esophageal cancer are squamous cell carcinoma and adenocarcinoma. Whereas squamous cell carcinoma is more evenly distributed throughout the length of the esophagus, adenocarcinoma is predominantly a disease of the distal esophagus and gastroesophageal junction.

Both types of esophageal cancer more commonly affect men older than 60 years. Risk factors for adenocarcinoma are different from those of squamous cell carcinoma. Adenocarcinoma of the esophagus is most commonly seen within a segment of Barrett's esophagus (chronic peptic sores in the lower esophagus). Squamous cell carcinoma occurs more commonly in people who heavily use tobacco and alcohol.

The esophagus has several unique properties that result in different behaviors for cancer in this organ than in other regions of the gastrointestinal tract. In contrast to the rest of the gastrointestinal tract, the esophagus has no serosa, thus reducing the resistance against local spread of invasive cancer cells. Furthermore, the esophagus has an extensive network of lymphatics, allowing for early regional tumor advancement. The result is local spread and invasion into surrounding tissue, with early metastatic disease developing in most patients. Lungs and liver are favored sites of hematogenous metastases.

The two most important prognostic indicators for esophageal cancer are depth of tumor penetration and nodal involvement. The most common symptoms are dysphagia, weight loss, and odynophagia. Hoarseness caused by invasion of the recurrent laryngeal nerve is a sign of unresectability.

Imaging studies in the evaluation of esophageal cancer include: barium studies, CT, and endoscopic ultrasound. Double-contrast barium studies are sensitive in detecting carcinoma of the esophagus and esophagogastric junction. On an esophagogram, esophageal tumors can be polypoid, infiltrative, varicoid, or ulcerative. CT is used to stage and follow esophageal tumors, and it is useful for defining the local extent of tumor. Infiltration of the tumor into the periesophageal fat on CT denotes a T3 tumor and adversely affects prognosis, although curative en-bloc resection may still be attempted. Tumor infiltration to involve adjacent mediastinal structures such as the aorta or tracheobronchial tree denotes a T4 lesion that is considered inoperable. Endoscopic ultrasound provides detailed images of the esophagus and immediately surrounding structures and has been used to define the layers of the esophageal wall and distinguish the depth of tumor penetration.

Radiologic Findings

Three consecutive images from a barium study show an infiltrative tumor in the lower third of the esophagus (Figs. 6.2.1, 6.2.2, and 6.2.3, *open arrows*). Contrast-enhanced CT depicts thickening of the esophageal wall without extension to the periesophageal fat (Fig. 6.2.4, *arrow*).

Case 3
Esophageal Fistula

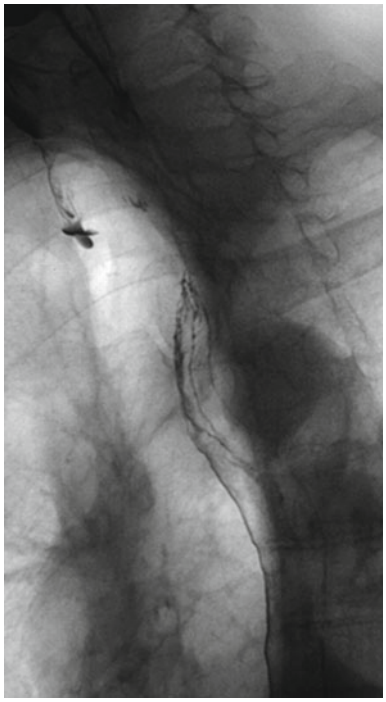

Fig. 6.3.1

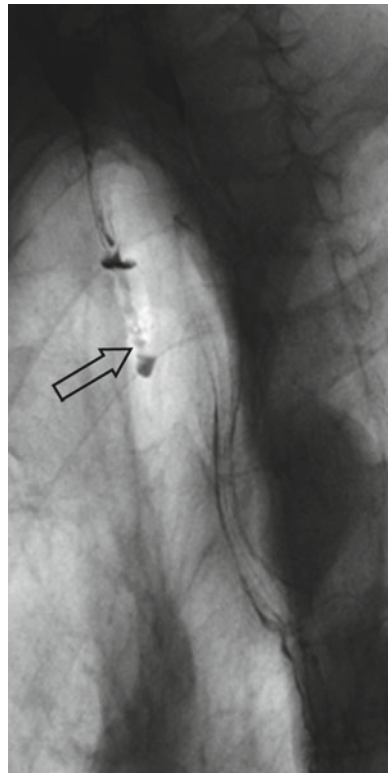

Fig. 6.3.2

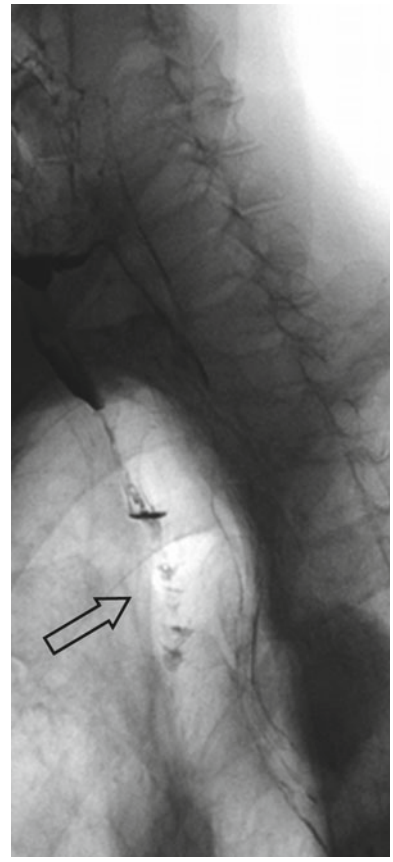

Fig. 6.3.3

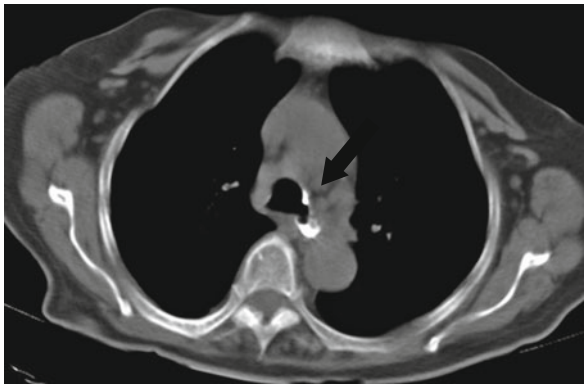

Fig. 6.3.4

A 49-year-old man developed a mediastinal abscess after dental extraction. During this process he complained of dysphagia, so a barium esophagogram and CT were performed.

Comments

Esophageal fistula (EF) is an unusual congenital malformation or acquired complication. It can be basically classified into tracheoesophageal fistula (TEF), bronchoesophageal fistula (BEF), esophagomediastinal fistula, anastomotic fistula, aortoesophageal fistula (EAF), and esophagopleural fistula (EPF).

Acquired EF usually results from direct invasion of the tracheobronchial tree in advanced esophageal cancer, often after radiotherapy. Other acquired causes include instrumentation, surgery, foreign body, trauma, infection, and radiochemotherapy. EF is usually associated with high morbidity and mortality. The most common symptom is episodes of violent coughing.

There is no single best test to diagnose EF. Plain radiography can give some clues but lacks of adequate sensitivity. It may show the widening and loss of the normal contours of the mediastinum; signs of pneumomediastinum may also be present.

Oral contrast studies performed with water-soluble material will often reveal a disruption, and this is often the safest method. However, several reviews have reported 20–50% false-negative rates for water-soluble contrast studies. This has led some authors to recommend barium swallow studies or endoscopy if the initial water-soluble study is negative.

CT and MRI are useful in defining the extent of mediastinal involvement and may be necessary for surgical planning. In patients with an abscess, a localized fluid-filled space, often containing air, is visible. An abscess may have a distinct wall, which enhances after contrast infusion.

Imaging Findings

Figures 6.3.1, 6.3.2, and 6.3.3: Barium esophagram shows the fistula between the esophagus and the upper left mediastinum, which is progressively opacified by the contrast (*open arrows*). Figure 6.3.4 Noncontrast axial CT (mediastinal window) shows a small air collection and oral contrast in the left paratracheal space (*arrow*).

Case 4
Esophageal Lymphoma

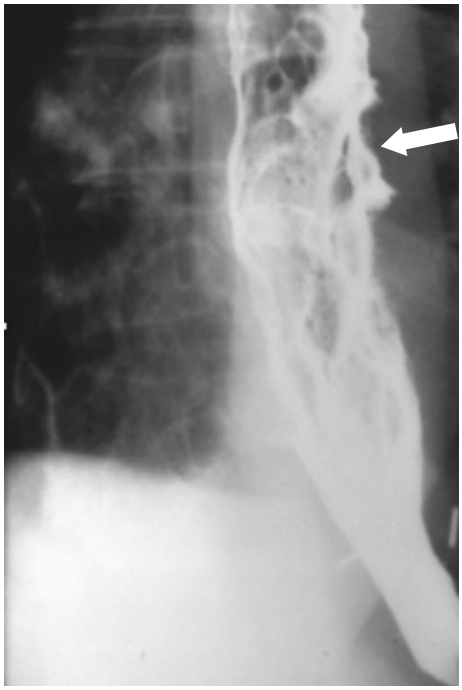

Fig. 6.4.1

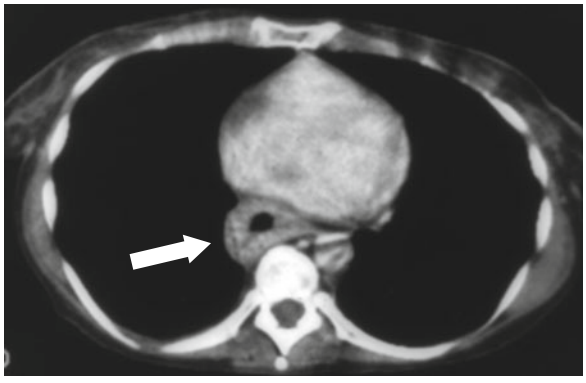

Fig. 6.4.3

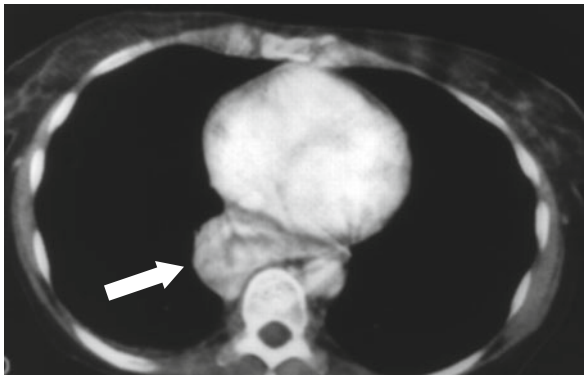

Fig. 6.4.2

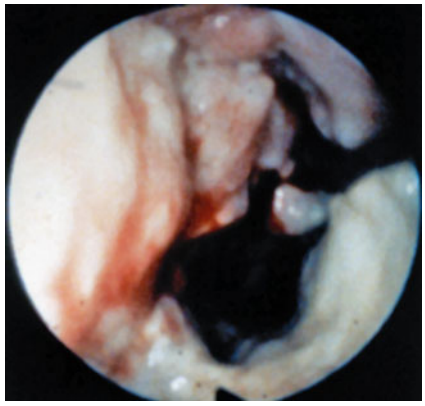

Fig. 6.4.4

A 42-year-old man with hepatitis C–induced cirrhosis received a liver transplant and cyclosporine for immunosuppression. Three months after the transplant, he presented dysphagia, odynophagia, and fatigue.

Comments

Lymphoma is a malignant neoplasm classically involving lymph and reticuloendothelial tissues. The gastrointestinal tract is the most common extranodal site for non-Hodgkin's lymphoma. The esophagus is the least common (<1%) gastrointestinal site for primary lymphoma. The etiology of esophageal lymphoma is unknown; however, HIV infections are a risk factor for development. Previous exposure to Epstein-Barr virus may play a role in the development of esophageal lymphoma. For a lymphoma to be correctly diagnosed as a primary lesion of the esophagus, five criteria must be met: (1) no concomitant palpable superficial lymph nodes, (2) no mediastinal adenopathy, (3) normal white blood cell count, (4) no hepatic or splenic involvement, and (5) the presence of an esophageal lesion. Lymphoma of the esophagus is often asymptomatic. Moreover, the symptoms of primary esophageal lymphoma are common to other esophageal diseases, making an accurate and timely diagnosis difficult: dysphagia, weight loss, hoarseness, and epigastric pain are the most common. Occasionally, symptoms of locally advanced disease such as vocal cord paralysis, esophagorespiratory fistula, or esophageal perforation occur.

Diagnosis may be very difficult. A variety of radiographic appearances, all nonspecific, have been reported for primary esophageal lymphoma. The most common include polypoid masses with or without erosions, stricture with ulceration mimicking esophageal cancer, thickening of the mucosal folds producing a varicoid appearance, narrowed distal segments, or submucosal nodules. Given such a diverse spectrum of plain film findings, CT must be performed and biopsy of the esophageal wall is needed to confirm the diagnosis.

Endoscopically, the presence of an intact mucosa, circumferential esophageal involvement, and the extremely scirrhous nature of submucosal mass should suggest the possible diagnosis of lymphoma. It is difficult to obtain tissue for the diagnosis during endoscopy because gastrointestinal tract lymphomas usually originate at the submucosa.

Radiologic Findings

Barium image shows stricture with ulceration mimicking esophageal cancer (Fig. 6.4.1, *arrow*). Noncontrast CT demonstrates the soft-tissue density mass arising from the esophagus (Figs. 6.4.2 and 6.4.3, *arrows*). Endoscopy shows an intact mucosa, circumferential esophageal involvement, and the extremely scirrhous nature of submucosal mass (Fig. 6.4.4).

Case 5

Esophageal Diverticula

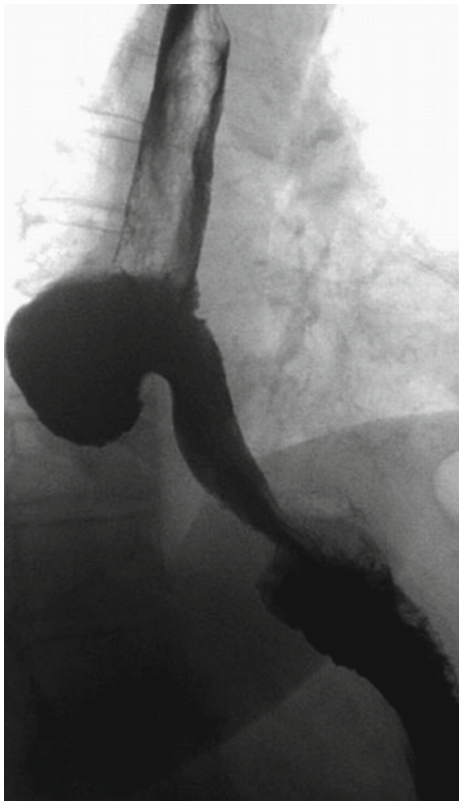

Fig. 6.5.1

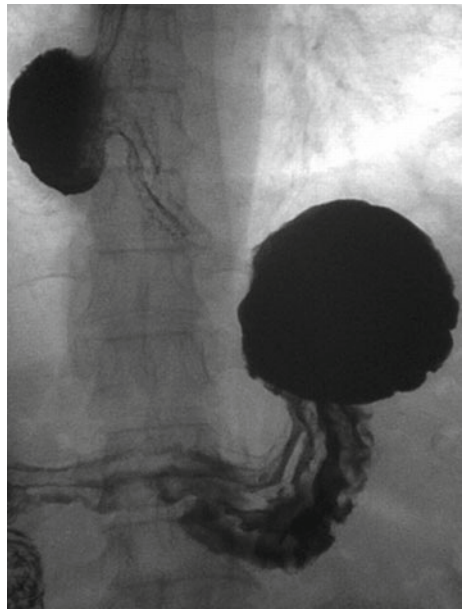

Fig. 6.5.2

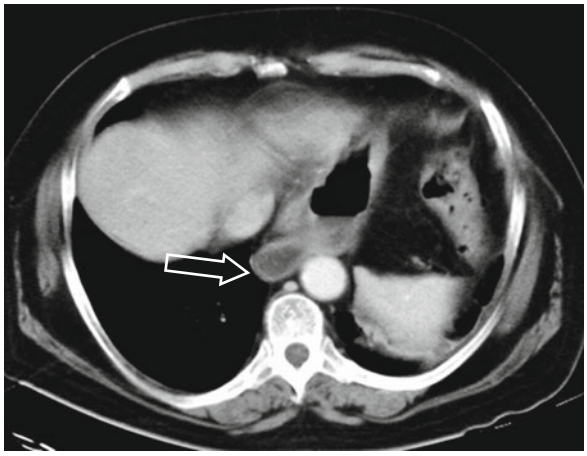

Fig. 6.5.3

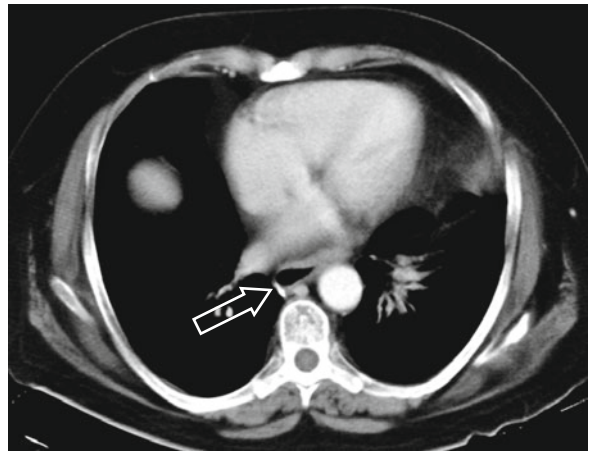

Fig. 6.5.4

A 70-year-old man presented with progressive dysphagia, regurgitation, and nocturnal cough that had worsened within the previous month.

Comments

Diverticula are outpouchings of one or more layers of the intestinal wall that may occur at any level of the esophagus. Based on their location in the esophagus, esophageal diverticula can be classified as Zenker's or pharyngoesophageal diverticula, hypopharyngeal or midesophageal diverticula, epiphrenic diverticula, or diverticula that involve the entire esophagus, which appear as minute, flask-like outpouchings called intramural pseudodiverticulosis. Based on their composition, they can also be classified as traction diverticula, which are composed of all esophageal layers, and pulsion diverticula, which are composed only of mucosa and submucosa herniating through the muscularis. Zenker's diverticulum is covered in another chapter.

The midportion of the esophagus is the most common site of esophageal diverticula. Midesophageal diverticula may develop as a result of either a pull on the esophagus by connective tissue in the chest cavity (traction diverticulum) or much less frequently by a force on the inside of the esophagus that pushes out to form a pouch (pulsion diverticulum). Food accumulation in midesophageal diverticula is rare.

Epiphrenic diverticula are pulsion diverticula that occur when the lower esophageal sphincter fails to relax normally during swallowing, which is often referred to as a motility disorder. Most pulsion diverticula are associated with diffuse esophageal spasm or achalasia.

Pseudodiverticulosis represents dilated excretory ducts of deep esophageal mucus glands and probably results from chronic irritation from different causes like esophageal reflux, diabetes, or chronic alcoholism.

Individuals with esophageal diverticula are often asymptomatic. Symptoms are more frequent in patients with diverticula related to diffuse esophageal spasm or achalasia. The most common symptoms are the sensation of food sticking in the throat, throat irritation, cough, excessive salivation, vomiting after eating, dysphagia, gurgling after swallowing, a metallic taste in the mouth, or halitosis.

Diagnostic modalities for pharyngeal and esophageal diverticula include barium swallow, upper endoscopy, esophageal manometry, CT, or any combination of the above. Traction diverticula often have a triangular or tented appearance resulting from traction on the diverticulum by the fibrotic process in the adjacent mediastinum. Pulsion diverticula appear on barium studies as rounded wide-necked outpouchings that fail to empty when the esophagus collapses. Pseudodiverticula appear as multiple flask-shaped outpouchings in the esophageal wall. On double-contrast esophagograms, most of the outpouchings are still filled with barium.

Imaging Findings

Barium swallow images (Figs. 6.5.1 and 6.5.2) show a large outpouching arising from the right anterolateral wall of the distal esophagus, suggestive of an epiphrenic diverticulum. The neck of the diverticulum is wide, and the gastroesophageal junction is in its normal anatomical position. Contrast CT images at two different levels also demonstrate the diverticulum and its neck filled with oral contrast (Figs. 6.5.3 and 6.5.4, *open arrows*).

Case 6

Gastroesophageal Reflux Disease

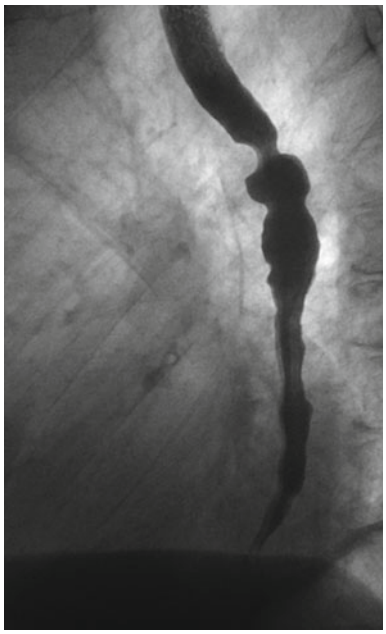

Fig. 6.6.1

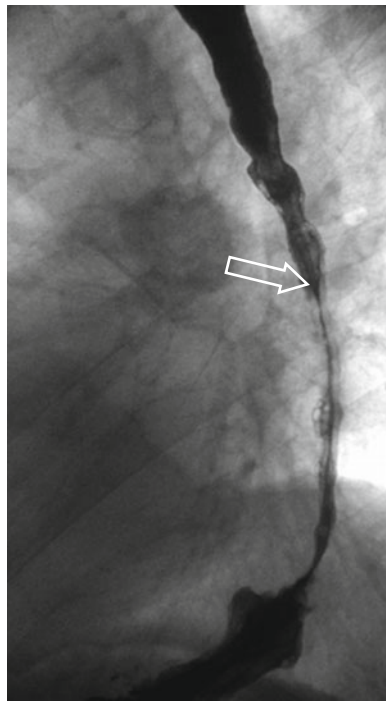

Fig. 6.6.2

Fig. 6.6.3

A 48-year-old man presented with liquid dysphagia and heartburn.

Comments

Gastroesophageal reflux occurs when stomach acid or, occasionally, bile refluxe into the esophagus. The cause is defective antireflux and luminal clearance mechanisms that can result from many conditions: hiatal hernia, achalasia, autonomic neuropathy, systemic sclerosis, pregnancy, and being overweight. When symptoms appear and/or injury to the esophageal epithelium occurs, the condition is termed gastroesophageal reflux disease (GERD).

GERD is the most common inflammatory disease of the esophagus. The classic symptoms of achalasia, which include chest pain, regurgitation, both solid and especially liquid dysphagia, and heartburn, may overlap with those of GERD. The benefits of medical versus surgical therapy (fundoplication) for GERD are under investigation. Preoperative evaluation may include pH monitoring, esophageal manometry, esophagogastric endoscopy, and barium swallow examination.

Barium swallow examination is the most sensitive test as it allows evaluation of:

- Esophageal peristalsis: It is crucial to detect motility disorders such as achalasia, diffuse esophageal spasm, or scleroderma. Up to 50% of GERD patients have ineffective swallowing or nonspecific motility disorders (Fig. 6.6.1).
- The presence and extent of complications of gastroesophageal reflux, esophagitis, stricture, and Barrett's esophagus.
- The presence and type of hiatal hernia.
- The presence of a shortened esophagus manifesting as a hiatal hernia.

Radiographic findings in esophagitis include mucosal granularity or edema (Fig. 6.6.2, *open arrow*), thickened folds, ulcerations, punctate shallow ulcers near the gastroesophageal junction (Fig. 6.6.3, *arrow*), and longitudinally oriented linear ulcers or erosions. These findings typically extend through the lower one-third to one-half of the esophagus. Radiographic findings related to stricture include circumferential peptic strictures, Schatzki ring, sacculations, and fixed transverse folds. Radiographic findings related to Barrett's esophagus include a high or midesophageal stricture or ulcer that is clearly situated above the gastroesophageal junction and a fine reticulonodular mucosal pattern.

Imaging Findings

Nonspecific motility disorders can be seen in the lower one-third of the esophagus (Fig. 6.6.1), with mucosal granularity or edema (Fig. 6.6.2, *open arrow*), diffuse thickened, irregular esophageal strictures, and punctate shallow ulcers near the gastroesophageal junction (Fig. 6.6.3, *arrow*) due to reflux esophagitis.

Case 7
Hiatal Hernia

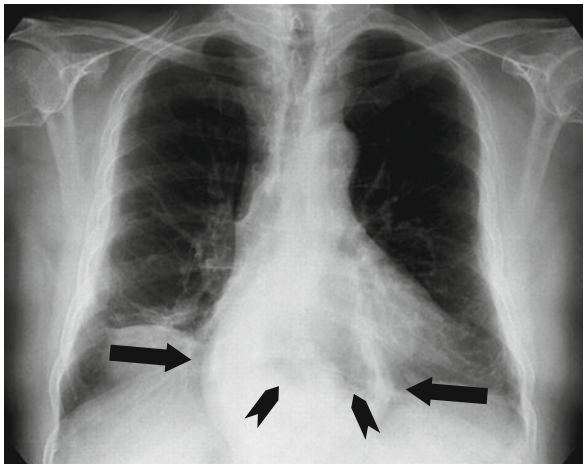

Fig. 6.7.1

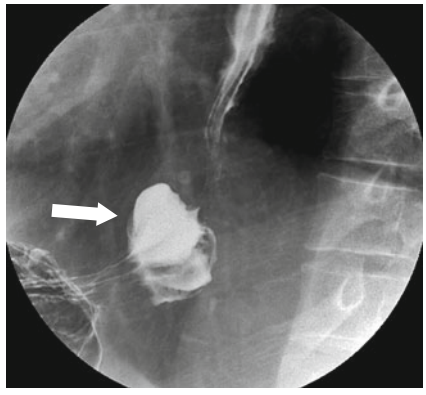

Fig. 6.7.2

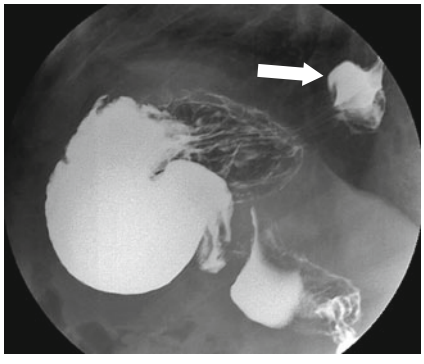

Fig. 6.7.3

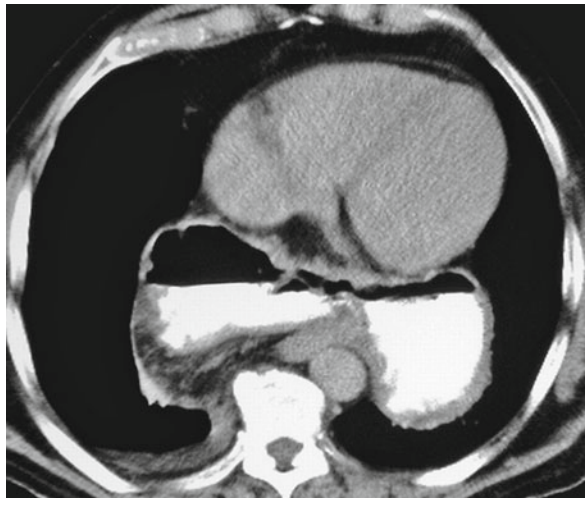

Fig. 6.7.4

A 76-year-old man presented with atypical chest pain.

Comments

Hiatal hernia is very common and affects more than 10% of the general population. It is by far the most common type of hernia, accounting for more than 90% of all hernias. Hiatal hernia occurs when the stomach protrudes through the esophageal hiatus to the chest. It is usually asymptomatic, although a wide range of clinical manifestations is possible. Hiatal hernia can be associated to diverticulosis, reflux esophagitis, duodenal ulcer, and gallstones. Hiatal hernia can be classified as:

- Sliding hiatal hernia, also known as axial or concentric hernia. This is the most common subtype (95%). It appears in 60% of people older than 60 years of age. Esophagogastric junction remains in chest. The ascent of the fundus and cardia is due to rupture or weakness of the phrenicoesophageal membrane. It is very commonly associated to esophagogastric reflux. It may be reductible in the erect position. Surgical repair is necessary only in symptomatic cases (severe esophagogastric reflux or advanced esophagitis).
- Paraesophageal hernia, also called parahiatal hernia (Fig. 6.7.4, unenhanced CT shows a giant paraesophageal hernia). Part of the stomach is displaced into the thorax, although the esophagogastric junction remains below the diaphragm. This type usually grows over time, and it is commonly asymptomatic, although when large can cause thoracic compression. It represents less than 5% of all hiatal hernia. Paraesophageal hernia is frequently nonreductible, and surgical repair is usually necessary.
- Mixed hiatal hernia, when both part of the stomach and esophagogastric junction are located within the thorax, is a very rare type of hernia (less than 1% of all hiatal hernias). Its treatment is also surgical.

Hiatal hernia is usually detected incidentally at chest X-ray or thoracic or abdominal CT or MR. When clinically suspected, upper gastrointestinal series or esophagogastric endoscopy is necessary to establish the diagnosis. CT is used in complicated cases to delineate the topography of the hernia before surgery. CT is also useful for ruling out complications such as strangulation or incarceration of the hernia.

Imaging Findings

An epigastric mass (*arrows*) with an internal air-fluid level (*arrowheads*) was seen on routine chest X-ray (Fig. 6.7.1). An upper gastrointestinal series carried out to rule out hiatal hernia showed the cardia and upper part of the fundus in the chest (*arrows*, Figs. 6.7.2 and 6.7.3). Associated gastroesophageal reflux was visualized during the examination and was probably the cause of the chest pain.

Case 8
Motility Disorders

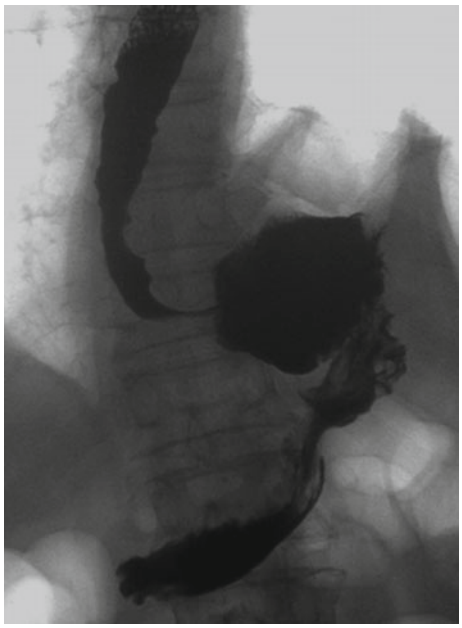

Fig. 6.8.1

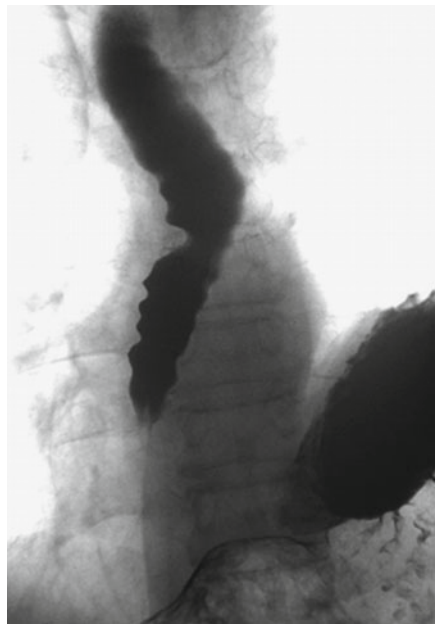

Fig. 6.8.2

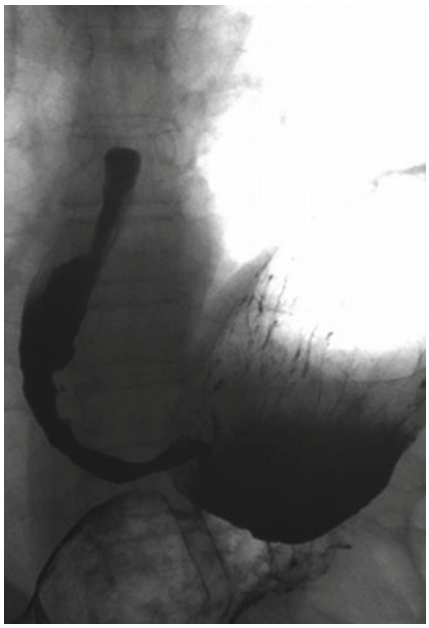

Fig. 6.8.3

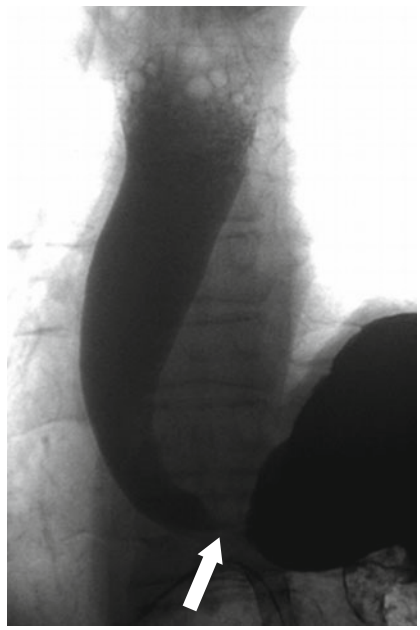

Fig. 6.8.4

A 62-year-old man presented with dysphagia. Findings at endoscopic examination of the esophagus were normal.

Comments

Propulsive defects can result from dysfunction of control mechanisms in the central nervous system, peripheral nerves, myenteric plexus, or intrinsic musculature.

The wide spectrum of motility disorders ranges from the well-defined primary esophageal motility disorders to very nonspecific disorders that may play a more indirect role in reflux disease, which might be otherwise asymptomatic. Esophageal motility disorders may occur as manifestations of systemic diseases, in which case they are referred to as secondary motility disorders.

Primary motility disorders include nonspecific esophageal motility disorder (NEMD), achalasia, diffuse esophageal spasm, nutcracker esophagus, and hypertensive lower esophageal sphincter. The pathophysiology of the primary esophageal motility disorders is poorly defined, with the exception of achalasia.

The secondary motility disorders, such as scleroderma involving the esophagus or esophageal motility disorder of diabetes, are better understood from the standpoint of the preexisting underlying disorders.

Symptoms of esophageal motility disorders include chest pain, dysphagia for liquids and solids, and regurgitation. A thorough history and physical examination, coupled with manometric, endoscopic, and radiologic evaluations, can readily identify all the most common esophageal motility disorders.

The criteria for diagnosis rely not only on compatible symptoms but also on exclusion of structural and metabolic disorders that might mimic the functional disorders.

Chest radiography is not required to establish the diagnosis. Radiologic findings in achalasia are described earlier in this chapter. Patients with NEMD can have nontransmitted waves, retrograde contractions, repetitive contractions, high-amplitude contractions, low-amplitude contractions, prolonged contractions, or spontaneous contractions (Figs. 6.8.1, 6.8.2, and 6.8.3), as well as incomplete lower esophageal sphincter relaxation (Fig. 6.8.4). These findings can be found in any combination. The classic finding in diffuse esophageal spasm, most commonly seen during a barium swallow study, is the "corkscrew" or "rosary-bead" appearance of the esophageal body during a simultaneous contraction. In "nutcracker esophagus", findings on barium swallows are often normal. Various nonspecific forms of tertiary activity have been reported; however, nutcracker esophagus is a manometric, not a radiologic, diagnosis.

Imaging Findings

Various appearances of contractions seen at barium esophagography: nontransmitted, retrograde, repetitive, high amplitude, low amplitude, prolonged, or spontaneous (Figs. 6.8.1, 6.8.2, and 6.8.3). Incomplete lower esophageal sphincter relaxation can be seen with NSED (Fig. 6.8.4, *arrow*).

Case 9

Radiation-Induced Esophagitis and Esophageal Stenosis

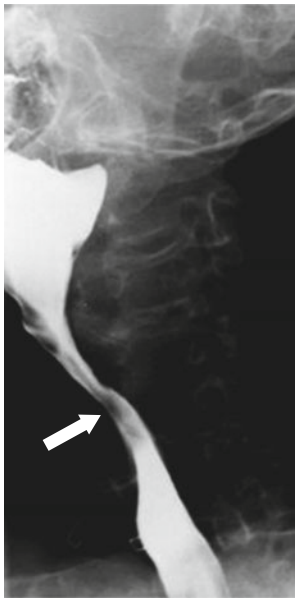

Fig. 6.9.1

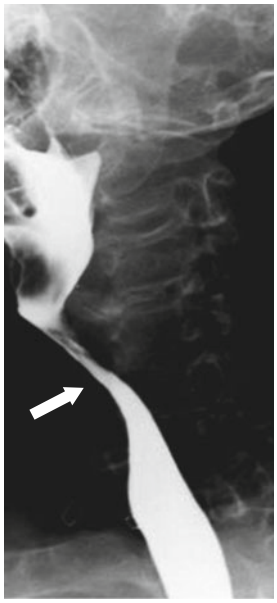

Fig. 6.9.2

Fig. 6.9.3

Fig. 6.9.4

A 70-year-old man presented with progressive dysphagia to solids and liquids. He had undergone radiation and chemotherapy for hypopharyngeal cancer 8 months before.

Comments

Esophagitis and esophageal stenosis can occur as a result of radiation therapy directed at organs and structures other than esophagus, such as the neck or mediastinum.

The nature and extent of complications depend on several factors, including the total dose and volume of irradiated tissue, homogeneity of dose, size of daily dose fractions, and time interval between fractions.

The frequency of esophageal toxicity increases whenever radiation therapy is performed with adjuvant chemotherapy. The submucosa is the first tissue to respond to radiation.

Histological examination soon after radiation therapy shows mucosal edema and vessel dilatation. In more severe cases, the epithelium is necrotic or eroded, and there is accompanying prominent submucosal edema.

In the late stage (6 months or more after radiation therapy), there may be epithelial atrophy or hyperplasia and the submucosal edema is replaced by fibrosis, which extends to surround the muscularis propia.

Clinical radiation esophagitis presents as dysphagia or a substernal burning sensation approximately 2 weeks after the beginning of radiation therapy. These symptoms typically resolve after 2 days without radiation treatment. Most commonly, chronic toxicity presents within 4–6 months after the end of radiation therapy. Patients with symptoms due to chronic radiation effects should be evaluated with barium swallow or upper endoscopy.

On double-contrast studies, acute radiation esophagitis is shown as a variable segment of esophageal narrowing with multiple discrete ulcers, serrations, small marginal filling defects, or a cobblestone pattern, identical to esophageal candidiasis.

Radiologic findings in chronic toxicity include stenosis of the esophagus, strictures, motility disorders, ulceration, pseudodiverticula, and fistulas. These patients are at risk of cancer recurrence or new primary cancers.

Strictures may result in edema and fibrosis, and they usually have a benign appearance with tapered margins and relatively smooth mucosal surfaces.

Imaging Findings

Figures 6.9.1, 6.9.2, 6.9.3, and 6.9.4: Barium esophagogram shows dysmotility and a large mild stenosis of the proximal esophagus (*arrows*).

Case 10
Zenker's Diverticulum

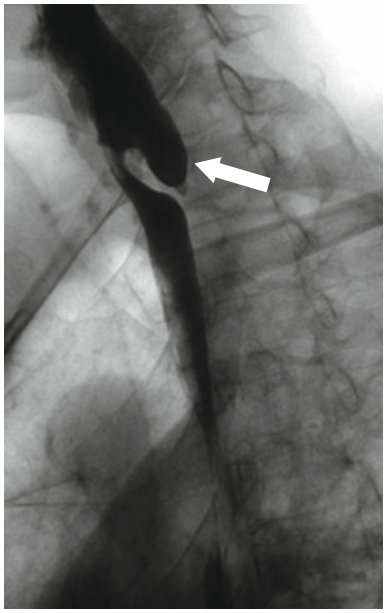

Fig. 6.10.1

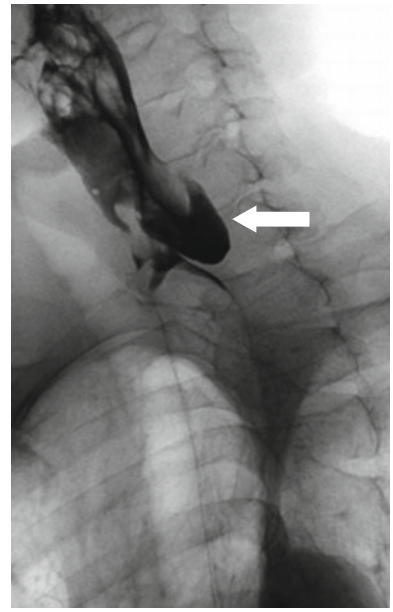

Fig. 6.10.2

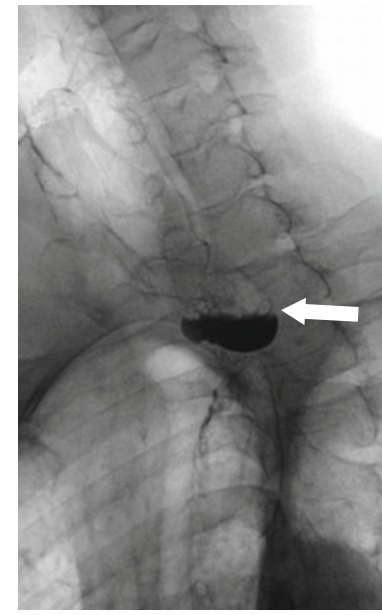

Fig. 6.10.3

A 71-year-old man presented with dysphagia, regurgitation of undigested food, and halitosis; he also complained of some changes in his voice.

Comments

Cricopharyngeal diverticulum or Zenker's diverticulum is the most frequent type of diverticulum of the upper gastrointestinal tract. It is a false diverticulum, consisting of mucosa and submucosa, that arises from the posterior portion of the inferior pharyngeal constrictor muscle (Killian's triangle). This process is more common in elderly men, with a peak incidence in the seventh to ninth decades of life.

The precise etiology is uncertain, although it is considered a pulsion type of diverticulum. It is thought to arise from increased intraluminal pressure caused by incoordination of the cricopharyngeus muscle. With time the diverticulum may become very large.

The clinical manifestations of Zenker's diverticulum include upper esophageal dysphagia, regurgitation and aspiration of indigested food, noisy deglutition, halitosis, and voice change.

Possibly dangerous complications include aspiration pneumonia, esophageal perforation, and carcinoma.

Treatment is diverticulectomy with cricopharyngeal myotomy.

Fluoroscopic barium esophagography is the mainstay of diagnosis of Zenker's diverticulum. The diverticulum appears as an outpouching arising from the midline of the posterior wall of the distal pharynx near the pharyngoesophageal junction. It is best identified during swallowing on the lateral view. Intradiverticular filling defects usually represent food, but carcinoma is in the differential diagnosis.

A large diverticulum can present on chest radiograph as a superior mediastinal mass.

Endoscopy is not required and involves a risk of inadvertent perforation.

Imaging Findings

Lateral view of a barium esophagogram shows a large diverticulum (Fig. 6.10.1, *arrow*) arising in the midline from the posterior wall of the cervical esophagus. Zenker's diverticulum in early (Fig. 6.10.2) and late phase of swallowing (Fig. 6.10.3) shows contrast material collected in the diverticulum (*arrows*).

Further Reading

Books

Eisenberg RL (2003) Gastrointestinal radiology: a pattern approach, 4th edn. Lippincott Williams & Wilkins, Philadelphia
Eisenberg RL (2010) Clinical imaging: an atlas of differential diagnosis, 5th edn. Lippincott Williams & Wilkins, Philadelphia
Ekberg O, Aksglaede K (2004) Radiology of the pharynx and the esophagus. Springer-Verlag, Berlin-Heidelberg
Gore RM, Levine MS (2010) High-yield imaging: gastrointestinal. Elsevier Health Sciences, Philadelphia
Shields TW, LoCicero J, Ponn RB (2009) General thoracic surgery, 7th edn. Lippincott Williams & Wilkins, Philadelphia

Web-Links

http://www.emedicine.medscape.com//
http://www.learningradiology.com//
http://www.acg.gi.org/physicians/guidelines//
http://esophagealcenter.ucla.edu//
http://www.wrongdiagnosis.com//

Articles

Adler DG, Romero Y (2001) Primary esophageal motility disorders. Mayo Clin Proc 76(2):195–200
Ahn SJ, Kahn D, Zhou S et al (2005) Dosimetric and clinical predictors for radiation-induced esophageal injury. Int J Radiat Oncol Biol Phys 61(2):335–347
Baker ME, Einstein DM, Herts BR et al (2007) Gastroesophageal reflux disease: integrating the barium esophagram before and after antireflux surgery. Radiology 243(2):329–339
Becker M, Schroth G, Zbären P et al (1997) Long-term changes induced by high-dose irradiation of the head and neck region: imaging findings. Radiographics 17(1):5–26
Canon CL, Morgan DE, Einstein DM et al (2005) Surgical approach to gastroesophageal reflux disease: what the radiologist needs to know. Radiographics 25(6):1485–1499
Do Nascimento FA, Lemme EM, Costa MM (2006) Esophageal diverticula: pathogenesis, clinical aspects, and natural history. Dysphagia 21(3):198–205
Eckardt AJ, Eckardt VF (2009) Current clinical approach to achalasia. World J Gastroenterol 15(32):3969–3975
Exarhos DN, Malagari K, Tsatalou EG et al (2005) Acute mediastinitis: spectrum of computed tomography findings. Eur Radiol 15(8):1569–1574
Ferreira LE, Simmons DT, Baron TH (2008) Zenker's diverticula: pathophysiology, clinical presentation, and flexible endoscopic management. Dis Esophagus 21(1):1–8
Hamed KA, Hoffman MS (1998) Primary esophageal lymphoma in AIDS. AIDS Patient Care STDS 12(1):5–9
Hoghooghi D, Coakley FV, Breiman RS et al (2006) Frequency and etiology of midesophageal diverticula at barium esophagography. Clin Imaging 30(4):245–247
Iyer R, Dubrow R (2004) Imaging of esophageal cancer. Cancer Imaging 4(2):125–132
Iyer RB, Silverman PM, Tamm EP et al (2003) Diagnosis, staging, and follow-up of esophageal cancer. AJR Am J Roentgenol 181(3):785–793
Kahrilas PJ (2000) Esophageal motility disorders: current concepts of pathogenesis and treatment. Can J Gastroenterol 14(3):221–231
Kim TJ, Kim HY, Lee KW et al (2009) Multimodality assessment of esophageal cancer: preoperative staging and monitoring of response to therapy. Radiographics 29(2): 403–421
Lacy BE, Weiser K, Chertoff J et al (2010) The diagnosis of gastroesophageal reflux disease. Am J Med 123(7):583–592
Levine MS, Rubesin SE (2005) Diseases of the esophagus: diagnosis with esophagography. Radiology 237(2):414–427
Levine MS, Rubesin SE, Laufer I (2008) Barium esophagography: a study for all seasons. Clin Gastroenterol Hepatol 6(1):11–25
Luedtke P, Levine MS, Rubesin SE et al (2003) Radiologic diagnosis of benign esophageal strictures: a pattern approach. Radiographics 23(4):897–909
Mesurolle B, Qanadli SD, Merad M et al (2000) Unusual radiologic findings in the thorax after radiation therapy. Radiographics 20(1):67–81
Patti MG, Herbella FA (2011) Achalasia and other esophageal motility disorders. J Gastrointest Surg 15(5):703–707
Smout AJ (2008) Advances in esophageal motor disorders. Curr Opin Gastroenterol 24(4):485–489
Soares R, Herbella FA, Prachand VN et al (2010) Epiphrenic diverticulum of the esophagus. From pathophysiology to treatment. J Gastrointest Surg 14(12):2009–2015
Weeratunge CN, Bolivar HH, Anstead GM et al (2004) Primary esophageal lymphoma: a diagnostic challenge in acquired immunodeficiency syndrome – two case reports and review. South Med J 97(4):383–387
Woodfield CA, Levine MS, Rubesin SE et al (2000) Diagnosis of primary versus secondary achalasia: reassessment of clinical and radiographic criteria. AJR Am J Roentgenol 175(3): 727–731

Stomach and Duodenum 7

Maria Boada, Joan C. Vilanova, Joaquim Barceló, and Pablo R. Ros

Contents

A. Luna et al., *Learning Abdominal Imaging*, Learning Imaging,
DOI 10.1007/978-3-540-88003-5_7,

Case 1
Gastrointestinal Stromal Tumor

A 65-year-old woman with stable ischemic heart disease presented with renal insufficiency (creatinine, 1.4). Ultrasound showed the absence of the right kidney. Abdominal CT to evaluate the absence of the

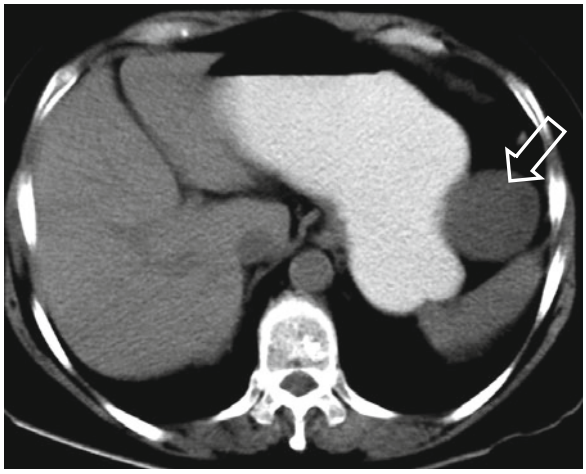

Fig. 7.1.1

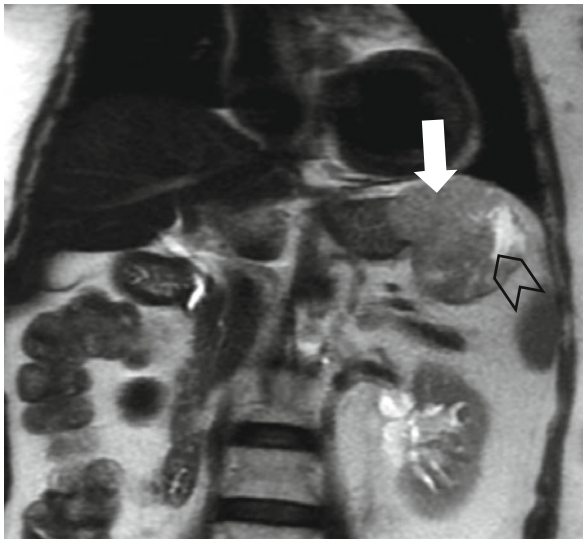

Fig. 7.1.3

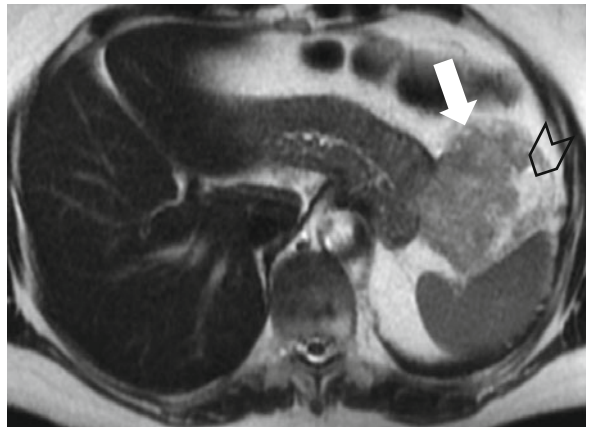

Fig. 7.1.2

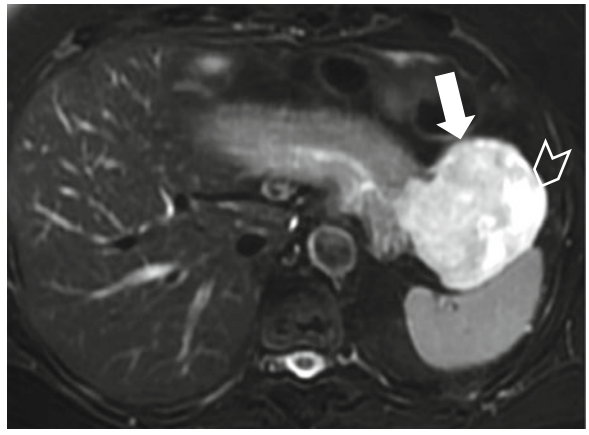

Fig. 7.1.4

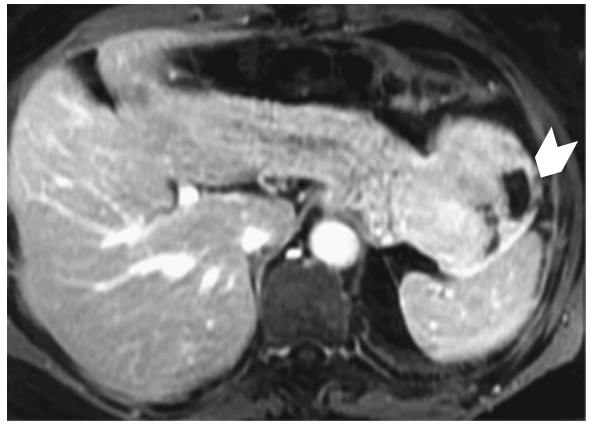

Fig. 7.1.5

kidney incidentally detected a tumor in the left hypochondrium, which was followed up with MRI 3 months later.

Comments

Gastrointestinal stromal tumor (GIST) is the most common mesenchymal tumor of the gastrointestinal (GI) tract, accounting for 2.2% of gastric malignancies and 13.9% of intestinal malignancies. It has no gender predilection, and it can occur at any age, although it is very rare in children (median age at presentation is 55 years).

GIST is a submucosal tumor of unknown etiology derived from interstitial cells of Cajal. It may occur anywhere in the GI tract; the most common sites are the stomach (60%), the small intestine, especially the duodenum (25%), and the anorectum (10%). The colon, appendix, esophagus, and extraintestinal sites are very rare locations. It appears as an exophytic submucosal mass of variable size; benign lesions are typically small (<3 cm) and malignant ones large (>5 cm). They may have ulcerations and necrosis. Malignant findings include invasion of adjacent organs and evidence of metastases. Microscopic malignant features include high mitotic rate, high nuclear rate, and high cellularity. At fluoroscopy, GIST typically appears as a bulky, well-circumscribed, lobulated mass, often polypoid, with smooth outer contours.

Calcification is seen on CT in 25% of cases. There can also present a cystic-like element (with low attenuation) secondary to liquefactive or coagulative necrosis and hemorrhagic component. GIST can be hypo- or hypervascular on contrast-enhanced CT.

At MRI, characteristic findings include a mass that is isointense on T1 weighted-image and hypo- or isointense on T2 weighted-image, with hyperintense areas of necrosis. The enhancement of the tumor varies because of its variable vascularity, and necrotic areas do not enhance.

Prognosis often depends on tumor size, with excellent prognosis for completely resected benign lesions. The treatment of choice is bloc resection and tyrosine kinase inhibitor chemotherapy (Gleevec) for metastatic disease. The liver, lung, and peritoneal cavity are common sites of metastases. PET is useful to predict the early response to Gleevec.

Other GI malignancies like lymphoma and exophytic gastric carcinoma should be considered in the differential diagnosis. Gastric lymphoma may be indistinguishable from GIST; however, it is usually associated with mesenteric and retroperitoneal adenopathies. Exophytic gastric carcinoma appears hypodense and less vascular than GIST on CT, and the focal thickening of adjacent gastric wall and gastric outlet obstruction help differentiate it from GIST. When gastric GIST is associated to pulmonary chondroma and extra-adrenal paraganglioma, it is known as Carney's triad.

Imaging Findings

Unenhanced CT shows a bulky exophytic gastric mass with well-circumscribed outer contours (Fig. 7.1.1, *open arrow*). No calcifications are present. MRI demonstrates a heterogeneous gastric mass, with a solid component and intermediate signal on axial and coronal T2-weighted images (Figs. 7.1.2 and 7.1.3, *arrows*) and high signal on fat-suppression T2-weighted image (Fig. 7.1.4, *arrow*). A hyperintense area corresponding to necrosis (Figs. 7.1.2, 7.1.3, and 7.1.4, *open arrowheads*) is also shown laterally. Delayed postcontrast phase on dynamic MRI shows contrast enhancement of the solid area of the mass and no enhancement of the necrotic area (Fig. 7.1.5, *arrowhead*).

Case 2
Linitis Plastica

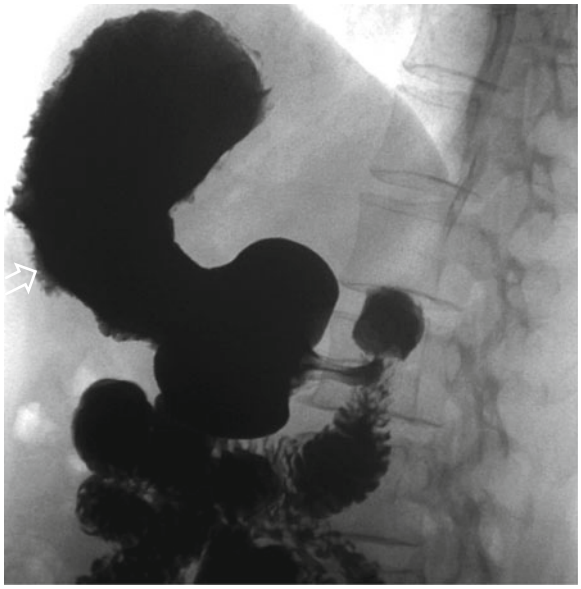

Fig. 7.2.1

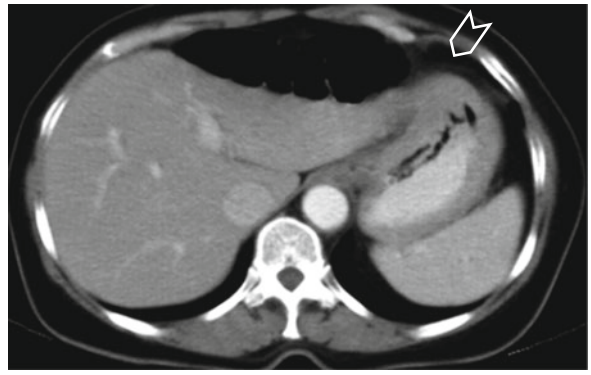

Fig. 7.2.2

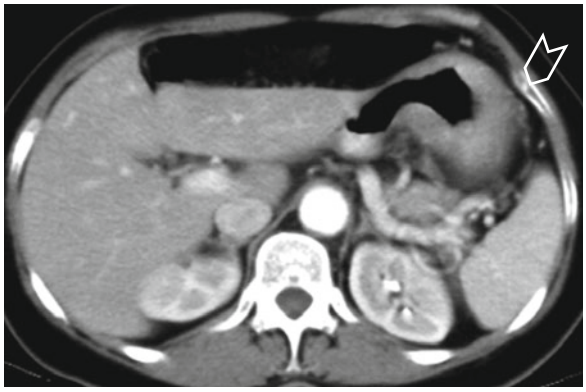

Fig. 7.2.3

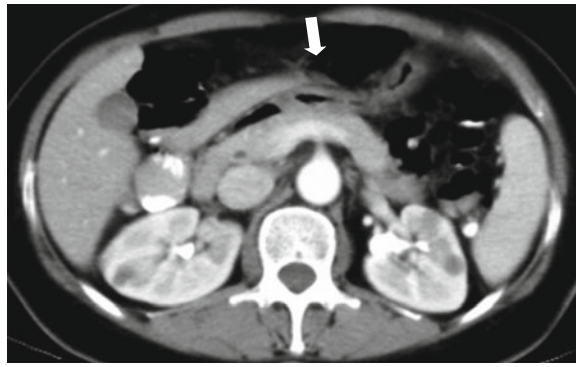

Fig. 7.2.4

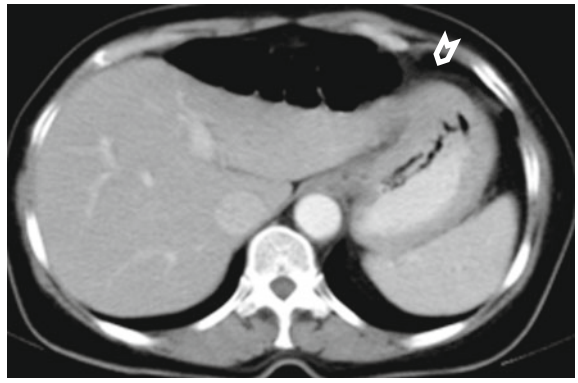

Fig. 7.2.5

A 68-year-old woman presented with severe epigastric pain and dysphagia. No relevant findings were observed at upper endoscopy, as she could not tolerate manometry, so an upper gastrointestinal series was done.

Comments

Gastric linitis plastica is a rare type of primary or secondary undifferentiated carcinoma, characterized by diffuse thickening and rigidity of the gastric wall resulting from inflammation and fibrosis. Linitis plastica can occur anywhere in the gastrointestinal tract, but it typically arises in the stomach. It accounts for 5% of all gastric tumors, and it is more frequent in patients under the age of 40.

The most common cause is a diffuse infiltrative gastric adenocarcinoma, but it can also result from metastatic breast carcinoma. The invasion of the gastric wall causes a desmoplastic response, and the stomach loses its elasticity and becomes contracted and tubular.

Patients usually complain of progressive dysphagia, abdominal pain, and weight loss.

The most common site of gastric linitis plastica is the antral and the pyloric regions. Histologically, it is characterized by a growth of the connective tissue with malignant cells being scarcely distributed in the fibrous stroma; it can affect all the gastric layers, although the gastric mucosa is often spared from malignant invasion. For this reason, standard endoscopic biopsy specimens, which usually contain only mucosa, are often negative for malignancy, and macrobiopsy or endoscopic ultrasound-guided biopsy are required.

At fluoroscopy, linitis plastica can appear as a narrowing of the gastric lumen. CT typically shows diffuse thickening of the gastric wall. Upper endoscopy may show marked thickening of the gastric mucosal folds with subsequent luminal narrowing and gastric wall rigidity. The mucosa can have a mosaic pattern with localized carmine-red nodular lesions.

The differential diagnosis includes benign conditions with enlargement of the gastric folds like lymphoid hyperplasia, granulomatous infiltration, or amyloidosis. Gastric malignancies like adenocarcinoma and infiltrative lymphoma should also be excluded, especially Hodgkin lymphoma, which can also cause a severe desmoplastic reaction and a similar radiologic appearance to linitis plastica.

Gastric linitis plastica has a very poor prognosis. The treatment is complete excision, but distant node metastases or carcinomatosis makes surgical excision rarely beneficial.

Imaging Findings

Upper gastrointestinal series shows a diffuse narrowing of the stomach and scalloping of the gastric contour (Fig. 7.2.1, *open arrow*). Abdominal CT after contrast injection and oral contrast administration (Figs. 7.2.2, 7.2.3, 7.2.4, and 7.2.5) shows a tubular stomach (*arrows*) with thickening of gastric wall (*open arrowheads*).

Case 3
Gastric Adenocarcinoma

A 59-year-old woman presented with ferropenic anemia and dyspepsia. Gastroscopy showed protruded and circumferential cancer, ulcerated from the body (2 cm from the cardia) and extending to the antrum.

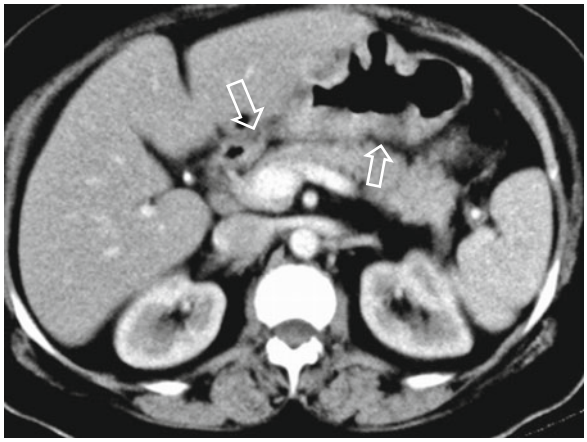

Fig. 7.3.1

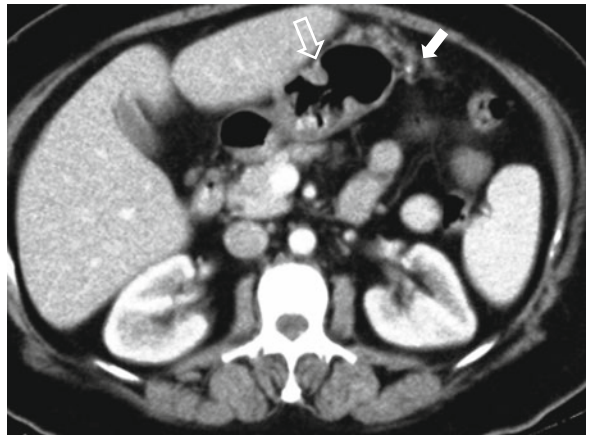

Fig. 7.3.2

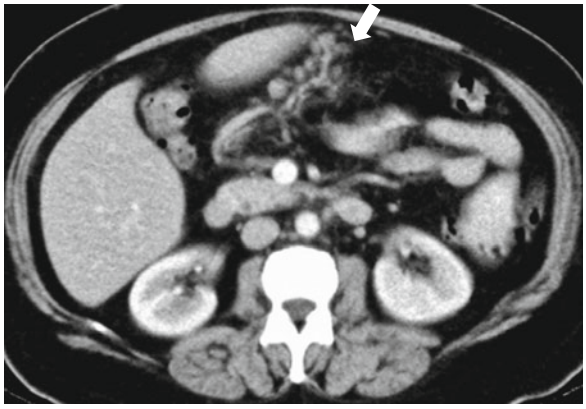

Fig. 7.3.3

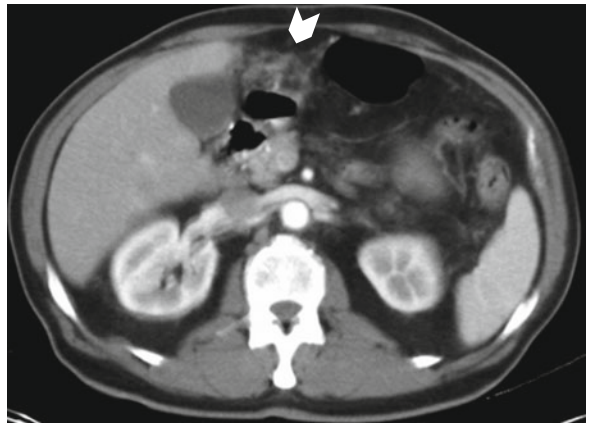

Fig. 7.3.4

Comments

Gastric cancer remains one of the most common cancers worldwide. Adenocarcinoma is the most common primary gastric tumor, accounting for 95% of cases. Environmental factors play an important role in the development of gastric cancer; *H. pylori* gastritis, Epstein-Barr virus infection, smoking, and a diet rich in nitrites or nitrates are some of the risk factors.

Early gastric cancer is defined as cancer confined to the mucosa or submucosa, irrespective of lymph node invasion. Most patients with early gastric cancer have symptoms of uncomplicated dyspepsia with no anemia, weight loss, or dysphagia. Early gastric cancer does not usually metastasize and can be resected endoscopically. However, most patients in the western world present with advanced gastric cancer.

Gastric adenocarcinoma can appear as a polypoid lesion, an ulcer, or an infiltrative lesion with narrowing of the gastric lumen (scirrhous type) like linitis plastica. Prognosis correlates with the stage of the tumor at presentation. One of the most important factors that affect the prognosis in patients with gastric cancer is lymph node involvement. Currently, the TNM staging system is a widely accepted method for assessing the prognosis of the disease and planning therapeutic strategies. CT is the staging modality of choice because it can help identify the primary tumor, assess for local spread, and detect nodal involvement and distant metastases. An adequate gastric distension is required for CT to indentify the primary lesion and determine the extent of abnormal wall thickness. One limitation of CT is the difficulty in detecting flat lesions that involve only the mucosa. CT cannot differentiate between T1 and T2 lesions. T3 can be suggested by identifying stranding into the adjacent perigastric fat, but differentiating between transmural extension and perigastric lymphadenopathy can be difficult. The diagnosis of T4 on CT relies on detecting contact between the tumor and contiguous organs or direct organ invasion.

Lymph node metastases are present at diagnosis in about 70% of gastric cancers, and liver metastases are present in about 15%. Hematogenous spread is the most common method of extension of gastric carcinoma. The most common sites of metastasis are the liver, lung, bone, adrenal glands, ovaries (Krukenberg tumor), and distant peritoneum. Metastatic disease of the peritoneum (carcinomatosis) is seen on CT as nodular thickening or enhancement of the peritoneum, omental masses, spiculated mesenteric masses, and ascites.

The differential diagnosis includes benign ulcer, gastritis, metastasis, Ménétrier disease, and lymphoma; deep biopsy is usually required for the diagnosis. Perigastric adenopathy is common in patients with gastric adenocarcinoma as well as in those with gastric lymphoma. However, adenopathy below the renal hila favors the diagnosis of gastric lymphoma over adenocarcinoma.

Imaging Findings

Contrast-enhanced CT (Figs. 7.3.1, 7.3.2, and 7.3.3) shows a nearly circumferential tumor located in the body and antrum (*open arrows*) with multiple perigastric lymph nodes (*arrows*). Contrast-enhanced CT image (Fig. 7.3.4) shows stranding of the adjacent perigastric fat with nodular thickening of the peritoneum representing peritoneal carcinomatosis from a gastric adenocarcinoma (*arrowhead*) in a different patient.

Case 4
Duodenal Diverticulum

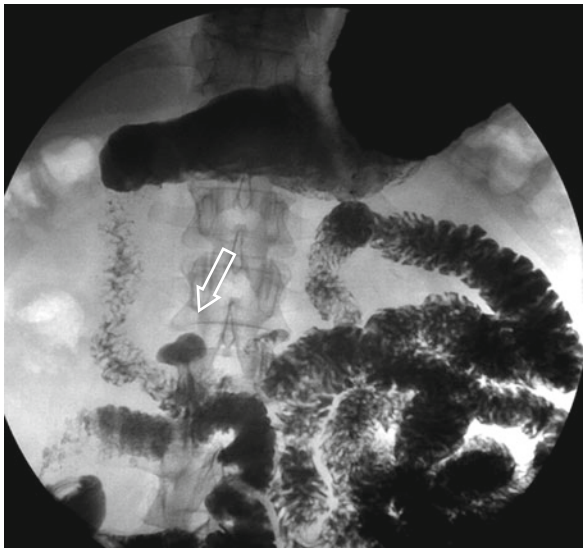

Fig. 7.4.1

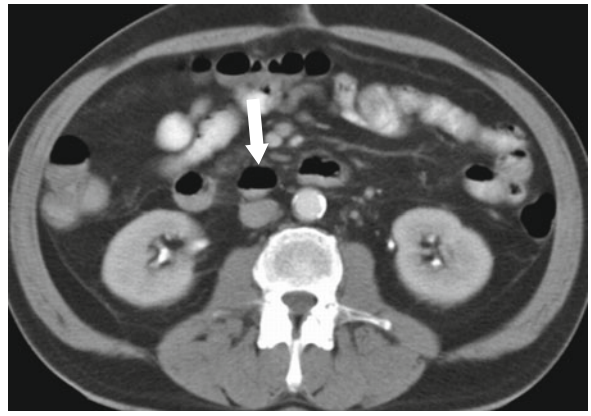

Fig. 7.4.2

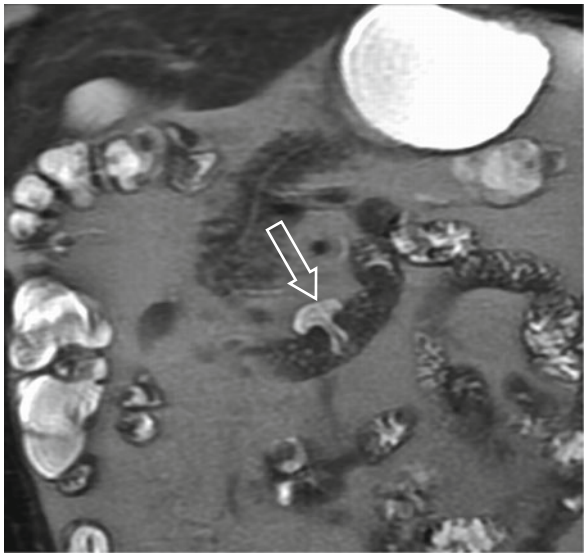

Fig. 7.4.3

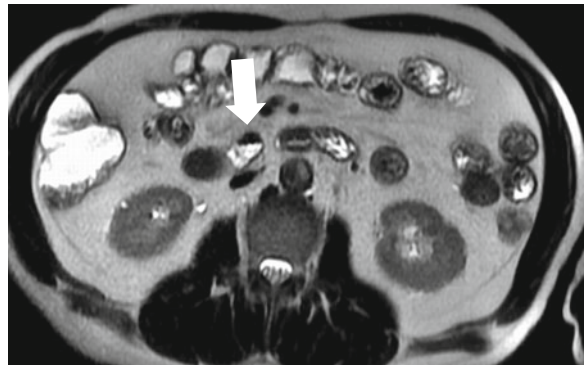

Fig. 7.4.4

A 76-year-old male was referred with epigastric and chronic abdominal pain for several years.

Comments

A diverticulum is a blind pouch leading off the alimentary tract, lined by mucosa that communicates with the lumen of the gut. The term true diverticulum implies that the pouch is composed of all layers of the intestinal wall, whereas a false diverticulum lacks a portion of the normal bowel. After the colon, the duodenum is the most common location for gastrointestinal diverticulum. They are easily recognized on upper gastrointestinal barium examinations, as well as on CT or MR imaging if they are filled with fluid and air.

Clinical diagnosis presents difficulty because a classic presentation does not exist. Symptoms are generally vague, <10% of the duodenal diverticulum are frankly symptomatic, and <1% to 2% will require surgical resection.

Perforation and bleeding are the most frequently reported complications. Duodenal diverticulum presents a major source of failure for endoscopic retrograde cholangiopancreatography (ERCP) if the common bile duct drains directly into a periampullary diverticulum, obscuring the orifice of the ampulla of Vatar. In rare cases, a duodenal diverticulum may become obstructed, resulting in associated duodenal diverticulitis.

Duodenal diverticula are incidentally discovered on upper gastrointestinal barium examinations in as many as 14.5% of patients and at autopsy in 22% of cadavers. Most duodenal diverticula are acquired, rather than congenital, abnormalities. They are easily recognized on upper gastrointestinal barium examinations as collections of gas and barium in round or oval saclike protrusions that usually arise from the medial aspect of the periampullary duodenum. CT appearance of a duodenal diverticulum has been described as a thin-walled rounded collection of gas and oral contrast material situated along the medial border of the junction of the second and third portions of the duodenum. On MR imaging, duodenal diverticula may contain both high-signal-intensity areas (related to the presence of fluid) and low-signal-intensity areas (related to the presence of gas).

Misinterpretation of a duodenal diverticulum on CT as a pancreatic tumor, metastatic lymph node, pancreatic pseudocyst, or pancreatic abscess has been reported. One may be unable to distinguish duodenal diverticula on CT or MR imaging if their content is purely fluid.

The differential diagnosis of a cystic lesion in the region of the head of the pancreas includes cystic pancreatic neoplasms, inflammatory processes (such as pseudocysts), and duodenal diverticula.

Imaging Findings

Radiograph from upper gastrointestinal barium series shows characteristic appearance of duodenal diverticulum (Fig. 7.4.1, *open arrow*). Axial CT (Fig. 7.4.2) scan obtained with IV and oral contrast materials shows a 10-mm air-filled cyst from the third portion of duodenum (*arrow*). Coronal MRI on T2-weighted image (Fig. 7.4.3) shows the diverticulum filled with fluid (*open arrow*), and the corresponding axial T2-weighted image depicts the fluid-air-filled lesion (*arrow*).

Case 5
Ménétrier Disease

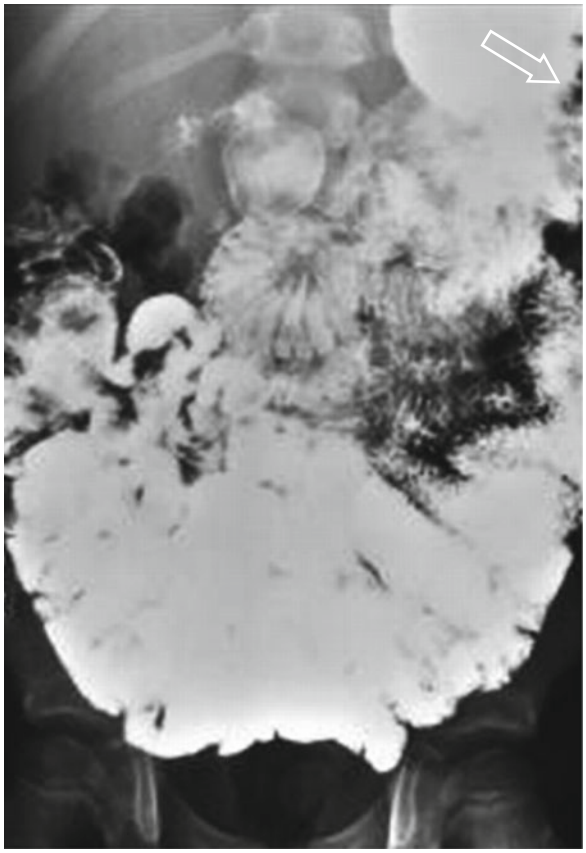

Fig. 7.5.1

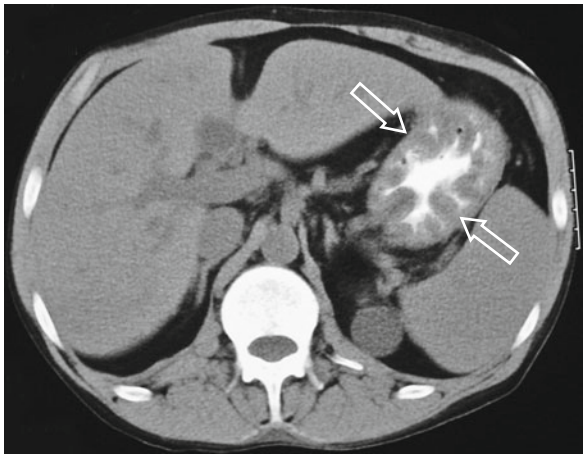

Fig. 7.5.3

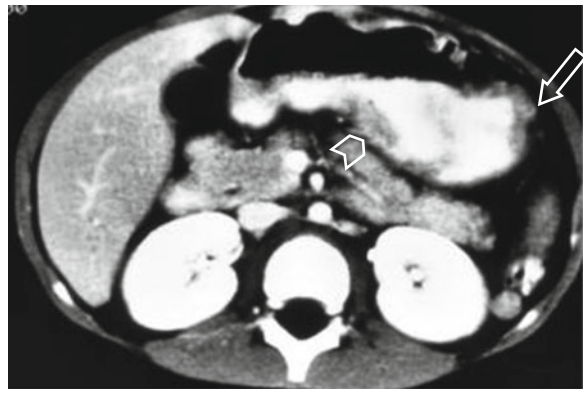

Fig. 7.5.2

Fig. 7.5.4

A 5-year-old boy underwent an upper gastrointestinal series and CT for abdominal distension and edema of 1 month's duration and laboratory findings of eosinophilia (12%) and hypoalbuminemia (2.2 g/dL).

Comments

Ménétrier disease is a rare chronic gastric disorder of unknown origin that is characterized by mucosal hypertrophy. It most commonly occurs in midlife, more often in men than in women, but there is a childhood form often linked to cytomegalovirus infection. The signs and symptoms of Ménétrier disease include anorexia, asthenia, weight loss, nausea, vomiting, gastrointestinal bleeding, diarrhea, edema, and hypoproteinemia (hypoalbuminemia). Hypoproteinemia is secondary to hyposecretion of acid and hypersecretion of mucus. The pathological findings include increased mucosal thickness caused by hyperplasia of epithelial cells. The hallmark of this disease is gastric mucosal hypertrophy; the submucosa and muscularis propia are not affected. Ménétrier disease usually affects the fundus and the body, and the greatest degree of fold thickening occurs on or near the greater curvature. The antrum is less commonly affected; however, it can be involved in the 46% of cases, and the diagnosis of Ménétrier disease should be considered when gastric rugal fold enlargement is seen in any region of gastric mucosa.

In fluoroscopic images, the mucosal hypertrophy is seen as thickened and lobulated mucosal folds. In contrast-enhanced CT images, the folds are seen as areas of thickened mucosa that project into the gastric lumen, usually with normal gastric mucosa between them, and a smooth serosal contour. The giant rugal folds can resemble convolutions of the brain. Endoscopy will show a hypertrophic gastric mucosa with swollen and spongy folds.

The differential diagnosis should consider other conditions with gastric fold thickening, including infectious causes like H. pylori gastritis or cytomegalovirus infection, infiltrative diseases, and malignancies like lymphoma or carcinoma. An increased risk for gastric malignancy has been hypothesized. Pediatric disease has a benign course and usually resolves spontaneously in weeks or months.

Imaging Findings

Radiograph from upper gastrointestinal barium series (Fig. 7.5.1) shows enlarged gastric fold, simulating a polypoid filling defect (*open arrow*). Contrast-enhanced CT (Fig. 7.5.2) shows thickening of the gastric wall in the greater curvature (*arrow*) and lesser curvature (*open arrowhead*). CT image from a different patient (Fig. 7.5.3) shows diffuse thickening of the gastric wall (*open arrows*). Photomicrograph (Fig. 7.5.4, original magnification, ×10; hematoxylin-eosin stain) appearance from the gastric mucosa of Ménétrier disease shows foveolar hyperplasia with elongation of pits, and glandular cystic dilatation.

Case 6
T-Cell Lymphoma

Fig. 7.6.1

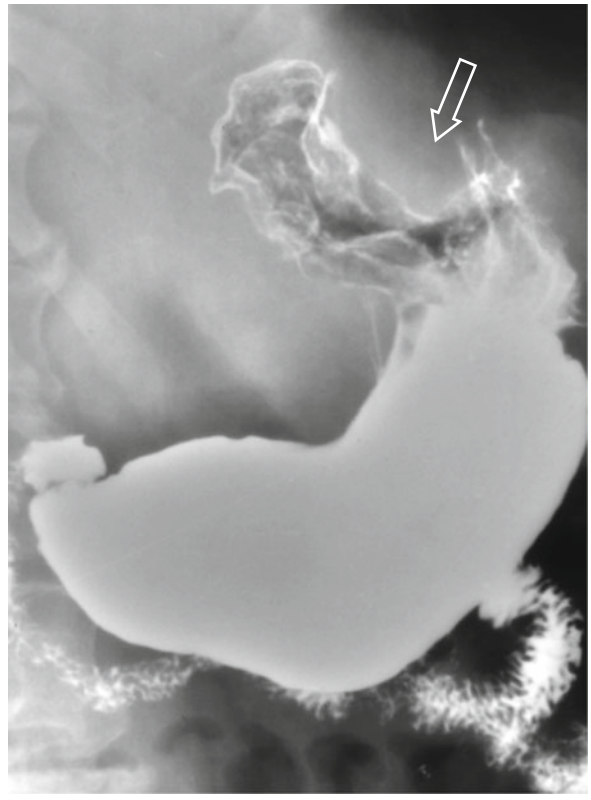

Fig. 7.6.2

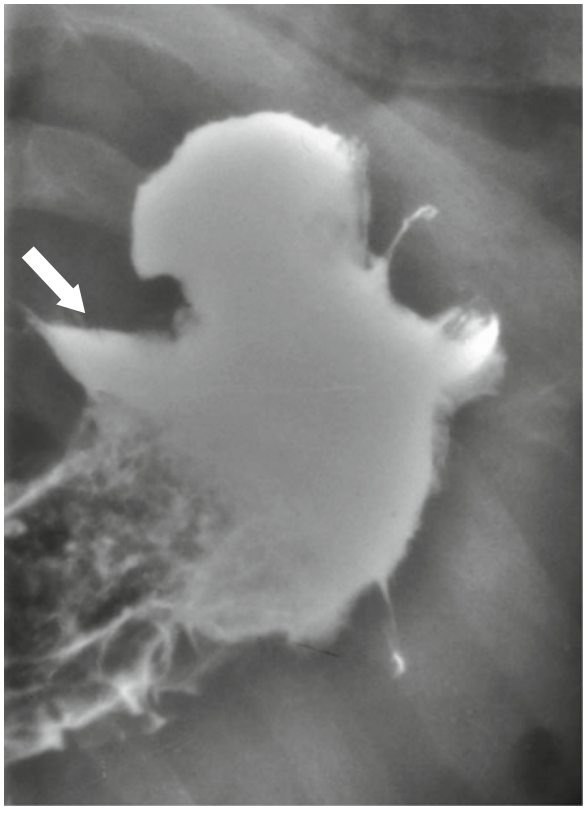

Fig. 7.6.3

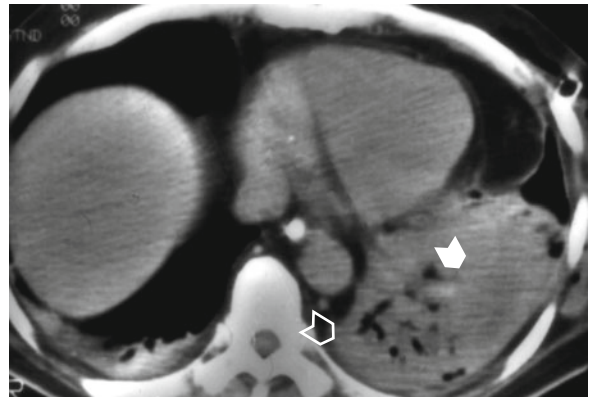

Fig. 7.6.4

A 62-year-old man presented with a 1-month history of an ulcer on his arm. A biopsy revealed an extranodal cutaneous T-cell lymphoma. One month later, he was admitted in the ER for important upper digestive bleeding.

Comments

Peripheral T-cell lymphoma (PTCL) is rare disease. It represents a small proportion of lymphomas, accounting for 5–30% of all non-Hodgkin lymphomas. The most common sites of extranodal involvement include bone marrow, skin, lung, and liver, but the gastrointestinal tract is rarely affected. Although PTCL is commonly associated with celiac disease, it can occur in patients without enteropathy. It can occur anywhere in the gastrointestinal tract, but in contrast to B-cell lymphomas, in which the stomach is the most frequent site, PTCL usually affects the upper part of the jejunum and duodenum, often causing bowel perforation. The course is aggressive, and death usually results from multifocal intestinal perforation caused by refractory malignant ulcers.

CT can depict PTCL involving the gastrointestinal tract if it is not confined to the mucosa. Moreover, CT provides information about both mural and extramural disease; it allows accurate staging and the evaluation of the presence or absence of lymphadenopathy, involvement of other organs (hepatomegaly, splenomegaly), and the response to treatment. Gastric PTCL commonly appears as diffuse or segmental infiltration with gastric wall thickening, but it can also appear as a localized polypoid lesion. Fluoroscopy can show narrowing of the gastric lumen or a filling defect. On gross pathology, the most common finding is the presence of ulcers.

Imaging Findings

Cutaneous ulcer on the arm (Fig. 7.6.1). Fluoroscopy shows a filling defect in the gastric fundus, representing an irregular polypoid gastric mass (Fig. 7.6.2, *open arrow*). There is also a filling defect in the lesser curvature (Fig. 7.6.3, *arrow*) at fluoroscopy. Contrast-enhanced CT (Fig. 7.6.4) demonstrates diffuse gastric wall thickening (*open arrowhead*) and an ill-defined mass in the gastric fundus with homogeneous hypoattenuation (*arrowhead*). There was not lymphadenopathy in the perigastric region or at other sites, and no other organ involvement was detected.

Case 7
Burkitt's Lymphoma

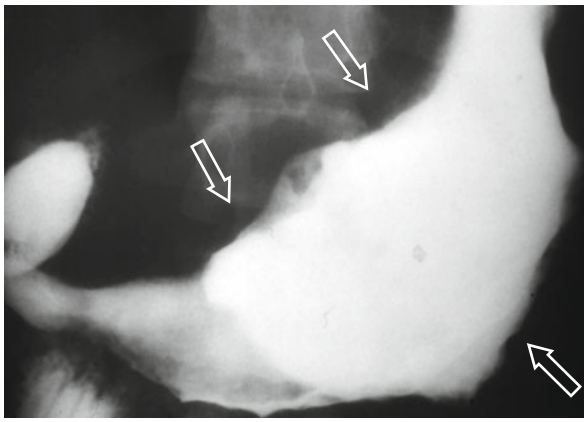

Fig. 7.7.1

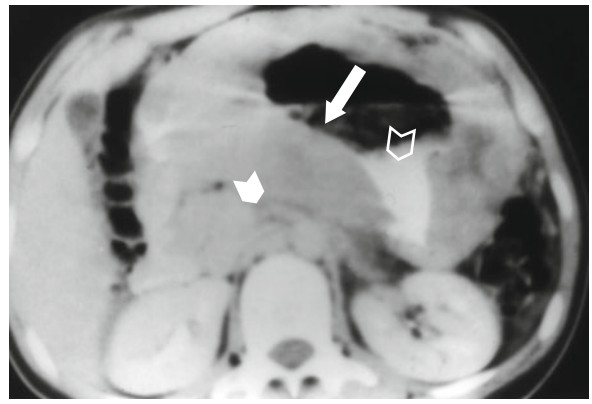

Fig. 7.7.2

A 17-year-old boy presented with 10- to 15-day history of vomiting and fever, as well as weight loss superior to 10% during the preceding month. Clinical examination revealed a left supraclavicular lymph node and a firm epigastric mass. Routine hematological and biochemical parameters were essentially normal. Upper gastrointestinal endoscopy revealed thickened gastric folds lacking distensibility, suggesting diffuse infiltration by a tumor.

Comments

Burkitt's lymphoma (BL) is a highly aggressive non-Hodgkin lymphoma arising from undifferentiated B-cell-derived lymphocytes. BL often presents in extranodal sites or as acute leukemia. The incidence of gastric BL is low compared to other types of gastric lymphomas, although its true incidence is not yet defined.

There are three main clinical variants: the endemic, the sporadic, and the immunodeficiency-associated variants. The endemic variant is found in tropical latitudes, and in some regions of Africa, it is the most common malignant disease of childhood. It usually involves extranodal sites, commonly beginning in the head and neck, especially in the jaw area, and a high percentage of cases are associated with antibodies to the Epstein-Barr virus. The sporadic variety is rare. It occurs in nonendemic areas but is histologically indistinguishable from the endemic variant; however, the age of onset is superior and intra-abdominal involvement is common. The immunodeficiency-associated variants are all associated with HIV and AIDS.

BL differs from other types of lymphoma in that it involves multiple extranodal sites; consequently, a different staging classification is used, depending on the extent of extra-abdominal and intra-abdominal masses or involvement. CT is the method of choice for diagnostic purposes and for assessing the full extent of intra-abdominal disease. The most common finding is an abdominal or pelvic mass, but BL can also appear as ascites, a retroperitoneal mass, splenomegaly, hepatic lesions, thickened gastric wall, or renomegaly. Bowel opacification with oral contrast helps in distinguishing lymphomatous masses from fluid-filled bowel on CT.

The treatment of choice is chemotherapy and surgical debulking when possible. CT examination is also useful to evaluate the response to chemotherapy, detect recurrences, or assess the adequacy of surgical debulking. The prognosis is poor, and it is related to tumor volume rather than to site of involvement.

Imaging Findings

Radiograph from upper gastrointestinal barium series (Fig. 7.7.1) shows a rigid, nondistended stomach (*open arrows*). Abdominal CT after contrast injection and oral contrast administration (Fig. 7.7.2) demonstrates diffuse thickening of the gastric wall (*open arrow*) with an ulceration (*open arrowhead*) and retroperitoneal lymph nodes (*solid arrowhead*).

Case 8
Gastric Pneumatosis

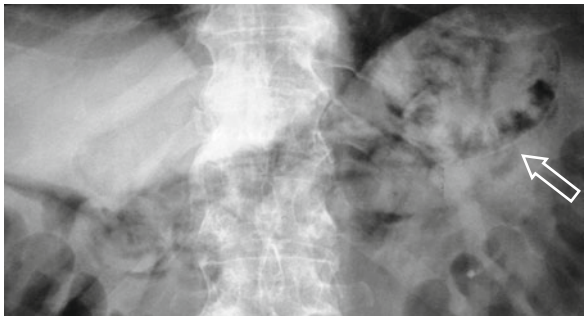

Fig. 7.8.1

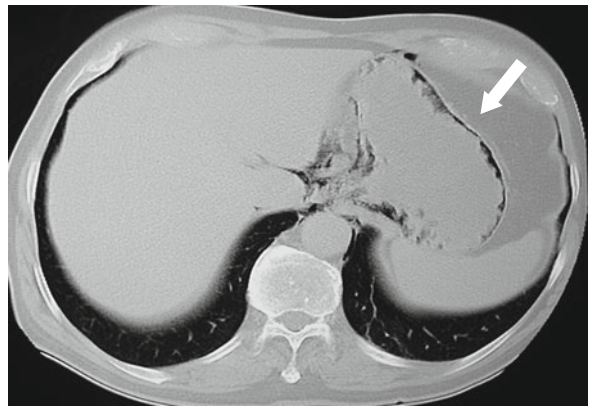

Fig. 7.8.2

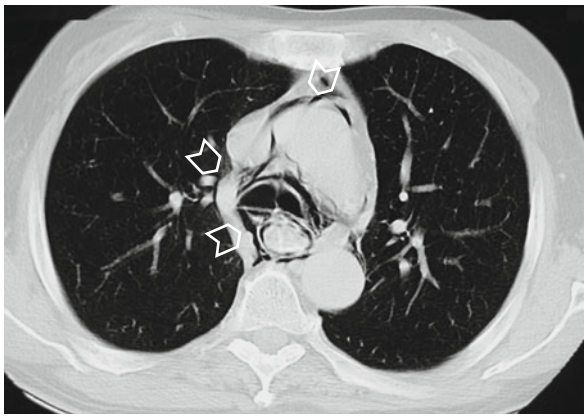

Fig. 7.8.3

A 62-year-old woman received a kidney transplant. After general anesthesia and intraoperative placement of a central venous catheter in the left internal jugular, the transplantation proceeded without complications. On postoperative day 11, when the internal jugular central venous catheter was removed in preparation for discharge, the patient developed chest crepitus and complained of shortness of breath.

Comments

Central venous catheters (CVCs) are commonly used in intensive care units to administer fluids, medications, and blood products. CVCs are associated with complications at the time of placement like pneumothorax or carotid artery puncture as well as with delayed complications like hydrothorax, cardiac tamponade, and catheter-related infection.

Gastric pneumatosis is rare. In children, it has been reported secondary to duodenal stenosis or hypertrophic pyloric stenosis, to child abuse, and to intramural malplacement of a feeding catheter, and to cardiac surgery in the neonatal period. In adults, it can be associated with a relatively benign disorder and is most often observed in a distended stomach after injury to the gastric mucosa from intubation or ulceration. It can also be caused by emphysematous gastritis, a rare infection of the stomach wall by a gas-producing organism that leads to high mortality. However, the radiologic appearance of gastric pneumatosis due to emphysematous gastritis is different, because it is usually associated with a collapsed stomach and typically presents as an edematous stomach wall with air collections within, rather than as linear pneumatosis.

Imaging Findings

Plain film shows a radiolucent line in the gastric wall, representing gastric pneumatosis (Fig. 7.8.1, *open arrow*). CT shows linear air within the gastric wall, representing gastric pneumatosis (Fig. 7.8.2, *arrow*). Chest CT shows pneumomediastinum (Fig. 7.8.3, *open arrowheads*).

Case 9
Gastric Leiomyoma

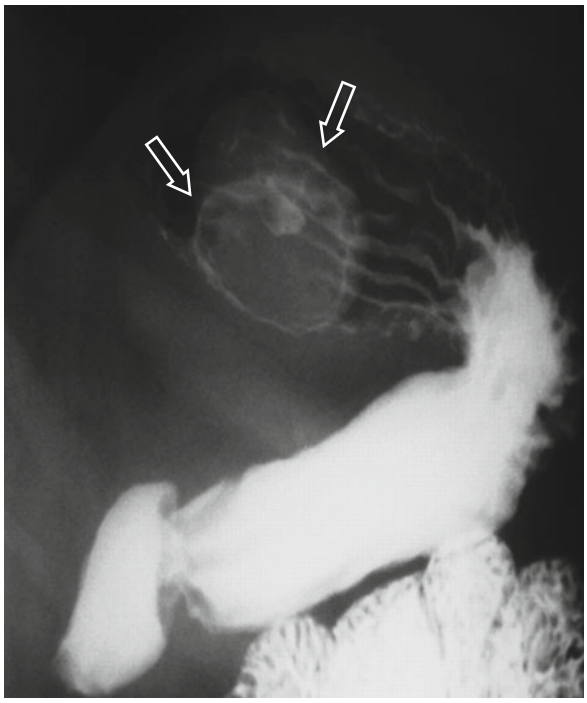

Fig. 7.9.1

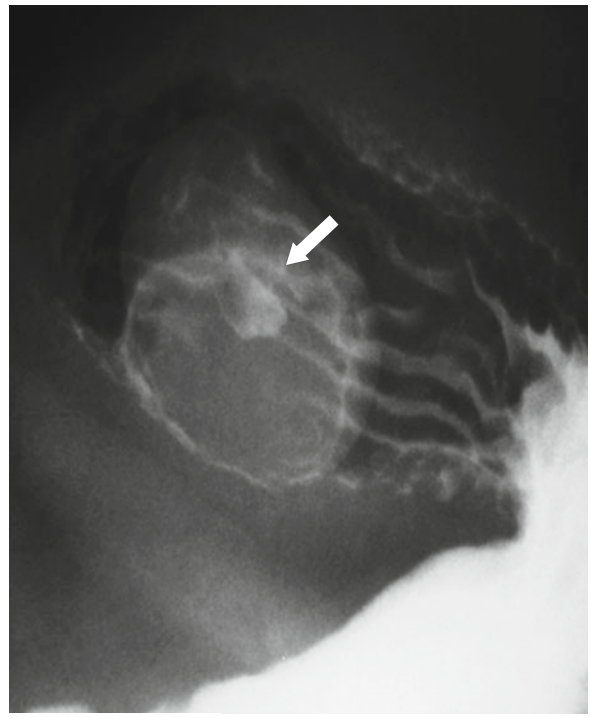

Fig. 7.9.2

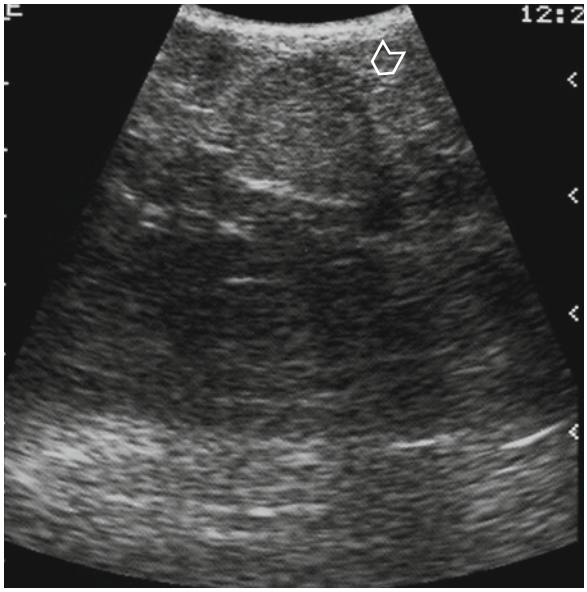

Fig. 7.9.3

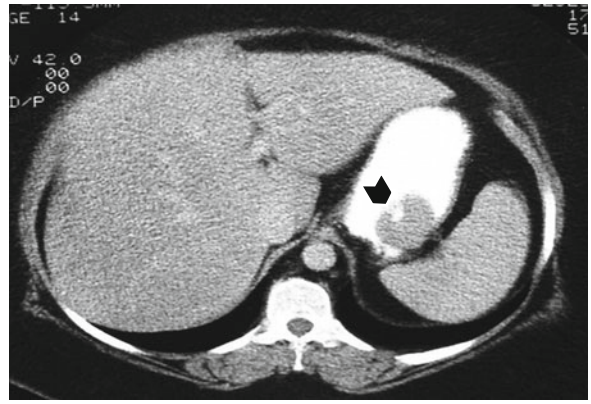

Fig. 7.9.4

A 53-year-old man presented with a history of episodes of hematemesis associated with dizziness, palpitation, and melena; he had no history of epigastric pain, anorexia, or weight loss. Anemia was detected and corrected by blood transfusion.

Comments

Gastric leiomyoma (GLM) is a submucosal lesion that represents 2.5% of gastric neoplasms and 6% of all benign gastric tumors. It originates from the muscularis mucosa or muscularis propia. The esophagus is the portion of the gastrointestinal tract most oftenly affected by leiomyoma. Gastric leiomyoma is usually located in the body and fundus of the stomach.

GLM is usually a small, solitary tumor, although tumors as large as 6 cm in diameter have been reported. GLM often appears as an ulcerated mass. Most commonly, GLM grows slowly, and is asymptomatic. Sometimes, it can become clinically apparent due to bleeding from ulceration of the overlying gastric mucosa. Malignant transformation is exceptional and may be announced by repeated hemorrhages or rapid growth.

On upper gastrointestinal serie, GLM is found as a filling defect of the gastric wall. Approximately 5% of GLMs have radiologically visible calcifications. On endoscopy, GLM is found as a submucosal mass. Endoscopic ultrasound (EUS) findings can distinguish leiomyomas from hemangiomas, cysts, and lipomas in the digestive tract wall. EUS can evaluate both the nature of the leiomyoma and its layer of origin. Gastrointestinal carcinoid has a similar appearance at ultrasonography, so it must be included in the differential diagnosis. Furthermore, the possibility of a leiomyosarcoma should be considered when the leiomyoma is larger than 4 cm, has erosion or ulceration on its surface, or has an inhomogeneous internal structure.

Surgical resection is the treatment of choice for GLM and it can also be treated with laparoscopic wedge resection. However, because of its slow growth, watchful waiting is another option in patients with small lesions or lesions originating from the muscularis propia.

Imaging Findings

Radiographs from upper gastrointestinal barium series (Figs. 7.9.1 and 7.9.2) show a polypoid mass with well-delineated contours (*open arrows*) and an ulceration in the middle of the mass (*arrow*). The mucosal folds around the filling defect are moved apart but not disorganized. Ultrasound shows a homogeneous mass with clear margins (Fig. 7.9.3, *open arrowhead*). Abdominal CT after contrast injection and oral contrast administration shows a well-defined polypoid mass arising from the posterior wall of the gastric fundus, with an ulceration (Fig. 7.9.4, *arrowhead*). There was not gastric wall thickening.

Case 10
Duodenal Hemangioma

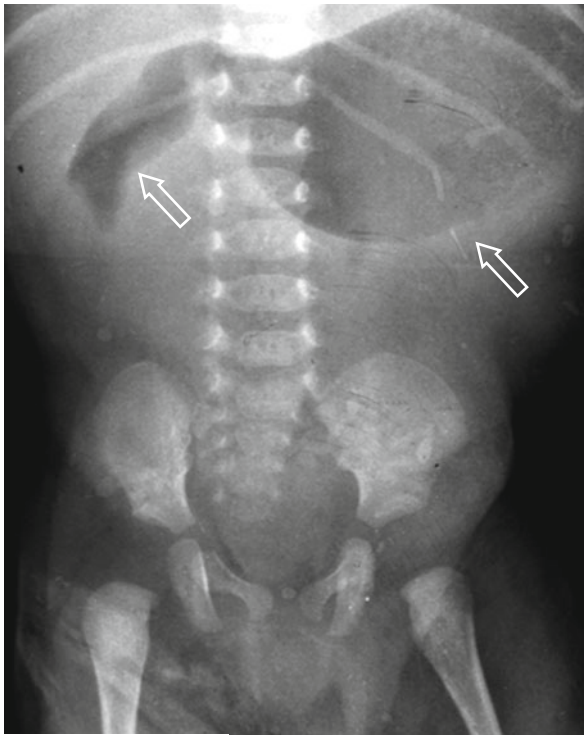

Fig. 7.10.1

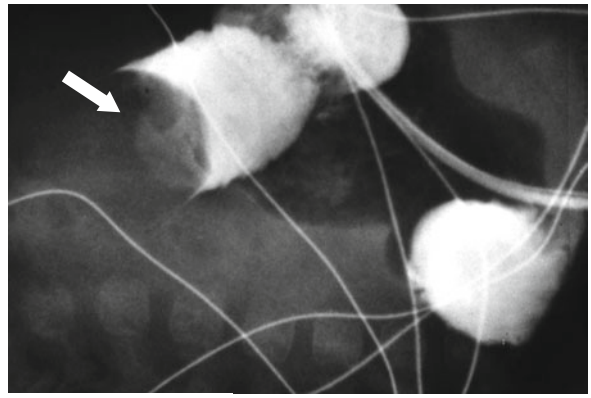

Fig. 7.10.2

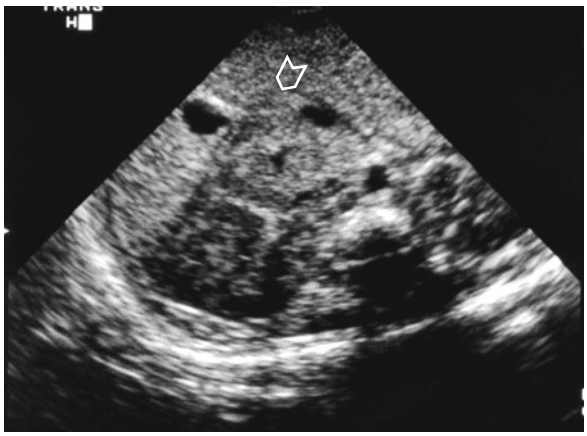

Fig. 7.10.3

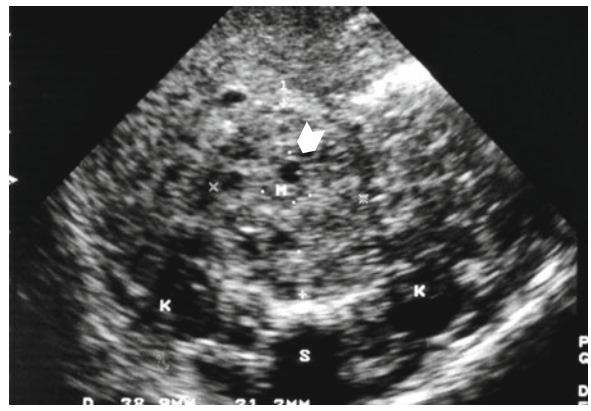

Fig. 7.10.4

A 7-week-old boy presented with a palpable right upper quadrant mass.

Comments

Hemangioma is a common benign vascular neoplasm that can occur in any organ. It represents <2% of benign tumors in the stomach and is even less common in the duodenum. In most cases, hemangiomas are multiple. They are usually asymptomatic. Their clinical importance lies on the risk of bleeding.

When located in the stomach or duodenum, hemangiomas appear as an intramural or sessile mass with a smooth surface. Although an uncommon finding, the presence of phleboliths on the plain film is pathognomonic of hemangioma. In the gross pathologic findings, hemangiomas can have numerous tiny vascular structures (capillary type) or large blood spaces or sinusoids lined with endothelial tissue (cavernous type). The differential diagnosis should include other benign gastroduodenal tumors that appear as intramural masses, like GIST (which is the most frequent mesenchymal gastric tumor), lipoma, leiomyoma, lymphangioma, or neurofibroma.

Imaging Findings

Abdominal plain film shows distension of the stomach and duodenum (Fig. 7.10.1, *open arrows*). There is an obstruction at the level of the duodenum, and no gas is seen in the small bowel or colon. Figure 7.10.2: Fluoroscopy confirms the duodenal obstruction secondary to a mass-filling defect (Fig. 7.10.2, *arrow*). Ultrasound (Figs. 7.10.3 and 7.10.4, *arrow*) shows a well-defined mass in the duodenum (*open arrowhead*). Notice the presence of vascular structures within the lesion (*solid arrowhead*).

Further Reading

Books

Eisenberg RL (ed) (2002) Gastrointestinal radiology. A pattern approach, 4th edn. Lippincott Williams & Wilkins, Baltimore

Federle MP (2004) Diagnostic imaging; abdomen, 1st edn. Amirsys, Salt Lake City

Federle MP (2008) EXPERTddx: abdomen, 1st edn. Lippincott Williams & Wilkins, Philadelphia

Semelka RC (2006) Abdominal-pelvic. MRI, 2nd edn. Wiley, Hoboken

Skucas J (2006) Advanced imaging of the abdomen, 1st edn. Springer-Verlag, Berlin, Heidelberg

Web-Links

American College of Gastroenterology: www.acg.gi.org

American Gastroenterological Association: www.gastro.org

British Society of Gastroenterology: www.bsg.org

European Society of Gastrointestinal and Abdominal Radiology: www.esgar.org

International Union Against Cancer (UICC): TNM classification of malignant tumors. 7th Edition Changes: www.uicc.org

Articles

Bajaj M, Ogilvy-Stuart AL (2004) Gastric pneumatosis/interstitial emphysema of the stomach. Arch Dis Child Fetal Neonatal Ed 89(2):F188

Ba-Ssalamah A, Prokop M, Uffmann M et al (2003) Dedicated multidetector CT of the stomach: spectrum of diseases. Radiographics 23(3):625–644

Byun JH, Ha HK et al (2003) CT findings in peripheral T-cell lymphoma involving the gastrointestinal tract. Radiology 227(1):59–67

Chourmouzi D, Sinakos E, Papalavrentios L et al (2009) Gastrointestinal stromal tumors: a pictorial review. J Gastrointestin Liver Dis 18(3):379–383

Faltas B, Kramer ZB (2009) Gastric Burkitt lymphoma associated with Efalizumab and Helicobacter pylori. Leuk Lymphoma 50(9):1538–1539

Fishman EK, Urban BA et al (1996) CT of the stomach: spectrum of disease. Radiographics 16:1035–1054

Flatley ME, Schapira RM (1993) Hydropneumomediastinum and bilateral hydropneumothorax as delayed complications of central venous catheterization. Chest 103(6):1914–1916

Friedman J, Platnick J et al (2009) Best cases from the AFIP. Ménétrier disease. Radiographics 29(1):297–301

Ghai S, Pattison J et al (2007) Primary gastrointestinal lymphoma: spectrum of imaging findings with pathologic correlation. Radiographics 27(5):1371–1388

Grayson DE, Abbott RM, Levy AD et al (2002) Emphysematous infections of the abdomen and pelvis: a pictorial review. Radiographics 22(3):543–561

Habermann CR, Weiss F et al (2004) Preoperative staging of gastric adenocarcinoma: comparison of helical CT and endoscopic US. Radiology 230:465–471

Haswell DM, Carsky EW (1979) Hepatic portal venous gas and gastric emphysema with survival. AJR Am J Roentgenol 133(6):1183–1185

Hong X, Choi H, Loyer EM et al (2006) Gastrointestinal stromal tumor: role of CT in diagnosis and in response evaluation and surveillance after treatment with imatinib. Radiographics 26(2):481–495

Horton KM, Fishman EK et al (2003) Current role of CT in imaging of the stomach. Radiographics 23(1):75–87

Kanne JP, Mankoff DA, Baird GS et al (2007) Gastric linitis plastica from metastatic breast carcinoma: FDG and FES PET appearances. AJR Am J Roentgenol 188(6): W503–W505

Kesik V, Safali M, Citak EC et al (2010) Primary gastric Burkitt lymphoma: a rare cause of intraabdominal mass in childhood. Pediatr Surg Int 26(9):927–929

Krudy AG, Dunnick NR et al (1981) CT of American Burkitt lymphoma. AJR Am J Roentgenol 136(4):747–754

Lee HJ, Im JG et al (2003) Peripheral T-cell lymphoma: spectrum of imaging findings with clinical and pathologic features. Radiographics 23(1):7–26; discussion 26–28

Lim JS, Yun MJ, Kim MJ et al (2006) CT and PET in stomach cancer: preoperative staging and monitoring of response therapy. Radiographics 26:143–156

Negreanu L, Assor P, Bumsel F et al (2007) An endoscopic view in gastric linitis. A case report. J Gastrointestin Liver Dis 16(3):321–323

Park SH, Han JK et al (1999) Unusual gastric tumors: radiologic-pathologic correlation. Radiographics 19(6): 1435–1446

Patel SD, Semeraro D, Hall RI (2005) Linitis plastica due to gastric diverticulosis. J R Soc Med 98(9):416–417

Sussman SK, Halvorsen RA et al (1988) Gastric adenocarcinoma: CT versus surgical staging. Radiology 167:335–340

Tarcoveanu E, Bradea C, Dimofte G et al (2006) Laparoscopic wedge resection of gastric leiomyoma. JSLS 10(3):368–374

Xu GQ, Zhang BL, Li YM et al (2003) Diagnostic value of endoscopic ultrasonography for gastrointestinal leiomyoma. World J Gastroenterol 9(9):2088–2091

Small Bowel

8

Sandra Baleato, Gabriel C. Fernández, Lidia Alcalá Mata, and Antonio Luna

Contents

A. Luna et al., *Learning Abdominal Imaging*, Learning Imaging,
DOI 10.1007/978-3-540-88003-5_8,

Case 1
Meckel's Diverticulum

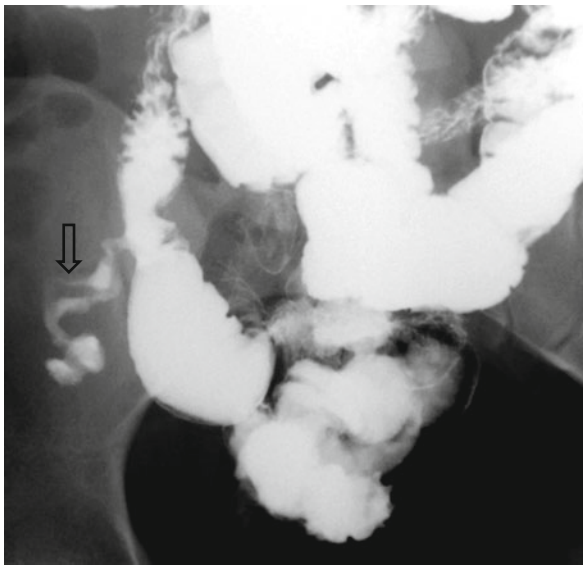

Fig. 8.1.1

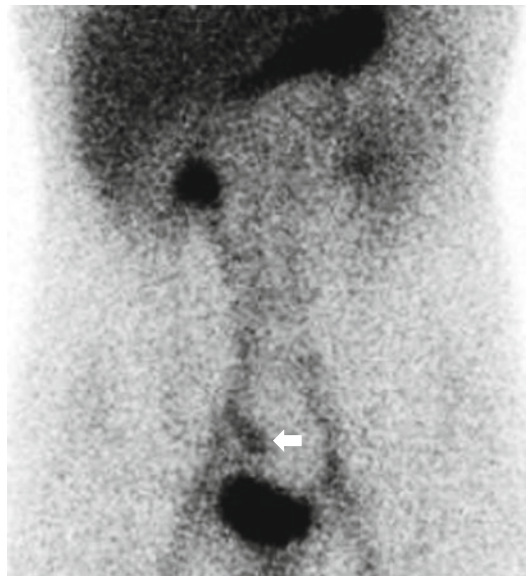

Fig. 8.1.2

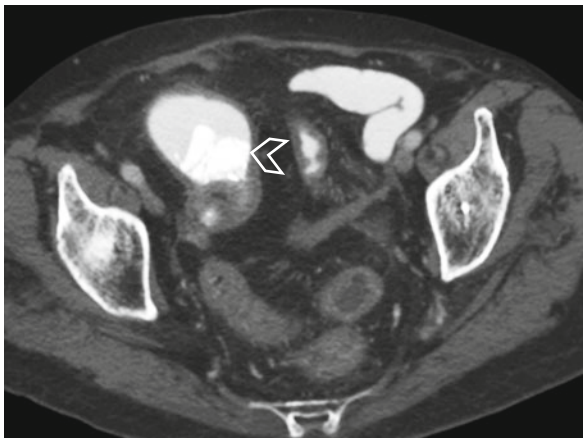

Fig. 8.1.3

A 23-year-old male presented at the emergency room with recurrent attacks of abdominal pain and gastrointestinal bleeding. A barium meal examination of the small intestine and Tc-99m pertechnetate scanning were performed preoperatively.

Comments

Meckel's diverticulum (MD) is the most common congenital abnormality of the small bowel and is estimated to occur in approximately 2% of the population. It results from improper closure and absorption of the omphalomesenteric duct, which connects the primitive midgut to the yolk sac during embryonic development.

An MD represents a true diverticulum that contains all three layers of the intestinal wall and arises from the antimesenteric border of the small bowel. The diverticulum generally occurs within 40–100 cm of the ileocecal valve, and 90% of diverticula range from 1 to 10 cm in length. Approximately 50% of Meckel's diverticula harbor heterotopic mucosa, more than 60% of which is the gastric type.

The majority of patients with this anomaly will remain asymptomatic; however, several complications may occur, including obstruction, intussusception, perforation, diverticulitis, and gastrointestinal hemorrhage. These complications may produce a variety of different clinical features and radiological appearances. Complications are much more common in males, and the incidence of complications decreases with age, with the majority occurring in the pediatric population. The most common presentation in the pediatric age group is painless rectal bleeding.

Radiological diagnosis of MD can be difficult, particularly when the diagnosis is not initially suspected. Ultrasound is often used in the setting of nonspecific abdominal pain, as it was in our patient; however, it is of limited value for diagnosing MD except in the case of intussusception. The technetium-99 m pertechnetate scan, or Meckel's scan, is generally regarded as the most accurate, noninvasive diagnostic technique. However, false-negative rates are higher in patients without bleeding, and ectopic gastric mucosa must be present in the MD for a positive result.

On CT, the diverticulum has been reported to appear as a rounded or tubular collection of air and fluid located in the abdomen or pelvis which communicates with the adjacent small bowel. Mesenteric inflammatory change is associated with this condition, and an enterolith may rarely be visualized as well. Radiologists should look for findings that might suggest Meckel's diverticulum when encountering lower abdominal inflammatory disorders.

Imaging Findings

A plain radiograph of the right side of the abdomen (Fig. 8.1.1) obtained during a follow-through GI barium series shows the pelvic ileal loops and a Meckel's diverticulum (*arrow*) with ectopic gastric mucosa visualized as a rugal pattern inside. A technetium-99 m-labeled heat-damaged RBC scan (Fig. 8.1.2) in the same patient shows a focus of intense activity

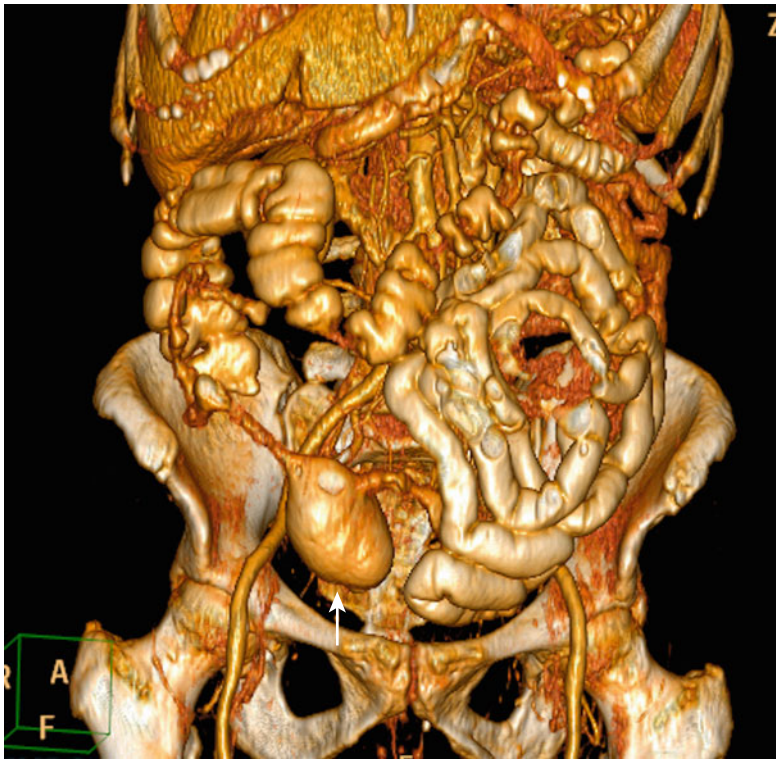

Fig. 8.1.4

(*arrow*) in the right lower quadrant on initial flow study. In a second different patient, unenhanced pelvic CT (Fig. 8.1.3) showed a blind-ending fluid structure in continuity with small bowel with multiple enteroliths inside (*open arrowhead*), corresponding to a MD. Volume rendering of the CT in the same patient (Fig. 8.1.4) showed the single diverticulum arising from the antimesenteric border of the distal ileum (*arrow*).

Case 2
Celiac Disease

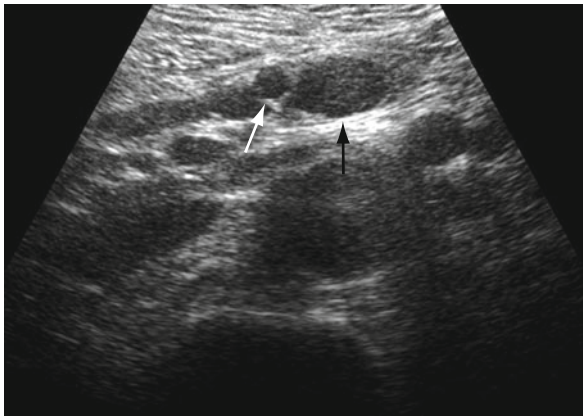

Fig. 8.2.1

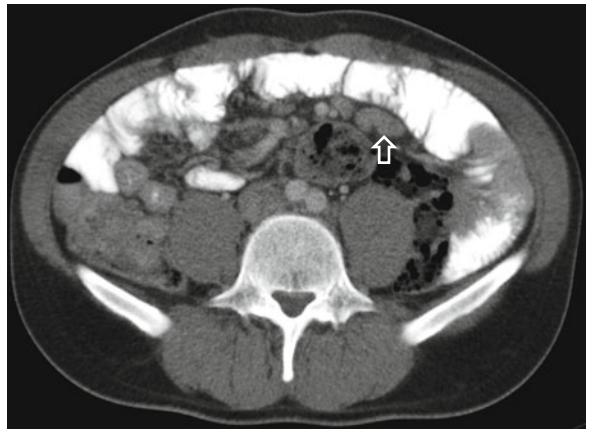

Fig. 8.2.2

Fig. 8.2.3

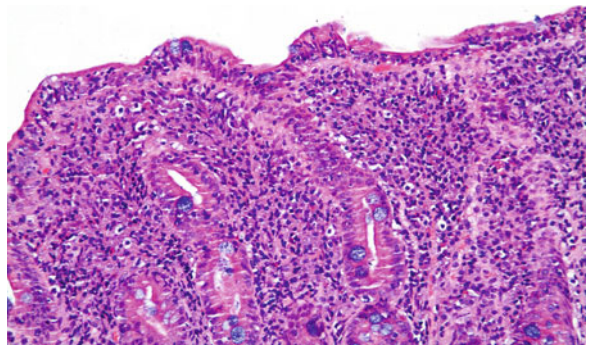

Fig. 8.2.4

A 33-year-old male presented with a history of abdominal pain, anemia, and deficit of folic acid.

Comments

Celiac disease (CD) is a chronic intolerance of gluten that induces intestinal mucosal lesions in genetically predisposed patients. Diagnosis is based on the presence of mucosa atrophy of the small bowel with crypt hyperplasia on duodenal or jejunal biopsies in case of a gluten containing diet, with improvement or return to normal after a gluten-free diet.

Some patients are asymptomatic, whereas other patients have symptoms ranging from fatigue and vague abdominal pain to weight loss, diarrhea, abdominal pain, and frank malabsorption with steatorrhea. A common complication in CD patients that present acute abdominal pain is transitory ileal intussusceptions.

The pathological changes of celiac disease are predominantly seen in the duodenum and proximal jejunum. However, the extent of the disease is extremely variable, ranging from segmental to full involvement of the small bowel.

Traditionally imaging techniques used to evaluate small intestine in patients with CD are represented by conventional barium studies. The most specific sign of disease at conventional barium is a decreased number of jejunal folds (<3 folds per inch) and an increased number of ileal folds (>5 per inch) depicting the so-called jejunoileal fold pattern reversal and barium flocculation due to dilution of contrast medium with intestinal fluids. Other common findings in untreated patients with CD are: small-bowel dilatation due to intestinal atony, mesenteric abnormalities that include lymph node enlargement (>1 cm in short axis), mesenteric vascular enlargement, and hyposplenism, which presents an incidence between 30% and 50% in celiac patients.

The development of malignancy is the most serious complication that occurs in patients with celiac disease. When compared to the general population, patients with celiac disease are at increased risk of lymphoma, adenocarcinoma, and squamous cell carcinomas. Abdominal CT is considered to play the key role in the evaluation of complications; however, small bowel barium studies remain as a fast and available technique for examining the small-bowel mucosa.

Imaging Findings

US (Fig. 8.2.1) and axial abdominal CT (Fig. 8.2.2) show multiple enlarged mesenteric lymph nodes (*arrows*). Coronal CT MPR (Fig. 8.2.3) demonstrates an ileoileal intussusception with the classic halo sign (*arrow*) that represents the different stratified layers of the small bowel wall and peritoneal fat tissue. Photomicrograph (original magnification, ×10; hematoxylin-eosin stain) of villous damage resulting from CD is shown in Fig. 8.2.4. The jejunal mucosa is flattened due to extensive loss of villi.

Case 3

Intramural Duodenal Hematoma

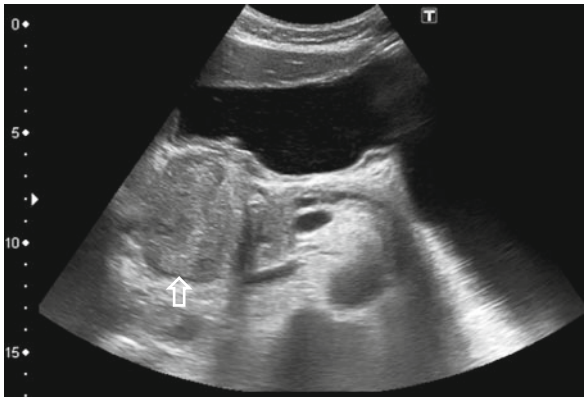

Fig. 8.3.1

Fig. 8.3.2

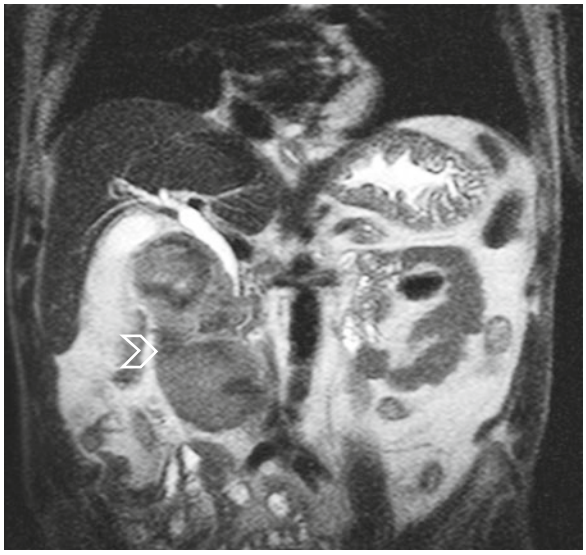

Fig. 8.3.3

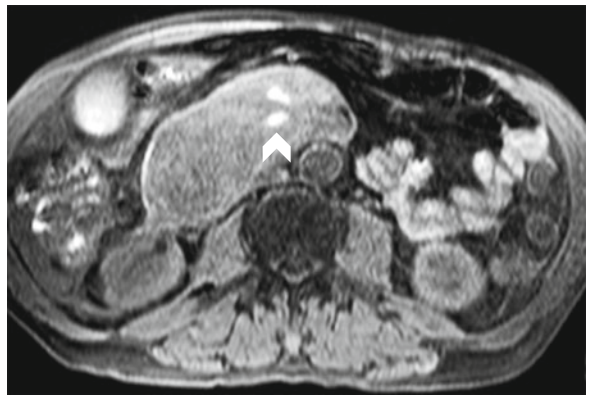

Fig. 8.3.4

A 69-year-old man complained of nausea, vomiting, and abdominal pain during hospitalization. There was no traumatic episode. An abdominal ultrasound, computed tomography, and MRI were performed consequtevely, as a heterogeneous mass at the level of the pancreatic head was demonstrated.

Comments

Intramural duodenal hematoma (IDH) is a rare but recognized complication that usually occurs in children secondary to blunt abdominal trauma. Common mechanisms include bicycle handlebar injuries, play or athletic injuries, and motor vehicle accidents. In adults, abdominal trauma accounts for >70% of cases. An IDH of the abdomen is most commonly observed in the duodenal wall of the gastrointestinal tract. It is believed that the hematoma results from the bowel being crushed between the anterior abdominal wall and the vertebral column. Because the duodenum is relatively fixed, it is therefore prone to this injury if enough force is applied to the anterior abdominal wall. The rich submucosal vascular supply of the duodenum may also contribute to the development of a hematoma. Children may be at higher risk than adults for duodenal injury because of their weaker abdominal musculature.

Nontraumatic IDH is particularly associated with coagulation abnormalities, including anticoagulant therapy, hemophilia, and von Willebrand's disease. Recently, cases of iatrogenic IDH due to duodenal biopsy or endoscopic retrograde cholangiopancreatography have been reported. Compared with traumatic IDH, which usually develops at the subserosal layer of the duodenum, nontraumatic IDH is more frequently located underneath the duodenal mucosa or submucosa.

Imaging plays a major role in their diagnosis. Both CT and MRI contribute to the early and accurate recognition of this condition. Normally, unenhanced CT shows a homogeneous and symmetric intramural thickening with hyperdense material in the bowel wall. The hyperdensity of the bowel can be seen during the first 10 days after the onset of symptoms. However, the hyperdensity decreases as the hematoma ages and evolves into a hypodense area that can mimic an intramural cystic lesion.

Whereas in the past, surgical evacuation or drainage was advised, current management of an intramural duodenal hematoma favors a conservative approach, including nasogastric suction and total parenteral nutrition. Surgical management should be reserved for patients with a suspected perforation or with severely damaged intestines. Complete resolution of the hematoma usually occurs within a few weeks after onset.

Imaging Findings

Transverse ultrasonography in the right upper quadrant (Fig. 8.3.1) shows a large heterogeneous mass (*arrow*) located at the level of the pancreatic head. Abdominal unenhanced CT (Fig. 8.3.2) demonstrates a round, encapsulated, hyperdense mass located along the second portion of the duodenum. No invasion of the surrounding tissues is detected. Coronal T2-weighted MRI (Fig. 8.3.3) reveals a large mass located in the lateral wall of the second portion of the duodenum (*open arrowhead*). On axial fat-saturated T1-weighted image (Fig. 8.3.4) at the same level than Fig. 8.3.2, the lesion has multiple hyperintense foci (*arrowhead*) due to hemoglobin degradation products.

Case 4
Aortoenteric Fistula

Fig. 8.4.1

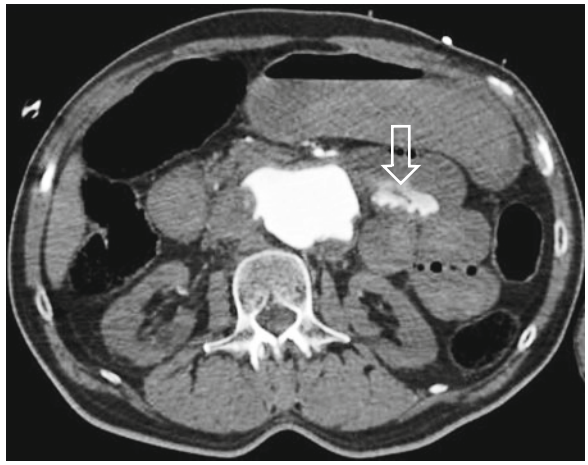

Fig. 8.4.2

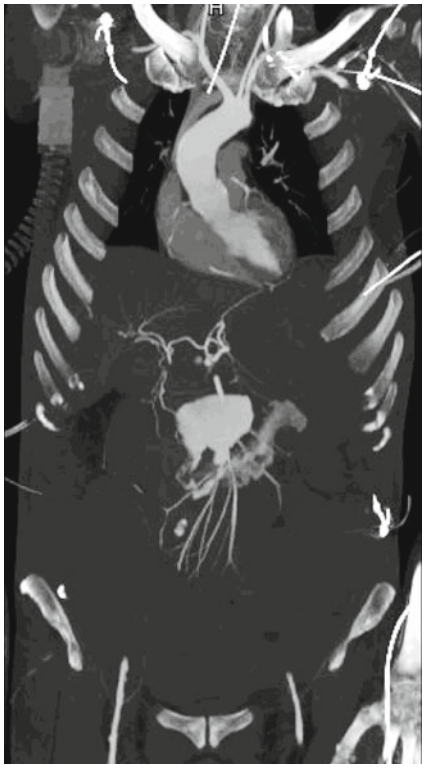

Fig. 8.4.3

Fig. 8.4.4

An 83-year-old man came to the emergency room with a history of supraumbilical abdominal pain and acute anemia. An abdominal CT was performed.

Comments

Aortoenteric fistulas (AFs) are a direct communication between the aorta and the adjacent bowel. They may be classified as primary or secondary. Primary AFs are a complication of atherosclerotic aortic aneurysm, whereas secondary aortoenteric fistulas are a complication of aortic repair with or without graft. Secondary fistulas that result from perigraft infection may occur between 2 weeks and 10 years after surgery. The clinical signs of aortoenteric fistula include hematemesis, melena, sepsis, and abdominal pain.

A total of 80% of AFs involve the duodenum. However, AFs secondary to aneurysms and following aortic surgery have been reported involving all portions of the gastrointestinal tract including the esophagus, stomach, and jejunum.

The most common causes of graft-intestinal fistulas are perforation of the duodenal wall, which is usually caused by impairment of the duodenal blood supply during surgical dissection, erosion by the graft, or false aneurysm at the anastomotic site. A large abdominal aortic aneurysm makes dissection more difficult, and this increases the likelihood of compromising the duodenal blood supply. The posterior wall of the third portion of the duodenum is the most common site of fistulas. This is due both to the close apposition of the anterior aortic wall to the duodenum and the location of the third duodenal segment between the aorta and superior mesenteric artery.

CT plays an important role in their diagnosis, and the characteristic radiological findings are ectopic gas adjacent to or within the aorta, loss of the normal plane that separates the aorta from bowel, extravasation of aortic contrast material into the enteric lumen, or leakage of enteric contrast material into the paraprosthetic space. Differential diagnosis includes retroperitoneal fibrosis, infected aortic aneurysm, infectious aortitis, and perigraft infection without fistulization. Prompt diagnosis of aortoenteric fistulas is imperative for patient survival.

Imaging Findings

Axial unenhanced CT image (Fig. 8.4.1) shows high attenuation content in the lumen of the small bowel. Axial CT after intravenous contrast administration (Fig. 8.4.2) shows a large aneurysm, loss of the fat planes separating the duodenum from the aorta, and extravasation of aortic contrast material into the gastrointestinal lumen (*arrow*). Coronal MIP (Fig. 8.4.3) and volume rendering (Fig. 8.4.4) CT images depict active bleeding into the third portion of the duodenum secondary to a primary aortoenteric fistula.

Case 5
Small-Bowel Obstruction

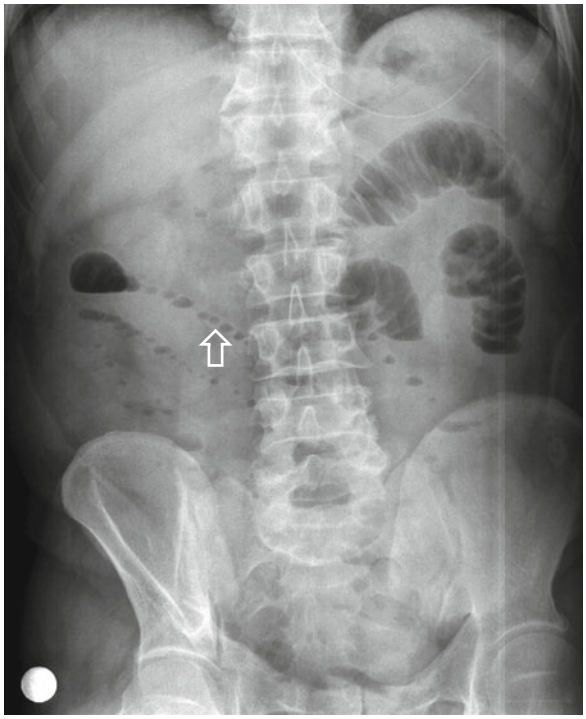

Fig. 8.5.1

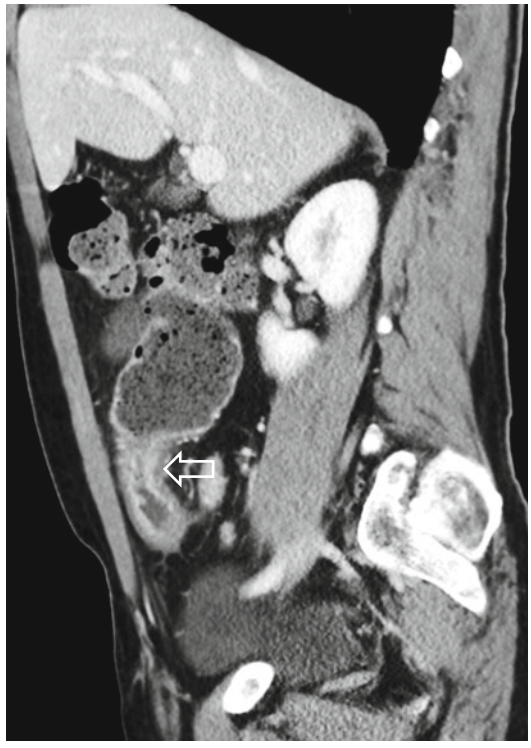

Fig. 8.5.2

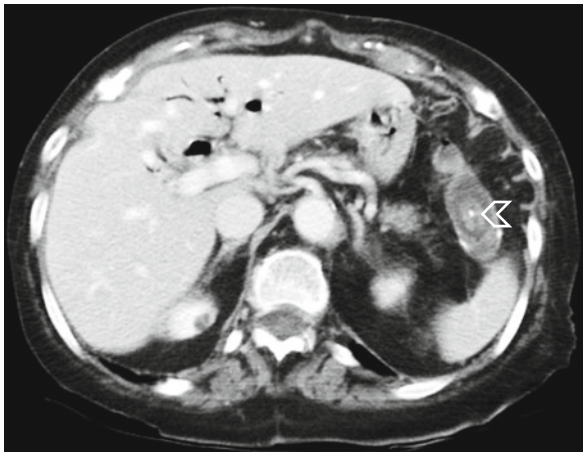

Fig. 8.5.3

A 63-year-old woman presented to the emergency room complaining of a 4-day history of nonlocalized pressure-like abdominal pain, vomiting, and diarrhea.

Comments

Small-bowel obstruction (SBO) is a common clinical condition secondary to mechanical or functional obstruction of the small bowel, preventing normal transit of its contents. It is responsible for 12–16% of admissions to the surgical service in patients with acute abdominal conditions. The three most common causes of SBO in the Western world are (1) adhesions, (2) Crohn's disease, and (3) neoplasia. Hernias still represent the predominant cause of SBO in many developing countries. The causes of SMO can be divided into intrinsic (inflammatory diseases, neoplasias, vascular lesions, hematoma, intussusceptions), intraluminal (gallstones, foreign bodies), and extrinsic (adhesions, hernias, endometriosis).

The diagnosis of mechanical SBO is straightforward when the classic findings of crampy abdominal pain, distention, nausea, and vomiting are present along with abdominal plain film findings of small-bowel distention, as multiple air-fluid levels, and decreased colonic gas and stool. Plain abdominal radiography continues to be the initial examination due to wide availability and relatively low cost.

CT plays a primary role in the evaluation of patients with acute SBO for several reasons: to confirm the diagnosis, to characterize the severity of obstruction, to identify the transition point, to identify the cause of obstruction, and to look for complications.

CT criteria for SBO are the presence of dilated small-bowel loops (diameter > 2.5 cm from outer wall to outer wall) proximally to normal-caliber or collapsed loops distally. The degree of obstruction can be mild, moderate, or high grade, depending on caliber difference between the dilated and nondilated segments of bowel. High-grade obstruction is greater than 50% difference in caliber of proximal dilated small bowel and collapsed distal small bowel. Identifying the transition point (transition point is the zone where the dilated loops abruptly change in caliber to normal/nondilated bowel) helps to evaluate the cause of obstruction and initiating appropriate treatment. Small-bowel "feces sign" is a useful CT finding that helps identifying the transition zone. It is defined as the presence of "feces-like material mixed with gas bubbles in the lumen of dilated loops of the small bowel proximal to the site of obstruction. Most of the intrinsic bowel lesions are identified at the transition point and manifest as localized mural thickening. Most of the extrinsic causes of SBO are located adjacent to the transition point and usually have associated extraintestinal manifestations. Most of the intraluminal causes manifest as endoluminal "foreign objects" with imaging characteristics different from those of the remaining enteric content.

SBO can be classified as simple or closed-loop obstructions. Closed-loop obstructions are diagnosed when a bowel loop of variable length is occluded at two adjacent points along its course. CT findings may include: a U- or C-shaped loop of small bowel; a spoke-like configuration of the mesentery demonstrating stretched vessels converging on the site where the twist may be identified; the appearance of the tightly twisted mesentery has been called the "whirl sign"; and the "beak sign" may be seen as a fusiform tapering at the site of the obstruction.

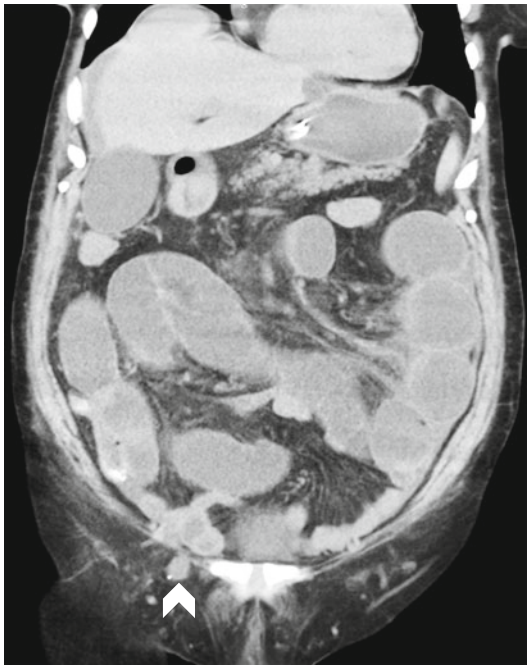

Fig. 8.5.4

Many patients with SBO are treated conservatively with small-bowel decompression and intravenous fluids. Surgical intervention may be necessary if there are signs and symptoms of strangulation, peritonitis, or lack of response to conservative treatment.

Imaging Findings

High-grade small-bowel obstruction. Plain abdominal radiograph in upright position (Fig. 8.5.1) shows multiple air-fluid levels. The small bowel is disproportionately dilated compared to the large bowel, which is collapsed. The curvilinear arrangement of air bubbles visualized (*arrow*) is known as the "string of pearls sign". The appearance is considered to be diagnostic of obstruction (as opposed to ileus) and is caused by small bubbles of air trapped in the valvulae of the small bowel.

Sagittal MPR of abdominal CT (Fig. 8.5.2) shows gas bubbles mixed with particulate matter in the small bowel proximally to the transition point (*arrow*), demonstrating the "small-bowel feces sign" in a patient with high-grade SBO secondary to Crohn's disease. Gallstone ileus in a second different patient, contrast-enhanced CT (Fig. 8.5.3) shows the migration of a large gallstone (*open arrowhead*) through a biliary intestinal fistula with subsequent impaction in the small bowel. The pathognomonic findings are: pneumobilia, ectopic gallstone, and SBO. Coronal unenhanced CT (Fig. 8.5.4) shows SBO secondary to an extrinsic cause: incarcerated inguinal hernia (*arrowhead*), in a third different patient.

Case 6
Bowel Ischemia

Fig. 8.6.1

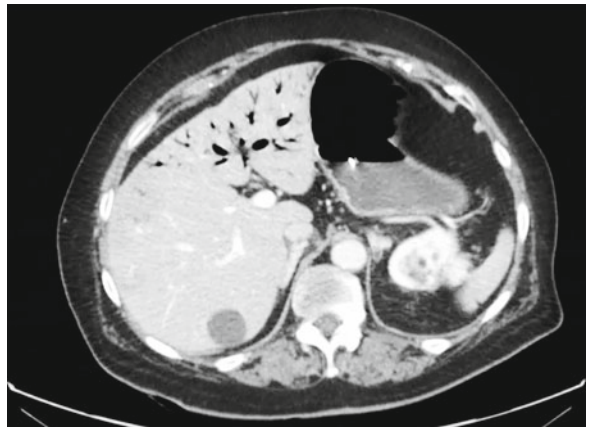

Fig. 8.6.2

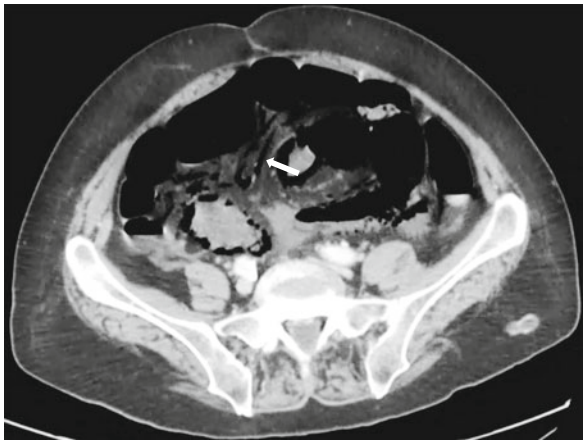

Fig. 8.6.3

Fig. 8.6.4

A 63-year-old man was admitted with complaints of sudden, severe, crampy abdominal pain. Physical examination revealed hypoactive bowel sounds, diffuse tenderness, and guarding. An abdominal CT was requested.

Comments

Vascular compromise of the gut is responsible for approximately 0.1% of all hospital admissions and 1% of admissions for an acute abdomen. Ischemic bowel results from acute or chronic insufficiency of blood flow to the intestine due to various causes, including thromboembolism, nonocclusive causes, bowel obstruction, neoplasms, vasculitis, abdominal inflammatory conditions, trauma, drugs (chemotherapy), radiation, and corrosive injury. Superior mesenteric artery (SMA) embolus associated with cardiovascular problems is the most common cause of acute mesenteric ischemia, accounting for approximately 50% of cases. Thrombosis in the SMA or superior mesenteric vein (SMV) is a less common cause.

Most oftenly, patients who have intestinal ischemia present with abdominal pain and other nonspecific symptoms, such as nausea, vomiting, diarrhea, and bloating. With delay in diagnosis and progression to full-thickness mural injury, the patients develop peritoneal signs of distention, guarding, rigidity, and hypotension. The diagnosis of mesenteric ischemia is often of exclusion after the exclusion of other more common possibilities, including bowel obstruction, appendicitis, diverticulitis, peptic ulcer disease, and gastroenteritis, has been excluded.

Most commonly, bowel ischemia occurs within the sixth and seventh decades of life. CT is the modality of choice for the evaluation of patients who are suspected of having acute and chronic intestinal ischemia.

CT findings in mesenteric ischemia include occlusion of the splanchnic vasculature, bowel distention, bowel wall thickening, either marked or absent enhancement of the bowel wall, intestinal pneumatosis, mesenteric edema, ascites, portomesenteric vein gas, and infarction of other organs. However, most of these signs are nonspecific and must occur in association with clinical signs suspicious for acute mesenteric ischemia to be considered significant for this disease entity. When CT demonstrates portomesenteric vein gas and clinical findings suggest the presence of mesenteric ischemia, surgery is mandatory.

Imaging Findings

A contrast-enhanced CT scan (Fig. 8.6.1) demonstrates a thrombus in the superior mesenteric artery (*arrow*). Extensive gas within portal vein is shown in the Fig. 8.6.2 as tubular areas of decreased attenuation in the periphery of the liver. Gas within SMV (*arrow* in Fig. 8.6.3) and pneumatosis intestinalis (*open arrowhead* in Fig. 8.6.4) attributable to small-bowel infarction are also evident on CT.

Case 7
Small-Bowel Intussusception

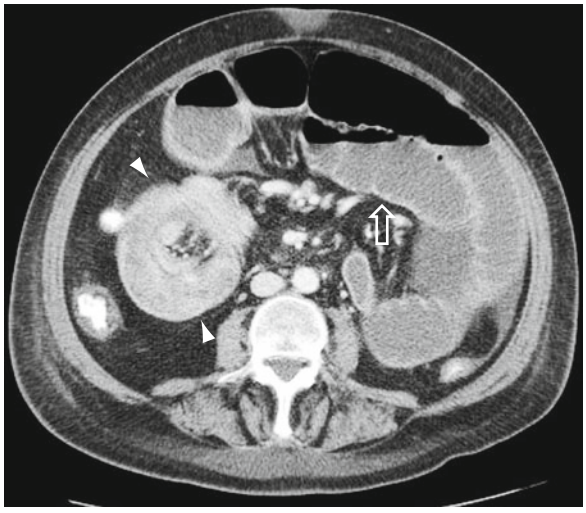

Fig. 8.7.1

Fig. 8.7.2

Fig. 8.7.3

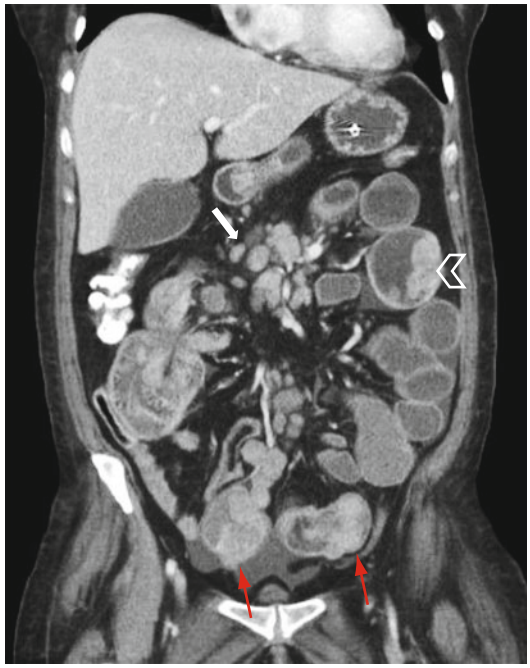

Fig. 8.7.4

A 53-year-old woman presented with abdominal pain. Her past medical history included a melanoma 9 years ago. A CT was performed.

Comments

An intussusception is the invagination of one segment of the intestine in another. Intussusception in adults is rare. Unlike children, about 90% of intussusceptions in adults are caused by a definitive underlying disorder such as a neoplasm or by a postoperative condition.

Small-bowel intussusceptions are secondary to benign lesions in a majority of cases, with malignant lesions causing 15% of cases and idiopathic intussusceptions accounting for approximately 20%. Benign causes include neoplasms such as gastrointestinal stromal tumors, polyps, congenital lesions such as Meckel's diverticulum and intestinal duplication, inflammatory lesions, and trauma. Malignant lesions causing intussusception in the small bowel include adenocarcinoma, malignant GIST, lymphoma, and metastasis.

The gastrointestinal tract is one the most common sites in which metastatic melanoma spreads, with reported incidences ranging from 30% to 50%. In addition, the most common cause of small-bowel metastasis is malignant melanoma. The patients could be asymptomatic, and the involvement is detected in a routine staging examination or symptomatic with abdominal pain or distension. Metastatic melanoma in the small bowel can occur as either single or multiple lesions, and it acts as the lead point to intussusception.

Diagnosis in adults is often more difficult because symptoms are usually nonspecific and sometimes chronic with recurrent episodes of subacute obstruction. CT is the modality of choice for the diagnosis. The classical finding on CT is the "target pattern" that occurs when an intraluminal soft-tissue mass and eccentric fat density are seen as a result of the intussusceptum and the intussuscepting mesentery. Imaging plays a major role in the evaluation and treatment of intussusception.

Imaging Findings

Axial contrast-enhanced CT (Fig. 8.7.1) shows the classic "target sign" of enteroenteric intussusception (*arrowheads*). There was also evidence of bowel obstruction (*arrow*). A second intussusception is depicted in the pelvis (Fig. 8.7.2, *arrow*). Coronal MPR of abdominopelvic CT images (Figs. 8.7.3 and 8.7.4) demonstrate multiple small-bowel metastatic implants of malignant melanoma (*open arrowhead* on Fig. 8.7.4 and added *red arrows*), large mesenteric nodes of metastatic origin (*white arrow*). Notice the presence of a sausage-shaped mass (*solid arrowhead* on Fig. 8.7.3), with a focal enhancing area representing the bowel wall of one segment of small bowel (intussusceptum) into adjacent segment (intussuscipiens). The central fatty density represents mesenteric fat (*arrowhead* on Fig. 8.7.3). Linear enhancing structures within mesenteric fat correspond to mesenteric blood vessels.

Case 8
Ampullary Tumor

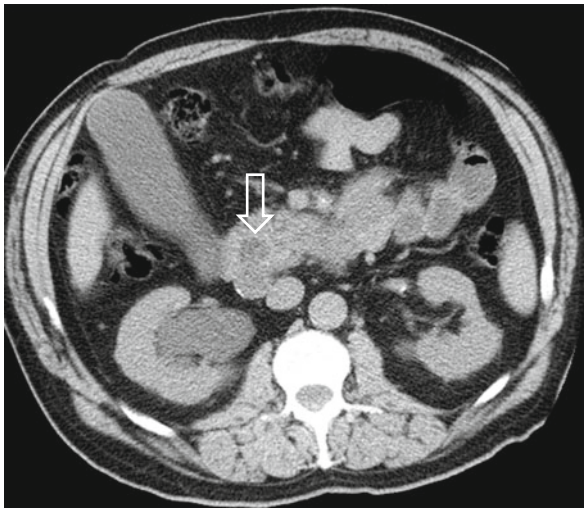

Fig. 8.8.1

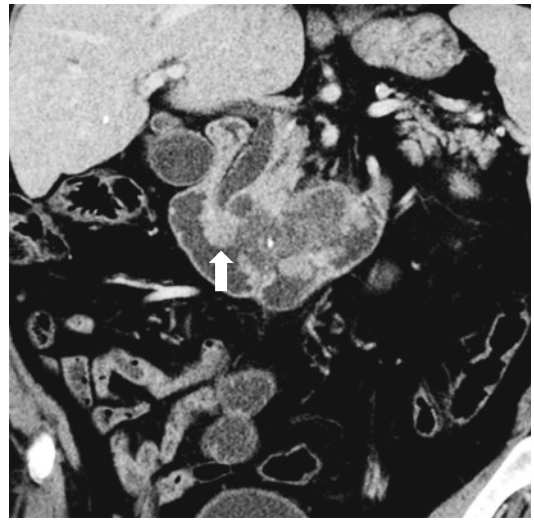

Fig. 8.8.2

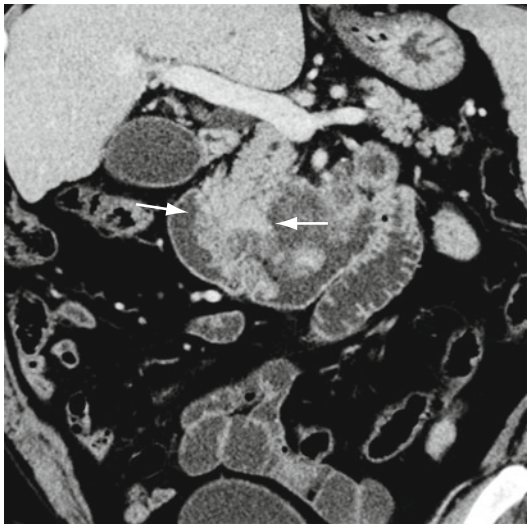

Fig. 8.8.3

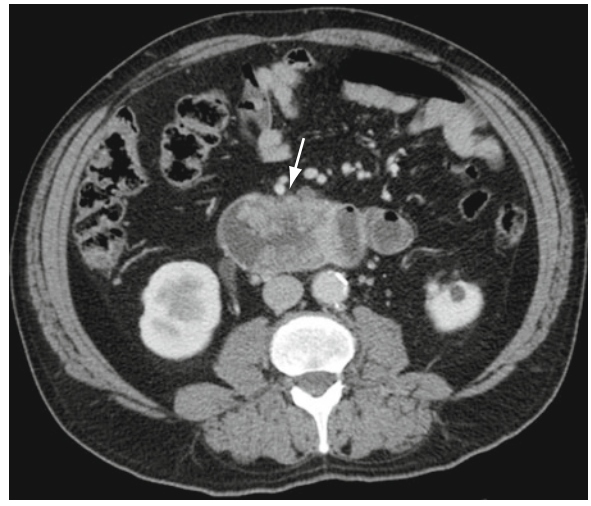

Fig. 8.8.4

A 66-year-old man presented with a 2-month history of fatigue, nausea, vomiting weight loss, and jaundice. Laboratory examination revealed direct hyperbilirubinemia.

Comments

Ampullary tumors are infrequent entities that represent about 0.2% of gastrointestinal malignancies. The periampullary tumors are a group of lesions arising within 2 cm of the major papilla in the duodenum. They include four different types of cancer with a different origin: ampullary; biliary, pancreatic, and duodenal malignancies. Because ampullary cancer has a better prognosis, differentiation among the various types of periampullary tumors is important for treatment planning.

Ampulla of Vater adenocarcinoma (AVAC) is the second most common periampullary adenocarcinoma, representing about 10–30% of patients undergoing Whipple resection. AVAC arises from the glandular epithelium of the ampulla of Vater. The patients are usually in their sixth to seventh decade of life. Clinical presentation includes vague abdominal pain, liver enzyme elevation, recurrent pancreatitis, or uncommon symptoms such as gastrointestinal bleeding or duodenal obstruction. However, ductal obstruction is a major source of symptoms. Classically, the jaundice associated with ampullary tumors is intermittent.

Ampullary cancers can be divided into three types according to gross morphologic features: protruded, ulcerative, and mixed.

AVAC may spread locally into the duodenal wall, the pancreas, or adjacent organs. Regional lymph node metastases occur in the nodes surrounding the head and body of the pancreas, anterior and posterior pancreaticoduodenal, pyloric, common bile duct, and proximal mesenteric areas. Hematogenous metastases to the liver are less common. All periampullary adenocarcinomas should be completely excised with wide margins as possible. The standard operation is the Whipple procedure.

Imaging Findings

Abdominal unenhanced CT (Fig. 8.8.1) reveals a mild dilated bile duct (*arrow*) without identifying the cause. Coronal MPR of pancreatic CT following the administration of intravenous contrast agent (Fig. 8.8.3) demonstrates a dilated common bile duct secondary to its obstruction by a soft-tissue mass (*arrow*) in the ampullary area. Oblique reformatted CT image (Fig. 8.8.3) confirms an irregular slightly hyperdense mass (*arrows*). Axial CT image shows duodenal wall invasion (Fig. 8.8.4, *arrow*).

Case 9
Gastrointestinal Carcinoid Tumor

Fig. 8.9.1

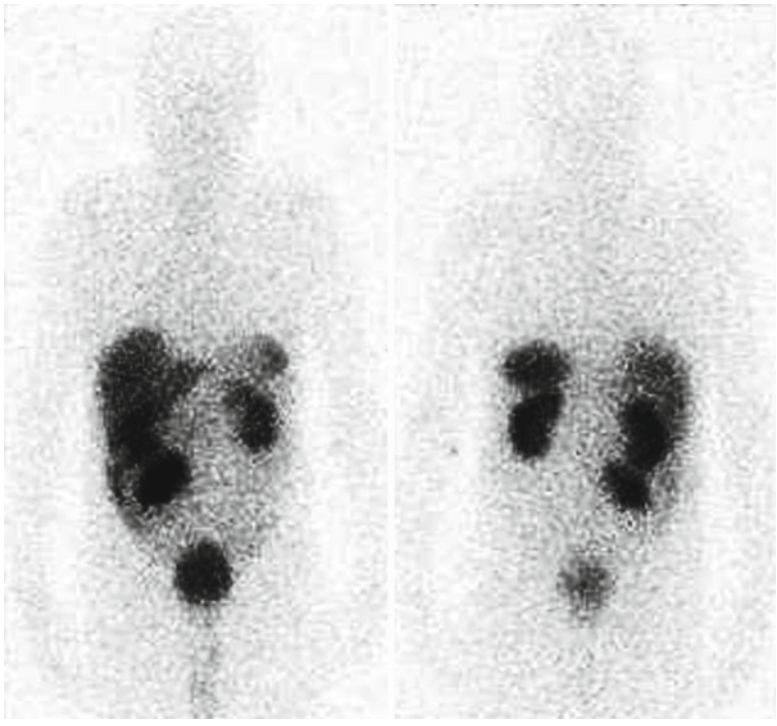

Fig. 8.9.2

A 55-year-old-man presented with abdominal pain and diarrhea. Contrast enhanced CT was performed.

Comments

Neuroendocrine tumors may arise from a wide range of organs and may occur in various locations in the body. These tumors arise from amine precursor uptake and decarboxylation (APUD) cells. They include carcinoid tumors, paragangliomas, medullary thyroid carcinomas, and islet cell tumors of the pancreas. Small-bowel carcinoids constitute approximately 2% of all gastrointestinal tumors. However, carcinoid tumors are the second most common small-bowel malignancy after adenocarcinomas.

Carcinoid tumors are characteristically slowly growing tumors that may go unrecognized for many years. Most commonly, these tumors occur in the fifth or sixth decade of life. Patients may be asymptomatic or have vague abdominal symptoms for many years and may present at a late stage after carcinoid syndrome has developed. Most of the small-bowel carcinoid tumors occur in the distal ileum.

The tumor arises in the wall of the bowel as a submucosal mass that may result in scarring and kinking of the surface. In their early stages, the tumors are small and confined to the bowel wall. Small-bowel series and enteroclysis may be more sensitive for detection than cross-sectional imaging showing a submucosal nodule, but primary tumors frequently are not detected. More commonly, small-bowel barium studies may demonstrate thickening, angulation, tethering, and fixation of ileal loops as a consequence of mesenteric fibrosis. As the tumor grows, extension outside the involved bowel loop may occur, with infiltration of the mesentery and development of a desmoplastic reaction, probably secondary to the secretion of serotonin or other active substances.

The characteristic CT finding is a well-defined mass of soft-tissue density in the root of the mesentery (in up to 40% of cases) associated with radiating strands (caused by thickened neurovascular bundles), giving the mass a speculated or stellate appearance. In an estimated 70% of cases, the mass contains calcification. Some 50–85% of patients who have gastrointestinal carcinoid (excluding cases of appendiceal involvement) have regional nodal metastases at presentation. The incidence of nodal or liver metastases is associated with the size of primary tumors. As the primary tumors, metastases are usually hypervascular and are well visualized on arterial phase of contrast-enhanced dynamic CT or MRI. However, the lesions are typically of low density on noncontrast CT. CT, MRI, and nuclear medicine studies play an important role in the diagnosis, preoperative evaluation, and posttreatment follow-up of patients who have neuroendocrine tumors.

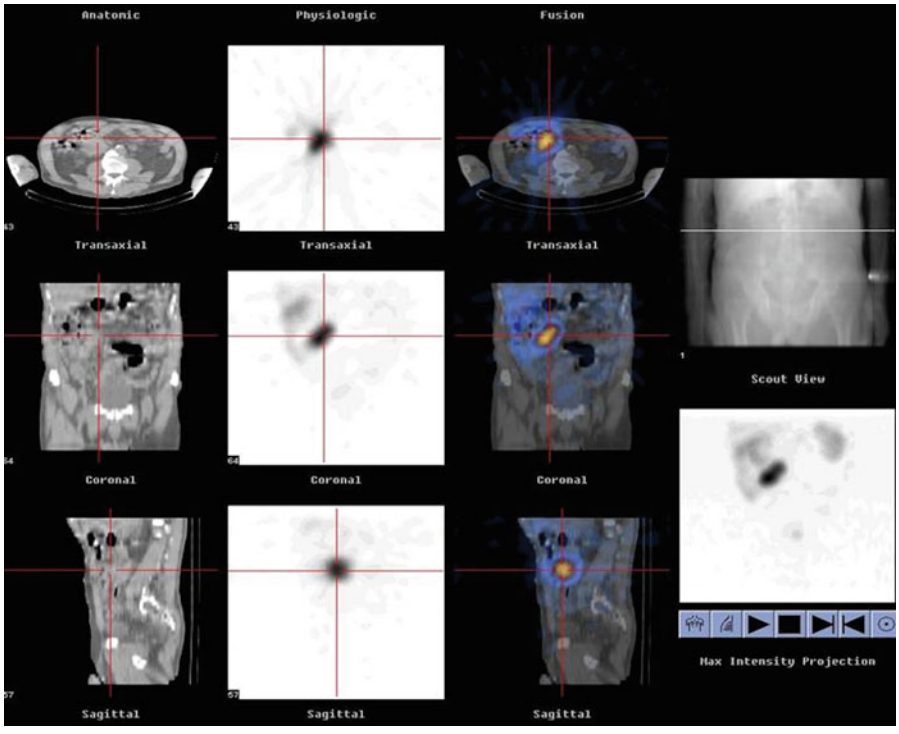

Fig. 8.9.3

Fig. 8.9.4

Imaging Findings

Abdominal contrast-enhanced CT (Fig. 8.9.1) shows a mesenteric mass with radiating soft-tissue strands surrounding it (*arrow*). This is the more usual imaging appearance of mesenteric nodal metastatic disease from a primary ileal carcinoid. Anterior (*left*) and posterior (*right*) images of whole-body scintigraphy obtained 24 h following the intravenous administration of In-111 octreotide (Fig. 8.9.2) show focal area of markedly increased activity of the small bowel. CT-SPECT fused images of the abdomen demonstrating this increased activity located in the ileum are shown in Fig. 8.9.3. Coronal MPR of abdominal enhanced CT in the portal phase allows to identifying nodal mesenteric involvement (*arrow*) and multiple hepatic metastases in (another) patient is shown in Fig. 8.9.4.

Case 10
Primary Small-Bowel Lymphoma

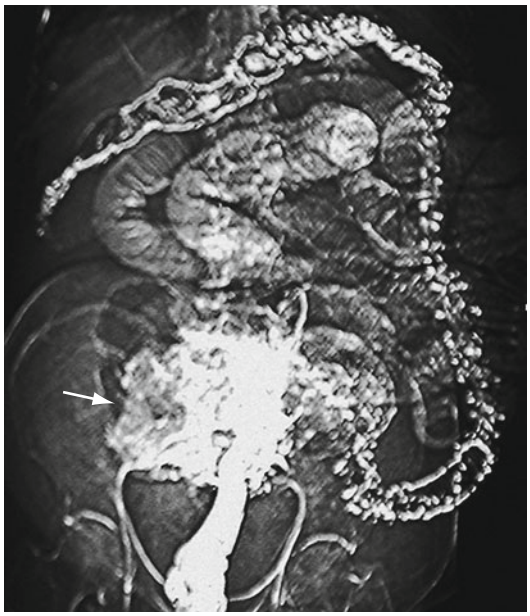

Fig. 8.10.1

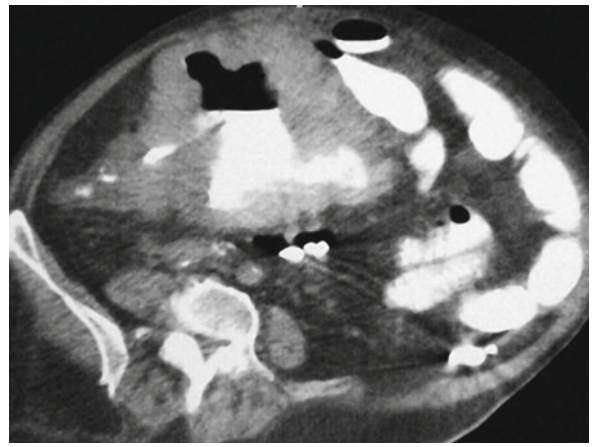

Fig. 8.10.2

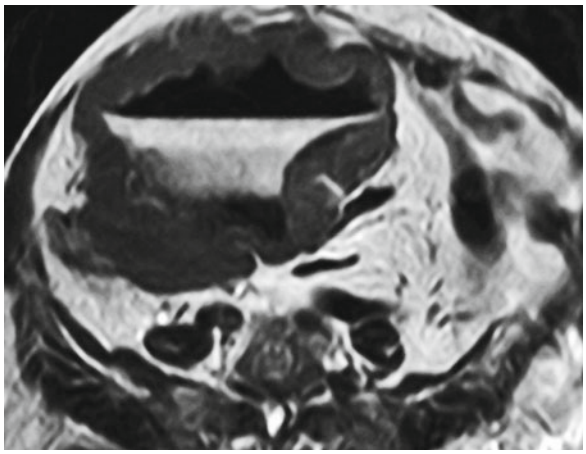

Fig. 8.10.3

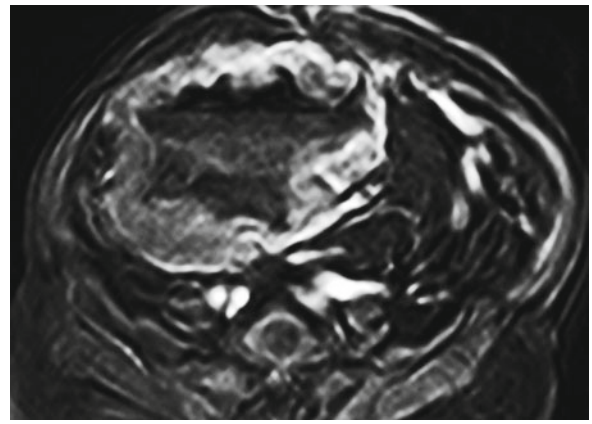

Fig. 8.10.4

An 82-year-old man presented fever in the previous week, weight loss, and recurrent abdominal pain in the previous 3 months. In physical exploration, a mass was detected in right lower quadrant.

Comments

Lymphoma is the most common malignant tumor in small bowel. It approximately represents the 25% of all malignant tumors of the small bowel. Small-bowel lymphoma can be classified either as primary or secondary. Primary lymphoma can be classified as localized or diffuse. Localized primary lymphoma, as the case shown, most commonly is a non-Hodgkin's lymphoma usually located in terminal ileum. Diffuse lymphoma or Mediterranean type is associated to parasitic infection as giardiasis. Secondary small-bowel lymphoma forms part of a generalized systemic process.

Cross-sectional imaging techniques are the most accurate tools to detect and characterize a small-bowel mass. The detection of the level of origin and the associated complications (obstruction, fistulas, etc.) helps to establish the diagnosis and therapeutic management.

Small-bowel lymphoma may have different types of presentation: infiltrating lymphoma with plaque-like, polypoid mass, endo-exo-enteric mass, and mesenteric and/or retroperitoneal adenopathy. Most of the time, due to this complex range of presentations, it is not possible to determine a specific diagnosis based on imaging findings, being necessary its histological analysis.

Small-bowel lymphoma must be differentiated of other small-bowel masses as small-bowel adenocarcinoma and carcinoid tumor. Small-bowel adenocarcinoma is most commonly located in the duodenum or jejunum. Carcinoid is usually located in terminal ileum; the presence of an endocrine syndrome (carcinoid syndrome), its hypervascular nature, and its peritumoral fibrotic reaction are differentiating features from intestinal lymphoma.

Imaging Findings

On the survey view of the CT (Fig. 8.10.1), an obstructive intestinal pattern was visualized, with dilatation of jejunal loops. An important leak of contrast in the right iliac fossa (*arrow*) and colonic diverticula were also present. The CT demonstrated the presence of a cavitated mass with origin in the terminal ileum (Fig. 8.10.2). This mass presented an internal air-fluid level and several fistulous tracks. The thickened walls of the mass were indicative of malignant neoplastic disease. MR confirmed the origin and characteristic of the mass (Fig. 8.10.3, axial HASTE). Intense capsular enhancement was seen (Fig. 8.10.4, axial postcontrast fat-suppressed GE T1-weighted image). After surgery, the histological analysis of the mass revealed a primary cavitated small-bowel lymphoma.

Further Reading

Books

Dalrymple NC, Leyendecker JR, Oliphant M (2009) Problem solving in abdominal imaging. Elsevier, Philadelphia

Federle M, Brooke Jeffrey R, Woodward PJ, Borhani A (2009) Diagnostic imaging: abdomen, 2nd edn. Amirsys, Salt Lake City

Gourtsoyiannis NC (ed) (2002) Radiological imaging of the small intestine. (Medical radiology/diagnostic imaging). Springer-Verlag, Berlin/Heidelberg

Skucas J (ed) (2006) Advanced imaging of the abdomen. Springer-Verlag, Berlin/Heidelberg

Stoker J (ed) (2010) MRI of the gastrointestinal tract (Medical radiology/diagnostic imaging). Springer-Verlag, Berlin/Heidelberg

Web-Links

http://eradiology.bidmc.harvard.edu
http://www.ctisus.com/teachingfiles
http://3s.acr.org/CIP/Default.aspx
http://www.radquiz.com/
http://www.mritutor.org/

Articles

Abbas MA, Collins JM, Olden KW (2002) Spontaneous intramural small-bowel hematoma: imaging findings and outcome. AJR Am J Roentgenol 179(6):1389–1394

Buck JL, Elsayed AM (1993) Ampullary tumors: radiologic-pathologic correlation. Radiographics 13(1):193–212

Buckley O, Brien JO, Ward E et al (2008) The imaging of coeliac disease and its complications. Eur J Radiol 65(3):483–490

Chung YE, Kim MJ, Park MS et al (2010) Differential features of pancreatobiliary- and intestinal-type ampullary carcinomas at MR imaging. Radiology 257(2):384–393

Fidler J (2007) MR imaging of the small bowel. Radiol Clin North Am 45(2):317–331

Fishman EK, Kuhlman JE, Shuchter LM et al (1990) CT of malignant melanoma in the chest, abdomen, and musculoskeletal system. Radiographics 10:603–620

Gore RM, Yaghmai V, Thakrar KH et al (2008) Imaging in intestinal ischemic disorders. Radiol Clin North Am 46(5):845–875

Hernandez-Jover D, Pernas JC, Gonzalez-Ceballos S et al (2011) Pancreatoduodenal junction: review of anatomy and pathologic conditions. J Gastrointest Surg 15(7):1269–1281

Idelevich E, Kashtan H, Mavor E et al (2006) Small bowel obstruction caused by secondary tumors. Surg Oncol 15(1):29–32

Kim S, Lee NK, Lee JW et al (2007) CT evaluation of the bulging papilla with endoscopic correlation. Radiographics 27(4):1023–1038

Kim YH, Blake MA, Harisinghani MG et al (2006) Adult intestinal intussusception: CT appearances and identification of a causative lead point. Radiographics 26:733–744

Levy AD, Sobin LH (2007) From the archives of the AFIP: gastrointestinal carcinoids: imaging features with clinicopathologic comparison. Radiographics 27(1):237–257, Review

Maglinte DD, Heitkamp DE, Howard TJ et al (2003) Current concepts in imaging of small bowel obstruction. Radiol Clin North Am 41(2):263–283, vi

Masselli G, Picarelli A, Gualdi G (2010) Celiac disease: MR enterography and contrast enhanced MRI. Abdom Imaging 35(4):399–406

Matos C, Serrao E, Bali MA (2010) Magnetic resonance imaging of biliary tumors. Magn Reson Imaging Clin N Am 18(3):477–496

Olson DE, Kim YW, Donnelly LF (2009) CT findings in children with Meckel diverticulum. Pediatr Radiol 39(7):659–663

Paolantonio P, Tomei E, Rengo M et al (2007) Adult celiac disease: MRI findings. Abdom Imaging 32(4):433–440

Rakita D, Newatia A, Hines JJ et al (2007) Spectrum of CT findings in rupture and impending rupture of abdominal aortic aneurysms. Radiographics 27(2):497–507

Rha SE, Ha HK, Lee SH et al (2000) CT and MR imaging findings of bowel ischemia from various primary causes. Radiographics 20(1):29–42

Schwartz SA, Taljanovic MS, Smyth S et al (2007) CT findings of rupture, impending rupture, and contained rupture of abdominal aortic aneurysms. AJR Am J Roentgenol 188(1):W57–W62

Sebastià C, Quiroga S, Espin E et al (2000) Portomesenteric vein gas: pathologic mechanisms, CT findings, and prognosis. Radiographics 20(5):1213–1224; discussion 1224–1226

Tamm EP, Kim EE, Ng CS (2007) Imaging of neuroendocrine tumors. Hematol Oncol Clin North Am 21(3):409–432; vii

Thurley PD, Halliday KE, Somers JM et al (2009) Radiological features of Meckel's diverticulum and its complications. Clin Radiol 64(2):109–118

Tresoldi S, Kim YH, Blake MA et al (2008) Adult intestinal intussusception: can abdominal MDCT distinguish an intussusception caused by a lead point? Abdom Imaging 33(5):582–588

Wiesner W, Khurana B, Ji H et al (2003) CT of acute bowel ischemia. Radiology 226(3):635–650

Colon

9

Anaberta Bermúdez Naveira, María Mercedes Liñares Paz, Carmen Villalba Martín, and Antonio Luna

Contents

A. Luna et al., *Learning Abdominal Imaging,* Learning Imaging,
DOI 10.1007/978-3-540-88003-5_9,

Case 1
Acute Apendicitis

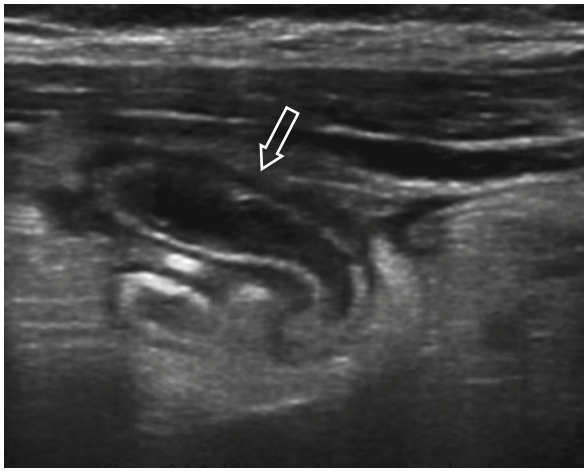

Fig. 9.1.1

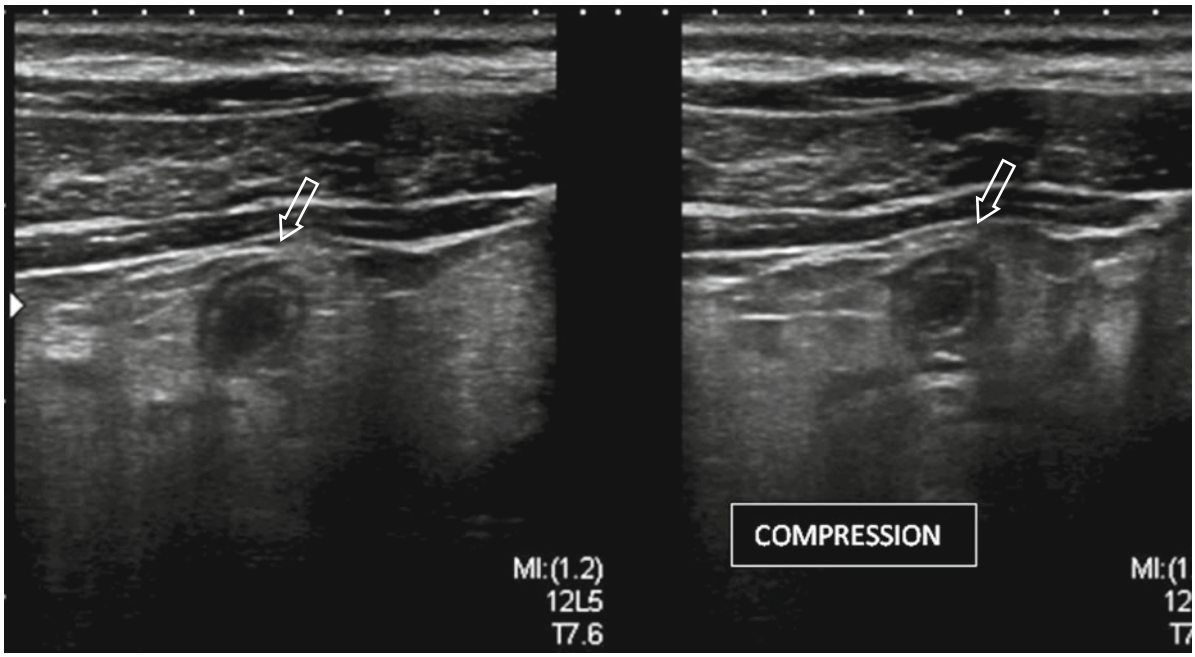

Fig. 9.1.2

A 38-year-old woman presented with right-lower-quadrant pain and a 3-day history of nausea, vomiting, and elevated white blood cell count.

Comments

The appendix is a long diverticulum with a maximum outer diameter of 6 mm that arises from the posteromedial wall of the cecum, approximately 3 cm below the ileocecal valve.

Appendicitis is the most common cause of acute abdominal pain that requires surgical intervention in the Western world.

At pathology, the first event of acute appendicitis is luminal occlusion with continued mucus accumulation. This fact increases luminal distension and intraluminal pressure. When the pressure inside the appendix excesses capillary perfusion, impaired venous drainage occurs at first, and later on, the arterial supply becomes affected. As the epithelial mucosal barrier is destroyed, luminal bacteria multiply and invade the appendiceal wall, causing transmural inflammation. Continued tissue ischemia results in appendiceal infarction and perforation with possible plastron or abscess formation.

There are many causes of appendiceal lumen obstruction. The most common are fecaliths and lymphoid hyperplasia.

Clinical diagnosis of acute appendicitis is based primarily on patient symptoms and on physical examination (localized periumbilical pain followed by nausea and vomiting, with subsequent pain migration to the right lower quadrant), but the classic presentation only occurs in 50–60% of cases. Unusual presentations most likely occur when the appendix is in an atypical location (due to its variable location in the abdominal cavity), and it is more common at extreme ages or in pregnant women.

Early surgical intervention in patients avoids appendiceal perforation, which is related to increased morbidity and mortality. Patients with classic presentation undergo early surgery without radiologic evaluation. Imaging is requested in patients with atypical or confusing clinical findings.

Imaging diagnosis of acute appendicitis can be performed due to:

- Identification of an abnormal appendix: The appearance of the abnormal appendix varies with the stage and severity of the disease process.
- Identification of a calcified appendicolith within pericecal inflammation, although the abnormal appendix is not seen.

The most important findings to identify an inflamed appendix are its maximum outer diameter (more than 6 mm) and a symmetric wall thickening. US should demonstrate a blind-ended, tubular, aperistaltic, and noncompressible structure.

Another hallmark of acute appendicitis is the inflammatory stranding of the fat surrounding the appendix. Fat hyperattenuation, phlegmon, local fascial fluid, free air bubbles, abscess, and adenopathies are frequent findings. Sometimes changes in the cecal apex are present (focal cecal apex thickening, arrowhead sign, and/or a cecal bar).

The presence of pericecal inflammatory changes in absence of an abnormal appendix or appendicolith are not diagnostic (many other inflammatory diseases such as Crohn's disease or diverticulitis have the same appearance). However, an abnormal appendix without pericecal inflammation is very suggestive of acute appendicitis.

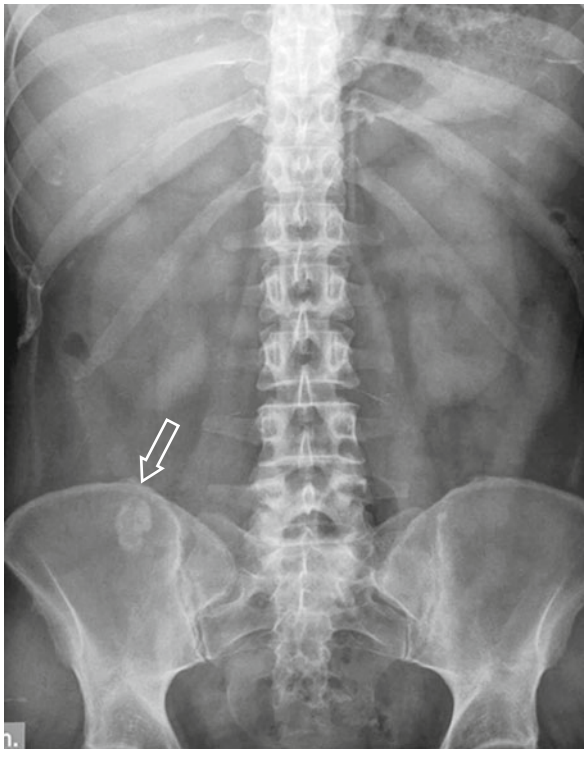

Fig. 9.1.3

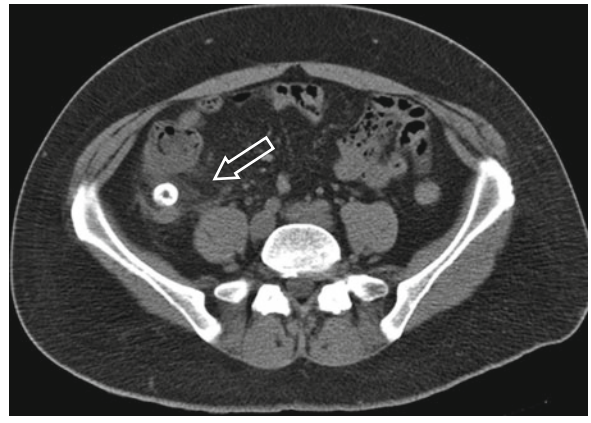

Fig. 9.1.4

Imaging Findings

Ultrasound images through the pelvis (Figs. 9.1.1 and 9.1.2, *open arrows*) demonstrate a blind-ended, tubular structure in the right lower quadrant of the abdomen surrounded by inflamed fat. In a transverse section, it shows an outer diameter >6 mm without compressibility.

In another patient, abdominal plain film (Fig. 9.1.3, *open arrow*) shows a calcification in the right lower quadrant of the abdomen. On unenhanced CT (Fig. 9.1.4, *open arrow*), this calcification is behind the cecum and surrounded by inflammatory fat changes. These features are diagnostic of an acute appendicitis even when the inflamed appendix is not seen.

Case 2
Crohn's Colitis

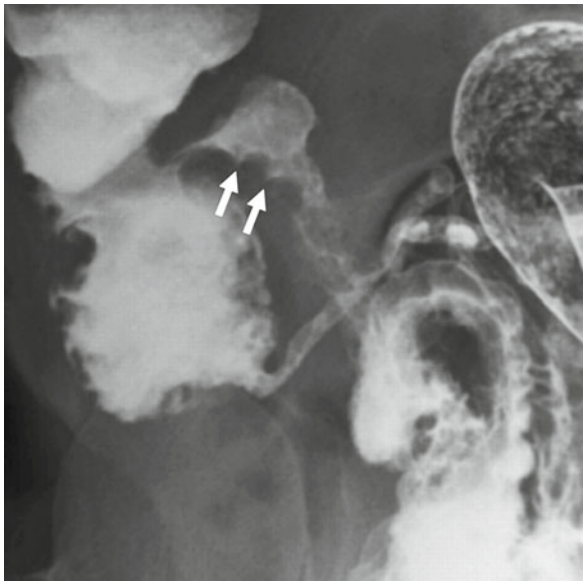

Fig. 9.2.1

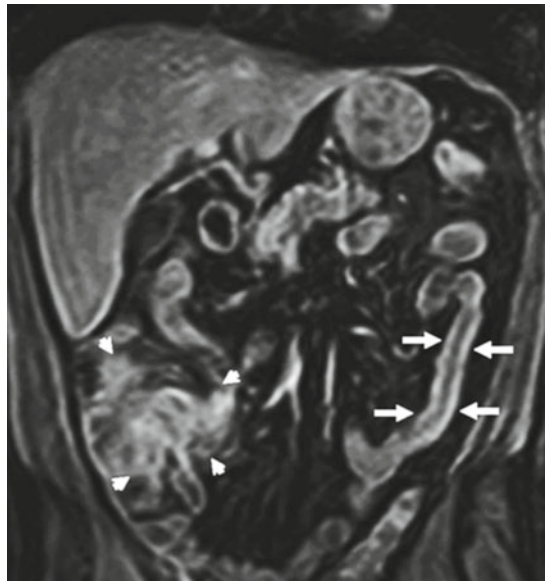

Fig. 9.2.2

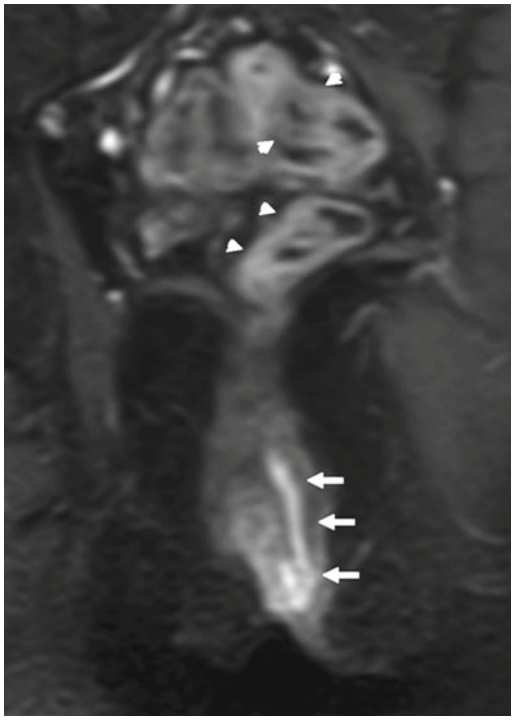

Fig. 9.2.3

Fig. 9.2.4

A 27-year-old woman presented with recurrent episodes of diarrhea, colicky abdominal pain, and progressive weight loss. She also referred perianal discomfort and low back pain. A small bowel series was performed.

Comments

The cause of Crohn's disease is unknown; it is characterized by discontinuous and asymmetric involvement of the entire gastrointestinal tract. The onset is usually before the third decade, and it has no sex preference. The most common areas of gastrointestinal tract involvement are terminal ileum (95%), small bowel (15–55%), rectum (14–50%), and colon (22–55%), although the esophagus, stomach, and duodenum can also be involved. The most common radiological findings are aphthous ulcers, skip lesions, cobblestone appearance of the involved segments, pseudopolyps, and focal strictures in the late phase. Enterocolic, enterocutaneous, sinus tract, and perianal fistulas are commonly found in patients with Crohn's disease. Extraintestinal manifestations of Crohn's disease are gallstones, sclerosing cholangitis, urolithiasis, erythema nodosum, uveitis, seronegative peripheral migratory arthritis, ankylosing spondylitis, and sacroiliitis.

In patients with diarrhea and abdominal pain, the presence of terminal ileitis suggests Crohn's disease, although the differential diagnosis includes yersinia ileitis, tuberculosis, anisakiasis, lymphoma, carcinoid tumor, and eosinophilic gastroenteritis.

Crohn's disease and ulcerative colitis form part of the spectrum of inflammatory bowel disease. It is sometimes possible to differentiate between both. Crohn's disease usually involves the terminal ileum and spares different segments of the colon and small bowel. Ulcerative colitis tends to involve the entire colon. CT and MR are useful to determine the regions involved and the presence of enteric fistulas. As shown in this case, MR is the technique of choice to evaluate the presence of perianal fistulas, which are common and usually complex in Crohn's disease.

Among the extraintestinal manifestations of Crohn's disease, ankylosing spondylitis and sacroiliitis are common. This case showed unilateral sacroiliitis in a patient with negative HLA-B27.

Imaging Findings

The terminal ileum (Fig. 9.2.1) was straightened and rigid, with a severe distal stenosis and multiple ulcers (*arrows*). The diagnosis of was established after a biopsy of colonic and terminal ileum mucosa. Figures 9.2.2 and 9.2.3 correspond to coronal postcontrast fat-suppressed T1-weighted sequences. Figure 9.2.2 shows diffuse enhancement of the terminal and distal loops of ileum, with infiltration of the adjacent fat and medial cecal involvement (*arrowheads*). Note the presence of parietal enhancement of the descending colon, indicating inflammatory activity in this segment (*arrows*). Figure 9.2.3 reveals the presence of an enhanced left transsphincteric perianal fistula (*arrows*). The enhancement of the rectal and sigmoid walls (*arrowheads*) also indicated involvement of these regions. An X-ray of the sacroiliac joints (Fig. 9.2.4) demonstrates loss of joint space, erosions, and reactive sclerosis in the right sacroiliac joint (*arrows*), indicative of unilateral sacroiliitis. Axial skeletal X-rays (not shown) were negative.

Case 3

Pseudomembranous Colitis

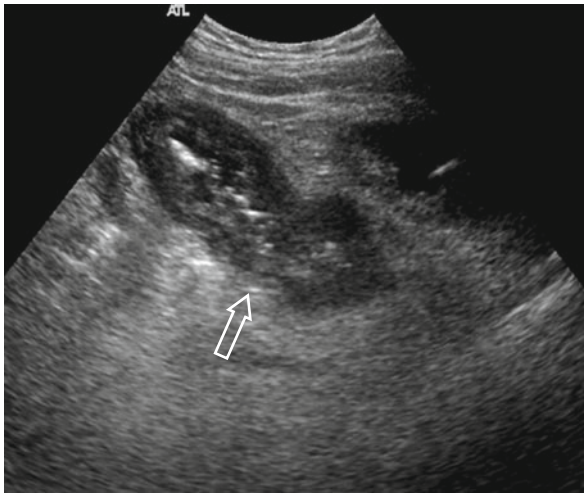

Fig. 9.3.1

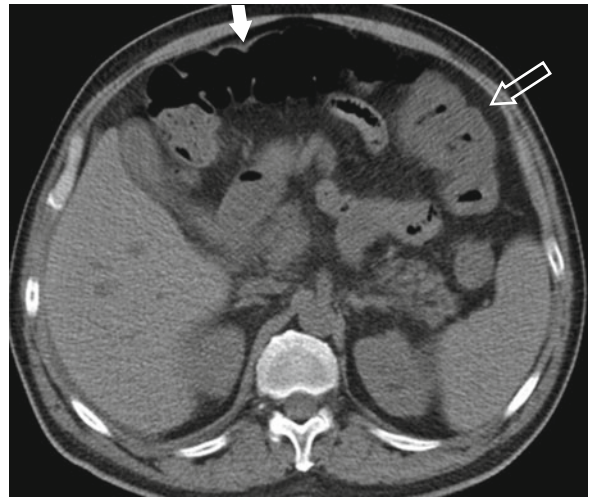

Fig. 9.3.2

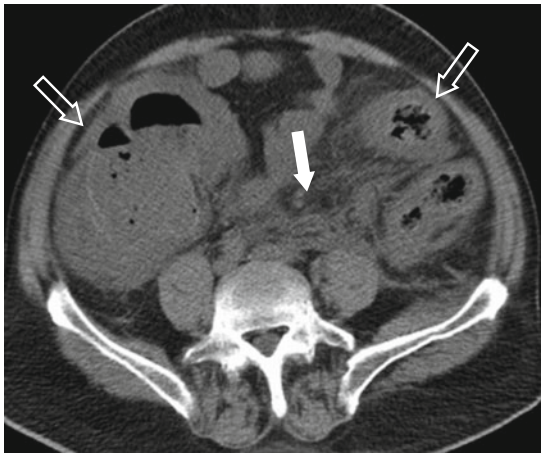

Fig. 9.3.3

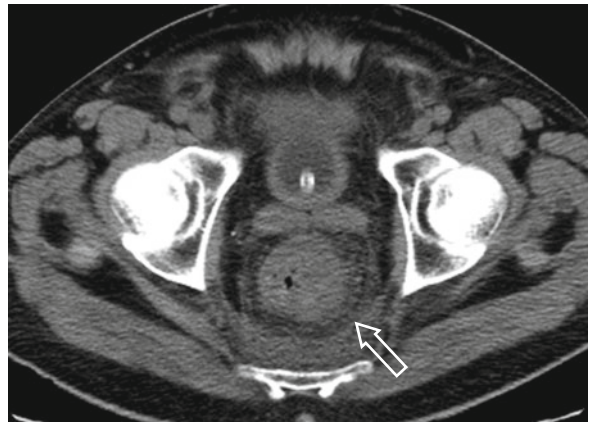

Fig. 9.3.4

A 59-year-old woman presented with a history of several atypical pneumonias after transplantation of umbilical cord cells due to acute lymphocytic leukemia. In the third posttransplantation month, she presented distension and diffuse abdominal pain.

Comments

Pseudomembranous colitis is a specific inflammatory colitis characterized by the presence of elevated yellow-white plaques forming pseudomembranes on the colonic mucosa. The main cause is certain pathogenic strain of *C. difficile* that produces two toxins (toxin A or enterotoxin and B or cytotoxin).

At histological studies, pseudomembranous colitis show inflammatory changes in the lamina propia with pseudomembranes which emerge through punctal superficial ulceration ("volcano" lesions) and are made up of fibrin, mucin, sloughed mucosal epithelial cells, and inflammatory cells. Most patients have a superficial mucosal disease, but in severe cases there are transmural lesions with increased risk of complications.

The diagnosis of PMC is based on clinical findings, demonstration of appropriate pathogen (in most cases, *C. difficile* toxins in the stool), and visualization of yellow-white plaques forming pseudomembranes in the endoscopic studies. Therefore, the two main aims of imaging studies are:

- Recognition of features that suggest this entity, as imaging techniques are generally used as a first step to study patients with abdominal pain.
- Diagnosis of potential complications: toxic megacolon or colonic perforation.

Pseudomembranous colitis can show generalized or segmental (with or without skip areas) colitis. The most affected areas are the rectum and sigmoid colon.

The radiological findings that may be seen depend on the severity and length of the disease because a negative imaging does not rule out *C. difficile* disease.

In the plain film, colonic ileus, nodular/polypoid mucosal thickening, thumbprinting sign, toxic megacolon, or pneumoperitoneum may be seen.

On CT images, the most common findings are mural thickening (the important degree of thickening is characteristic of this entity, with an average of 14 mm), the "target sign" (identification of the wall layers due to enhancement of serosal and mucosal layers and hypodensity of submucosal one), the "accordion sign" (entrapment of oral contrast between thickened haustral folds), pericolonic stranding, ascites, or pneumatosis coli with or without air in the mesenteric/portal veins.

Imaging Findings

Ultrasound image (Fig. 9.3.1, *open arrow*) shows circumferential, symmetric, homogeneous, hypoechoic thickening of ascending colon.

Axial unenhanced CT shows (Figs. 9.3.2, 9.3.3, and 9.3.4) marked wall thickening of the cecum, ascending, descending, and sigmoid colon, and rectum (*open arrows*) with pericolic stranding (*arrows*) and small quantity of free fluid. Notice how the transverse colon is not involved.

Case 4
Complicated Diverticulitis

Fig. 9.4.1

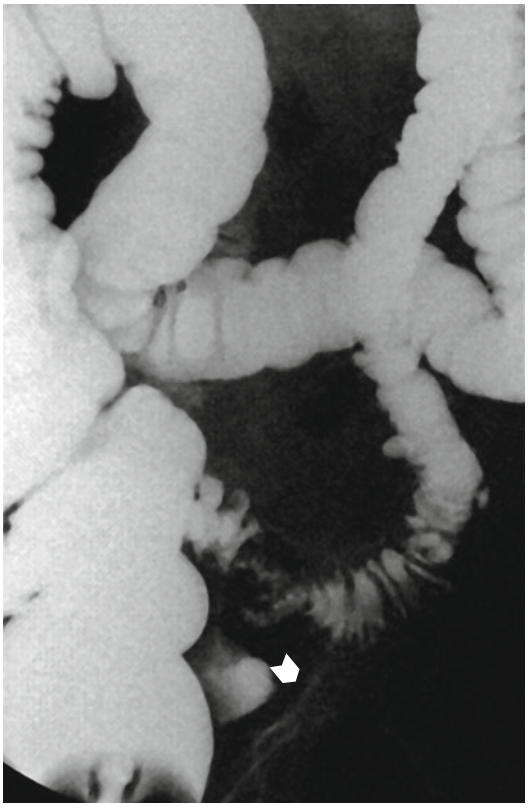

Fig. 9.4.2

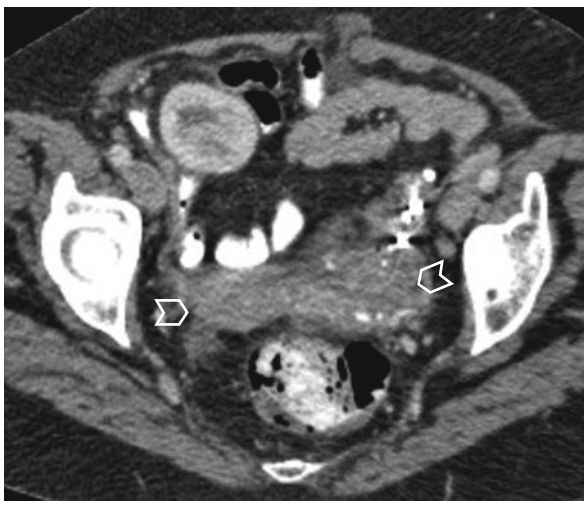

Fig. 9.4.3

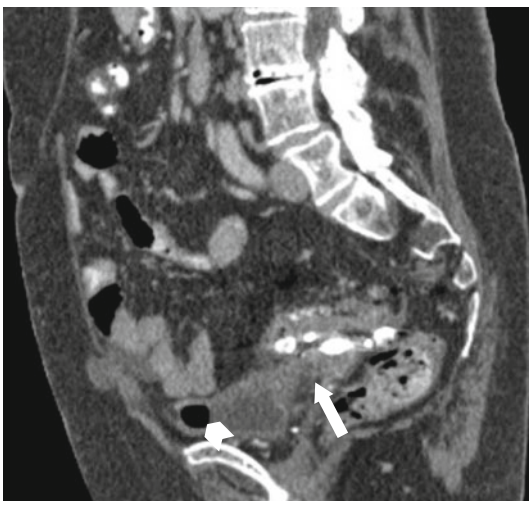

Fig. 9.4.4

A 78-year-old woman presented to the emergency room with left iliac fossa pain, dysuria, tenesmus, and fecal smelling urine.

Comments

The presence of diverticula or diverticulosis is very common, with an incidence of 5–10% in individuals over 45 years of age and of 80% in individuals over 85 years. This condition is characterized by small sacs or pouches (diverticula) in the wall of the colon. If the diverticula become inflamed, they cause a condition known as diverticulitis, which occurs in a 10–25% of cases of diverticular disease. Diverticula appear more commonly in the sigmoid colon, although any other colonic location is possible. Clinically, the most common symptoms are pain, local tenderness, and mass in the left lower quadrant, together with fever and leukocytosis. Common complications are perisigmoid abscess formation, colon perforation, and fistula formation (to the bladder, small bowel, or vagina).

The presence of diverticula and segmental involvement of colon are hallmarks of diverticulitis. As in other colonic inflammatory conditions, concentric wall thickening and pericolonic inflammatory changes can be visualized. The differential diagnosis includes colonic adenocarcinoma, infectious or ischemic colitis, and Crohn's colitis. Imaging evaluation enables their differentiation on many occasions. CT is the preferred imaging technique to evaluate patients over 50 years with left-lower-quadrant pain. CT helps to establish the diagnosis of diverticulitis, to determine its extension, and to rule out complications.

The barium contrast enema was the classical test of choice for suspected diverticulitis, although evaluation of extraluminal changes was limited. Ultrasound has a role, but CT is the most useful imaging technique in the evaluation of diverticulitis. CT allows global evaluation of the stenotic segment, pericolic inflammation, and extracolonic complications. CT is more accurate than barium enema in the detection of fistulas. MR has also shown great accuracy in the detection of colonic and small bowel fistulas, thanks to its multiplanar capabilities and great sensitivity for inflammatory changes.

Imaging Findings

Barium enema detected a large stenotic segment of sigmoid colon associated to multiple diverticula (Fig. 9.4.1). A linear contrast extravasation, connecting the sigmoid colon to the bladder, was also observed (Fig. 9.4.2, *arrowhead*). Contrast-enhanced CT confirmed the diverticulitis associated to colonic bladder fistula. In Figs. 9.4.3 and 9.4.4, axial and sagittal MPR of enhanced CT show multiple diverticula in the sigmoid colon with inflammatory changes, a complex collection (Fig. 9.4.3, *open arrowheads*) in Douglas space, communication between the sigmoid colon and the bladder (Fig. 9.4.4, *arrow*), bladder wall thickening, and an air-fluid level (Fig. 9.4.4, *arrowhead*) within the bladder confirming the fistula.

Case 5
Epiploic Appendagitis

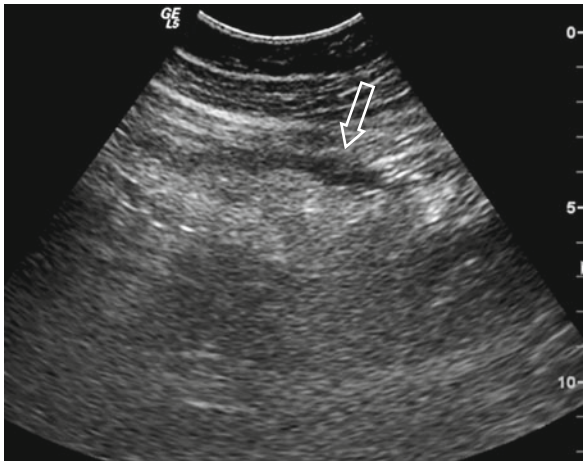

Fig. 9.5.1

Fig. 9.5.2

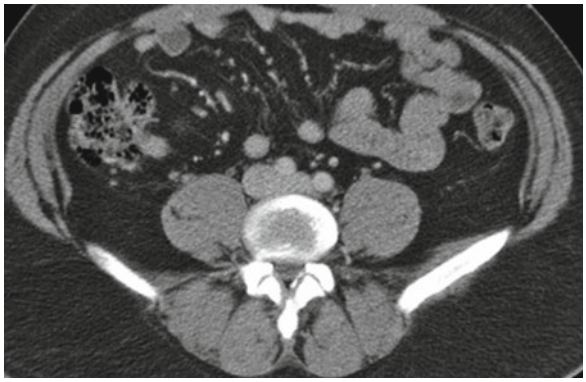

Fig. 9.5.3

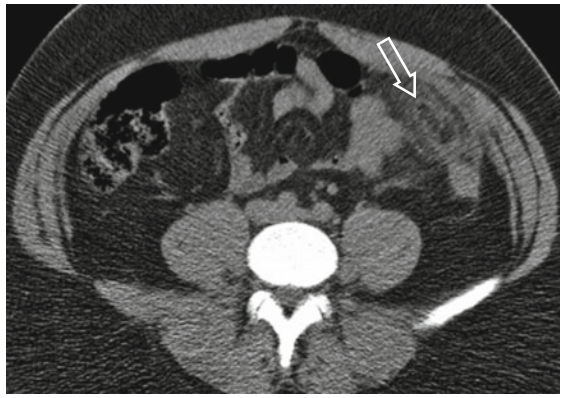

Fig. 9.5.4

A 37-year-old woman presented with intense left-lower-quadrant pain.

Comments

Epiploic appendages are visceral peritoneal outpouchings that arise from the surface of the colon; they contain fat and blood vessels and are attached by a vascular stalk (pedunculated structure). They are arranged in two rows along the colon from the cecum to sigmoid colon.

Epiploic appendagitis is an inflammatory and ischemic entity due to torsion or spontaneous venous thrombosis. It can appear anywhere in the colon, but the most common sites are areas adjacent to the sigmoid colon, the descending colon, and the right colon.

Acute epiploic appendagitis can manifest at any age, but most commonly, in the fourth or fifth decades of life. It is associated with obesity, hernia, and lack of exercise.

The main symptom is acute onset of abdominal pain. In the physical examination, there is a circumscribed tenderness that elicits with pressure.

Management of epiploic appendagitis is usually conservative, thus the diagnosis based on imaging is very important to avoid unnecessary surgery.

Epiploic appendages are only identified on imaging studies when they are surrounded by fluid and/or inflamed. The signs for acute epiploic appendagitis are:

- At US, a hyperechoic noncompressible intra-abdominal mass at the site of maximum tenderness that abuts the anterior colon wall. It can be associated with a central hypoechoic area, which represents a thrombosed vessel or hemorraghic changes, and with a hypoechoic rim surrounding this lesion which corresponds to inflamed visceral peritoneal lining.
- At CT, a fatty pericolic lesion about 1.5–3.5 cm in diameter with a hyperattenuating well-defined rim that abuts the anterior colon wall is the typical appearance. This rim corresponds to thickening visceral peritoneum, and this sign is virtually pathognomonic for epiploic appendagitis. Surrounding this rim, there are inflammatory changes on pericolonic fat. Sometimes a central high-attenuation dots that represent thrombosed vessels.

This entity is not usually associated with adjacent colonic wall thickening.

The main differential diagnoses are acute inflammatory processes in the large bowel (especially, appendicitis and acute diverticulitis) and omental infarction (fatty lesions that are larger and more heterogeneous, without a hypoechoic/hyperattenuating rim and a central hyperattenuating dot).

Imaging Findings

Ultrasound image (Fig. 9.5.1, *open arrow*) demonstrates a hyperechoic noncompressible intra-abdominal mass at the site of maximum tenderness. Contrast enhanced CT (Fig. 9.5.2, *open arrow*) shows a focal lesion in the pericolic fat with a hyperdense rim and inflammatory changes adjacent to the descending colon. CT image (Fig. 9.5.3) demonstrates the complete resolution of the lesion in 5 months. Figure 9.5.4 corresponds to a contrast-enhanced CT of another patient, which shows inflammed epiploic appendages (*open arrow*), surrounded by ascites.

Case 6

Ischemic Colitis

Comments

A 53-year-old woman presented with a history of a crampy abdominal pain of 5 hours associated to rectal bleeding.

Ischemic colitis is the most common form of gastrointestinal ischemia (50–60%) and the second most common cause of lower gastrointestinal bleeding.

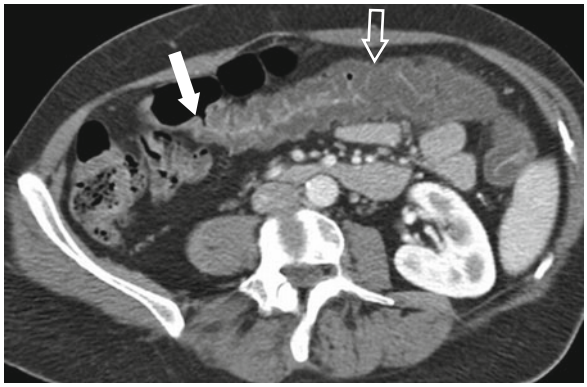

Fig. 9.6.1

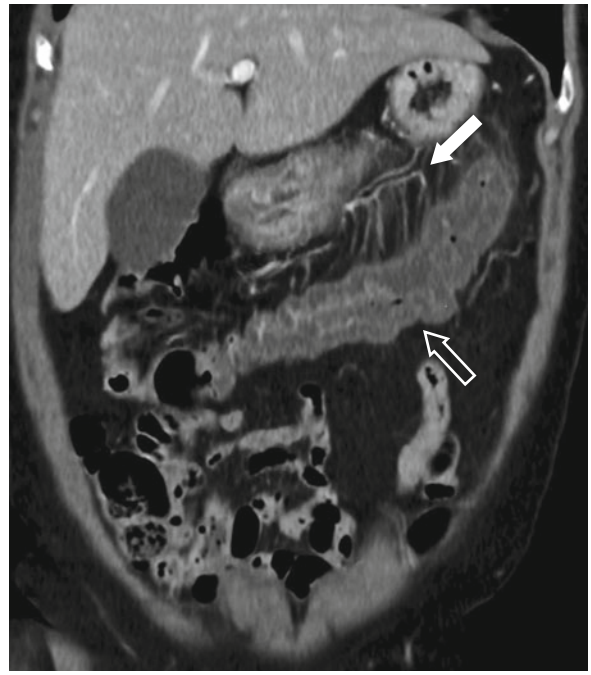

Fig. 9.6.2

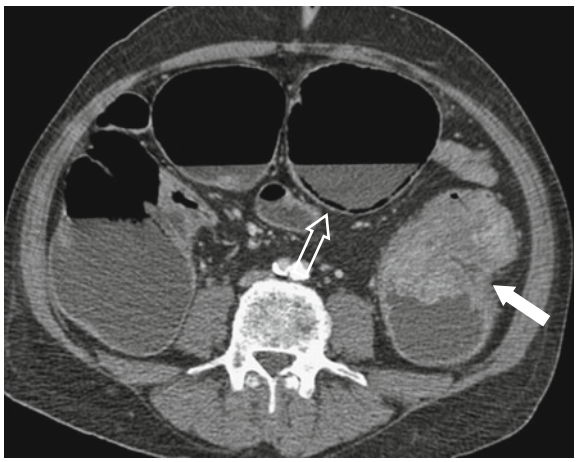

Fig. 9.6.3

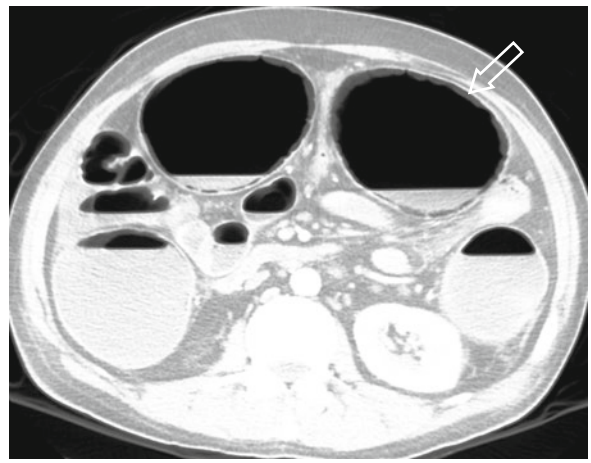

Fig. 9.6.4

The ischemic events are due to compromised blood flow in the colon. The causes can be divided into occlusive (direct injury in the mesenteric vasculature by thrombus, embolus, or tumor) and nonocclusive (NOMI), due to secondary vasospasm of the splanchnic arteries related to hemodynamic instability.

More than half of the blood supply in the bowel wall is used for the mucosa and submucosa; therefore these layers are more sensitive to ischemia. Based on this, there are two forms of ischemic colitis: (a) nongangrenous form (80–85%), in which changes are mainly limited to mucosa and submucosa (usually is self-limited and generally only need a medical management) and (b) the gangrenous form, in which there is transmural necrosis, so increased risk of perforation, peritonitis, and sepsis, therefore these patients usually require surgical resection.

The diagnosis of ischemic colitis is made of a combination of clinical evaluation, radiological studies, and colonoscopy.

In these patients, the most requested imaging studies are plain radiographs (to rule out visceral perforation and pneumoperitoneum) and CT (to rule out other entities than arises with similar clinical findings to colitis ischemia, especially a mesenteric ischemia).

At CT, ischemic colitis shows circumferential, symmetric wall thickening (mean 8 mm) with either low (submucosa edema) or high attenuation (intramural hemorrhage). Initially (the wet appearance), the wall preserves the stratification with enhancement (reperfusion: double-halo or target sign), but these latter features are going to disappear as ischemia-necrosis keeps on (the dry appearance). Colon involvement is usually segmental, without discontinuity and about 10 cm in length or more. The most common involved area is the left colon, especially the splenic flexure (25%) followed by rectosigmoid colon (75%), probably because they are watershed areas, and so susceptible to ischemic insults. Pericolic fat may present inflammatory change, more significant in the wet phase. Pneumatosis is not a pathognomonic sign of ischemic colitis, but it suggests a worse prognosis, especially if it is associated with air in the vessel or into peritoneal cavity (perforation).

At color Doppler US, ischemic colitis usually shows barely visible or no color Doppler signal.

The main differential diagnoses are neoplasm, acute diverticulitis, and inflammatory infectious colitis.

Imaging Findings

Axial and coronal MPR contrast-enhanced CT (Figs. 9.6.1 and 9.6.2) show symmetric, homogeneous thickening of the wall of the transverse colon (*open arrow*) with sharp transition (*solid arrow* in Fig. 9.6.1). It is associated to mucosal enhancement (target sign) and vascular engorgement in mesocolon (solid arrow in Fig. 9.6.2).

In another patient, axial contrast-enhanced CT (Figs. 9.6.3 and 9.6.4) demonstrate severe dilatation of the colon with pneumatosis and little inflammatory changes in pericolic fat (*open arrow*) due to focal concentric thickening of the descending colon wall. Notice the presence of a thickened segment of descending colon corresponding to an area of chronic diverticulitis (*solid arrow*). An irregular mucosal contour in the nondependent bowel wall is also seen (Fig. 9.6.4, *open arrow*).

Case 7
Colonic Obstruction

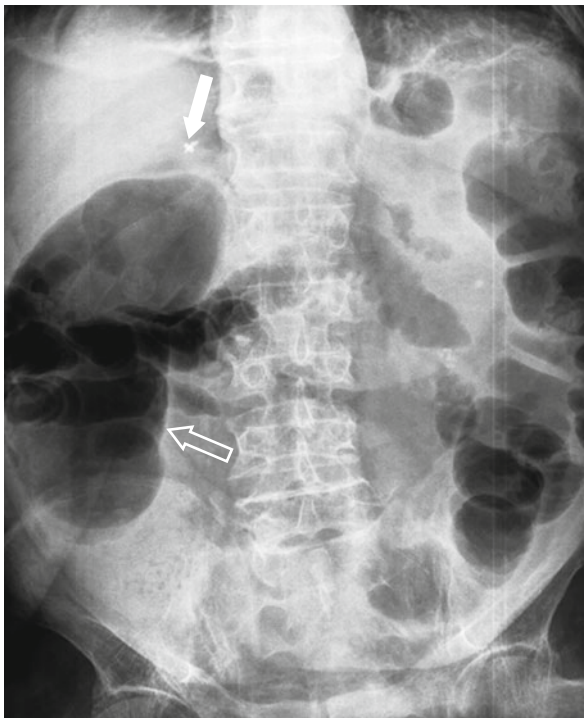

Fig. 9.7.1

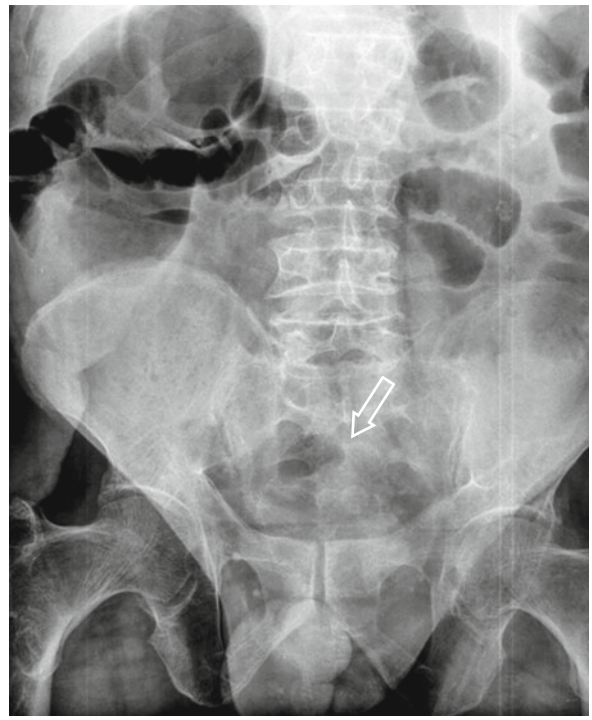

Fig. 9.7.2

A 50-year-old patient presented with abdominal pain, nausea, and vomiting.

Comments

Obstruction of the colon is less common than small bowel obstruction (representing only 25% of bowel obstructions). Colonic obstruction is caused by malignant lesions in more than 50% of the cases. The differential diagnosis also includes inflammatory diseases (ulcerative colitis and Crohn's disease), granulomatous infections (tuberculosis, actinomycosis, and lymphogranuloma venereum), extrinsic bowel diseases (volvulus, hernias, tumor, abscess, bladder distension, endometriosis, pancreatitis, and mesenteritis), luminal occlusion (fecal impaction, intussusception, calculus, and foreign bodies), and congenital diseases (colonic atresia, anorectal malformations, and meconial peritonitis).

The obstruction usually occurs in the sigmoid colon, where the bowel is narrower and the stool more solid, followed by the rectum, colonic flexures, cecum, and ascending colon.

On abdominal plain films, large bowel obstruction is manifested by dilated, gas-filled loops of large bowel down to the point of obstruction and absence or paucity of gas in distal colon or rectum. It may be accompanied by small bowel dilatation if the ileocecal valve becomes incompetent. But when the ileocecal valve remains competent, the small bowel shows few gas while the colon, and particularly the cecum, can develop a closed-loop obstruction with a high perforation risk. Supine plain film can be enough to make a diagnosis, but to confirm the lack of gas distal to the obstruction point, prone or right lateral decubitus (these positions facilitate gas entrance to the rectum) films can be obtained.

Although abdominal plain film is diagnostic in 60–70% of the cases, other techniques should be considered to exclude a pseudoobstruction and confirm the lesion. Single-contrast barium or water-soluble enema, colonoscopy, and CT can be used.

Barium studies were the standard of reference in diagnosing and characterizing intestinal obstruction, but nowadays the use of CT has many advantages, mainly in predicting the danger of intestinal ischemia due to its ability to demonstrate the bowel wall and its accuracy to detect pneumoperitoneum.

On CT images, we will find out the site, level, and cause of obstruction. The easiest sequence is to evaluate the large bowel in a retrograde way, following the course of the distal colon proximally until dilated loops are found. MDCT with its capability to obtain of multiplanar reformats allows to identifying better and easier the point of transition and its cause.

A careful study of the bowel wall proximal to the obstruction point is mandatory in order to exclude bowel ischemia due to the elevated pressure inside the loop. Due to Laplace's law, the widest point suffers the maximum pressure; in the colon the widest segment is the cecum. Cecum diameters of 9–12 cm should be considered to have a high perforation risk.

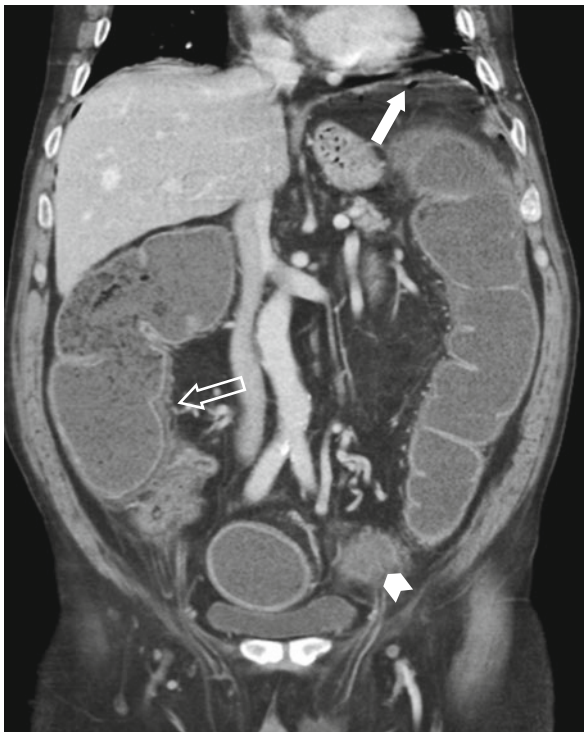

Fig. 9.7.3

Fig. 9.7.4

Imaging Findings

Supine abdominal plain film (Fig. 9.7.1, *open arrow*) shows a dilated large bowel with small amount of gas in rectum and small bowel, due to ileocecal valve incompetence. Incidentally, laparoscopic cholecystectomy surgical material is also seen in the right upper quadrant (*arrow*).

Prone abdominal plain film (Fig. 9.7.2) confirms the absence of gas in the distal sigmoid colon and rectum (*open arrow*).

Coronal MPR of contrast-enhanced CT (Fig. 9.7.3) reveals dilated colonic loops with soft fecal material. The cecal wall is enlarged with hyperattenuating mucosa, hypoattenuating muscular layer, and a small amount of free fluid representing the vascular compromise (intestinal ischemia, *open arrow*). Note also the small free air bubbles under the diaphragm (pneumoperitoneum, *arrow*). These findings are associated with a high-grade obstruction due to a sigmoid colon carcinoma (*arrowhead*) with intestinal ischemia.

Sagittal MPR of contrast-enhanced CT image (Fig. 9.7.4) reveals the point of transition and the cause (an obstructing carcinoma, *arrowhead*), as well as a small amount of free air (*arrow*).

Case 8
Sigmoid Volvulus

Fig. 9.8.1

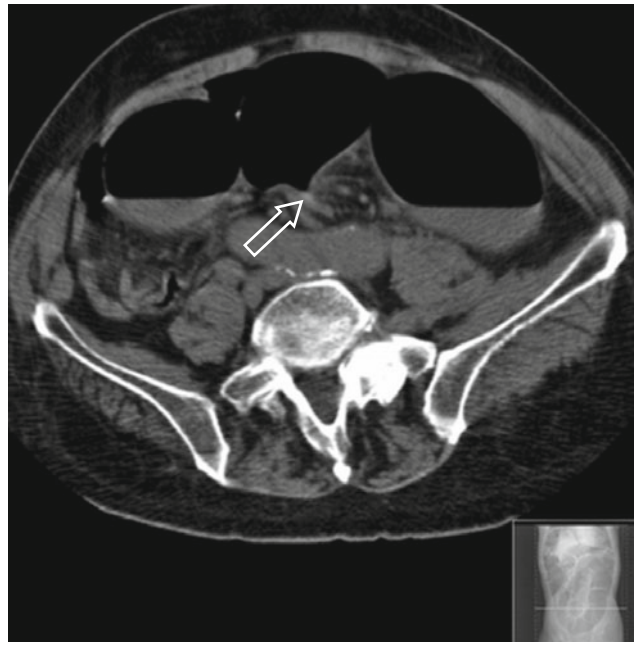

Fig. 9.8.2

A 76-year-old man presented with abdominal discomfort and constipation.

Comments

Sigmoid volvulus is caused by torsion of its mesenteric pedicle. According to the degree of twisting, it can be developed from closed-loop obstruction (>180°) to a vascular compromise (>360°). Sigmoid volvulus is the third most common cause of acute colonic obstruction in adults and makes up more than half of colonic volvulus.

The most important predisposing factor is a redundant, mobile sigmoid colon (dolichosigmoid colon) with a tight mesenteric pedicle.

Clinical features are nonspecific and range from chronic and insidious history of constipation and abdominal distension to acute distal colonic obstruction and perforation. Physical examination is also nonspecific and varies from tenderness to peritonitis.

In developed countries, volvulus is usually found in elderly people, but in endemic areas, it is found in younger patients.

In the majority of cases, the diagnosis of sigmoid volvulus is based on imaging features or during surgery.

The emergency treatment of choice is endoscopic reduction in uncomplicated patients and laparotomy in complicated ones, but afterward, both groups should be submitted to sigmoid resection to avoid recurrence.

In a high percentage of cases, the features of plain films can suggest or diagnose this entity. It can be usually seen a disproportionate enlargement of the sigmoid colon related to the rest of the colon with an inverted U shape, with the following findings:

- The edges are close and converge downward in the pelvis (pelvic convergence sign).
- The apex is very high, overlapping hepatic silhouette or extending above the tenth thoracic vertebrae, up to the left hemidiaphragm or above the transverse colon (northern exposure sign).
- Two apposed arms of the sigmoid coIon cause the three lines sign (these lines represent both outer walls of the arms and the apposed medial walls that converge in the pelvis), the white stripe sign (the apposed medial walls), and the coffee bean, bent inner tube, omega, or horseshoe sign.

It is usually associated with effaced haustral outpouchings and the absence of rectal gas.

In half of the cases, proximal colonic dilatation can be also seen, therefore alternative diagnoses are considered, such as distal colonic obstruction due to other causes, colonic pseudoobstruction, and colonic ileus.

A contrast enema has a high sensitivity to diagnose the sigmoid volvulus. It manifests the bird's beak or corkscrew signs.

Currently, CT is the imaging study of choice to study unspecific gastrointestinal disease. Some features which can be found are:

- The same aforementioned features can be seen on MPR coronal images.
- The whirl sign: The point of torsion is identified by spiral loops of collapsed bowel and their mesentery around their vascular supply.

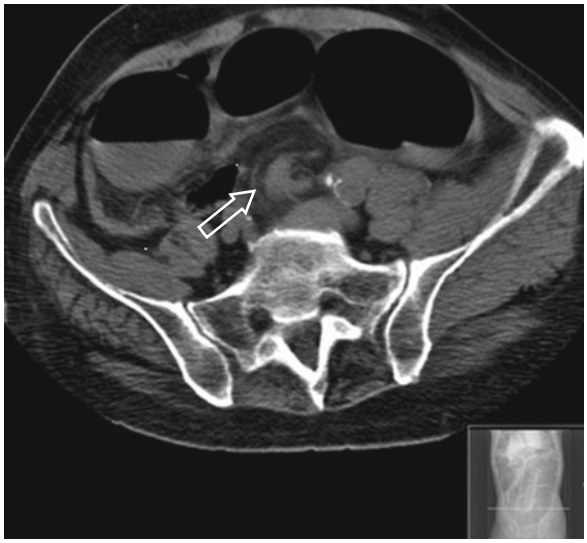

Fig. 9.8.3

Fig. 9.8.4

- Split-wall sign: This feature is seen in incomplete torsion and represents the mass effect of the twisting mesentery on the distal sigmoid loop which adopts a bilobed or C shape or even may simulate to be divided into two loops.
- The X-marks-the-spot sign: This finding is seen in tight torsion with at least two crosses, where the projection of both crossed loops in a single virtual image forms an "X."

Features that suggest vascular compromise (wall thickening, mesenteric infiltration, or pneumatosis intestinalis), or perforation (pneumoperitoneum) should also be ruled out by CT.

Imaging Findings

CT scanogram (Fig. 9.8.1) shows a disproportionate enlargement of the sigmoid colon in relation to the rest of the colon with an inverted U shape and absence of distal gas (*open arrow*). Its apex extends cephalad to transverse colon (northern exposure sign) and overlaps the hepatic silhouette. Two apposed arms of the sigmoid coIon cause the three lines sign and the coffee bean appearance. Axial CT images (Figs. 9.8.2 and 9.8.3) demonstrate the abrupt stop of one of the colonic loops with the bird's beak appearance (Fig. 9.8.2, *open arrow*) and the point of torsion which is identified by spiral loops of collapsed bowel and their mesentery, the whirl sign (Fig. 9.8.3, *open arrow*).

Single-contrast barium enema (Fig. 9.8.4) from another patient shows a severe stenosis due to a complete twist of the two limbs of dilated sigmoid colon (corkscrew sign, *open arrow*).

Case 9
Appendiceal Mucocele

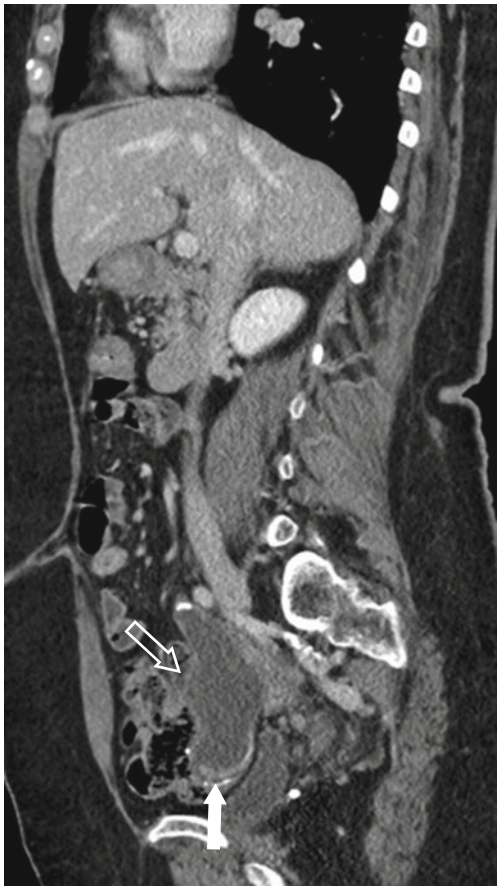

Fig. 9.9.1

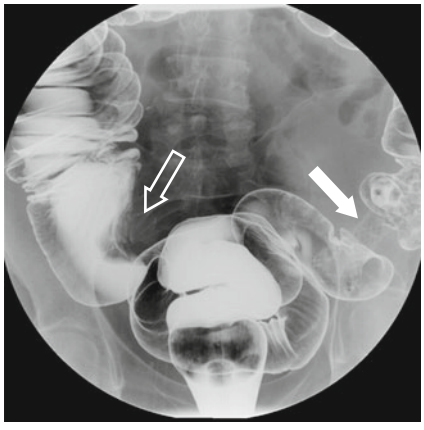

Fig. 9.9.3

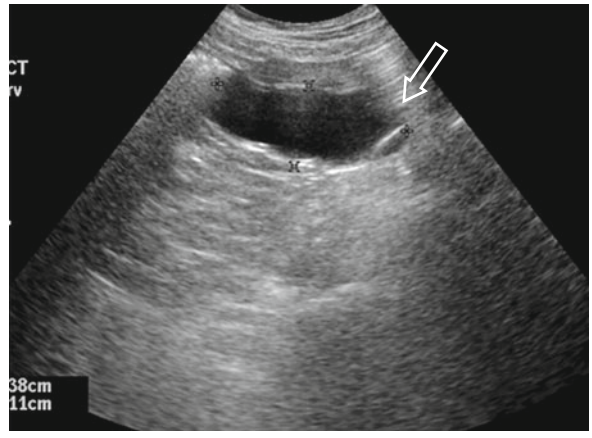

Fig. 9.9.2

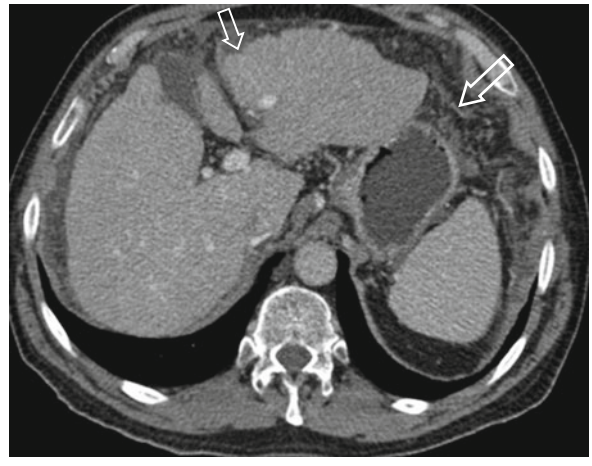

Fig. 9.9.4

A 60-year-old man presented with nausea and epigastric pain.

Comments

Appendiceal mucocele is a macroscopic description which represents a chronic cystic dilatation of the appendiceal lumen due to obstruction and secondary accumulation of mucus. This lesion represents four histologic entities: (1) simple or retention mucoceles (about 20%); (2) focal or diffuse hyperplasia (approximately 5–25%); (3) mucinous adenomas/cystadenomas—they are the most common histologic subtype and represent about 60–80% of the mucoceles, and they show adenomatous villous epithelium with some degree of atypias (these neoplasms usually are low grade); (4) mucinous adenocarcinomas (10–20%).

A simple mucocele or mucosal hyperplasia usually shows a mild dilatation of appendiceal lumen, and they rarely measure more than 2 cm. However, neoplastic mucoceles are larger with luminal distention of 6 cm or more, therefore they have an increased risk for perforation, and it can lead to pseudomyxoma peritonei.

The average age at diagnosis is over 50 years, and the gender distribution is similar for males and females. The clinical presentation of a mucocele is usually nonspecific. Up to 50% are found incidentally at abdominal imaging or at the time of operation.

The most common complications are acute appendicitis intestinal obstruction (due to a volvulus or a ileocolic intussusceptions, in which a mucocele is the lead point), torsion with gangrene and hemorrhage, and pseudomyxoma peritonei.

An appendiceal mucocele is a cystic mass in the expect region of the appendix. Therefore it is essential to demonstrate its relation with the cecal pole at all imaging modalities.

Depending on the mucin content, it can show some degree of internal echogenicity in relation to the number of acoustic interfaces at sonography, different degree of attenuation at CT, and high signal intensity on T1-weighted images.

The chance of malignancy is associated with focal nodules on the walls of mucoceles but not related to the thickness or irregularity of the wall.

Curvilinear or punctuate wall calcification suggests strongly the diagnosis of appendiceal mucocele, but it is only seen in less than 50% of cases. The diffuse calcification of the wall is called a porcelain appendix.

The differential diagnosis might include periappendiceal abscess, enteric duplication cysts, peritoneal inclusion cysts, fallopian tube cysts, or ovarian cystic lesions.

Imaging Findings

Sagittal MPR of contrast-enhanced CT shows incidentally a near-water-density mass abutting cecal pole (*open arrow*) with punctate and lineal wall calcifications (*solid arrow*) due to an appendiceal mucocele (Fig. 9.9.1). The lesion is also evaluated with sonography (Fig. 9.9.2), showing a cystic appearance with few internal echoes and prominent distal acoustic shadowing (*arrow*). The double-contrast barium enema (Fig. 9.9.3) demonstrates an extrinsic compression of the medial aspect of the cecum, and absence of filling of the appendix (*open arrow*). A circumferential filling defect with affected mucosa is also seen in descending colon corresponding to a known colon cancer (apple-core sign, *arrow*). Figure 9.9.4 corresponds to an enhanced CT from another patient with appendiceal cystadenoma. This figure shows thickening of all peritoneal surfaces and gastrocolic ligament (*open arrows*) related to pseudomyxoma peritonei due to a ruptured appendiceal cystadenoma (not shown).

Case 10
Colorectal Cancer

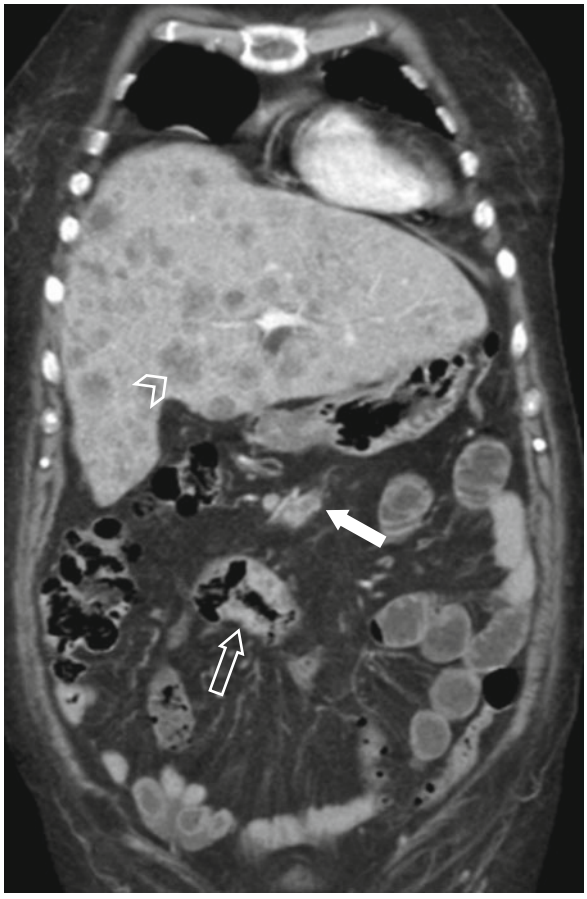

Fig. 9.10.1

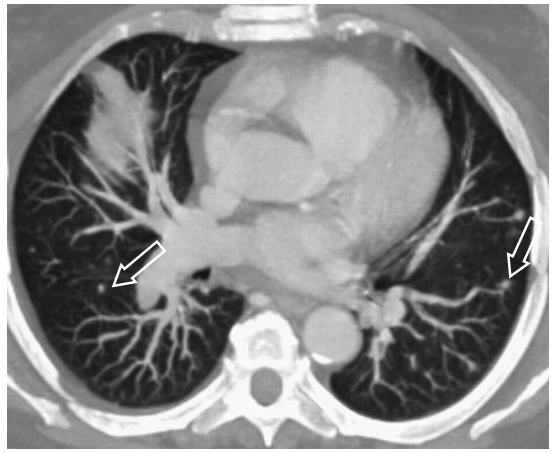

Fig. 9.10.2

A 62-year-old woman presented with epigastric pain and weight loss.

Comments

Colorectal cancer is the third most common malignant neoplasm and the second one in either men or women. Its incidence increases as age advances (it is most frequent after age 50) and is especially common in North America, Northern Europe, and Australia.

Most carcinomas arise from preexisting benign adenomatous polyps, and the incidence of cancer increases with polyp size (90–95% of cancers are presented in polyps whose size is more than 1 cm). There are high-risk factors for developing colonic cancer such as a strong family of colorectal cancer or polyps, history of chronic inflammatory bowel disease, history of polyps or colorectal cancer in the individual, and hereditary colorectal cancer syndrome.

The main roles of imaging in colonic cancer are staging (assessment of local extension and metastatic disease) and follow-up surveillance. A CT of the thorax, abdomen, and pelvis is usually the technique of choice.

On cross-sectional imaging, the tumor presents as a focal wall thickening. Multidetector CT enables to differentiate colonic cancers according to their local stage, in those with good prognosis (T1 or T2: outer margin of tumor is smooth or with few thin strands into pericolonic fat) and poor ones (T3 or T4: the margins are usually irregular, nodular, with thick strands, loss of fat planes, or invasion into adjacent structures). MR imaging is not oftenly used in local staging of colonic cancer due to technical problems (colonic peristalsis, variability in the location of the transverse and sigmoid colon, and difficulty in obtaining true axial images of the tumor because of a tortuous colon).

CT is inaccurate for assessment of metastatic lymph nodes, because the used criterion of maximum transverse diameter has demonstrated to be inaccurate. Regional nodes are located along the border of the antimesenteric colon, the vascular arcades of the marginal artery, and the course of the major vessels supplying the colon. New functional MRI techniques as diffusion-weighted imaging has demonstrated promising in this task, but their role has still to be validated.

Colonic cancer commonly metastasizes to the liver and the lungs, but almost any organ can be affected. In liver, MR imaging using liver-specific contrast agents and diffusion-weighted sequences is the preoperative technique with the highest sensitivity and specificity, therefore it is used for assessing the distribution and the respectability of hepatic metastases. Although the use of intraoperative ultrasound is recommended because it has greater sensitivity and allows to detect more and smaller hepatic metastatic lesions, generally <1 cm.

FDG PET is used to detect unsuspected extrahepatic disease (it is recommended in patients before planning hepatic resection or metastasectomy) or suspected recurrence due to CEA elevation when routine serial CT has failed to show it.

The incidence of recurrence in colon cancer is related to several prognosis factors (TNM stage, tumor regression grade, the presence of oncogene KRAS, or extramural venous spread). Local recurrence usually develops at the anastomotic or perianastomotic area.

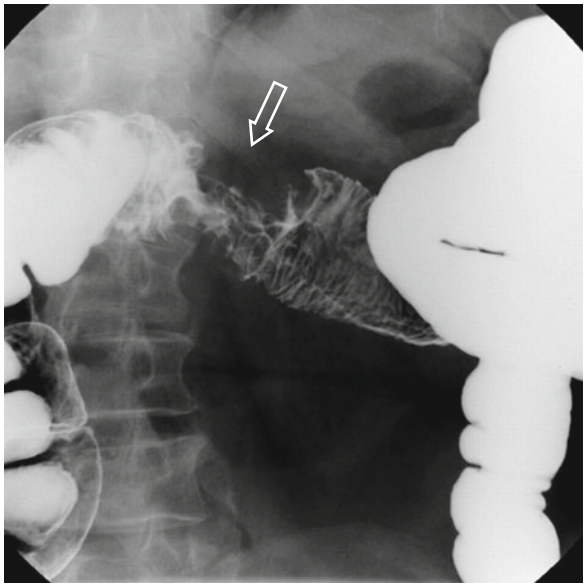

Fig. 9.10.3

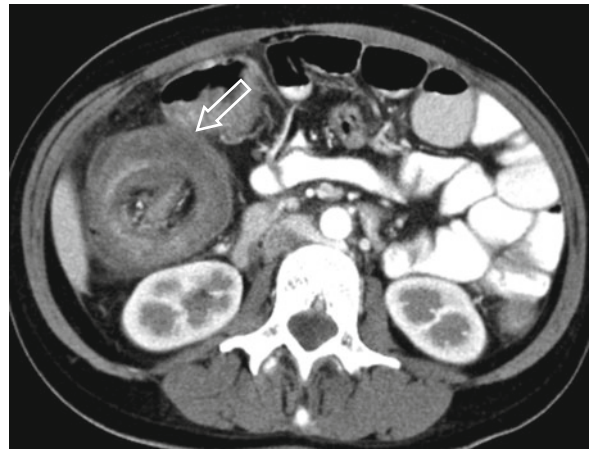

Fig. 9.10.4

Imaging Findings

Coronal MPR of contrast-enhanced CT image (Fig. 9.10.1) shows segmental circumferential thickening of the transverse colon with luminal narrowing (*open arrow*). Stranding of the pericolic fat is suggestive of local extension of tumor. A heterogeneous regional lymph node suggestive of metastatic infiltration can also be identified (*arrow*). The liver shows multiple hypoattenuating lesions that represent metastases (*open arrowhead*). Axial MIP of thoracic CT (Fig. 9.10.2) shows multiple pulmonary nodules corresponding to metastatic disease (*open arrows*). Double-contrast barium enema image (Fig. 9.10.3) shows a constricting lesion with eccentric lumen, ulcerated mucosa, and overhanging edges ("apple-core" lesion, *open arrow*) confirming the diagnosis of colon carcinoma.

Axial contrast-enhanced CT (Fig. 9.10.4) from another patient shows a target-like mass with alternating rings of soft tissue and fat (the wall of the intussusceptum, mesenteric fat, and the wall of the intussuscipiens) that represent an intussusception in the hepatic flexure due to colon cancer (*open arrow*), which is one of the complications of this entity.

Further Reading

Books

Eisenberg RL (2003) Gastrointestinal radiology: a pattern approach, 4th edn. Lippincott Williams & Wilkins, Philadelphia

Gore RM, Levine MS (eds) (2008) Textbook of gastrointestinal radiology, 3rd edn. W.B. Saunders, Philadelphia

Husband J, Rexnek RH (eds) (2010) Imaging in oncology, 3rd edn. Informa Healthcare, London

Lee KT, Sagel SS, Stanley RJ, Heiken JP (2005) Computed body tomography with MRI correlation, 4th edn. Lippincott Williams & Wilkins, Philadelphia

Rumack CM, Wilson SR, Charboneau JW, Levine D (eds) (2011) Diagnostic ultrasound, 4th edn. Mosby, St. Louis

Web-Links

www.auntminnie.com.
www.ctisus.org
www.learningradiology.com.
www.radiologyassistant.nl
www.wikiradiography.com

Articles

Bartone G, Severino BU, Armellino MF et al (2008) Clinical symptoms of intestinal vascular disorders. Radiol Clin North Am 46(5):887–889

Birnbaum BA, Wilson SR (2000) Appendicitis at the millennium. Radiology 215(2):337–348

Dachman AH, Lichtenstein JE, Friedman AC (1985) Mucocele of the appendix and pseudomyxoma peritonei. AJR Am J Roentgenol 144(5):923–929

Dixit A, Robertson JH, Mudan SS et al (2007) Appendiceal mucocoeles and pseudomyxoma peritonei. World J Gastroenterol 13(16):2381–2384

Honnef I, Moschopulos M, Roeren T (2008) Appendiceal mucinous cystadenoma. Radiographics 28(5):1524–1527

Horton KM, Corl FM, Fishman EK (2000) CT evaluation of the colon: inflammatory disease. Radiographics 20(2):399–418

Hurley BW, Nguyen CC (2002) The spectrum of pseudomembranous enterocolitis and antibiotic-associated diarrhea. Arch Intern Med 162(19):2177–2184

Javors BR, Baker SR, Miller JA (1999) The northern exposure sign: a newly described finding in sigmoid volvulus. AJR Am J Roentgenol 173(3):571–574

Kawamoto S, Horton KM, Fishman EK (1999) Pseudomembranous colitis: spectrum of imaging findings with clinical and pathologic correlation. Radiographics 19(4):887–897

Levsky JM, Den EI, DuBrow RA et al (2010) CT findings of sigmoid volvulus. AJR Am J Roentgenol 194(1):136–143

Martin MJ, Steele SR (2010) Twists and turns: a practical approach to volvulus and intussusception. Scand J Surg 99(2): 93–102

Moyle PL, Kataoka MY, Nakai A et al (2010) Nonovarian cystic lesions of the pelvis. Radiographics 30(4):921–938

Navaneethan U, Venkatesh PG, Shen B (2010) *Clostridium difficile* infection and inflammatory bowel disease: understanding the evolving relationship. World J Gastroenterol 16(39):4892–4904

Paterno F, Longo WE (2008) The etiology and pathogenesis of vascular disorders of the intestine. Radiol Clin North Am 46(5):877–885

Pereira JM, Sirlin CB, Pinto PS et al (2004) Disproportionate fat stranding: a helpful CT sign in patients with acute abdominal pain. Radiographics 24(3):703–715

Pickhardt PJ, Levy AD, Rohrmann CA Jr et al (2003) Primary neoplasms of the appendix: radiologic spectrum of disease with pathologic correlation. Radiographics 23(3):645–662

Rao PM, Mueller PR (1998) Clinical and pathologic variants of appendiceal disease: CT features. AJR Am J Roentgenol 170(5):1335–1340

Raveenthiran V, Madiba TE, Atamanalp SS et al (2010) Volvulus of the sigmoid colon. Colorectal Dis 12(7 Online):e1–e17, Epub Mar 10, 2010

Rexroad JT (2003) The CT arrowhead sign. Radiology 227(1):44–45

Singh AK, Gervais DA, Hahn PF et al (2005) Acute epiploic appendagitis and its mimics. Radiographics 25(6):1521–1534

Sun MY, Maykel JA (2007) Ischemic colitis. Clin Colon Rectal Surg 20(1):5–12

Taourel P, Aufort S, Merigeaud S et al (2008) Imaging of ischemic colitis. Radiol Clin North Am 46(5):909–924

Thoeni RF, Cello JP (2006) CT imaging of colitis. Radiology 240(3):623–638

van Breda Vriesman AC (2003) The hyperattenuating ring sign. Radiology 226(2):556–557

van Breda Vriesman AC, Puylaert JB (2002) Epiploic appendagitis and omental infarction: pitfalls and look-alikes. Abdom Imaging 27(1):20–28

Rectum-Anus 10

Guadalupe Garrido and Xavier Merino-Casabiel

Contents

A. Luna et al., *Learning Abdominal Imaging*, Learning Imaging,
DOI 10.1007/978-3-540-88003-5_10, © Springer-Verlag Berlin Heidelberg 2012

Case 1
Tailgut Cyst

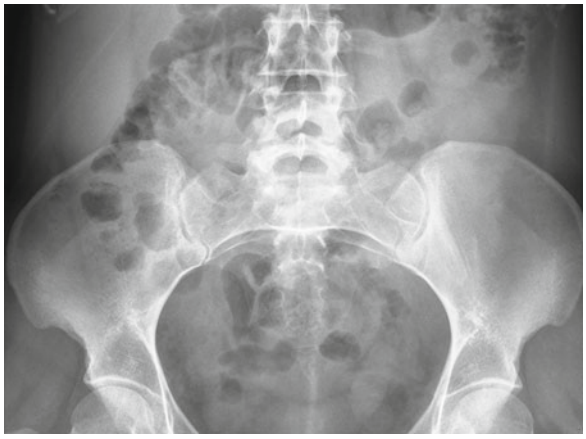

Fig. 10.1.1

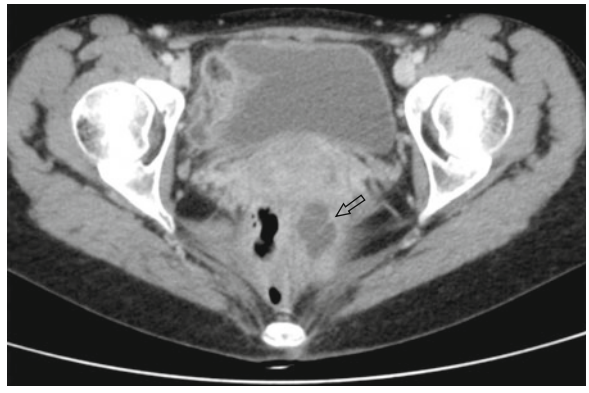

Fig. 10.1.2

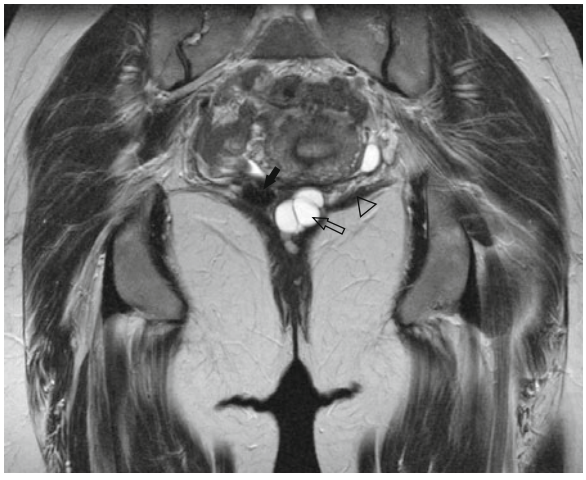

Fig. 10.1.3

Fig. 10.1.4

Asymptomatic incidental imaging finding in a 35-year-old woman with a history of gastric carcinoma (T2N1) treated surgically 4 years previously. There was no imaging or laboratory evidence of recurrent tumor, the patient had no history of anal fistula, and there was no pelvic pain.

Comments

Tailgut cysts are rare congenital developmental lesions derived from the remnant embryonic gut and typically located in the retrorectal space. They are usually diagnosed in middle-aged women, but can occur at any age. Tailgut cysts are commonly an incidental imaging finding, but patients occasionally experience symptoms related to local compression (pelvic pain, constipation, or rectal fullness) when the cyst is large. Possible complications of tailgut cysts include infection with a recurrent fistula, bleeding, and malignant degeneration.

Imaging studies, in particular MRI, are helpful to define the extent of the cystic lesion and its relationship with surrounding structures, in order to select the best surgical approach. Abdominal plain films are of little help and mainly serve to exclude conspicuous sacrococcygeal abnormalities related to other retrorectal cysts (e.g., sacral bone defects in anterior sacral meningocele). CT generally shows a well-defined, thin-walled, hypodense, unenhanced lesion in the retrorectal space, with no evidence of internal fat or calcification. MRI is superior to CT for tissue characterization because of its better soft-tissue contrast resolution. MRI shows a well-defined, multiloculated, thin-walled retrorectal cystic lesion, usually with low signal intensity on T1-weighted image and high signal intensity on T2-weighted image. Areas of high signal intensity may sometimes be seen on T1-weighted image, related to mucinous material, high protein content, or hemorrhage within the cyst.

The differential diagnosis is wide and difficult because the definite diagnosis is made on pathological examination after surgical resection, but there are some useful diagnostic keys. Other developmental cysts (e.g., epidermal cyst, dermoid cyst, or rectal cyst duplication) may have a similar appearance, but they are usually unilocular. The presence of fat within the lesion suggests a dermoid cyst, and rectal duplication cysts usually communicate with the rectal lumen. Anal gland cysts are generally lower and close to the anal sphincter. Lastly, in anterior sacral meningocele, there is partial agenesis of the sacrum with associated communication of the cyst with the thecal sac.

Imaging Findings

Plain film (Fig. 10.1.1) shows no significant morphological abnormalities of the sacrum. Contrast-enhanced CT (Fig. 10.1.2) shows a nonspecific, well-defined, hypodense, unenhanced lesion in the pararectal space (*open arrow*) with no evidence of calcification or sacrococcygeal communication. No adjacent soft-tissue inflammatory changes are seen. Coronal T2-weighted image (Fig. 10.1.3) shows multiple small cysts clustered together (*open arrow*) between lower rectum (*arrow*) and left levator ani muscle (*open arrowhead*). Axial fat-suppressed T1-weighted image (Fig. 10.1.4) demonstrates subtle high signal intensity within the cyst (*open arrow*), related to the protein-rich mucinous content.

Case 2

Fistulizing Rectal Crohn's Disease

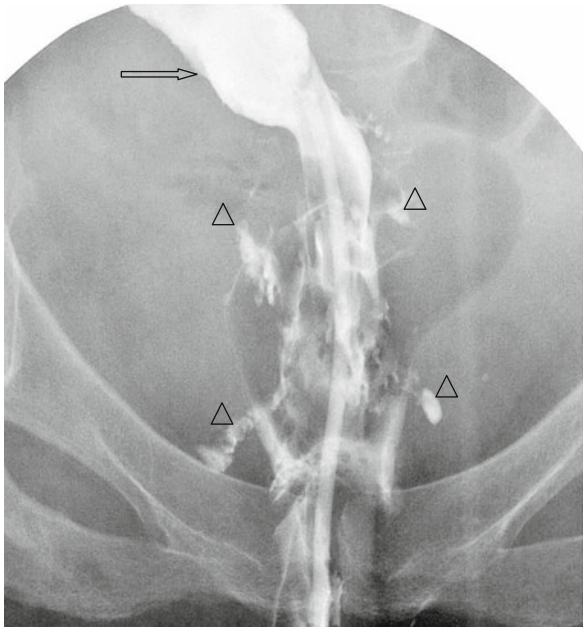

Fig. 10.2.1

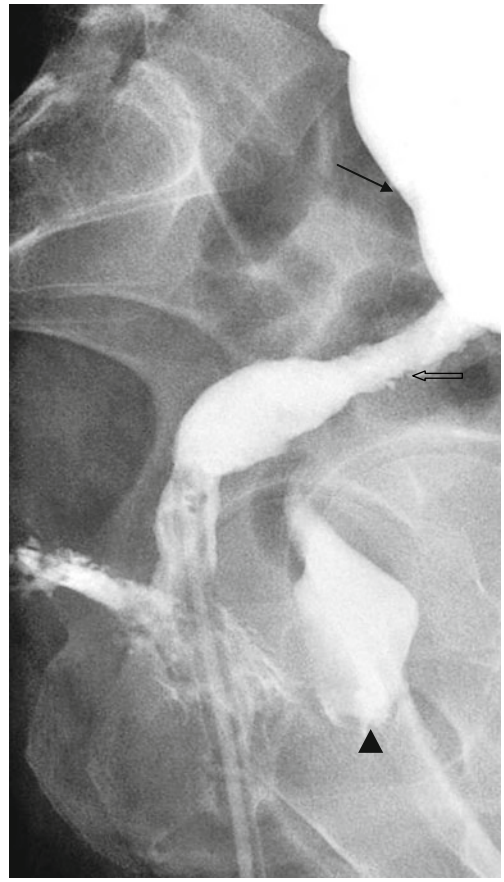

Fig. 10.2.2

Fig. 10.2.3

Fig. 10.2.4

A 35-year-old woman with a history of Crohn's disease and ileocecal resection presented with lower abdominal pain, low-grade fever, and constipation. Fluoroscopy-guided barium enema was requested. Based on the findings, contrast-enhanced abdominopelvic CT was performed.

Comments

Crohn's disease is a chronic, segmental, transmural inflammatory bowel disease of unknown etiology. It can affect any part of the gastrointestinal tract from mouth to anus, but is most common in the terminal ileum and proximal colon. The rectum is involved in 14–50% of cases.

Rectal Crohn's disease manifestations on fluoroscopic barium enema include wall thickening with luminal narrowing and associated proximal dilatation, deep collar-button ulcers, sacculations, fistulas, sinus tract, and fissures. Sinuses and fissures are blind-ended inflammatory tracts that penetrate through the full thickness of the muscular layer. Fistulas communicate with other structures; they can be reliably detected when contrast material is found within them.

Transrectal sonography may show mural thickening, abscesses, and fistulas. Anal sphincter heterogeneity may also be observed.

CT can be helpful for assessing the distribution, extension, and severity of Crohn's disease and detecting complications. Intestinal wall thickening and surrounding inflammatory changes are easily visualized on CT. On postcontrast images, the target sign may be observed, with enhancing inner mucosa and outer muscularis propia, but lower-density edematous submucosa. As the changes progress, luminal narrowing may increase and the target sign may disappear. Perianal disease and extramural complications, such as fistulas, sinus tracts, and abscesses can also be evaluated by CT.

MRI can show mural thickening and the extent and severity of the disease and is sensitive for evaluating perianal lesions and detecting sinuses, abscesses, and fistulas.

The differential diagnosis of rectal Crohn's disease mainly includes ulcerative colitis, ischemic colitis, infectious colitis, and radiation colitis.

Imaging Findings

Barium enema (Figs. 10.2.1 and 10.2.2) shows marked thickening of the rectum and sigmoid colon (*open arrows*) with prestenotic dilatation (*arrow*). Multiple sinus tracts affecting the rectum wall and a rectovaginal fistula are present, and contrast material is visualized within the sinus tracts (*open arrowheads*) and vagina (*arrowhead*).

Axial CT image (Fig. 10.2.3) shows luminal narrowing and rectal wall thickening with the target sign (*open arrow*), as well as marked surrounding inflammatory changes with fat stranding and an abnormal soft-tissue attenuation in the presacral space (*arrow*).

Axial CT image (Fig. 10.2.4) obtained at a level lower than Fig. 10.2.3 shows substantial thickening of the rectum and a hypodense linear tract between rectum and vagina related to the rectovaginal fistula (*open arrow*).

Case 3

Rectal Gastrointestinal Stromal Tumor

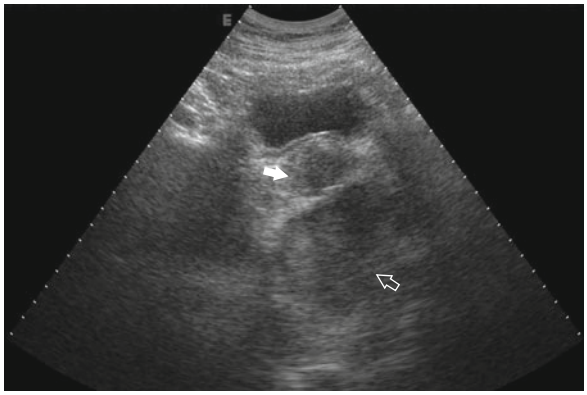

Fig. 10.3.1

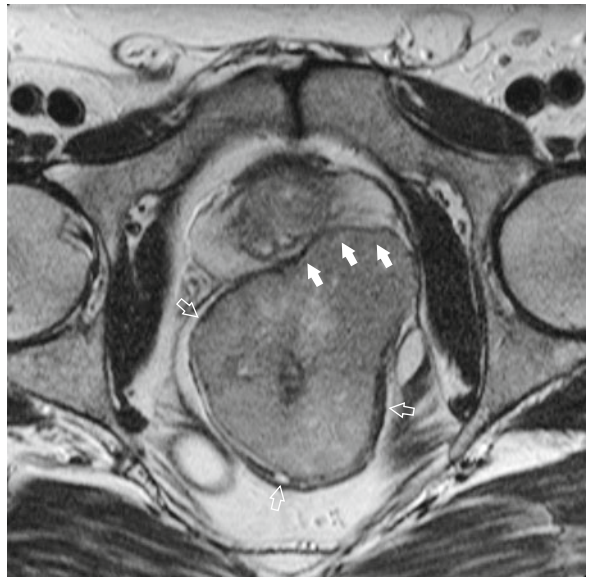

Fig. 10.3.2

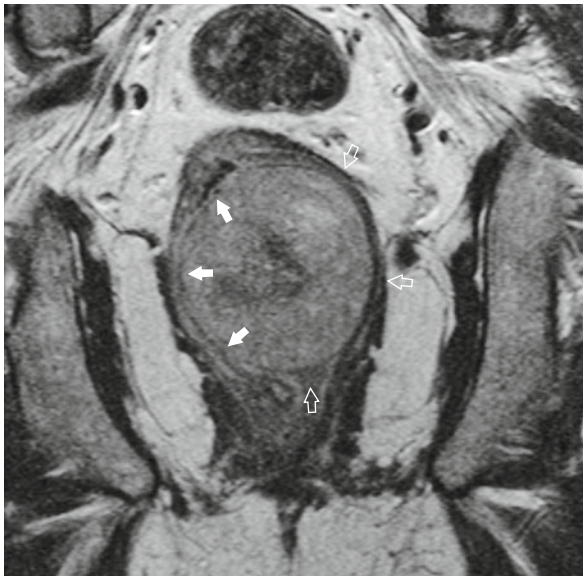

Fig. 10.3.3

Fig. 10.3.4

A 55-year-old man presented with progressively increasing constipation, pain in the low abdomen, and signs of prostatic hypertrophy with micturition difficulty. Laboratory tests, including PSA level, were normal. The patient underwent colonoscopy and pelvic ultrasound.

Comments

Gastrointestinal stromal tumor (GIST) is the most common mesenchymal tumor of the gastrointestinal tract, affecting any segment. The typical locations of GIST are the stomach (60–70%) and small bowel (20–25%). Only about 5% of all GISTs occur in the rectum. These tumors are derived from interstitial cells of Cajal and almost always express a specific tyrosine kinase growth factor receptor known as c-KIT, which is the key to the pathologic diagnosis.

Patients with GIST are usually older than 50 years, and both sexes are equally affected. When this tumor presents in young adults or children, a specific syndrome should be suspected (neurofibromatosis type 1, familial GIST, or the Carney's triad: gastric GIST, extra-adrenal paraganglioma, and pulmonary chondroma). The symptoms of rectal GIST are similar to those of other rectal masses, but prostate compression may occasionally develop, and the mass may be incidentally detected on US examination of the prostate.

Because of its mesenchymal origin, GIST usually grows as a well-defined round-oval endophytic or exophytic mass, parallel to the bowel lumen, with an intact overlying mucosa. Occasionally, the overlying mucosa shows signs of necrosis or ulceration. Hence, on endoscopic examination, GIST appears as a smooth deformity of the rectal wall, usually covered with normal mucosa. Endoscopic ultrasonography can be useful for differentiating an intramural lesion (GIST) from extrinsic compression. On US, these tumors are usually seen as solid, well-defined polylobulated hypoechoic masses. On CT, GIST appears as a well-defined, homogeneous, round, or polylobulated, endophytic, or exophytic mass. On MRI, in addition to these typical imaging signs, GIST displays a low signal intensity on T1-weighted image and is hyperintense or isointense with some hyperintense areas on T2-weighted image. Large tumor size and imaging findings of central necrosis, ulceration, and heterogeneous contrast enhancement have been reported as indicative of greater aggressive behavior. Tumor size and a pathologic mitotic rate are the most important and easily applicable criteria to predict tumor behavior.

The differential diagnosis of rectal GIST includes all the remaining neoplasms of the anorectal region: rectal adenocarcinoma, anal squamous cell carcinoma, lymphoma, malignant melanoma, neuroendocrine tumors, and true leiomyoma or leiomyosarcoma.

Imaging Findings

Suprapubic pelvic US (Fig. 10.3.1) shows a large well-defined hypoechoic mass (*open arrow*), apparently originating in the left prostatic lobe with posterior extension (*arrow*). Axial T2-weighted image (Fig. 10.3.2) shows an eccentric, well-defined, 6-cm, homogeneous submucosal tumor (*open arrows*) deforming and indenting the prostate gland (*arrows*). The prostate and the tumor are both delimited by a narrow hypointense line. No evidence of tumor invasion of the prostate was seen on pathological analysis. Coronal T2-WI (Fig. 10.3.3) shows the tumor (*open arrows*) located only 3.5 cm from the anal verge. Because of the submucosal location of the tumor, it displaces the rectal lumen

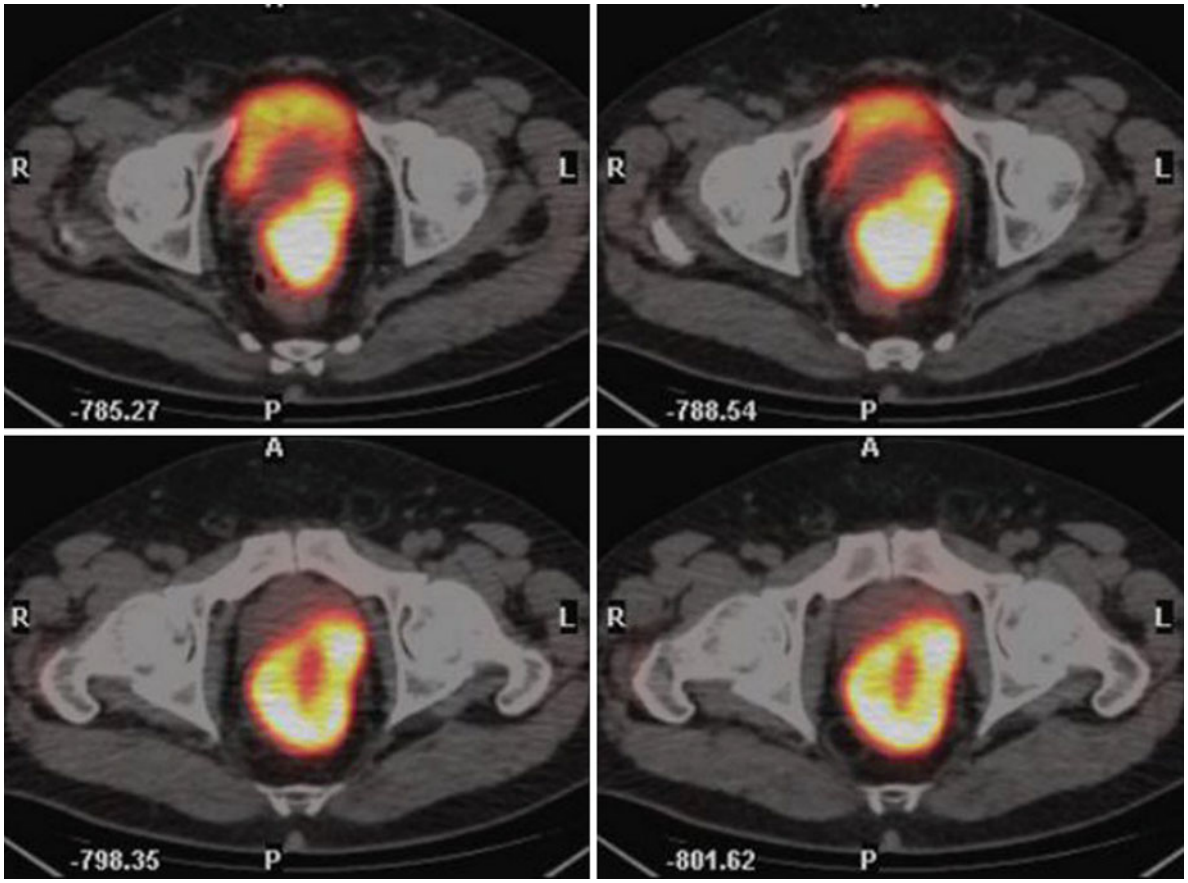

Fig. 10.3.5

to the right (*arrows*). There is no significant lymph node enlargement. Unenhanced CT (Fig. 10.3.4) shows a well-defined homogeneous rectal mass with no signs of calcification or intratumoral necrosis (*open arrows*). The lesion demonstrates intense metabolic activity on the fused PET-CT images of the pelvis (Fig. 10.3.5).

Case 4

Mucinous Rectal Adenocarcinoma

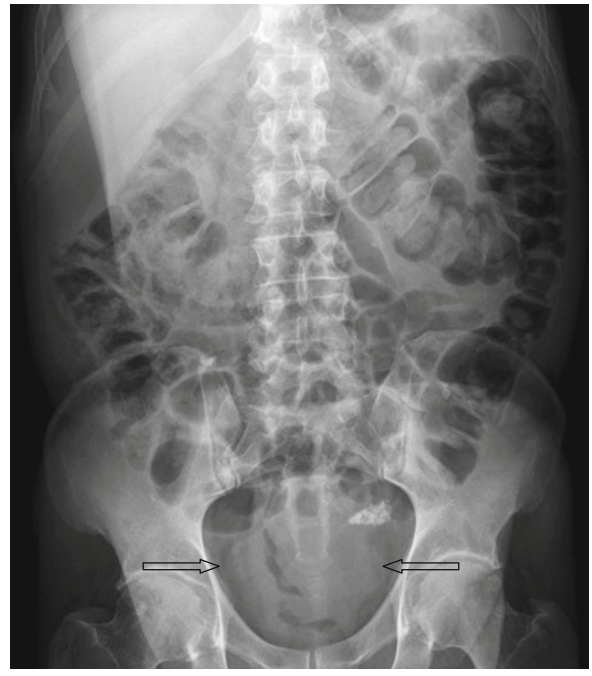

Fig. 10.4.1

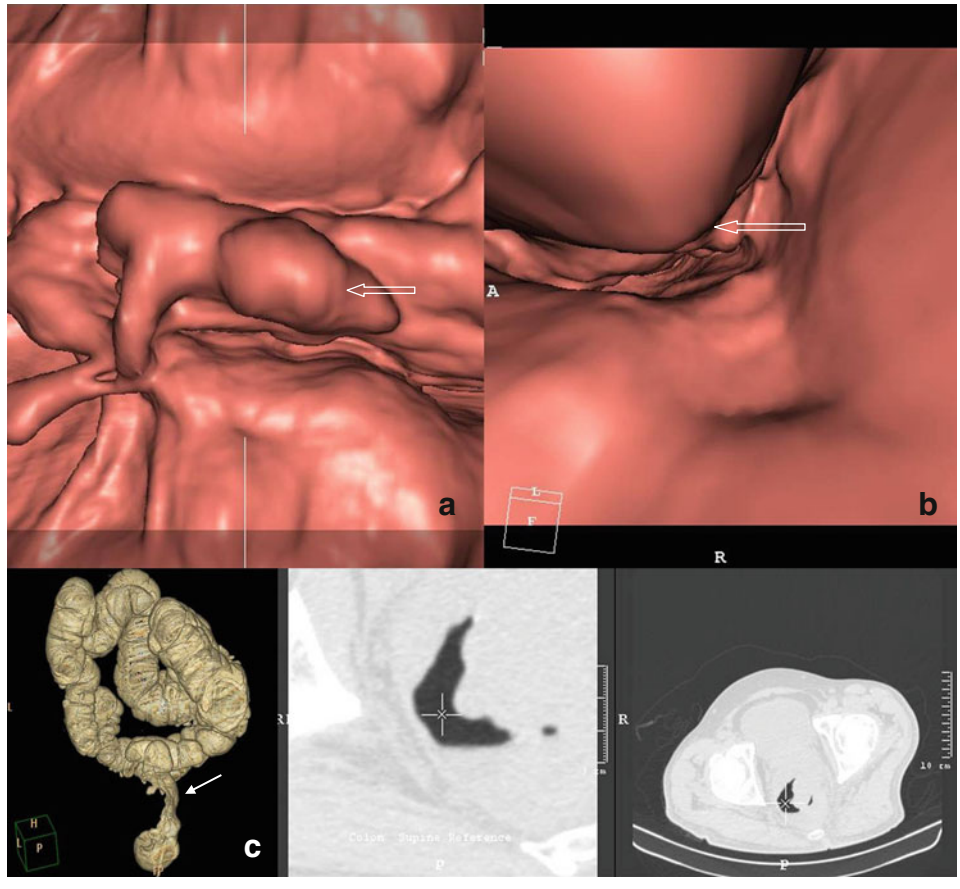

Fig. 10.4.2

A 60-year-old man presented with a 1-year history of change in bowel habits and blood on stool. Abdominal plain film revealed a space-occupying mass in the pelvis. CT colonography and abdominal CT were then performed to rule out a rectal tumor. Once suspected tumor was confirmed, MRI was requested for preoperative staging.

Comments

Colorectal cancer is the third leading cause of cancer deaths worldwide. Rectal carcinomas account for approximately 15% of colorectal carcinomas. Mucinous adenocarcinoma is a histologic subtype of rectal adenocarcinomas characterized by abundant extracellular mucin production. Mucinous adenocarcinoma is known to be a highly infiltrative lesion with an unfavorable prognosis.

Fluoroscopy-guided barium enema is the best imaging tool for detecting rectal cancer.

Endorectal US is probably the imaging modality that best assesses local disease because of its ability in identifying up to five layers of the rectal wall and thus determining the degree of mural infiltration. Rectal cancer may appear as a hypoechoic mass with disruption of wall segments or as focal or circumferential wall thickening. Perirectal lymph nodes may also be depicted.

Cross-sectional imaging is the most useful modality for evaluating advanced disease, complications, and recurrent disease. On CT scans, mucinous adenocarcinoma can be recognized by its low attenuation, in part due to the large pools of extracellular mucin within the tumor and, less commonly, by calcification.

MR imaging, performed with high-resolution sequences is useful for local staging of rectal tumors because of its high accuracy for evaluating the depth of invasion, spread to the mesorectal fascia and surrounding organs, and lymph node involvement. On MRI, mucinous tumors typically display markedly high signal intensity on T2-weighted fast SE images (higher than that of nonmucinous tumors), a finding presumably related to the mucous lakes. After contrast medium administration, mucinous tumors usually show peripheral or heterogeneous enhancement, differing from the most often homogeneous enhancement of nonmucinous tumors.

Due to their high signal intensity on T2-weighted images, mucinous tumors should be differentiated from a number of other malignant and benign conditions, such as necrotic tumors, fluid collections, and cysts.

Imaging Findings

Abdominal plain film (Fig. 10.4.1) reveals a space-occupying mass in the pelvic area (*open arrows*) with a paucity of gas distally.

Virtual colonoscopy (Fig. 10.4.2a, b) shows an irregular mass in the rectal wall, narrowing the rectal lumen (*open arrows*). Oblique volume-rendered image (Fig. 10.4.2c) demonstrates the classic "apple core" appearance of rectal cancer (*arrow*).

Sagittal contrast-enhanced CT scan (Fig. 10.4.3) depicts a large rectal mass with heterogeneous enhancement (*open arrows*), perirectal stranding, and enlarged local lymph nodes (*arrow*). Large hypodense areas are observed related to the mucinous lakes.

Axial T1-weighted MR image (Fig. 10.4.4) shows the large hypointense tumor spreading through the rectal wall into the surrounding fat (*open arrow*). Note the presence of mesorectal lymph nodes (*arrows*).

Fig. 10.4.3

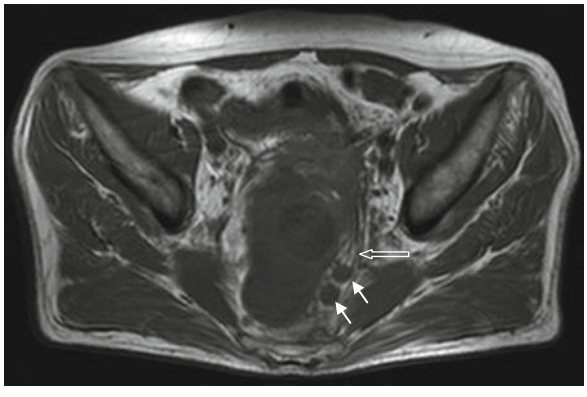

Fig. 10.4.4

Fig. 10.4.5

Sagittal T2-weighted MR image (Fig. 10.4.5) shows the predominantly high-signal-intensity rectal mass interlaced with strands of lower intensity, typical findings of mucinous tumors.

Case 5
Anorectal Melanoma

Fig. 10.5.1

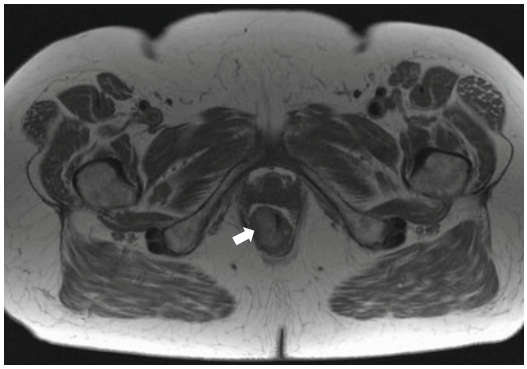

Fig. 10.5.2

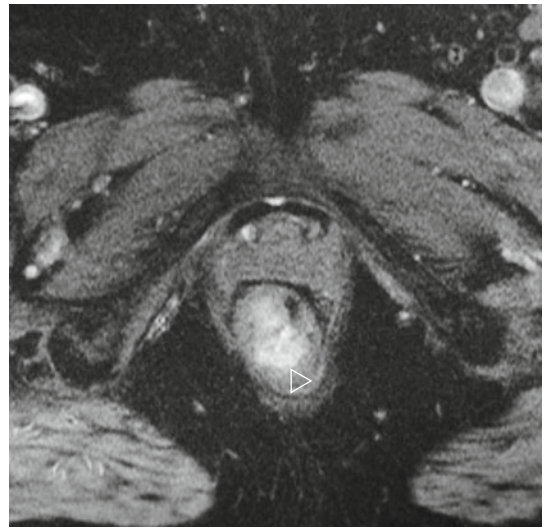

Fig. 10.5.3

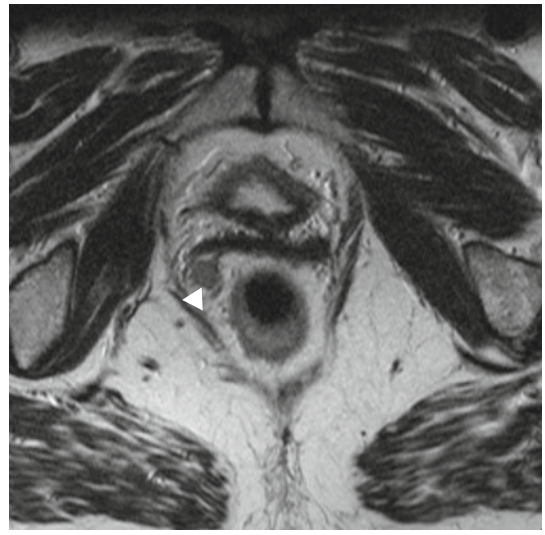

Fig. 10.5.4

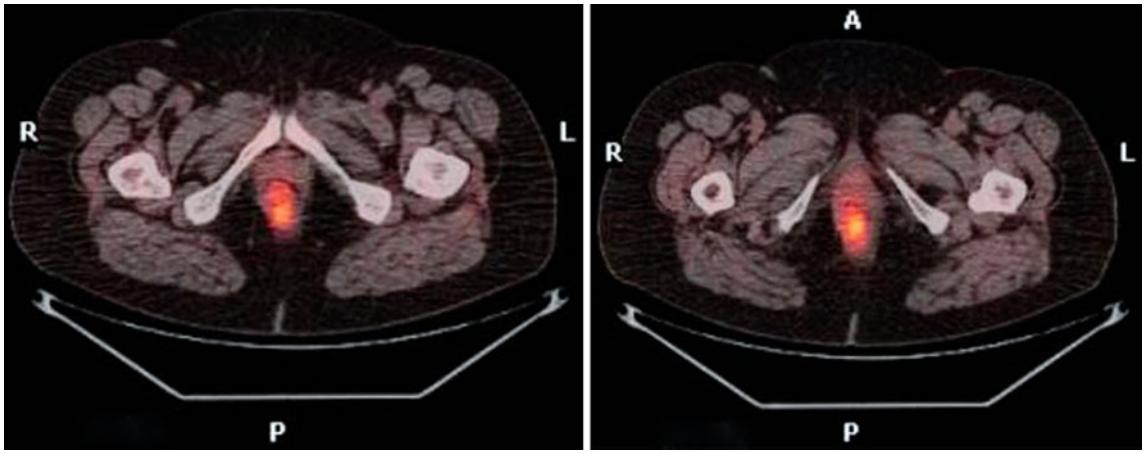

Fig. 10.5.5

A 74-year-old woman presented with bleeding when passing stool. Digital examination revealed a tumor protruding from the anal canal. Laboratory tests were normal. The patient underwent colonoscopy and biopsy.

Comments

Although primary anorectal melanoma is rare (0.1–5% of anal tumors and 0.5–1.6% of all melanomas), the anorectal region is the most common site for primary melanoma within the gastrointestinal tract. Malignant anorectal melanoma has a very poor prognosis, with a median survival of 24 months and a 5-year survival of approximately 10–20%. Almost 60% of patients have disseminated disease at diagnosis.

Patients with malignant anorectal melanoma are older (fifth to eighth decade), and there is a slight female sex predominance. Rectal bleeding and anorectal pain are the most common symptoms at initial presentation. The definitive diagnosis is based on pathologic examination, in which immunohistochemical data are important; specifically, expression of protein S-100, melanoma antigen HMB-45, and Melan-A, which are typical of melanoma. Anorectal melanoma may not be pigmented in 10–30% of cases. Amelanotic melanomas have a poorer prognosis because they are more invasive than melanotic lesions and much more difficult to diagnose.

Endoluminal ultrasound is a helpful technique for evaluating anorectal melanoma, defining the extent of the mass and potential sphincter involvement. On CT, anorectal melanoma generally appears as a bulky intraluminal mass in the distal rectum-anal canal. Perirectal infiltration and enlarged lymph nodes are also seen. Melanin pigments are paramagnetic and have a specific MRI behavior: high-in-low intensity on T1-weighted image and mixed intensity on T2-weighted image. The differential diagnosis of an anorectal mass with high-in-low intensity on T1-weighted image should also include postbiopsy hemorrhage. Enlarged lymph nodes with hemorrhagic changes or melanin pigments may occasionally be seen on MRI. The role of PET-CT in the management of patients with melanoma is rapidly evolving, but whole-body PET-CT is currently a highly effective imaging modality to stage patients.

Imaging Findings

Contrast-enhanced CT image (Fig. 10.5.1) shows a subtle, small, nodular, minimally enhancing lesion adjacent to the right levator ani muscle (*open arrow*).

Axial T1-weighted image (Fig. 10.5.2) confirms a small bulky endoluminal mass in the lower rectum-anal canal (*arrow*). Note in this image the slight diffuse hyperintensity of the lesion relative to the adjacent muscles, which is related to its melanin content and that is confirmed (*open arrowhead*) in the corresponding axial fat-suppressed T1-weighted image (Fig. 10.5.3).

Axial T2-weighted image (Fig. 10.5.4) shows a small, nonenlarged, but heterogeneous, perilesional lymph node (*arrowhead*).

Fused PET-CT images of the pelvis (Fig. 10.5.5) demonstrate the lesion with intense metabolic activity.

Case 6

Anal Squamous Cell Carcinoma

Fig. 10.6.1

Fig. 10.6.2

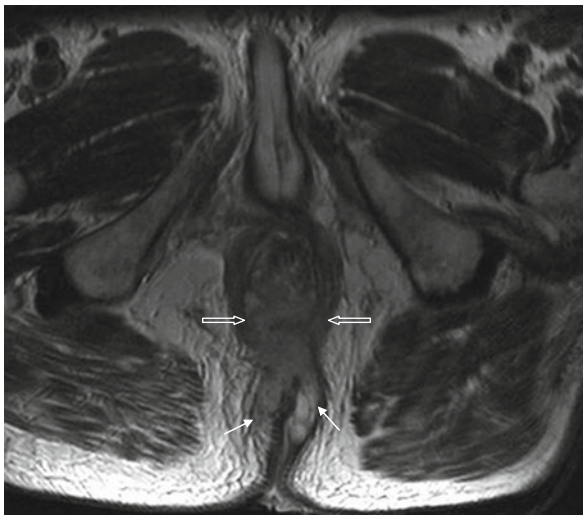

Fig. 10.6.3

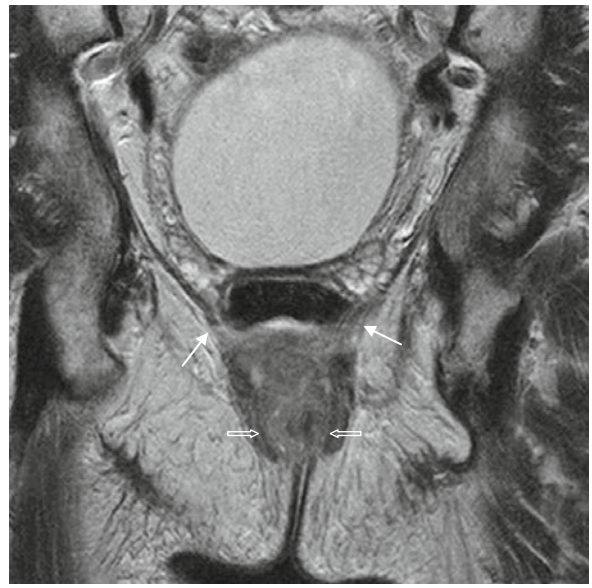

Fig. 10.6.4

A 68-year-old man presented with a history of pain, swelling, and intermittent bleeding in the perianal region. Physical examination revealed a mass in the anal canal. Proctoscopy was performed, and a biopsy was obtained, revealing an infiltrative squamous cell carcinoma. The preoperative work-up included abdominopelvic contrast-enhanced CT and pelvic MRI.

Comments

Anal canal tumors are uncommon, accounting for 1–6% of all malignant anorectal tumors. In general, the various histologic types of anal carcinoma are best considered as variants of epidermoid carcinoma. Most anal cancers are squamous cell carcinomas (95% of cases).

Anal canal carcinoma usually develops as a hard nodular mass infiltrating surrounding structures or as an ulcerating lesion with an indurated base. Less commonly, it appears as an exophytic mass.

Anal endosonography accurately stages early anal carcinoma, but as occurs in endoluminal MRI the limited field of view restricts the staging of advanced disease.

CT and MRI are best indicated to establish the extent of the primary lesion, the invasion of adjacent organs, and the presence of enlarged lymph nodes or distant metastasis.

CT findings of anal canal tumor include of a soft-tissue mass, with or without necrosis, or an asymmetry of the perineal structures, including asymmetric thickness of the sphincter or levator ani muscles. Associated linear stranding in the ischiorectal fossa may be present. Gas in the perineum may be a secondary sign of an anal canal tumor.

High-resolution MRI of the anorectal region with an external phased array coil enables detailed visualization of the muscles of the sphincter complex, providing accurate information about locoregional disease extent. This technique also provides information about nodal involvement. Anal canal tumors usually display low or intermediate signal intensity on T1-weighted images and high to intermediate signal intensity relative to skeletal muscle on T2-weighted images.

The differential diagnosis should be established with secondary involvement from direct extension of adjacent primary tumors, infectious or inflammatory lesions, and hematomas.

Imaging Findings

Contrast-enhanced CT scan (Fig. 10.6.1) shows bilateral thickening and bulging of the levator ani (*open arrows*) with blurring of the normal perianal fat line and marked thickening of the anal notch (*arrows*).

CT image obtained a few centimeters distal to the view in Fig. 10.6.1 (Fig. 10.6.2) shows anal canal tumor invading the external anal sphincter (*open arrow*) and the anal notch (*arrow*) and extending into the ischiorectal fossa (*open arrowhead*).

Axial T2-weighted MR image (Fig. 10.6.3) demonstrates a lobulated high-signal-intensity mass arising from the posterior wall of the anal canal, infiltrating the external anal sphincter (*open arrows*), and extending beyond the anal margin to affect the subcutaneous and cutaneous layers of the natal cleft (*arrows*).

Coronal T2-weighted MR image (Fig. 10.6.4) shows the anal canal mass infiltrating the external anal sphincter (*open arrows*) and levator ani muscles (*arrows*) bilaterally.

Case 7
Primary Rectal Syphilis

Fig. 10.7.1

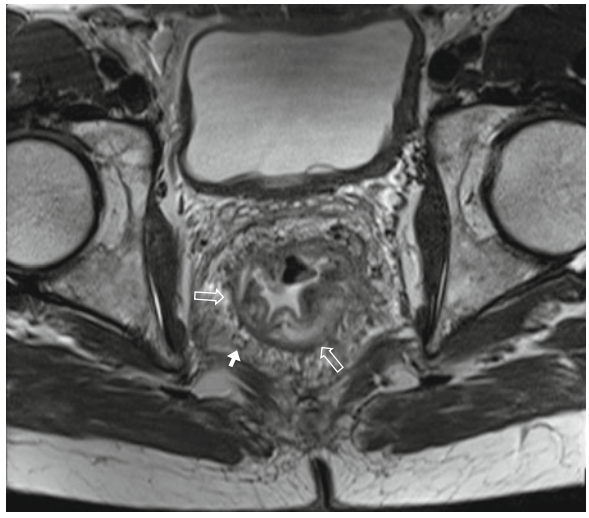

Fig. 10.7.2

Fig. 10.7.3

A 74-year-old man with a history of prostate carcinoma treated surgically 6 years previously was referred to our hospital for suspected rectal cancer. He reported anal pain and intermittent rectal bleeding. On physical examination, no enlarged lymph nodes were detected. On digital examination of the rectum, an indurated mass was palpated in the right posterolateral side of the anorectum. HIV antibody testing was negative. Laboratory tests were normal. Colonoscopy showed a poorly defined mass in the lower rectum with a deep ulcer extending from the anal canal that was not typical of carcinoma. Direct identification of spirochetes in the biopsy specimen and positive serology established the diagnosis of primary rectal syphilis.

Comments

Inflammatory conditions of the rectum are occasionally confused with rectal cancer. Although primary rectal syphilis is very rare, the prevalence of this condition has increased in recent years because of a rise in sexual risk behavior, such as unprotected anal intercourse. Rectal syphilis is known as one of the great masqueraders because of its variable clinical presentation, which includes bleeding, tenesmus, anal discharge, or defecation urgency, and its wide spectrum of endoscopic findings, including proctitis, rectal mass ulcers, or pseudotumors, hence being easily confused with rectal cancer. Despite the increase incidence of proctitis of other rare etiologies (syphilis, lymphogranuloma venereum), the most common source of rectal infection is anorectal inflammatory disease. Other causes of proctitis are rectal perforation, surgical complications, or spread from an adjacent pelvic infection. Imaging findings include inflammatory edematous thickening of the rectal wall with associated cellulitis and, sometimes, a soft-tissue abscess or fistula. MRI is useful for assessing the extent and severity of the disease and detecting complications, such as supralevator or infralevator abscesses.

In addition to rectal cancer, the differential diagnosis should include other inflammatory conditions, such as inflammatory bowel disease (ulcerative colitis and Crohn's disease), prior radiation therapy (radiation proctitis), and other causes of infection.

Imaging Findings

Contrast-enhanced CT image (Fig. 10.7.1) shows severe, irregular rectal wall thickening (*open arrow*) with multiple, small perirectal lymph nodes (*arrows*).

Axial and coronal T2-weighted MR images (Fig. 10.7.2 and Fig. 10.7.3) depict mucosal and submucosal wall thickening of the lower rectum with high signal intensity (*open arrows*) and associated diffuse perirectal edematous infiltration (*arrows*). Enlarged mesorectal lymph nodes are also seen (*arrowhead*).

Case 8
Fecaloma

Fig. 10.8.1

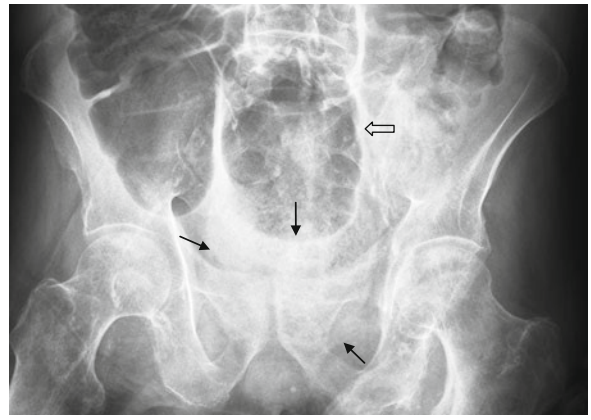

Fig. 10.8.2

Fig. 10.8.3

Fig. 10.8.4

An 80-year-old man presented to the emergency department with abdominal pain, vomiting, chronic constipation, and abdominal distention. An abdominal plain film was taken. Contrast-enhanced abdominal CT was performed to investigate suspected mechanical large bowel obstruction.

Comments

The most common causes of colonic obstruction are colorectal neoplasms and chronic diverticular disease. Colonic obstruction secondary to fecal impaction occurs most frequently in the elderly and less often in neurologically impaired young patients.

Stercoral colitis is an inflammatory condition involving the colonic wall related to maintained fecal impaction. Prolonged increased intraluminal and colonic wall pressures may lead to a decrease of the local blood supply. If left untreated, ischemic pressure necrosis, ulceration, and perforation can occur.

Abdominal plain film is useful in the diagnosis of fecal impaction, usually demonstrating a dilated rectum with soft-tissue density content or a bubbly pattern of large mass of stool within it. When obstruction occurs, dilated colon or dilated colon and small bowel may be present.

Although the diagnosis of fecal impaction is usually straightforward, CT is useful for detecting stercoral colitis. Fecaloma is usually seen as massive fecal impaction in a distended colon with thin walls. Stercoral colitis is suspected when focal thickness of the colonic wall and stranding of the pericolonic fat are seen. Other signs, such as hyperdense mucosa on unenhanced CT scans and mucosal enhancement alteration of the affected segment on contrast-enhanced CT scans, have also been described. Perforation is suspected when extraluminal gas or an abscess is detected.

The differential diagnosis should include other causes of large bowel obstruction (such as colorectal neoplasms and diverticulitis), ischemic colitis, inflammatory colitis, and infectious colitis.

Imaging Findings

Abdominal (Fig. 10.8.1) and pelvic (Fig. 10.8.2) plain films show colonic dilatation (*open arrows*) until rectum, where soft-tissue density content is seen within it (*arrows*). No air is seen distally, suggesting a mechanical obstruction.

Contrast-enhanced abdominal axial (Fig. 10.8.3) and sagittal MPR (Fig. 10.8.4) CT images show a dramatically distended rectum with fecal impaction and proximal dilatation of the colon. Focal thickening of the posterior aspect of the rectum (*open arrowheads*) and fat stranding in the presacral space (*arrowhead*) are observed.

Case 9
Deep Endometriosis

Fig. 10.9.1

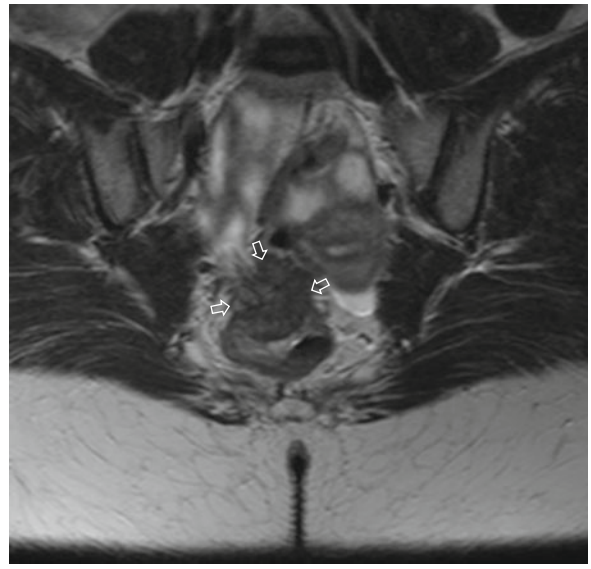

Fig. 10.9.2

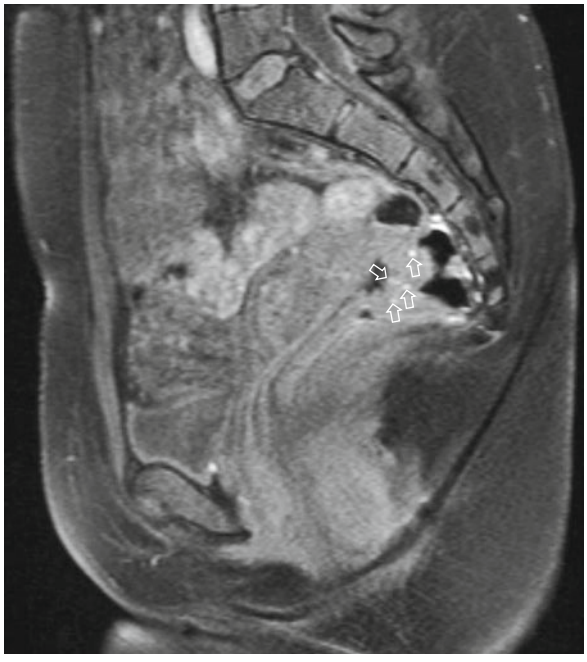

Fig. 10.9.3

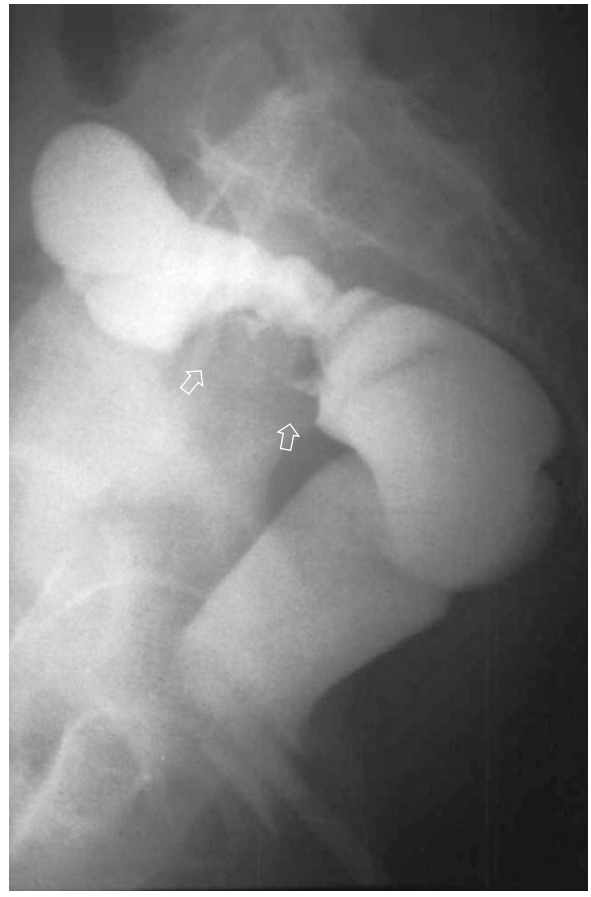

Fig. 10.9.4

A 36-year-old woman was referred for dysmenorrhea and rectal bleeding. A painful, fixed, indurated retrouterine mass was palpated on digital vaginal-rectal examination. Colonoscopy showed a focal nodular lesion in the anterior upper rectum, which, on biopsy study, was consistent with an endometrial implant.

Comments

Endometriosis is defined as the presence of functional endometrium outside the uterine cavity and myometrium. Deep pelvic endometriosis is a specific condition characterized by infiltration of endometrial implants under the surface of the peritoneum; that is, implants in the posterior cul-de-sac, uterosacral ligaments, rectum, rectovaginal septum, vagina, or bladder. These endometrial implants are usually associated with a severe desmoplastic response within the surrounding tissues and with secondary adhesions and fibrotic bands or soft-tissue nodules.

Deep endometriosis affects childbearing age women and has an estimated prevalence of approximately 10%. Clinically, patients with deep endometriosis can experience noncyclical pelvic pain, dysmenorrhea, dyspareunia, infertility, and gastrointestinal/urinary symptoms. Complete surgical excision of all endometrial implants is the treatment of choice.

The rectum and distal sigma are often affected by deep pelvic endometriosis. Rectosigmoid endometrial implants are commonly associated with obliteration of the posterior cul-de-sac. Although the reference standard to evaluate and stage endometriosis is laparoscopy, the affected region cannot be properly assessed when there is fixed retroversion of the uterus secondary to cul-de-sac adhesions or fibrosis; in these cases, MRI is of great value. Transvaginal sonography can be useful in the diagnosis of deep endometrial implants in the pelvis, but it is operator-dependent and has a relative limited field of view.

MRI is accepted as a noninvasive imaging tool for the preoperative work-up of patients with deep pelvic endometriosis. MRI diagnosis of this condition is based on the presence of signal intensity abnormalities, associated with adjacent soft-tissue fibrosis. On MRI, rectosigmoid endometrial implants appear as irregular areas of bowel thickening, sometimes associated with small hemorrhagic foci that are hyperintense on T1-weighted image, fat-suppressed T1-weighted image, and T2-weighted image. In addition, there are often associated direct signs (faint, spiculated, low-signal-intensity strands) or indirect signs (angulation of intestinal loops, elevated posterior vaginal fornix, posterior displacement of the uterus, or ovary in a medial position) of adhesions to adjacent pelvic organs.

Imaging Findings

Sagittal and oblique T2-weighted image (Fig. 10.9.1 and Fig 10.9.2) show a dense low-signal fibrotic nodule in the anterior aspect of the rectosigmoid colon (*open arrows*), with associated fibrotic obliteration of the pouch of Douglas and evidence of a low-signal-intensity area of tissue retraction (*arrow*). Note the retraction and elevation of the posterior vaginal fornix.

Fat-suppressed T1-weighted image (Fig. 10.9.3) demonstrates the presence of small high-signal-intensity foci (*open arrows*) within the mass, related to hemorrhagic content.

Barium enema in another patient with rectosigmoid endometrial implant (Fig. 10.9.4) shows a single intramural defect involving the upper rectum-sigmoid colon (*open arrows*), with no evidence of significant fibrosis or bowel retraction.

Case 10
Rectocele and Pelvic Floor Weakness

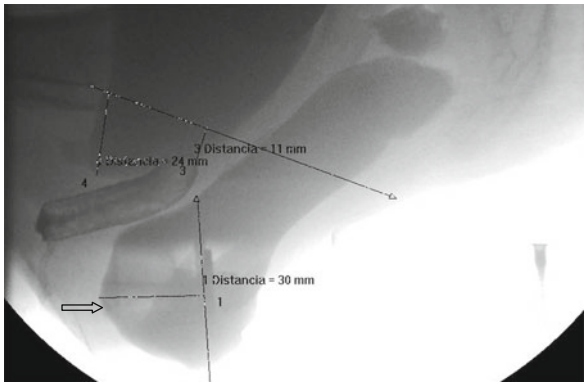

Fig. 10.10.1

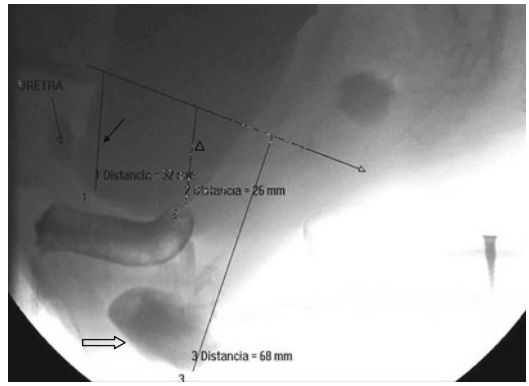

Fig. 10.10.2

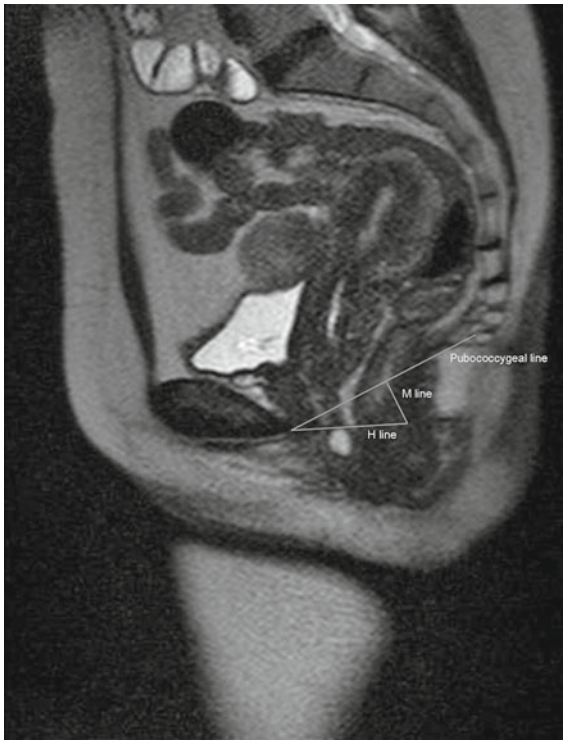

Fig. 10.10.3

Fig. 10.10.4

A 40-year-old woman with a history of chronic constipation presented symptoms of perineal pressure and a sensation of incomplete evacuation. A dynamic cystoproctography was requested. Dynamic MRI of the pelvic floor was then performed to plan a complex, multicompartment repair.

Comments

Rectocele is an outpouching of the rectum, commonly occurring in the anterior rectal wall. Anterior rectocele is considered to result from an anatomic weakness of the rectovaginal septum and is almost always present in women with pelvic floor weakness.

At physical examination, rectocele is palpated as a bulge in the posterior wall of the vagina.

Defecography or dynamic cystoproctography is the imaging technique of choice for evaluating anorectal dysfunction. Combined with opacification of other pelvic viscera, defecography can also be used to assess pelvic floor movement and pelvic organ prolapse. At defecography, rectocele is usually seen as an outpouching of the anterior rectal wall occurring during evacuation. The size of the rectocele is measured relative to a line drawn along the anterior margin of the axis of the anal canal. Barium may be retained within a rectocele after rectal evacuation. Concomitant cystocele, uterovaginal prolapse, or rectoanal intussusception are sometimes seen in patients with anterior rectocele.

MR imaging provides a global view of the pelvic viscera and pelvic floor musculature and can be used to evaluate pelvic floor movement. On sagittal T2-weighted MR images, an anterior bulge in the contour of the rectum, with a depth greater than 2 cm relative to a line drawn through the anterior wall of the anal canal, indicates a rectocele.

Pelvic floor weakness and pelvic organ prolapse are evaluated in sagittal images acquired while the patient is at rest and during pelvic strain. The pubococcygeal line (which represents the level of the pelvic floor), the H line (anteroposterior width of the levator hiatus), the M line (vertical descent of the levator hiatus), and the angle of the levator plate with the pubococcygeal line are evaluated. Excessive elongation of these lines during the Valsalva maneuver indicates pelvic floor laxity, and increased caudal inclination of the levator plate suggests a loss of posterior muscular support. Pelvic viscera prolapse is evaluated by measuring organ descent below the pubococcygeal line.

Imaging Findings

Cystoproctogram image obtained during the early phase of defecation (Fig. 10.10.1) shows an outpouching arising anteriorly from the rectum, indicating a rectocele (*open arrow*).

Cystoproctogram image taken during straining after rectal evacuation (Fig. 10.10.2) shows barium trapping within the rectocele (*open arrow*). A cystocele (*arrow*) and vaginal vault prolapse (*open arrowhead*) are also seen.

Sagittal MR images of the patient at rest (Fig. 10.10.3) and during pelvic strain (Fig. 10.10.4) demonstrate a global pelvic floor weakness (H line >5 cm, M line >2 cm, levator plate nearly vertical [*open arrow*]) with involvement of the three pelvic compartments. The descent and anterior bulging of the rectum observed is consistent with a rectocele (*dashed red line*). The cystocele (*arrow*) and vaginal vault prolapse (*open arrowhead*) are also evident.

Further Reading

Books

Dähnert W (2011) Radiology review manual, 7th edn. Lippincott Williams & Wilkins, Philadelphia

Federle MP, Brooke Jeffrey R, Woodward PJ, Borhani B (2009) Diagnostic imaging. Abdomen, 2nd edn. Amirsys Publishing Inc, Salt Lake City

Lee JKT, Sagel SS, Stanley RJ, Heiken JP (2005) Computed body tomography with MRI correlation, 2nd edn. Lippincott Williams & Wilkins, Philadelphia

Ros PR, Mortele KJ, Lee S, Pelsser V (2006) CT and MRI of the abdomen and pelvis: a teaching file, 2nd edn. Lippincott Williams & Wilkins, Philadelphia

Siegelman ES (2005) Body MRI, 1st edn. Elsevier Saunders, Philadelphia

Web Links

http://3s.acr.org/CIP/
http://rad.usuhs.edy/medpix/
http://www.eurorad.org/
http://www.learningradiology.com/
http://www.mypacs.net/cases/

Articles

Beets-Tan RG, Beets GL (2004) Rectal cancer: review with emphasis on MR imaging. Radiology 232:335–346

Beets-Tan RG, Beets GL, van der Hoop AG et al (1999) High-resolution magnetic resonance imaging of the anorectal region without an endocoil. Abdom Imaging 24:576–581

Blomqvist L, Machado M, Rubio C et al (2000) Rectal tumor staging: MR imaging using pelvic phased-array and endorectal coils vs endoscopic ultrasonography. Eur Radiol 10:653–660

Chung JJ, Kim MJ, Lee JT et al (2000) Large villous adenoma in rectum mimicking cerebral hemispheres. AJR Am J Roentgenol 175:1465–1466

Dahan H, Arrivé L, Wendum D et al (2001) Retrorectal developmental cysts in adults: clinical and radiologic-histopathologic review, differential diagnosis, and treatment. Radiographics 21:575–584

Fielding JR (2002) Practical MR imaging of female pelvic floor weakness. Radiographics 22:295–304

Fishman EK, Wolf EJ, Jones B et al (1987) CT evaluation of Crohn's disease: effect on patient management. AJR Am J Roentgenol 148:537–540

Healy JC, Halligan S, Reznek RH et al (1997) Dynamic MR imaging compared with evacuation proctography when evaluating anorectal configuration and pelvic floor movement. AJR Am J Roentgenol 169:775–779

Hoeffel CC, Azizi L, Mourra N et al (2006) MRI of rectal disorders. AJR Am J Roentgenol 187:W275–W284

Horton KM, Abrams RA, Fishman EK (2000a) Spiral CT of colon cancer: imaging features and role in management. Radiographics 20:419–430

Horton KM, Corl FM, Fishman EK (2000b) CT evaluation of the colon: inflammatory disease. Radiographics 20:399–418

Hussain SM, Outwater EK, Siegelman ES (1999) Mucinous versus nonmucinous rectal carcinoma: differentiation with MR imaging. Radiology 213:79–85

Kim KW, Ha HK, Kim AY et al (2004) Primary malignant melanoma of the rectum: CT findings in eight patients. Radiology 232:181–186

Klas JV, Rothenberger DA, Wong WD, Madoff RD (1999) Malignant tumors of the anal canal. The spectrum of disease, treatment, and outcomes. Cancer 85:1686–1693

Koh DM, Dzik-Jurasz A, O'Neill B et al (2008) Pelvic phased-array MR imaging of anal carcinoma before and after chemoradiation. Br J Radiol 81:91–98

Llauger J, Palmer J, Perez C et al (1998) The normal and pathologic ischiorectal fossa at CT and MR imaging. Radiographics 18:61–82

Maglinte DDT, Kelvin FM, Hale DS et al (1997) Dynamic cystoproctography: a unifying diagnostic approach to pelvic floor and anorectal dysfunction. AJR Am J Roentgenol 169:759–767

Paley MR, Ros PR (1998) MRI of the rectum: non-neoplastic disease. Eur Radiol 8:3–8

Pannu HK, Kaufman HS, Cundiff GW et al (2000) Dynamic MR imaging of pelvic organ prolapse: spectrum of abnormalities. Radiographics 20:1567–1582

Rafal RB, Nichols JN, Cennerazzo WJ et al (1995) MRI for evaluation of perianal inflammation. Abdom Imaging 20:248–252

Roach SC, Hulse PA, Moulding FJ et al (2005) Magnetic resonance imaging of anal cancer. Clin Radiol 60:1111–1119

Scherrer A, Reboul F, Martin D et al (1990) CT of malignant anal canal tumors. Radiographics 10:433–453

Silva AC, Vens EA, Hara AK et al (2006) Evaluation of benign and malignant rectal lesions with CT colonography and endoscopic correlation. Radiographics 26:1085–1099

Thoeni RF (1997) Colorectal cancer: radiologic staging. Radiol Clin North Am 35:457–485

Zerhouni EA, Rutter C, Hamilton SR et al (1996) CT and MR imaging in the staging of colorectal carcinoma: report of the Radiology Diagnostic Oncology Group II. Radiology 200:443–451